ELUCIDATING THE REGULATION OF SPAK AND OSR1 KINASES BY UBIQUITYLATION

A thesis submitted for the degree of

Doctor of Philosophy in Cardiff University

by

Binar Asrining Dhiani

September 2019

Cardiff School of Pharmacy and Pharmaceutical Sciences

Cardiff University

SUMMARY

The WNK-SPAK/OSR1 signalling pathway is a master regulator of ion homeostasis. The WNK kinases, whose mutations cause an inherited form of hypertension, activate SPAK and OSR1 kinases via phosphorylation. Upon phosphorylation by WNK kinases, SPAK and OSR1 kinases, consequently, phosphorylate an array of sodium, potassium and chloride ion co-transporters leading to either their activation or inhibition. WNK kinases phosphorylate SPAK and OSR1 kinases on their *N*-terminal threonine-rich region (termed the T-loop) as well as their serine-rich region (termed the S-motif). Although T-loop phosphorylation of SPAK and OSR1 kinases is known to activate these kinases, the function of their S-motif phosphorylation remains unclear. This project was aimed to unravel the function of SPAK and OSR1 S-motif phosphorylation by WNK kinases.

Using peptide pull-down assays that employed SPAK and OSR1 peptide sequences derived from their S-motifs, followed by mass spectrophotometry analysis, the E3 ubiquitin ligases Cullin 4A and 4B (CUL 4A and B) were identified as novel binders of SPAK and OSR1 S-motif. Additionally, the adaptor protein DDB1, which is known to form a complex with CUL4A/B, was also identified along with two other proteins known as WDR3 and WDR6. This binding of these proteins to SPAK and OSR1 kinases was subsequently verified using pull-down assays of overexpressed proteins in cells as well as immunoprecipitation of the endogenous proteins and followed by Western blotting. The results showed that these proteins bind SPAK and OSR1 kinases when unphosphorylated on their S-motif, while phosphorylation on these sites by WNK-kinases compromises the binding.

Given that CUL4A/B E3 ubiquitin ligases ubiquitylate their protein substrates, overexpressed SPAK and OSR1 kinases, along with the proteasome inhibitor, MG132, and the neddylation inhibitor MLN4924 were used to investigate whether SPAK and OSR1 kinases are ubiquitylated by the CUL4A/B-DDB1-WDR3/6 complex. The results indicated that SPAK and OSR1 are constitutively ubiquitylated under resting conditions, whereas under osmotic stress when SPAK and OSR1 kinases are phosphorylated by WNK kinases, the ubiquitylation of these proteins is significantly reduced.

Together, the data presented in this work represents the first example of an E3 ubiquitin ligase system that binds SPAK and OSR1 kinases. Critically, it provides a new molecular insight that links the CUL4A/B-mediated protein ubiquitylation to ion homeostasis and the regulation of blood pressure through SPAK and OSR1 kinases.

For my Ibu Ningrum and the late Bapak Asriyanto,

For my beloved husband Tunggul

and wonderful children Silmi, Salman, Syamil,

For my teachers.

ACKNOWLEDGEMENTS

I would first and foremost like to thank my lead supervisor Dr. Youcef Mehellou for his invaluable teaching, guidance and supports.

I am also hugely grateful to my second supervisor Dr. William Ford and my PhD advisor Dr. Meike Heurich-Sevcenco, whose support and input have helped to enrich the project.

I would like to express my gratitude to all my fellow lab members and friends especially for the past members: Dr. Abdulrahman Elzwawi, Dr. Hachemi Kadri, Dr. Mubarak Alamri, and Dr. Ageo Miccoli whose support, advice and technical assistances was greatly helpful. My warmest thanks also to others from the School of Pharmacy: Mr. Christopher Smith, Olivia Ogle, Sara Almadani, Catia Neto, Dr. Silvia Ziliotto, Dr. James Blaxland, Dr. Giulio Nannetti, Evans Ahortor, Ahmed Eissa, and Faizah Binjubair for all kind help and fruitful discussion.

I would like to thank our collaborator Prof. Dario Alessi at MRC-PPU University of Dundee, whose generosity with resources have been greatly enhanced the project. Also, I would like to thank the scientists at MRC-PPU University of Dundee for useful advice on the project troubleshooting.

Thanks also to Dr. Kathryn Taylor, Dr. Julia Gee, Dr. Stephen Hiscox, Prof. Les Baillie, Prof. James Birchall, Prof. Jean-Yves Maillard and Dr. Yi Jin for kindly allowing me to use their laboratory facilities.

For my former supervisor Prof. Nicholas Barnes at University of Birmingham along with the staff in Medical School and School of Pharmacy University of Birmingham, I would like to convey my gratitude for all support during my first year of my study.

I am extremely grateful to Indonesia Endowment Fund for Education (LPDP) for generous funding for my PhD study. Thanks also to University Muhammadiyah of Purwokerto Indonesia for general funding support.

Thank you so much to all Indonesian community in the United Kingdom, especially in Birmingham and Wales, for always being a great supporter throughout my study.

Last and most importantly, I would like to express my deepest thanks to my amazing family: my Ibu Sri Multiningrum and the late Bapak Asriyanto, my husband Tunggul Adi Purwonugroho and my sisters Fusi Asrining Dhini and Visi Asrining Njani for their endless love, encouragement and support in all my pursuits.

TABLE OF CONTENTS

LIST OF FIGURES

LIST OF TABLES

LIST OF PUBLICATIONS

Mubarak A Alamri, Dr. Hachemi Kadri, **Binar A Dhiani**, Shumail Mahmood, Abdulrahman Elzwawi, Dr. Youcef Mehellou, 2017, *WNK-Signaling Inhibitors as Potential New Antihypertensive Drugs*, ChemMedChem 12(20):1677-1686.

Youcef Mehellou, Mubarak A Alamri, **Binar A Dhiani**, Hachemi Kadri, 2018, *C - terminal phosphorylation of SPAK and OSR1 kinases promotes their binding and activation by the scaffolding protein MO25*, Biochem BioPhys Res Comm 503(3): 1868-1873.

Ageo Miccoli, **Binar A Dhiani**, Youcef Mehellou, 2019, *Phosphotyrosine Prodrugs: Design, Synthesis and Anti-STAT3 Activity of ISS-610 Aryloxy Triester Phosphoramidate Prodrugs***,** MedChemComm 10(2), 200-208.

Binar A Dhiani, Youcef Mehellou, 2019, *The Cul4-DDB1-WDR3/WDR6 Complex Binds to SPAK and OSR1 Kinases in A Phosphorylation-Dependent Manner*, ChemBioChem, https://doi.org/10.1002/cbic.201900454, first published 15 Oct 2019.

(The publication which covers Chapter III section 3.1., 3.2. and 3.3.2. of this thesis)

Ageo Miccoli, **Binar A Dhiani**, Peter J Thornton, Olivia A Lambourne, Edward James, Hachemi Kadri, Youcef Mehellou, 2019, *Aryloxy Triester Phosphoramidates as Phosphoserine Biocleavable Masking Motifs***,** published as preprint on ChemRxiv, chemrxiv.org/articles/Aryloxy_Triester_Phosphoramidates_as_Phosphoserine_Biocleavable_Masking_Motifs/10260887/1, published online 13 Nov 2019.

LIST OF ABBREVIATIONS

AATYK	Apoptotic–Associated Tyrosine Kinase
AMP	Adenosine Mono Phosphate
APS	Ammonium Per Sulphate
ATP	Adenosine Tri Phosphate
BPA	Beta Propeller A
BPB	Beta Propeller B
BPC	Beta Propeller C
BSA	Bovine Serum Albumin
BTB	Bric-a-Brac, Tramtrack and Broad complex
CAND1	Cullin-Associated NEDD8-Dissociated 1
CCC	Cation Chloride Cotransporter
CCT	Conserved Carboxy Terminal
CNS	Central Nervous System
CRISPR	Clustered Random Interspaced Short Palindromic Repeat
CRL	Cullin RING Ligase
CSN	COP9 signalosome
CTD	C-Terminal Domain
CUL	Cullin
DCAF	DDB1-Cullin Associating Factor
DCT	Distal Convoluted Tubules
DDB1	DNA Damage Binding 1
DMP	Dimethyl Pimelimidate
DMSO	Dimethyl Sulfoxide
DNA	Deoxyribo Nucleic Acid
ECL	Enhanced Chemiluminescence
ECM	Extra Cellular Matrix
EDTA	EthyleneDiamineTetraacetic Acid
EGTA	Ethylene Glycol-bis(β-aminoethyl ether)-N,N,N′,N′-Tetraacetic Acid
ELOC	Elongin C
ERK1/2	Extracellular signal Regulated Kinase
FBS	Fetal Bovine Serum
FDA	Food and Drug Administration

GABA	γ-Amino Butiric Acid
GCK	Germinal Centre Kinase
GFP	Green Fluoroscence Protein
GST	Glutathione S Transferase
HDR	Homology-Directed Repair
HECT	Homologous to the E6-AP C-terminus
HEK293	Human Embryonic Kidney 293
HSP	Heat Shock Protein
HTS	High Through-put Screening
IMiD	Immunomodulatory Drugs
IRK	Inward Rectifier K^+
JNK	c-Jun N-terminal Kinase
KCC	K^+, Cl^- Cotransporter
KLHL3	Kelch-Like 3
KO	Knock Out
LC	Liquid Chromatography
LKB1	Liver Kinase B1
LRR	Leucine-Rich Repeat
MAPK	Mitogen-Activated Protein Kinase
MEK1	MAP Kinase Kinase 1
MO25	Mouse Protein 25
MRC-PPU	Medical Research Council-Protein Phosphorylation and Ubiquitylation
MS	Mass Spectrophotometry
MST	Mammalian Ste-20-like
NAE	NEDD8-activating enzyme
NCC	Na^+, Cl^- Cotransporter
NFκB	Nuclear Factor kappa-light-chain-enhancer of activated B cells
NHEJ	Non-Homologous End Joining
NKCC	Na^+, K^+, Cl^- Cotransporter
NTD	*N*-Terminal Domain
OSR1	Oxidative Stress Response 1
PARC	Parkin-like cytoplasmic protein
PBS	Phosphate Buffer Saline
PCR	Polymerase Chain Reaction
PDB ID	Protein Data Base Identification

PEI	Polyethyleneimine
Penstrep	Penicillin Streptomycin
PHAII	Pseudoaldosteronism Type II
RBR	RING-Between-RING
RING	Really Interesting New Gene
RNA	Ribonucleic Acid
RVD	Regulatory Volume Decrease
RVI	Regulatory Volume Increase
SCF	Skp-Cullin- F Box
scRNA	Scrambled RNA
SDS/PAGE	Sodium Dodecyl Sulphate/Polyacrylamide Agarose Gel Electrophoresis
sgRNA	Single guided Ribonucleic Acid
shRNA	Short hairpin RNA
siRNA	Short interference RNA
SLK	Ste-20 Like Kinase
SOCS	Supressor Of Cytokine Signalling
SOK1	Ste20/Oxidant stress response Kinase-1
SPAK	Ste-20 Proline-Alanine Rich Kinase
SR	Substrate Receptor
SREF	Substrate Receptor Exchange Factor
STRAD	Ste20-Related Kinase Adapter
TAE	Tris Acetate EDTA
TAL	Thick Ascending Limb of Henle
TBS	Tris-Cl Buffer Saline
TEMED	Tetramethylethylenediamine
TUBE	Tandem-repeated Ubiquitn-Binding Entities
Ub	Ubiquitin
UBA	Ubiquitin-Associated
UV-Vis	UltraViolet-Visible
VHL	Von Hippel Lindau
WDR	WD Repeat
WHO	World Health Organization
WNK	With No K (Lysine)
WT	Wild Type

CHAPTER I.

INTRODUCTION

CHAPTER I. INTRODUCTION

1.1. THE WNK-SPAK/OSR1 SIGNALLING PATHWAY

The With No Lysine (K) Kinases 1-4 (WNK 1-4) signalling pathway plays an important role in the regulation of salt homeostasis and, thus, the control of blood pressure (Alessi *et al.*, 2014). In humans, mutations in the WNK genes, which encode WNK kinases, have been found to cause an inherited form of hypertension and hyperkalemia named Pseudoaldosteronism Type II (PHAII) or Gordon's syndrome (Wilson *et al.*, 2001).

The ability of the WNK signalling pathway to regulate ion homeostasis is now understood to be due to its ability to regulate the function of a series of sodium, potassium and chloride ion co-transporters (**Figure 1.1.**) (Moriguchi *et al.*, 2005, Anselmo *et al.*, 2006, Vitari *et al.*, 2006, Richardson *et al.*, 2008). Indeed, it is now established that under resting conditions, WNK kinases are inactive, and they become activated under osmotic stress (Zagórska *et al.*, 2007). Although the mechanism of their activation of WNK kinases is not entirely understood, it is thought to involve chloride-sensing (Moriguchi *et al.*, 2005, Richardson *et al.*, 2008).

Once activated, WNK kinases phosphorylate two other protein kinases termed Ste-20/SPS1-related Proline/Alanine-rich Kinase (SPAK) and Oxidative Stress Responsive 1 (OSR1). Specifically, WNK kinases phosphorylate SPAK and OSR1 kinases on their highly conserved catalytic threonine-rich region (T-loop) residues, T233 and T185, respectively (Kahle *et al.*, 2003, Vitari *et al.*, 2005). This SPAK and OSR1 T-loop phosphorylation turns on their catalytic activity (Vitari *et al.*, 2005). Additionally, WNK kinases phosphorylate SPAK and OSR1 kinases on their serine-rich region (S-motif) primarily at S373 and S325, respectively (Vitari *et al.*, 2005). Upon WNK phosphorylation, SPAK and OSR1 kinases bind to the scaffolding protein mouse protein-25 (MO25) (Filippi *et al.*, 2011) through their highly conserved *C*-

terminal domain (CCT domain) (Mehellou *et al.*, 2018). The binding of WNK-phosphorylated SPAK and OSR1 kinases to MO25 leads to 80- to 100-fold increase in their catalytic activities (Filippi *et al.*, 2011). Subsequently, SPAK and OSR1 kinases in complex with MO25 phosphorylate sodium, potassium and chloride ion cotransporters (CCCs) such as Na^+- K^+- Cl^- cotransporters (NKCCs), Na^+- Cl^- cotransporter (NCC) and K^+- Cl^- cotransporters (KCCs) (Filippi *et al.*, 2011).

CCCs are responsible for transporting chloride (Cl^-) and potassium (K^+) into or out of cells (Alessi *et al.*, 2014). There are two types of CCCs: Cl^- importing and Cl^- exporting CCCs (Alessi *et al.*, 2014). The first type is driven by sodium, and these include N[K]CCs, i.e. NCC, NKCC1 and NKCC2 and the second type is potassium-driven CCCs, which include KCCs (KCC1-4) (Alessi *et al.*, 2014). Given their critical roles in regulating essential ion homeostasis, CCCs play vital roles in human health and diseases (Kahle *et al.*, 2009, Alessi *et al.*, 2014, Murthy *et al.*, 2017). In fact, these ion co-transporters are the molecular targets of many antihypertensive loops and thiazide diuretics, which target NKCC1/2 and NCC, respectively.

The binding of SPAK and OSR1 kinases to their downstream ion co-transporters is achieved by the binding of SPAK and OSR1 highly conserved *C*-terminal domains to the tetramer RFXV/I peptide motifs that are present in the ion co-transporters (Piechotta *et al.*, 2002) (**Figure 1.1.**). Notably, such interaction is also similar to that mediates WNK kinases binding to SPAK and OSR1 as this binding is also achieved by the binding of SPAK and OSR1 *C*-terminal domains to the tetramer RFXV/I peptide motifs that are present in the four upstream WNK kinase isoforms (Vitari *et al.*, 2005, Vitari *et al.*, 2006).

WNK kinases are regulated by its upstream regulator, an E3 ubiquitin ligase CUL3-KLHL3. At first, it was found that the mutation in CUL3 and KLHL3 cause PHAII (Boyden *et al.*, 2012, Louis-Dit-Picard *et al.*, 2012). CUL3-KLHL3 then was known to interact and ubiquitylate WNK isoforms (Ohta *et al.*, 2013).

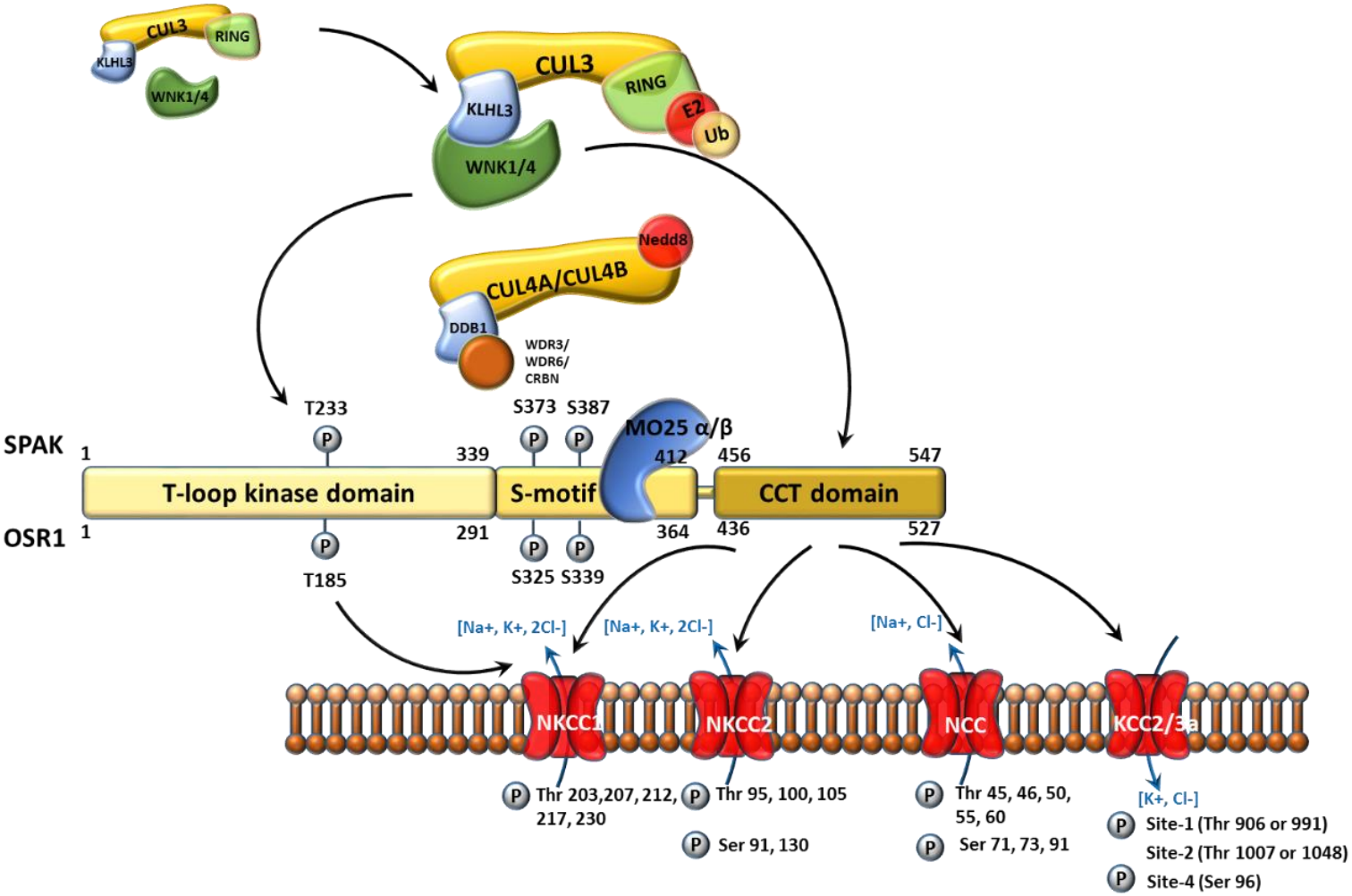

Figure 1.1. (Continued on the following page)

Figure 1.1. A schematic representation of the WNK-SPAK/OSR1 signalling pathway. Active WNK kinases phosphorylate SPAK and OSR1 in multiple sites; T233 of SPAK or T185 of OSR1 in the T-loop kinase domain; S373 and S387 of SPAK or S325 and S339 of OSR1 in the S-motif domain. The phosphorylation of SPAK and OSR1 leads to further phosphorylation and activation of a series of ion cotransporters protein; NKCC1 (Thr203, 207, 2112, 217 and 230), NKCC2 (Thr95, 100 and 105, Ser91 and 130), NCC (Thr 45, 46, 50, 55 and 60, Ser71, 73 and 91) and KCC2/3a (Thr906 or 991, Thr 1007 or 1048, and, Ser96) which affecting cellular ion homeostasis. The activity of SPAK/OSR1 is enhanced by the binding of MO25 protein via CCT domain. E3 ubiquitin ligases, which play a role in this signalling pathway, are shown; CUL3/KLHL3, and CRL4 complex, which is proposed in this study. The figure is adapted and modified from (Alessi *et al.*, 2014). WNK, with-no-lysine kinase; SPAK, Ste-20 proline/alanine-rich kinase; OSR1, oxidative stress response 1; T/Thr, threonine; T-loop, threonine-loop; S/Ser, serine; S-motif, serine-motif; NKCC, Na^+- K^+- Cl^- cotransporter; NCC, Na^+- Cl^- cotransporter; KCC, K^+- Cl^- cotransporter; MO25, mouse protein-25; CCT, conserved carboxy-terminal; CUL, cullin; KLHL3, Kelch-like family member 3; CRL4, cullin ring ligase 4.

1.1.1. Regulation of WNK-SPAK/OSR1 signalling pathway by cellular ion concentration

Cellular ion concentration regulates WNK-SPAK/OSR1 pathway mainly through cellular chloride and potassium concentrations. Chloride ion exporting, which lowers the amount of intracellular chloride and eventually cause cell shrinkage, increases the activity of NCC, NKCC1, and NKCC2 but inhibit KCCs (Gagnon *et al.*, 2006, Pacheco-Alvarez *et al.*, 2006). Reciprocally, Cl^- importing, which causes cell swelling by Cl^- accumulation inside the cell, inhibit NKCCs and promote KCCs activity (Gagnon *et al.*, 2006).

The chloride-binding pocket in the catalytic domain of WNK1 kinase, which is established by Leu369 and Leu371 in the Aspartic Acid - Leucine - Glycine (DLG) motif, affect the activity of WNK kinases (**Figure 1.2.**) (Piala *et al.*, 2014). The binding of Cl^- prevents WNK1 autophosphorylation. Thus, the increased level of intracellular Cl^- lowers the level of WNK1 autophosphorylation (Piala *et al.*, 2014). The low Cl^- concentration/hypotonic stress exposure promotes WNK1 autophosphorylation (Zagórska *et al.*, 2007), leading to its activation and phosphorylation of its substrates, SPAK and OSR1 kinases (Moriguchi *et al.*, 2005). The WNK1 Cl^- binding pocket is conserved across the four WNK isoforms, and thus the activation of these kinases

and their downstream signalling are regulated by intracellular Cl^- concentration with the WNK4 isoform being the most sensitive (Hadchouel *et al.*, 2016, Murthy *et al.*, 2017).

The WNK-SPAK/OSR1 signalling is also regulated by extracellular K^+ concentrations (**Figure 1.3.**). In the distal convoluted tubules (DCT) cells, the level of phospho-NCC and phospho-SPAK were directly affected by the concentration of K^+ outside cells. Low extracellular K^+ concentrations increase the phosphorylation and activation of SPAK and NCC (Naito *et al.*, 2010). The presence of chloride sensor in WNKs could explain the effect of extracellular K^+ concentration to NCC function via the changes of intracellular Cl^- concentration. The mutation in the chloride sensor motifs of WNKs was found to trigger increased levels of phospho-WNK in HEK293 cells even though no chloride could bind WNKs and inhibit their autophosphorylation (Hadchouel *et al.*, 2016, Murthy *et al.*, 2017).

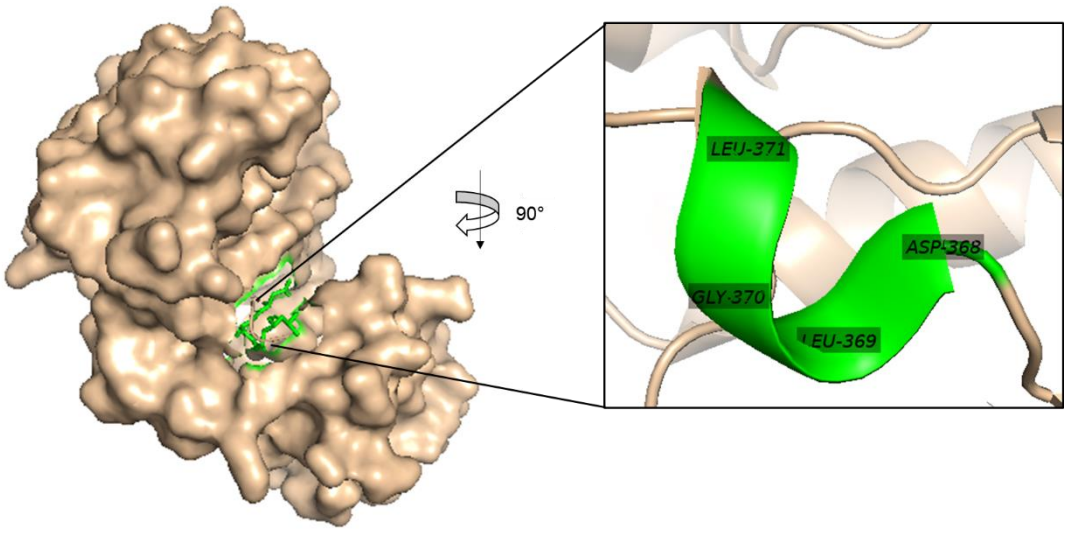

Figure 1.2. Chloride binding pocket in WNK1. Crystal structure of WNK1 (PDB ID:4PWN) showing the chloride binding pocket in its DLGL motif (coloured in green). The Cl^- binding pocket lies on conserved Leu369 and Leu371 residue of WNK kinases (Piala *et al.*, 2014). The structure was visualised using PyMOL software. WNK1, with-no-lysine kinase 1; LEU/Leu, leucine; GLY, glycine; ASP, Aspartic Acid; DLGL, aspartic acid-leucine-glycine-leucine.

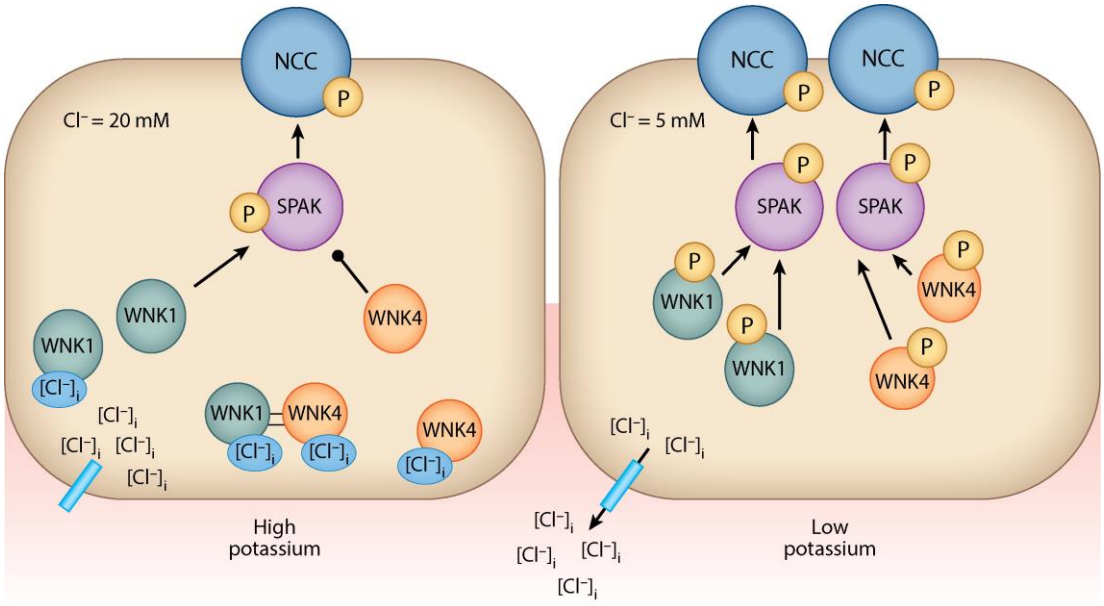

Figure 1.3. Mechanism of WNK-SPAK-NCC regulation by intracellular Cl^- and extracellular K^+ concentration. When the extracellular K^+ concentration is at normal-high, the intracellular Cl^- concentration is at around 20 mM. In this condition, WNKs autophosphorylation is inhibited due to chloride binding to the WNKs. Decreasing extracellular K^+ concentration depolarises the cells and stimulates chloride export, thus decreasing intracellular Cl^- concentration. This condition promotes the WNKs phosphorylation and activity, thus phosphorylate and activates more SPAK, which eventually increased phosphorylation and activation of NCCs (Hadchouel *et al.*, 2016, Murthy *et al.*, 2017). SPAK, Ste-20 proline/alanine-rich kinase; NCC, Na^+- Cl^- cotransporter; WNK, with-no-lysine kinase.

1.1.2. Human ion homeostasis-related diseases

Imbalances in cellular ion concentrations could cause diseases in humans (Richardson and Alessi, 2008, Glover *et al.*, 2011, Vitvitsky *et al.*, 2012). For instance, electrolyte dysregulation, particularly in Na^+, K^+, and Cl^- levels, has been reported to cause hypertension and various neurological disorders (Glykys *et al.*, 2017, Murthy *et al.*, 2017)

The link between the WNK-SPAK/OSR1 signalling proteins with hypertension and neurological disorders was initially determined from several patients who had a genetic mutation in their CCCs protein (Simon *et al.*, 1996a, Simon *et al.*, 1996b, Howard *et al.*, 2002). For instance, Gitelman Syndrome (a mirror of Gordon's syndrome) and Bartter Syndrome, in which patients are characterised by having

hypotension and hypokalemic alkalosis, are caused by loss-of-function mutations in NCC and NKCC2 (Simon *et al.*, 1996a, Simon *et al.*, 1996b). Additionally, lack of KCC3 function in neurons in the development phase causes Andermann Syndrome (Howard *et al.*, 2002). Patients with Andermann Syndrome show the absence or malformation of connecting tissue between the left and right halves of the brain (agenesis of the corpus callosum) (Howard *et al.*, 2002).

1.1.2.1. Hypertension and WNK-SPAK/OSR1 pathway

It is estimated that one billion people worldwide have elevated blood pressure (hypertension). As one of the leading causes of cardiovascular diseases, hypertension is a global problem that causes ten million deaths annually (NCD-RFC, 2016).

As mentioned above, there are genetic evidences in humans that links the WNK-SPAK/OSR1 pathway to the regulation of blood pressure by mediating the activation of NCC and NKCC2 in the kidney (Wilson *et al.*, 2001). The NCC and NKCC2 activation are responsible for renal salt reabsorption, which is essential for maintaining cell volume, thus affecting blood pressure and electrolyte homeostasis (Vitari *et al.*, 2005, Richardson *et al.*, 2008).

There are several studies on the proteins upstream of the WNK kinases, which play a role in the regulation of blood pressure. Loss-of-function mutations in CUL3-KLHL3 and KLHL3 degron-binding site causes an increase in blood pressure through an increased abundance of WNK1 and WNK4 kinases as a result of a reduction in their proteasomal degradation (Boyden *et al.*, 2012, Louis-Dit-Picard *et al.*, 2012, Yoshida *et al.*, 2018). This CUL3/KLHL3 interaction leads to the ubiquitination (Ohta *et al.*, 2013) and degradation of WNK isoforms, which regulate electrolyte homeostasis and cause hypertension (Shibata *et al.*, 2013).

Using mouse models of human PHAII, gain-of-function mutation of WNK1 and WNK4, also resulted in hypertension as phosphorylation and activity of NCC and NKCC2 was increased (Vidal-Petiot *et al.*, 2013, Takahashi *et al.*, 2014). Also, in SPAK knockout and SPAK or OSR1 knock-in mice, reduction of NCC or and NKCC2 activation by phosphorylation resulted in hypotension (Rafiqi *et al.*, 2010, Yang *et al.*, 2010, Chiga *et al.*, 2011).

A more recent review specifically discussed the molecular mechanisms of WNK-regulated blood pressure and the various WNK-SPAK/OSR1 mouse models and their impact on blood pressure (Murthy *et al.*, 2017). For instance, the import of Cl^- into smooth muscle generally depolarises the membrane potential and results in smooth muscle contraction (Chipperfield and Harper, 2000). Vascular smooth muscle contraction increases the vascular resistance caused by the reduced vascular diameter, so the higher blood pressure is occurred (Touyz *et al.*, 2018). NKCC1, which is the only NCC expressed in the aorta when the mice were NKCC1 double allele knocked-out, the blood pressure of the mice was lower than wild-type controls (Meyer *et al.*, 2002). Confirmation of SPAK involvement in the lowering blood pressure was exhibited by the reduced aortic phospho-NKCC1 in SPAK knock-out mice that had low blood pressure (Zeniya *et al.*, 2013).

WNK-SPAK/OSR1 signalling was shown to be associated with cardiac physiology, which could affect blood pressure. WNK and OSR1 regulate the IRK (Inward Rectifier K^+) channels, Kir2.1 and Kir2.3 (Taylor *et al.*, 2018). IRK channels are cardiomyocytes proteins which control vital processes including the circulatory system, vasculature and neuronal excitability. Active OSR1 increased the Kir2.1 and Kir2.3 channel activity by increasing their current density in the whole-cell patch-clamp experiments, which trigger the cardiac action potential (Taylor *et al.*, 2018). The cardiac action potential regulates the opening of sodium channels, thus affecting the cellular Na^+ transport and later regulate the circulatory system (Taylor *et al.*, 2018).

1.1.2.2. Neurological disorders and WNK-SPAK/OSR1 pathway

Neurological disorders are the second leading cause of death (up to 9 million) and the leading cause of disabilities (276 million) worldwide (Feigin *et al.*, 2019). This number was reported from systematic analysis about the burden of neurological studies between 1990-2016, which included 195 countries of 15 neurological disorders (Feigin *et al.*, 2019). These 15 neurological disorders are tetanus, meningitis, encephalitis, stroke, brain and other cancers related to central nervous system, traumatic brain injury, spinal cord injury, Alzheimer's disease and other dementias, Parkinson's disease, multiple sclerosis, motor neuron diseases, idiopathic epilepsy, migraine, tension-type headache, and a residual category for other less common neurological disorders). Among these neurological disorders, stroke was the most significant contributor to neurological disability (Feigin *et al.*, 2019).

Ion co-transporters are associated with the pathophysiology of neurological disorders. CCCs play a role as a counter-response when the intra and extra-cellular osmolarity of the neurons is changed as a result of several pathological conditions, e.g. stroke, ischemia, and brain trauma, which induce changes in cytoplasmic volume (Glykys *et al.*, 2017). In response to neuron shrinkage, changes in the Regulatory Volume Increase (RVI) occur, and the Regulatory Volume Decrease (RVD) mechanisms are activated in response to swelling (Glykys *et al.*, 2017). RVI counters the cell shrinkage when there are water and solute loss from neurons by the activation of NKCC1 to trigger Na^+, K^+, and Cl^- accumulation in the neurons. On the other hand, RVD promotes cytoplasmic K^+, and Cl^- loss as a response to acute cell swelling through the activation of KCCs (Glykys *et al.*, 2017, Huang *et al.*, 2019).

A ligand-gated Cl^- -permeable, GABA receptors, are regulated by CCCs activity (Kahle *et al.*, 2009). Activation of GABA receptor triggers milliseconds hyperpolarisation of the neuron, thus inhibits neurotransmitter in the adult central neuron system (Dzhala *et al.*, 2005). The increase of KCC2 activity to export Cl^-

relative to NKCC1 activity to import Cl^-, lowers the Cl^- concentration in the neurons to the level which promotes GABA receptor-mediated hyperpolarisation, so the neurotransmission is inhibited. The pathogenesis of several human neurological disorders, such as epilepsy, autism, neuropathic pain from peripheral nerve injury and post-traumatic spasticity, have been associated with KCC2 and NKCC1 activity (Kahle *et al.*, 2009). KCC2 down-regulation and NKCC1 up-regulation, which promotes the increase of Cl^- concentration in the neurons, facilitate GABA receptors-mediated depolarisation (Kahle *et al.*, 2009).

1.2. PROTEINS INVOLVED IN WNK-SPAK/OSR1 SIGNALLING PATHWAY

1.2.1. With No K (lysine) protein kinases (WNKs) protein

WNK kinases have a unique branch within the families of human kinome (**Figure 1.4.**) (Manning *et al.*, 2002). WNK kinases are serine/threonine-protein kinase. They are structurally related to Sterile-20 (Ste-20) kinases, *e.g.* SPAK and OSR1, and possess ~30% sequence identity (Dan *et al.*, 2001).

The first identified WNK gene was the WNK1 gene from cDNA library of rat brain (Moore *et al.*, 2000, Xu *et al.*, 2000). Within the human genome, there are three other kinase genes, which share the same domain structure as WNK1; WNK2, WNK3 and WNK4. They share more than 95% sequence identity in their catalytic domain (Cope *et al.*, 2005) (**Figure 1.5.**), an autoinhibitory region, protein interaction motifs in their regulatory domain and tissue-specific expression in the heart and kidney (Xu *et al.*, 2000, Wilson *et al.*, 2001, Delaloy *et al.*, 2003).

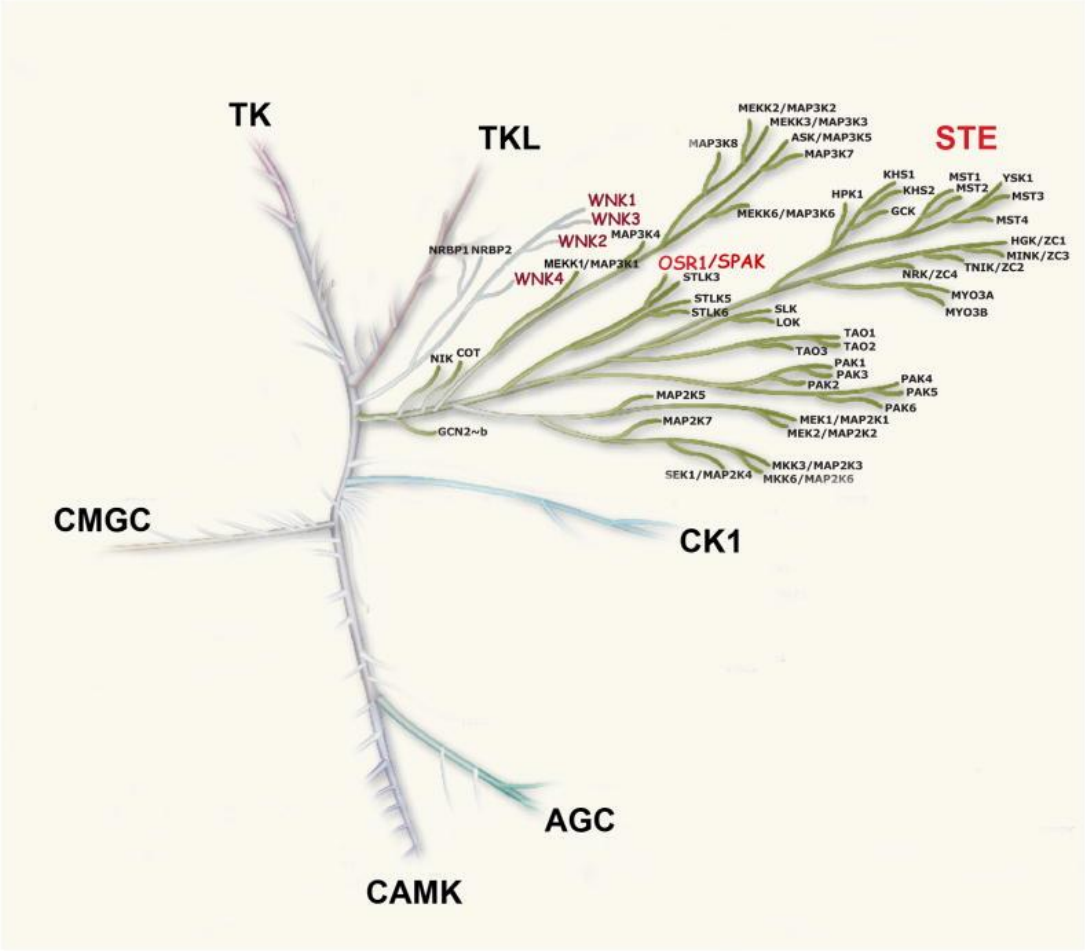

Figure 1.4. Phylogenetic tree of major families human kinome. SPAK and OSR1 belong to STE kinase family and closely related to WNKs. The figure is retrieved from (McCormick and Ellison, 2011). CMGC, cyclin-dependent kinases mitogen-activated protein kinases glycogen synthase kinases and CDK-like kinases; CAMK, Ca^{2+} /calmodulin-dependent kinases; AGC, protein kinase A, G, and C families; CK1, casein kinase 1; TK, tyrosine kinase; TKL, tyrosine kinase-like; STE, serine/threonine kinases.

Unlike the typical kinases, which have catalytic lysine residue in subdomain II (position 250 in WNK1), WNK kinases possessed cysteine in this residue (Xu *et al.*, 2000). The lysine residue (K233 in WNK1) is conserved across the WNKs. Mutation in lysine residue (K233A) vanished WNK kinase activity, and mutation on C250 failed to restore it (Xu *et al.*, 2000). Autophosphorylation of WNKs occurs in two Serine residues within the activation loop (S378 and S382). This autophosphorylation site directly affects WNK1 kinase activity since WNK1 mutations in this residue resulted in the loss of kinase activity (Xu *et al.*, 2002).

WNK function was unknown until it was identified the mutation in WNK1 and WNK4 in PHAII patients (Wilson *et al.*, 2001). It was later found that the PHAII patients carried WNK4 mutation different from the mutation in WNK1. In PHAII patients, WNK1 mutations are large deletions of the first intron that result in the increased of mRNA of WNK1 (Vidal-Petiot *et al.*, 2013), whereas mutations in WNK4 are missense mutations that are clustered in the highly conserved acidic motif (Na *et al.*, 2013).

Despite its high sequence homology, WNK kinases exhibit functional diversity related to their capability to control and regulates ion transporters and their role in MAPK signalling, including the cell cycle, apoptosis, and cell proliferation (McCormick and Ellison, 2011). Gordon's syndrome was identified in families with WNK1 and WNK4 mutation (Wilson *et al.*, 2001). Both kinases are known to play a key role in the homeostasis of electrolytes (Kahle *et al.*, 2003, Moriguchi *et al.*, 2005, Vitari *et al.*, 2005, Takahashi *et al.*, 2014). The link between WNKs and hypertension was also reported via two ubiquitin E3 ligase, Kelch-like 3 (KLHL3) and Cullin 3 (Boyden *et al.*, 2012, Louis-Dit-Picard *et al.*, 2012).

Physiological function WNK2 and WNK3 are less studied compare to WNK1 and WNK4. However, to date, it is known that WNK2 kinase regulates the cation-chloride cotransporters in the mammalian brain through its activation, via phosphorylation, of NKCC1 (Rinehart *et al.*, 2011). Protein kinase WNK2 inhibits cell proliferation by negatively modulating the activation of MEK1/ERK1/2 (Moniz *et al.*, 2007). As regulatory kinases of NKCC1, WNK3 has been implicated in reducing ischemia (Begum *et al.*, 2015).

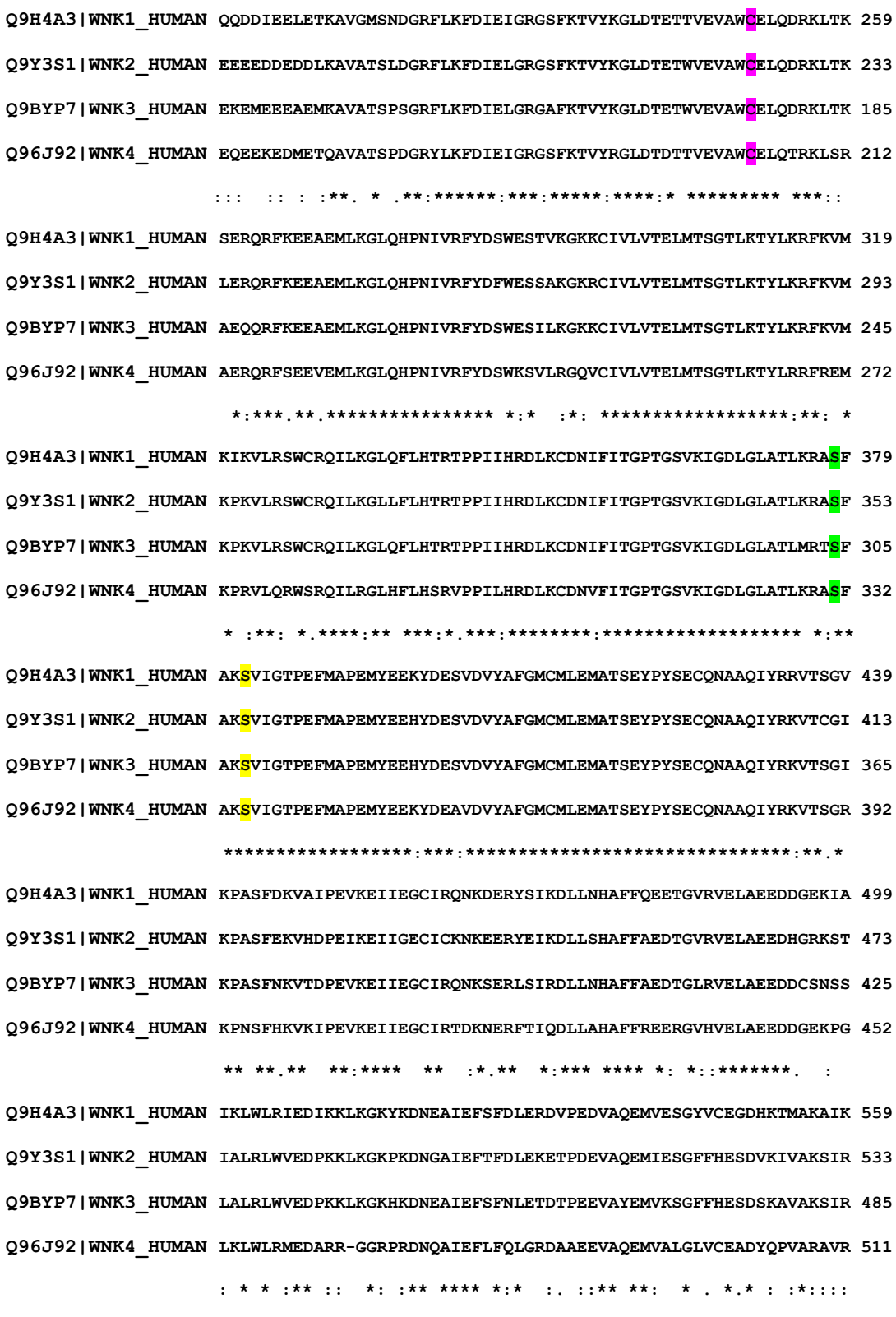

Figure 1.5. Multiple alignments of highly conserved kinase domain sequence of human WNKs. 'C' in purple highlight is C250 residue, a unique feature of WNKs as a protein kinase. Serine residues (S378 and S382) in the activation loop where WNK autophosphorylation occurs, are highlighted in lime and yellow, respectively. An asterisk indicates identical residues, double dotted line indicates the non-similarity region. The sequences are retrieved from https://www.uniprot.org.

1.2.2. SPAK and OSR1 protein kinases

1.2.2.1. SPAK and OSR1 proteins are members of the Ste20 family of protein kinases

Germinal Center Kinases (GCKs) form one of the groups of Ste20 family of protein kinases, which has 5' or amino-terminal catalytic domain (Gagnon and Delpire, 2012). Another group of Ste20 family kinase is p21 activated kinases (PAKs), which had 3' or carboxyl-terminal catalytic domain (Gagnon and Delpire, 2012). Eight subgroups of GCKs are grouped based on their localisation, structure and function and named GCK-I to GCK-VIII (**Figure 1.6.**) (Gagnon and Delpire, 2012). SPAK and OSR1 kinases are members of the GCK-VI subfamily. Mst proteins (Mst3/Mst4), which were reported to be regulated by MO25 (Filippi *et al.*, 2011), are grouped as GCK-III.

Beside SPAK and OSR1, there are two other members of the GCK-VI subgroup, STRADα and STRADβ. They share 90% sequence identity with SPAK and OSR1 catalytic domain, even though several important key residues are not present (Gagnon and Delpire, 2012). Originally, it was proved that STRAD interacted with LKB1 (Boudeau *et al.*, 2003). This interaction stabilises the activation loop of LKB1, which then induces a conformational change that allows substrate binding. STRAD in complex with MO25 and LKB1 form a protein complex that is an upstream regulator of AMP kinases (Zeqiraj *et al.*, 2009).

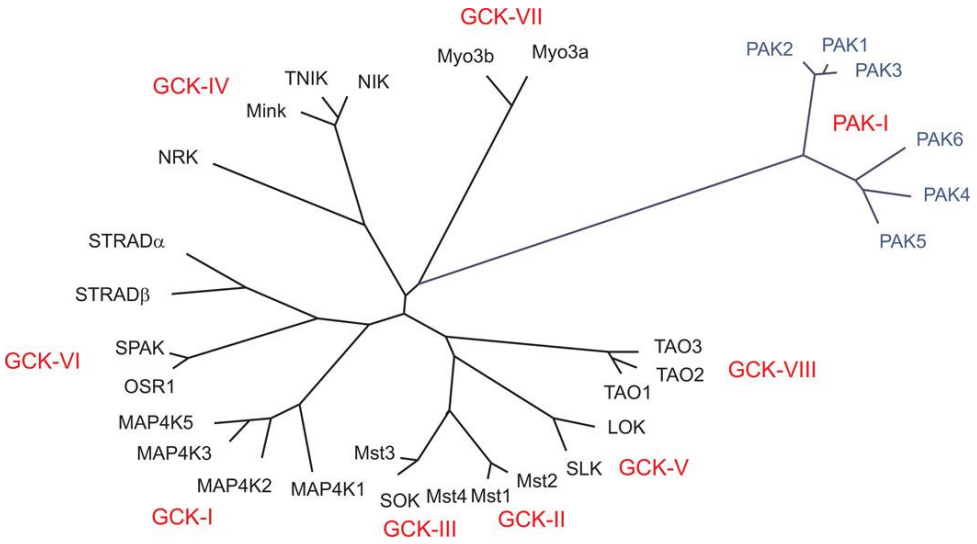

Figure 1.6. Cluster dendrogram of mammalian Ste20 kinase. SPAK and OSR1 are a member of GCK-VI within Ste20 kinase family. STRADs protein as members of other subgroups in GCK-VI (Gagnon and Delpire, 2012). SPAK, ste-20/SPS1-related proline alanine kinase; OSR1, oxidative stress response 1; GCK, germinal center kinase; STRAD, ste20-related kinase adapter protein; PAK, p21-activated kinase.

1.2.2.2. Molecular and functional characters of SPAK and OSR1 proteins and their tissue distribution

SPAK was initially identified from the immunoblotting using poly (ADP-ribose) polymerase (PARP) of rat brain tissue lysate. It was identified as a protein with molecular weight (MW) 66 kDa and comprised of 553 amino acid. SPAK was at first referred to PASK (proline-alanine-rich Ste20-related kinase) because of its unique proline-alanine (PAPA box) in its N-terminus (Ushiro *et al.*, 1998). Later, it was known that this PAPA box differentiates SPAK from OSR1 (Tamari *et al.*, 1999). A year later, OSR1, which encoded 527 amino acid protein with MW 58 kDa, were mapped with 39% sequence homology to human Ste-20/oxidant stress response kinase-1 or SOK1 (Tamari *et al.*, 1999).

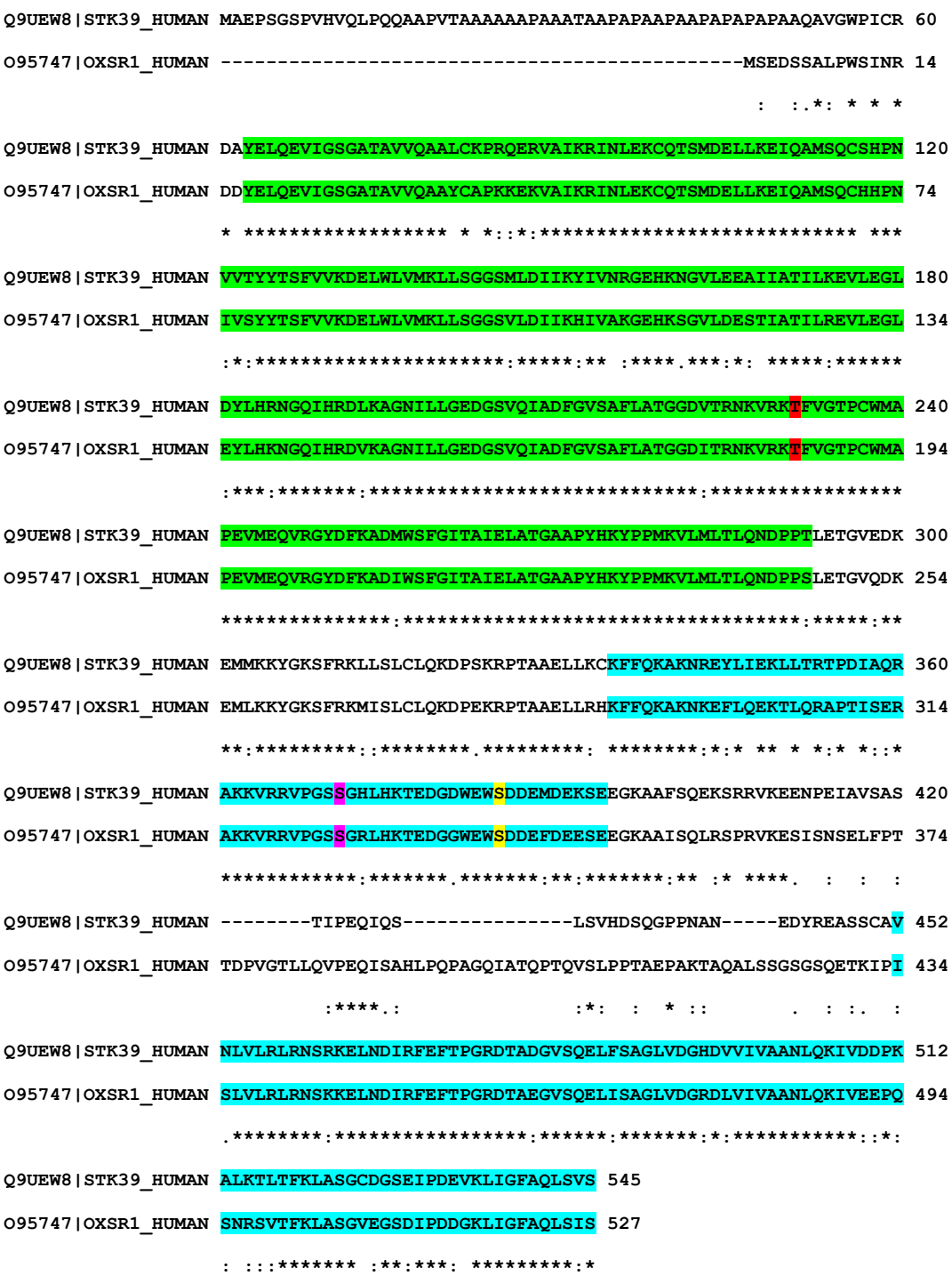

Figure 1.7. **Sequence homologies between SPAK (STK39) and OSR1 (OXSR1)**. Indicated region are kinase domain showed by light green highlight, an asterisk indicates identical residues, double dotted line indicates the non-similarity region of SPAK and OSR1. T in red highlight is marked threonine residue (T185 of OSR1) phosphorylated by WNKs, purple highlighted S (S325 OSR1) and yellow highlighted S (S339 OSR1) showing non-catalytic serine residue phosphorylated by WNKs, and tosca colour highlight indicates PF1 and PF2 region.

SPAK and OSR1 share 65-67% sequence identity, with higher sequence identity found in the catalytic domain (89%) (Piechotta *et al.*, 2002, Chen *et al.*, 2004). Furthermore, two regions of similarity were also found in the regulatory domains, namely the PF1 and PF2 domain (PF stands for PASK and Fray, the Drosophila homolog) (Leiserson *et al.*, 2000). PF1 domain is located immediately after the catalytic kinase domain, and PF2 domain is in the terminal 90-amino acid residues of the *C*-terminal (Chen *et al.*, 2004).

The catalytic domain of SPAK (63-292) and OSR1 (17-245) kinases lies at the *N*-terminal domain, while the regulatory domains, the PF1 (291-344 in OSR1) and PF2 (434-527 in OSR1), at the *C*-terminal domain (**Figure 1.7.**). The PF1 domain is required for enzyme activity (Chen *et al.*, 2004), whereas the PF2 domain contains the RFx[V/I] tetrapeptide motifs, which mediate the binding to these kinases down- and upstream protein binders (Piechotta *et al.*, 2003). Notably, the PF2 does not seem to be unique to SPAK and OSR1 kinases as WNK kinases also possess a PF2 domain (Delpire and Gagnon, 2008). Unlike in SPAK and OSR1, however, the PF2 domain in WNK kinases (PF2-like) is located in their catalytic domain. This domain was also shown to bind RFx[V/I] domains (Delpire and Gagnon, 2008) (**Figure 1.8.**).

The interaction between SPAK and OSR1 kinases with mouse KCC3 and NKCCs was identified initially via yeast-two-hybrid with alanine scanning mutagenesis (Piechotta *et al.*, 2002). There was a vital 9-amino acid region (RFQVTPTKI), which contained the RFx[V/I] motif, which fitted into the pocket of PF2 domain of SPAK (Piechotta *et al.*, 2002). Additionally, WNK2, WNK4, gelsolin, apoptotic–associated tyrosine kinase (AATYK), heat shock protein (HSP) 105 and otoferlin were also found to bind SPAK *C*-terminal domain in yeast two-hybrid system (Gagnon and Delpire, 2012). SPAK as WNK1 interactor was identified by another approach, *i.e.* immunoprecipitations followed by mass spectrometry analysis (Moriguchi *et al.*, 2005, Vitari *et al.*, 2005).

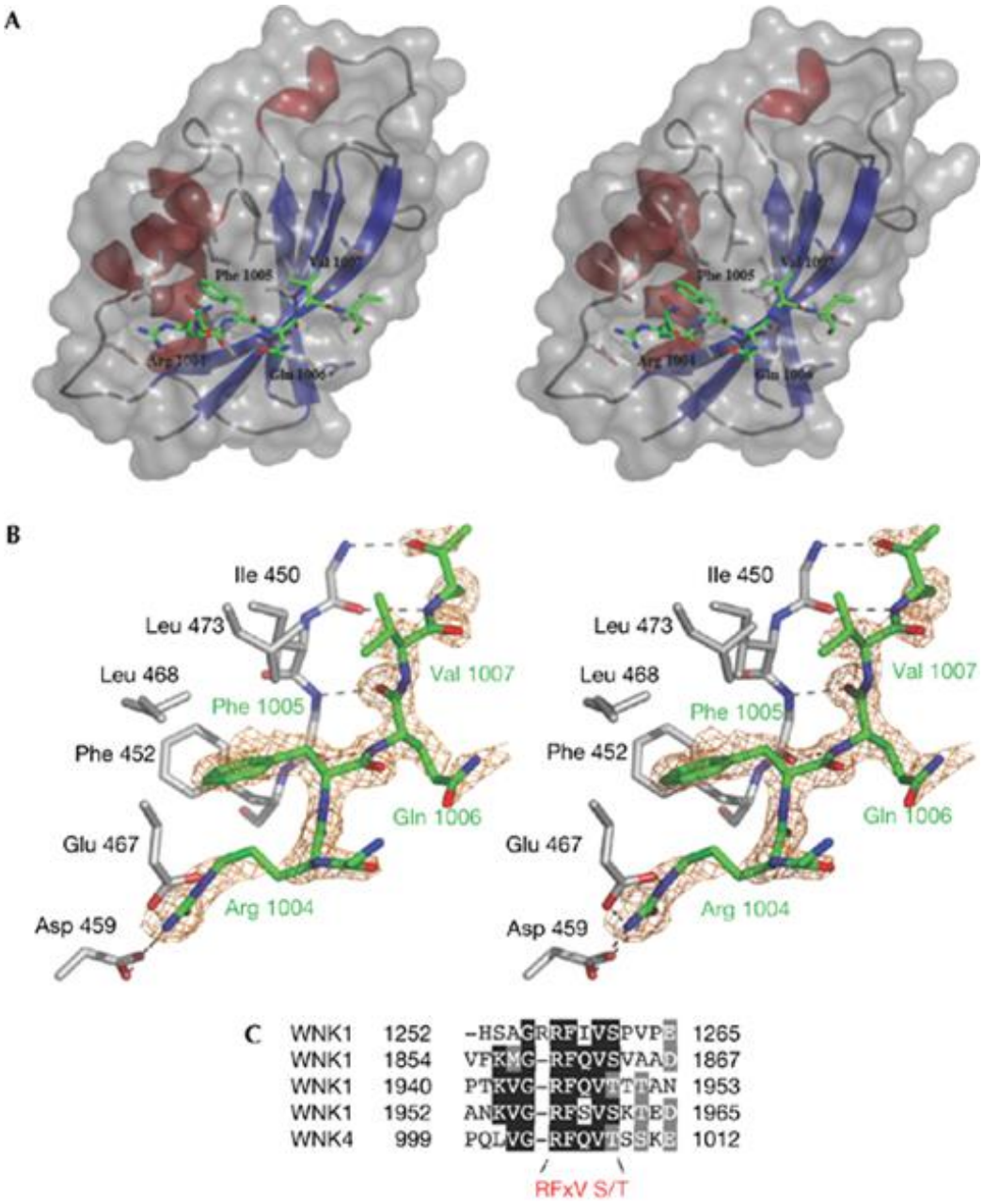

Figure 1.8. Interaction of RFXV peptide with OSR1 CCT domain in the molecular level. A. 3D view of OSR1 CCT domain (residue 434-527) (blue β-strand and red α-helices) in complex with GRFQVT from WNK4 (green). B. Stick representation on the interaction of residue of CCT OSR1 (grey) with the GRFQVT peptide (green). C. Multiple sequence alignment of RFXV motif in WNKs (Villa *et al.*, 2007). RFXV, arginine-phenylalanine-any amino acids-valine; OSR1, oxidative stress response 1; CCT, conserved carboxyl-terminal; GRFQVT, glycine-arginine-phenylalanine-glutamine-valine-threonine.

The SPAK and OSR1 proteins are expressed in various tissues. Northern and Western blotting revealed that SPAK is distributed in rat brain, salivary glands, thymus, heart, lung, spleen, liver, stomach, small intestine, large intestine, adrenal

gland, kidney, testis, epididymis, skeletal muscle, ovary and uterus (Ushiro *et al.*, 1998). In lung, kidney, heart, liver, spleen, skeletal muscle, small intestine, and testis, OSR1 is expressed in mRNA and protein level (Tamari *et al.*, 1999, Chen *et al.*, 2004). SPAK and OSR1 were also found in the white and grey matter in the spinal cord and co-expressed in Node of Ranvier with NKCC1, even though OSR1 expression was lower than SPAK (Piechotta *et al.*, 2003). Kidney-specific NKCC2 and NCC were found to be colocalised with both SPAK and OSR1 in the thick ascending limb of Henle (TAL) and distal convoluted tubule (DCT), respectively (Lin *et al.*, 2011, McCormick *et al.*, 2011).

1.3. SMALL MOLECULE INHIBITORS OF WNK-SPAK/OSR1 SIGNALLING PATHWAY

There are four molecular targets that have been explored in discovering WNK-SPAK/OSR1 signalling inhibitors (AlAmri *et al.*, 2017b). These are 1) WNK kinases, 2) the binding of WNK to SPAK and OSR1 kinases, 3) SPAK and OSR1 kinases, and 4) the binding of SPAK and OSR1 to MO25 (**Figure 1.10.**). Herein, the small molecules that have been discovered to date as inhibitors of WNK-SPAK/OSR1 are discussed.

a. WNK463

WNK463 is the first reported ATP-competitive WNK kinase inhibitor (Yamada *et al.*, 2016). The discovery of this inhibitor utilised the unique structural characteristic of WNKs compare to the structure of common protein kinases, which has catalytic lysine residue (Lys233) within their ATP binding site. This catalytic Lys233 is absent in WNK1 and occupied by cysteine residue (Cys250). The presence of Cys250 in WNK1, instead of Lys233, result in the availability of a large cavity in the back of the ATP-binding site nearby the Cys250 of WNK1 (Min *et al.*, 2004) (**Figure 1.9.**). Thus,

this characteristic was exploited for the discovery of WNK1 ATP-binding site-specific inhibitors (Yamada *et al.*, 2016).

WNK463 molecule inhibited the four WNK isoforms in the nanomolar range (Yamada *et al.*, 2016). In HEK293 cells, WNK463 was found to be a potent inhibitor of WNK kinases IC_{50} = 106 nM. *In vivo* studies showed that WK463 decreased blood pressure in spontaneous hypertensive mice and analysis of protein lysates from the kidneys showed decreased phosphorylation of WNK kinase substrates, SPAK and OSR1 (Yamada *et al.*, 2016). Unfortunately, the development of this molecule to treat hypertension was halted due to pre-clinical safety issues (AlAmri *et al.*, 2017b).

A.

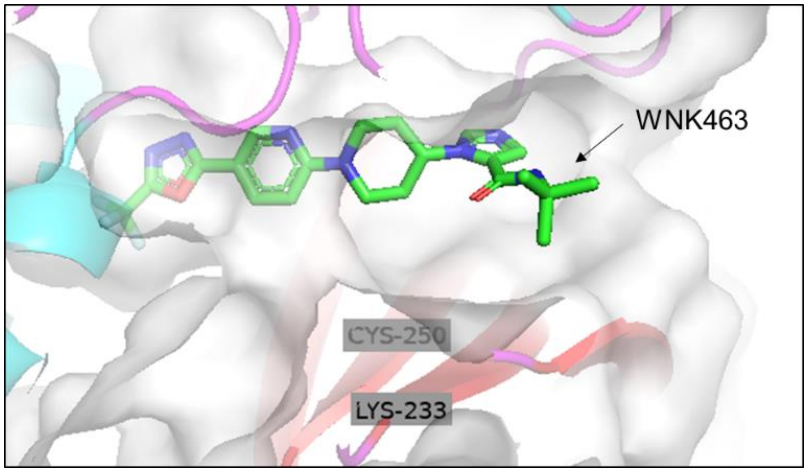

B.

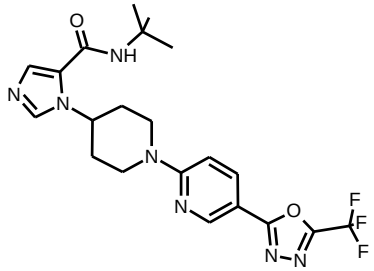

Figure 1.9. Co-crystal structure of WNK1 kinase domain and WNK kinase inhibitor WNK463 (PDB ID: 5DRB). A. The WNK463 structure (as cartoon shown in green) is shown bind to the large cavity at the back of Cys250 residue in WNK1. The catalytic lysine residue Lys233 of WNK1 is also shown. The 3D structure visualisation was performed using PyMol software. B. The chemical structure of WNK463 was drawn using ChemSketch program. WNK1, with-no-lysine kinase 1; Cys, cysteine; Lys, Lysine.

b. STOCK1S-50699

The first inhibitor of WNK kinases binding to SPAK and OSR1 kinases was STOCK 1S-50699. This molecule was discovered by high-throughput screening of 17,000 compounds (Mori *et al.*, 2013). This high-throughput screening utilised the labelling of the RFQV peptide with a fluorophore and measured the binding of tested compounds to GST-tagged SPAK *C*-terminal domain. STOCK1S-50699 was found to inhibit WNK-SPAK/OSR1 phosphorylation of the NKCC1 at low micromolar concentrations. Screening this molecule against a panel of 150 protein kinases showed that it has good selectivity. Subsequently, this molecule was also found to inhibit SPAK and OSR1 kinases, independent of WNK kinases, via the binding to a highly conserved pocket in the *C*-terminal domain of SPAK and OSR1 kinases (Mori *et al.*, 2013).

c. Closantel

Using a cell-screening method, closantel was found to be a specific SPAK inhibitor with low micromolar potency (Kikuchi *et al.*, 2015). The inhibition of total and phosphorylated NCC was achieved by this molecule in a dose-dependent manner in two different cell lines. The administration of closantel in mice promoted a reduction in blood pressure and heart rate in a short time, which was suggested this outcome was not caused by cation imbalance but vasodilation (Kikuchi *et al.*, 2015). It was also exhibited that the phosphorylation of NCC in the kidney and of NKCC1 in the aorta was reduced in the mice treated with closantel (Kikuchi *et al.*, 2015). Subsequently, the anti-parasitic agent Rafoxanide, which is structurally related to closantel, was found to inhibit OSR1 by binding to an allosteric *C*-terminal pocket of OSR1 (AlAmri *et al.*, 2017a).

d. HK01

The discovery of small molecules that inhibit the interaction between SPAK and OSR1 with MO25 was initiated by Mehellou group (Cardiff, UK). The driver for this approach was the previous finding that SPAK and OSR1 kinase activity increased by up to 100-fold upon binding to MO25 (Filippi *et al.*, 2011). Using a high throughput screening assay, HK01 exhibited inhibition of SPAK and OSR1 binding to MO25 (Kadri *et al.*, 2017). Despite its promise, HK01 lacked potency (IC_{50} = 78 μM) to be developed further as an indirect SPAK and OSR1 kinases inhibitor (Kadri *et al.*, 2017).

e. Verteporfin

The photosensitising agent, Verteporfin, was reported to bind the kinase domain of SPAK and OSR1 and inhibit their catalytic activity (AlAmri *et al.*, 2018). This discovery was made following a high-throughput screening assay that utilised 1,200 compounds from the FDA-approved library of compounds. The inhibition of SPAK and OSR1 kinases by verteporfin led to reduced phosphorylation of NKCC1 in HEK293 cells (AlAmri *et al.*, 2018).

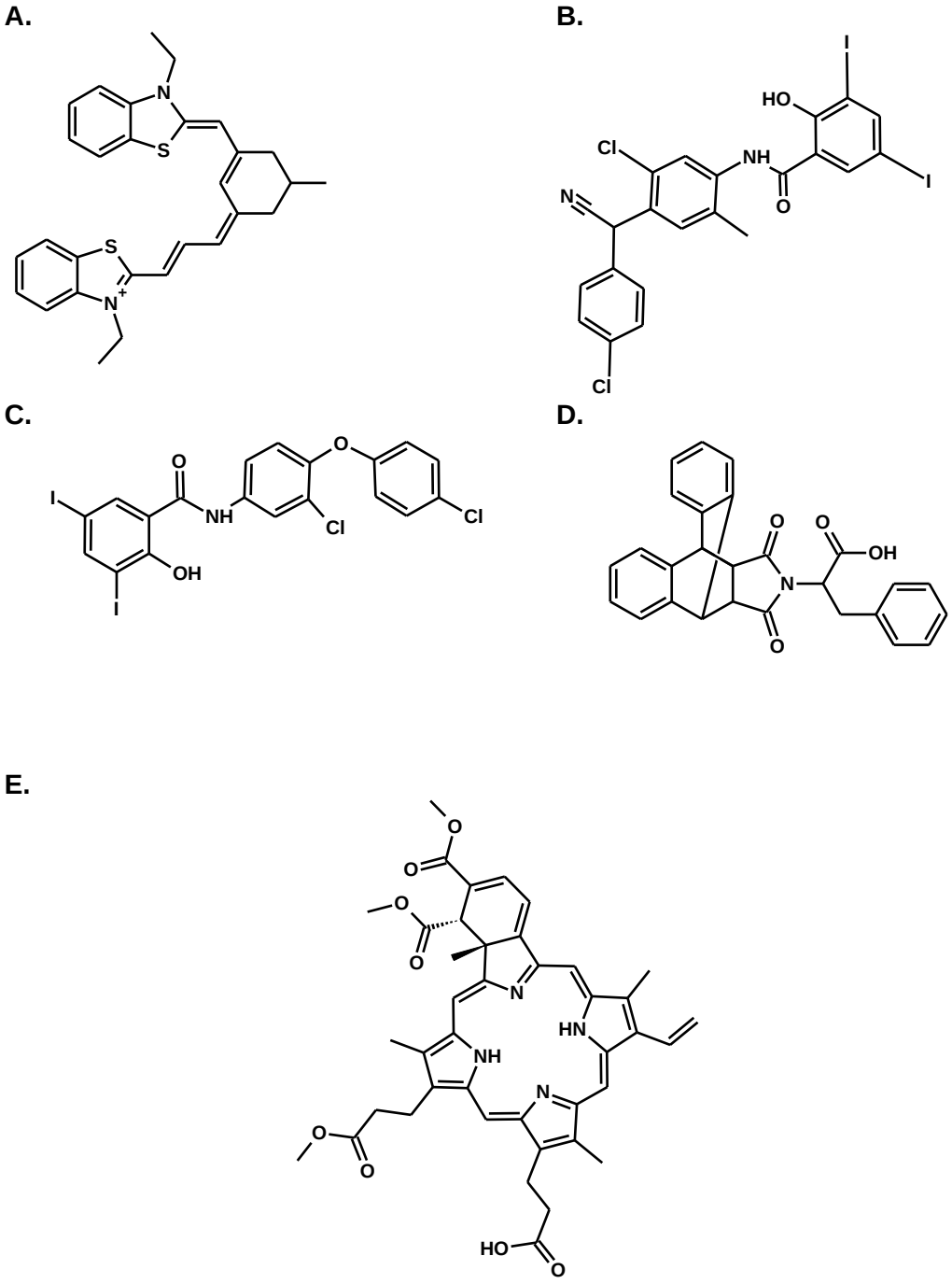

Figure 1.10. Chemical structure of small molecule inhibitors of WNK-SPAK/OSR1 signalling. A. STOCK 1S-50699 (WNK to SPAK and OSR1 binding inhibitor, B. Inhibitor of SPAK and OSR1 kinase activity, Closantel, and C. Rafoxanide, D. Binding inhibitor of SPAK and OSR1 to MO25, HK01, E. Verteporfin, a SPAK and OSR1 inhibitor.

1.4. PROTEIN UBIQUITYLATION

Protein degradation is an important process for the cell, as this event regulates diverse cellular processes (Petroski and Deshaies, 2005). Among the primary protein degradation strategies is the ubiquitin-mediated proteolytic pathway. Ubiquitin is a small protein (ca. 8 kDa) that is made up of 76 amino acids (Bosu and Kipreos, 2008).

The ubiquitylation (or also referred to ubiquitination) cascade starts with the binding of ubiquitin to an E1 enzyme in the presence of ATP-Mg^{+2}, and this then catalyses ubiquitin *C*-terminal acyl adenylation at glycine residue (Hershko *et al.*, 1983). A catalytic cysteine on the E1 enzyme then attacks the ubiquitin-AMP complex through acyl substitution, which then forms a thioester bond and an AMP leaving group simultaneously (**Figure 1.11.**). The transfer of ubiquitin to the E2 enzyme occurs via a trans-thioesterification reaction, in which the E2 catalytic cysteine attacks the E1-ubiquitin complex. Subsequently, the E2 protein forms a complex with the E3 ubiquitin ligase E3 (Hershko *et al.*, 1983). The ubiquitin protein ligase identifies substrate protein targets and catalyses the transfer of ubiquitin to the lysine residue of the protein as an isopeptide (Bosu and Kipreos, 2008, Jackson and Xiong, 2009). This repetition of this catalytic cycle builds a polyubiquitin chain, which targets the substrate to the 26S proteasome, where it gets degraded (Merlet *et al.*, 2009) (**Figure 1.11.**).

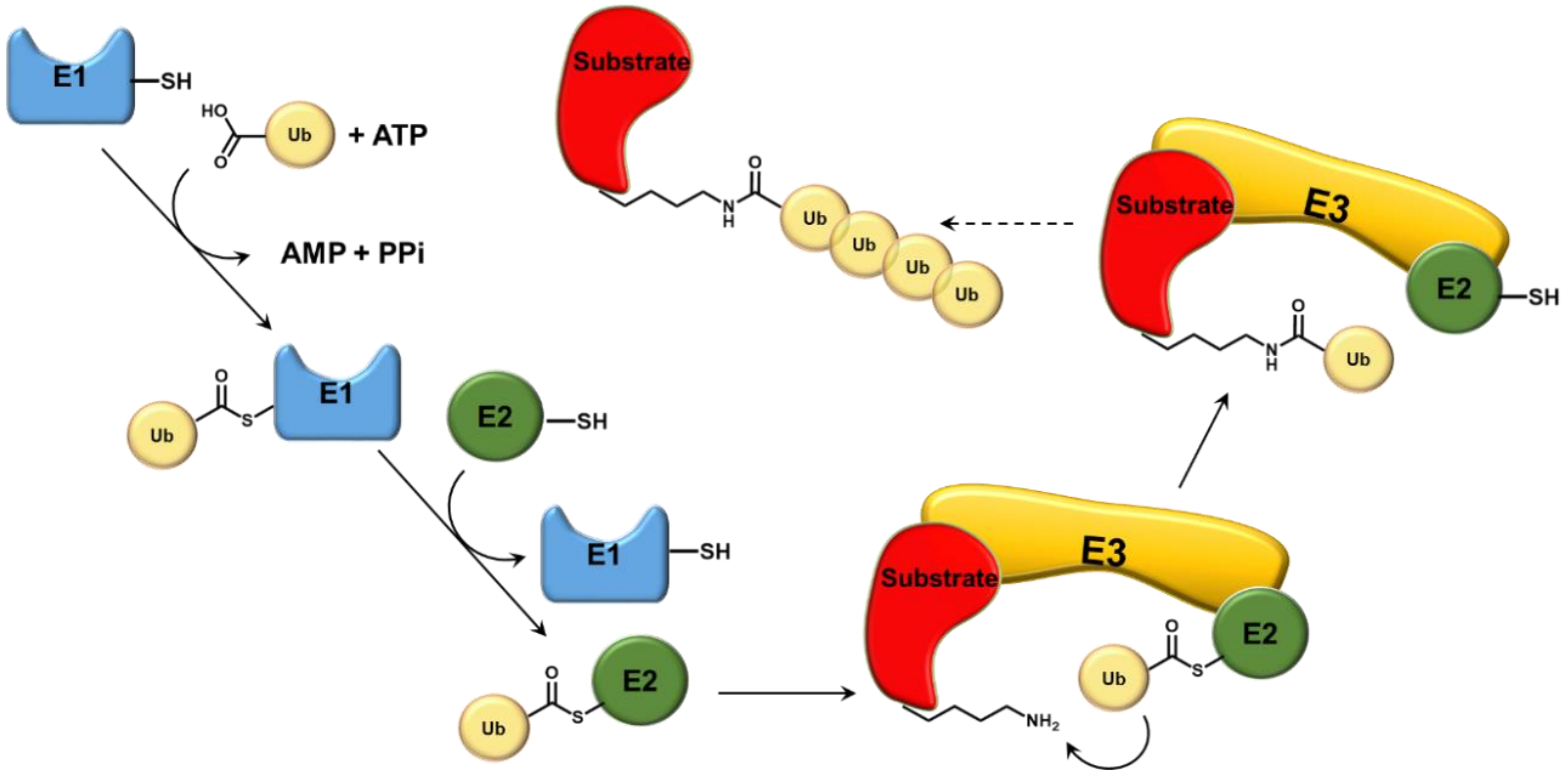

Figure 1.11. Schematic diagram of ubiquitylation mechanism. Polyubiquitin chain is assembled from a repetition catalytic cycle performed by E1 (ubiquitin-activating enzyme) (blue), E2 (ubiquitin-conjugating enzyme) (green), and E3 (ubiquitin ligase) (yellow). The scheme represents the ubiquitylation in the Really Interesting New Gene (RING) Family E3s. In Homologous to the E6-AP C-terminus (HECT) and RING between RING (RBR) family E3s, the E2 is transferred to the cysteine residue in the E3 before binds to the substrate. ATP, adenosine triphosphate; AMP, adenosine monophosphate; Ub, ubiquitin.

1.4.1. Types of Ubiquitylation

It is long established that there are eight different types of ubiquitin linkages, which are known to be able to attach the ubiquitin to the protein substrates (termed as canonical ubiquitylation) (Freiman and Tjian, 2003). These linkages occur between the *C*-terminus of ubiquitin and the ε-amino groups of lysine (K) residues; Lys6 (K6), Lys11 (K11), Lys27 (K27), Lys29 (K29), Lys33 (K33), Lys48(K48), Lys 63 (K63), and to the α-amino groups of N-terminal Met1 (M1) residue (Akutsu *et al.*, 2016). Additionally, since non-canonical ubiquitylation (or non-lysine ubiquitylation) could also occur in cysteine or serine/threonine/tyrosine residues with the same mechanism as lysine ubiquitylation (McDowell and Philpott, 2013), later it was found that threonine residue is indeed able to be ubiquitylated (Pao *et al.*, 2018).

The ubiquitin chains forms could be divided into three general types: mono-ubiquitylation, multi-monoubiquitylation, and polyubiquitylation (**Figure 1.12.**) (Komander, 2009). Mono-ubiquitylation is characterised by the addition of one ubiquitin on a single lysine residue of the protein substrate. Multi-monoubiquitylation is the addition of ubiquitin to multiple lysine residues. Lysine residues, which form single linkages are K6, K11, K27, K29 and K33. Poly-ubiquitylation occurs in two forms, homotypic- and heterotypic polyubiquitylation. Homotypic polyubiquitylation forms ubiquitin chains, which contain a single linkage-type, while heterotypic poly-ubiquitylation consists of different types of linkages. Both forms, homotypic- and heterotypic- can form chains in a linear or branched linkage by K63 or K48 linkages (Komander, 2009, Emmerich and Cohen, 2015).

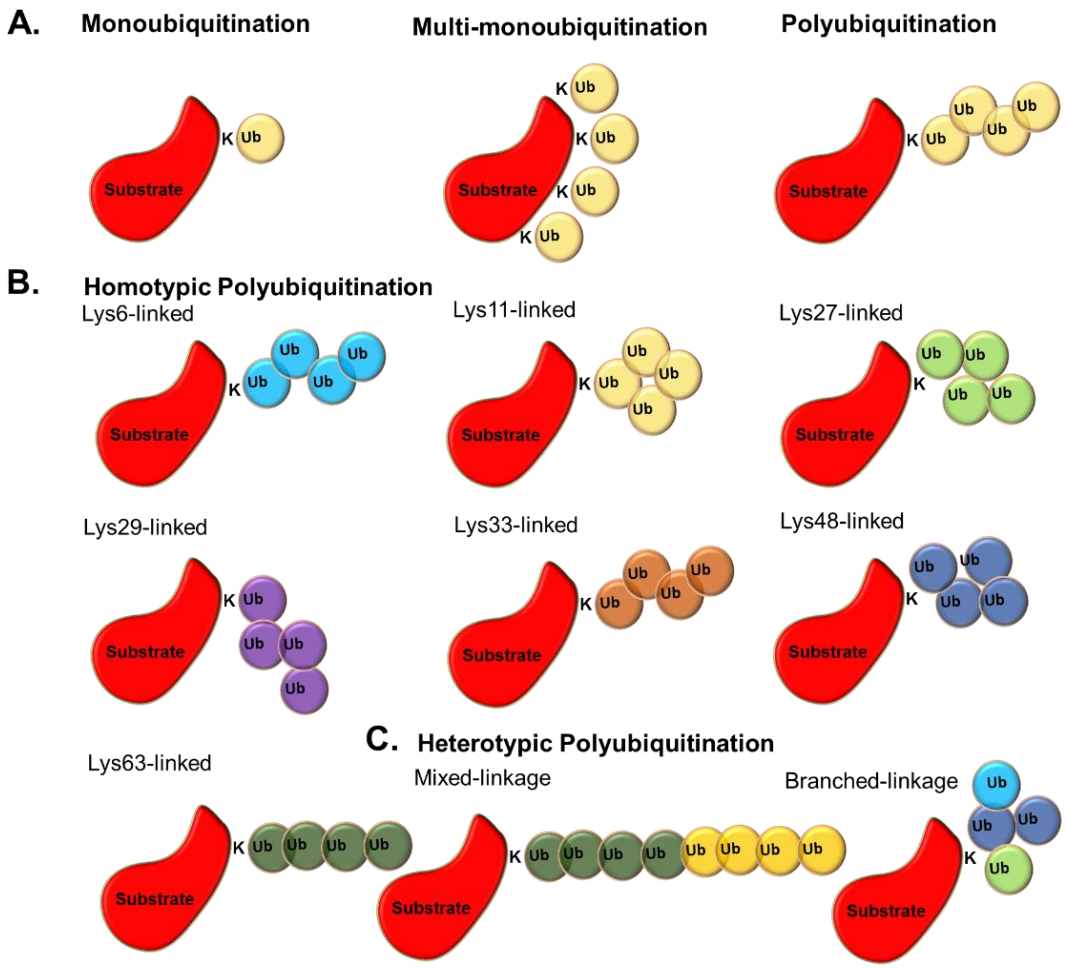

Figure 1.12. Different types of ubiquitylation and its type of linkages by lysine residues. A. Three types of ubiquitylation; monoubiquitylation, multi-monoubiquitylation, and polyubiquitylation. Polyubiquitylation with ubiquitin chain contains single ubiquitin linkages (B. Homotypic polyubiquitylation) or different ubiquitin linkages (C. Heterotypic polyubiquitylation) (Komander, 2009). Lys/K, Lysine; Ub, ubiquitin.

1.5. CULLIN RING E3 UBIQUITIN LIGASES (CRLs)

1.5.1. E3 Ubiquitin Ligases

It is estimated that there are more than 600 E3 ubiquitin ligases encoded in the human genome (Li *et al.*, 2008). E3 ubiquitin ligases play a central role in the ubiquitin-proteolytic system, as they identify the protein substrates and mediate the addition of ubiquitin to these proteins (Freiman and Tjian, 2003). There are three main classes of E3 ubiquitin ligases, and these are characterised by conserved structural domains and the mechanism of the E2 transfer to the substrates. These three classes are: 1)

Really Interesting New Genes (RINGs), 2) Homologous to the E6-AP *C*-Terminus (HECTs), and 3) RING Between RINGs (RBRs) (Berndsen and Wolberger, 2014). RING E3s bind directly to the protein substrates by providing lysine residues as a docking site to receive ubiquitin from E2 (Deshaies and Joazeiro, 2009). The HECT and RBR families of E3 ubiquitin ligases undergoes two-step reaction, which involves ubiquitin transfer from the E2 to the active cysteine residue in the E3 and this is then followed by ubiquitin transfer from E3 to the substrate (Berndsen and Wolberger, 2014).

There are approximately 30 HECT E3 ubiquitin ligases present in the human genome (Rotin and Kumar, 2009). The HECT E3 ubiquitin ligases are defined by a homologous *C*-terminal catalytic domain, which adopts a characteristic bilobal structure with a short hinge (Zheng and Shabek, 2017). A flexible interlobe configuration is necessary to allow the cysteine active site of E3 ubiquitin ligase, which lies on the *C*-lobe to become closer in proximity to the N-lobe-bound E2 enzymes (Zheng and Shabek, 2017). The HECT E3 ubiquitin ligases are also used in polyubiquitylation of protein substrates with specific chain linkage (Metzger *et al.*, 2012).

The RBR family of E3 ubiquitin ligases is considered as a new class of E3 ubiquitin ligase, which has a unique characteristic of RING-HECT hybrid (Wenzel *et al.*, 2011). RBR E3 ubiquitin ligases are characterised by a homologous sequence, which comprises two predicted RING fingers, RING1 and RING2, a central in-between-RING (IBR) zinc-binding domain (Wenzel *et al.*, 2011). There are more than ten RBR E3 encoded in the human genome (Spratt *et al.*, 2014). One of the examples of RBR E3 ubiquitin ligase is PARKIN, encoded from the *PARK2* gene, which is mutated in Parkinson disease (Kitada *et al.*, 1998). The RBR E3 ubiquitin ligases also have a unique sequence of N- and or *C*-terminal flanking domains in addition to the central of RING1-IBR-RING2 sequence, which is responsible for its ligase activity regulation

(Spratt *et al.*, 2014). Even though the RBR E3 ubiquitin ligase shows a common linear arrangement, the crystal structure of the PARKIN exhibited a compact architecture, in which structural domains are entangled and intertwined by flexible interdomain linkers (Riley *et al.*, 2013). The RING2 domain and RING1-IBR domains are physically separated by a domain outside the RBR module and bury its active site cysteine (Zheng and Shabek, 2017). Just like the HECT E3 ubiquitin ligases, the chain type specificity is defined by the catalytic domain of the RBR E3 ubiquitin ligases (Zheng and Shabek, 2017).

Due to relevance to WNK-SPAK/OSR1 signalling, RING E3 ubiquitin ligases, especially Cullin-RING E3 Ubiquitin ligases are described in more details in this thesis.

1.5.2. General Features of CRLs

CRLs were first discovered and identified in *C.elegans* around twenty years ago (Kipreos *et al.*, 1996). The CRLs are a superfamily of RING E3 ubiquitin ligases, and they are involved in approximately 20% ubiquitin-dependent protein turnover in the cells (Soucy *et al.*, 2009). The SCF (Skp1-Cullin-F-box) is one of the first RING domains, which was discovered to have a link with the ubiquitin-proteolytic system (Skowyra *et al.*, 1997). The SCF complex is comprised of a cullin scaffold subunit (Cdc53 in budding yeast/CUL1 in mammals), the adaptor protein SKP1, and the RING-H2 finger protein RBX1 (also called HRT1 or ROC1) (Duda *et al.*, 2011). The *N*-terminal of CUL1/Cdc53 is linked to the F-box by SKP1, and in its *C*-terminal lies an RBX1 binding site which is a docking site for E2 binding for ubiquitin transfer (Lydeard *et al.*, 2013). The SCF complex provides an architectural model of a larger family of cullin-based ubiquitin ligases (see **Figure 1.13.** and **Figure 1.14.A.**) (Duda *et al.*, 2011, Lydeard *et al.*, 2013).

Six types of cullins genes are encoded in the human genome; CUL1, CUL2, CUL3, CUL4A/4B, CUL5 and CUL7 (**Figure 1.13.**) (Lydeard *et al.*, 2013). There are also another two proteins known to contain a cullin homology domain, but they are different from the typical cullins. These are PARC (Parkin-like cytoplasmic protein) (Skaar *et al.*, 2007) and APC2 (a subunit of the APC/C complex) (Tang *et al.*, 2001).

These cullin genes form the central CRL scaffold in an elongated horseshoe-like structure (see the general feature of CRLs in **Figure 1.13.**) (Lydeard *et al.*, 2013). The *C*-terminus of the cullin binds the *N*-terminus of the RING finger protein, RBX1, for all types of cullins, except for CUL5 which is bound exclusively to RBX2 (Huang *et al.*, 2009). In the *C*-terminal of RBX1/2, the E2 binds and mediates the ubiquitin transfer. The *N*-terminus of cullin binds to the various substrate-receptor module to recruit the different proteins targets, mainly the modules use a BTB (Bric-a-Brac, Tramtrack and Broad complex)-fold adaptor to interact with the amino-terminal domains of cullin (Lydeard *et al.*, 2013). As this *N*-terminus domain in cullin is only conserved between cullin orthologues, it provides specificity for the interaction with the various substrate-recognition modules (Duda *et al.*, 2011).

There are three classes of substrate-recognition modules. 1) BTB for CUL3, which interacts with the *N*-terminal of CUL3 and other protein-interaction domains that bind to protein substrates (Zhuang *et al.*, 2009), 2) SKP1 and ELOC (one of the two BTB-fold protein) for CUL1, CUL2, CUL5 and CUL7, which interact with the *N*-terminal of their respective cullins (Kamura *et al.*, 1998, Zheng *et al.*, 2002b), and 3) the substrate module for CUL4A/4B which is made up of DDB1 and members of the DDB1-Cullin Associating Factor (DCAF) family of substrate receptors (He *et al.*, 2006) (**Figure 1.13.**). Although DDB1 is unrelated to SKP1 and ELOC, it also associates with the *N*-terminus of the cullin. The DDB1 structure contain the WDR40 binding domain, which serves as the Aspartic Acid – Tryptophan – Aspartic acid (DWD) motif for substrate binding (Lydeard *et al.*, 2013).

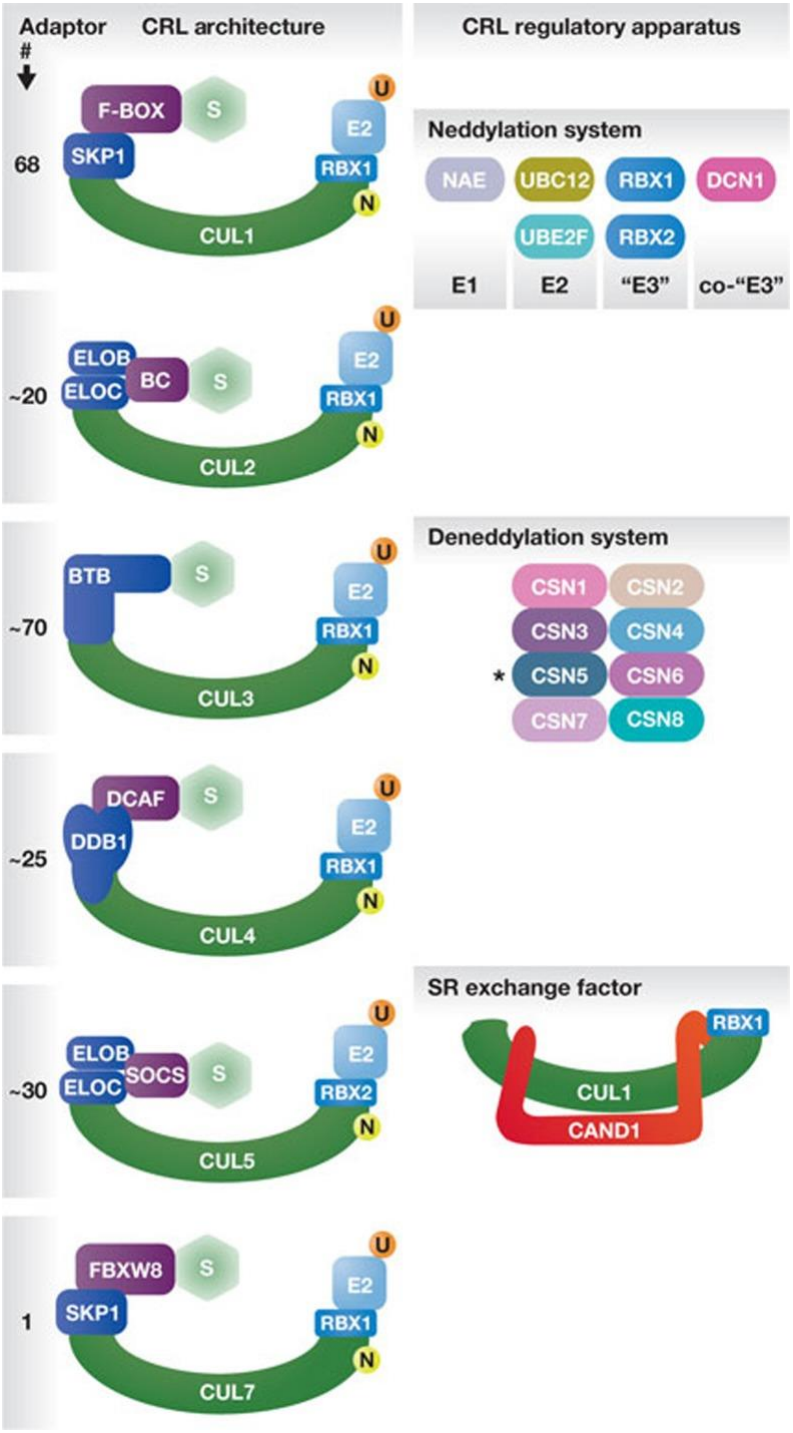

Figure 1.13. The general architecture of human Cullin-RING E3 ubiquitin ligases. The number of substrate adaptors for each type of CRLs is written on the left. The CRLs regulatory apparatus consists of the neddylation system, deneddylation system and the substrate receptor (SR) exchange (Lydeard *et al.*, 2013). CRL, cullin RING ligase; SKP1, S-phase kinase-associated protein 1; CUL, cullin; RBX, RING box protein; S, substrate; U, ubiquitin; N, Nedd8; NAE, Nedd8 activating enzyme; UBC, polyubiquitin-C; UBE2F, ubiquitin-conjugating enzyme E2 F; DCN1, defective in cullin neddylation protein 1; ELO, elongin; BTB, BR-C ttk bab; CSN, COP9 signalosome complex subunit; DDB1, DNA damage binding protein 1; DCAF, DDB1-cullin associated factor; SOCS, suppressor of cytokines signalling; CAND1, cullin-associated Nedd8-dissociated protein 1; FBXW8, F-box and WD repeat domain containing 8.

1.5.2.1. Structural assembly of SCF-Skp2, CRL2 and CRL5

The model structure of SCF-Skp2 provides several key canonical characteristics of CRLs. The model structure was obtained from superimposing Skp1-Skp2 complex and CUL1-Rbx1-Skp1-Skp2-F-box domain structure (**Figure 1.14.**) (Zimmerman *et al.*, 2010). These key characteristics are, firstly, the central scaffold CUL1 shows horseshoe-like structure comprising the stalk-like *N*-terminal domain and globular *C*-terminal domain. Secondly, Skp1 binds to CUL1 through two conserved α-helices close to CUL1 *N*-terminus, whereas Rbx1 lies at the other end of the CUL1 *C*-terminal domain. Thirdly, the entire SCF complex featured tight-packed interfaces suggesting that the E3 ubiquitin ligase machinery act as a rigid platform to promote the transfer of ubiquitin from the E2 to the substrate protein. Fourthly, the structural configuration of SCF escorts the substrate-binding leucine-rich repeat (LRR) of Skp2 to the same orientation of E3 ubiquitin ligase scaffold. However, the 50Å distance between the substrate-binding site of the E3 ubiquitin ligase and the active site of E2 is accessible suggested that the configuration is a rigid and open arrangement (Bosu and Kipreos, 2008, Hotton and Callis, 2008, Zimmerman *et al.*, 2010, Lydeard *et al.*, 2013).

Based on the sequence homology, CRL2 and CRL5 components share a typical characteristic with SCF complex, which consists of CUL1 as the scaffold protein and Skp1 as the adaptor protein (Zimmerman *et al.*, 2010). Elongin C/B is the adaptor protein for CRL2 and CRL5 (Mahrour *et al.*, 2008). The von Hippel-Lindau (VHL) tumour suppressor and suppressors of cytokine signalling (SOCS) proteins are a substrate receptor for CUL2 and CUL5, respectively, and they are recruited by the binding with Elongin C/B (Kamura *et al.*, 2004). Furthermore, the interaction between ElonginC/B and BTB fold of Elonginc C (BC-box) motif is very similar to the assembly of Skp1 binding to the F-box protein (Zimmerman *et al.*, 2010). In general, CRL1, CRL2 and CRL5 shared similar architecture and assembly (Zimmerman *et al.*, 2010, Lydeard *et al.*, 2013)

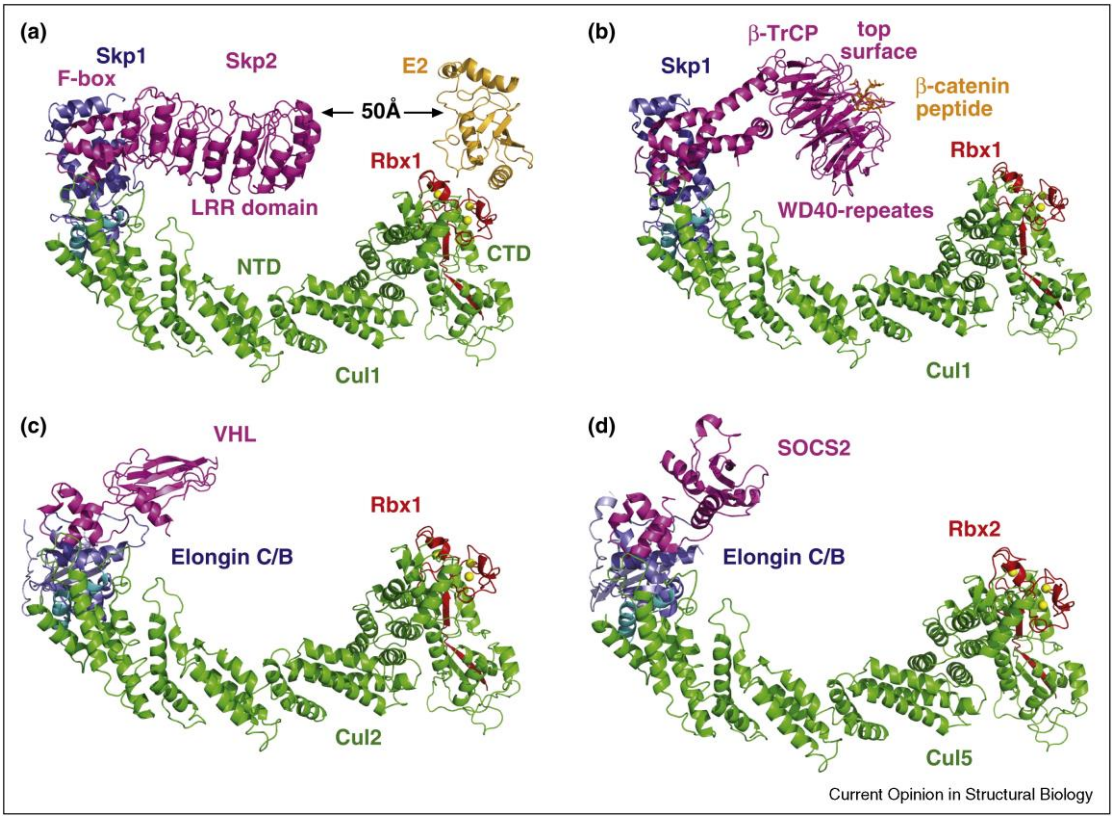

Figure 1.14. Structural assembly of CRL1, CRL2 and CRL5. a) structural model for SCF-Skp2 showing LRR domain of Skp2 and its gap with E2. b) structural model of SCF-β-TrCP in complex with phosphorylated β-catenin degron peptide. c) structural model for CRL2-VHL. d) structural model for CRL5-SOCS2 (Zimmerman *et al.*, 2010). Skp, S-phase kinase-associated protein; LRR, lysine arginine arginine; NTD, N-terminal domain; Cul, cullin; CTD, C-terminal domain; RBX, RING box protein; SCF, Skp1-cullin-F-box protein complex; β-TrCP, beta-transducin repeats-containing proteins; WD40, tryptophan aspartic acid repeat containing protein 40; VHL, von Hippel-Lindau; SOCS, suppressor of cytokines signalling.

1.5.2.2. Structural assembly of CRL3

CRL3 structure is dissimilar to other CRLs by the integrated function of its adaptor protein and substrate receptor into a single polypeptide (**Figure 1.15.**) (Zimmerman *et al.*, 2010). This single polypeptide forms an obligate dimer (Ahmad *et al.*, 1998). The substrate receptors of CUL3 are the BTB domain proteins, which allow for the interaction between the cullin scaffold and the Kelch, MATH, ZnF, or another protein-protein interaction domain to bind to the substrates. CRL3, with BTB as the adaptor proteins, has been known its ability to induce dimerisation of the CRL3 with two

substrate-binding sites and two catalytic cores located opposed to each other in a close distance (Zimmerman *et al.*, 2010).

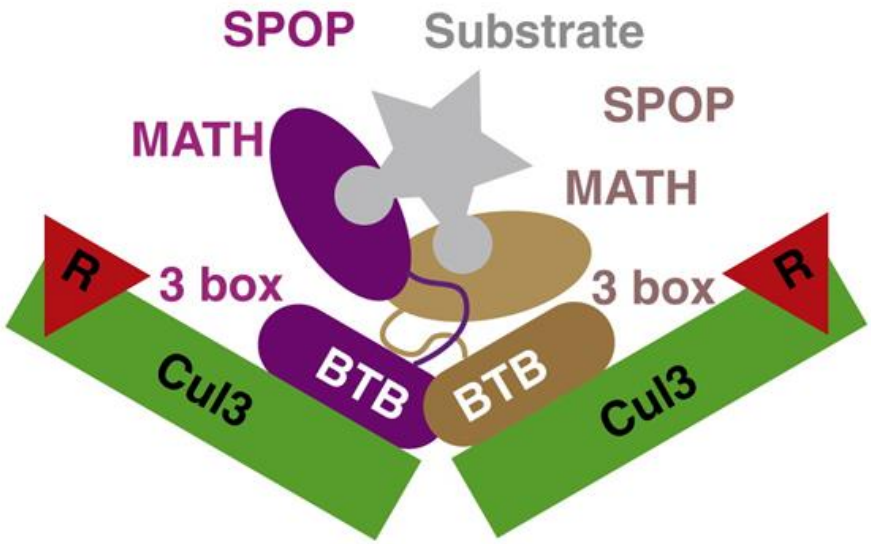

Figure 1.15. Schematic diagram of the structural assembly of CRL3. Asymmetric CRL3 substrate receptor, SPOP dimerise and recruits two copies of CUL3-Rbx1 via BTB domains and can bind to a single substrate polypeptide by recognising two degrons via two MATH domains (Zimmerman *et al.*, 2010). SPOP, speckle-type POZ protein; MATH, meprin and TRAF-C homology; R, Rbx protein; BTB, BR-C ttk bab.

1.5.2.3. Structural assembly of CRL4

The architecture of CRL4 is distinct to the typical structural assembly of CRL1, CRL2 and CRL5 as it has a relatively more complex structure. CRL4 is conserved from yeast to human and has a horseshoe-like structure (Jackson and Xiong, 2009). The adaptor protein of the CRL4 is DDB1, which lacks BTB fold (He *et al.*, 2006). DDB1 contains three WD40-like β-propeller domains designated BPA, BPB, and BPC, and a *C*-terminal helical domain (**Figure 1.16.**) (Angers *et al.*, 2006, Li *et al.*, 2006). The interaction between DDB1 and CUL4A features the binding between the BPB domain to CUL4A N-terminal domain, whereas the BPA and BPC point away from the cullin scaffold (Angers *et al.*, 2006). Interestingly, the BPB domain of DDB1 interacts with the N-terminal domain of CUL4A by the same two α-helices correspondings to that is

observed in the binding between CUL1 and Skp1, even though there was no sequence homology or structural similarity between the two adaptor proteins (Higa and Zhang, 2007). Thus, in general, the position of the adaptor proteins, Substrate Receptor (SR) and Rbx1, on the cullin scaffold is conserved among CRLs (Angers *et al.*, 2006, Higa *et al.*, 2006, Higa and Zhang, 2007, Zimmerman *et al.*, 2010, Lydeard *et al.*, 2013, Hannah and Zhou, 2015).

The endogenous substrate receptor of CRL4s, named DDB1 and CUL4A Association Factors (DCAFs) were identified from several DDB1 protein interactors analysis studies (He *et al.*, 2006, Higa *et al.*, 2006, Higa and Zhang, 2007). These substrate receptors are characterised by having six or more of the WD40 motifs, which feature propeller blades and forms radial topology around a central axis to generate a complete β-propeller domain (see **Figure 1.16.A.** for DDB1 structure) (He *et al.*, 2006, Higa and Zhang, 2007, Biedermann and Hellmann, 2011, Hannah and Zhou, 2015).

The first report which uncovered the mode of DDB1 binding to DCAF was the co-crystal structure of DDB1 with SMV-5, a hijacker protein virus (**Figure 1.16.**) (Angers *et al.*, 2006, Li *et al.*, 2006). The N-terminal domain of SMV-5 forms an α-helix and inserts in the deep pocket between BPA and BPC domains of DDB1, while the *C*-terminal domain of SMV-5 forms an additional interaction with the BPC domain of DDB1 (Angers *et al.*, 2006). The ability of SMV-5 to recruit unnatural targets to CRL4 suggested that SMV-5 mimics the DDB1 endogenous substrate receptors and competes with the endogenous DCAF proteins for DDB1 interaction though it does not feature the WD40 propeller domains (Angers *et al.*, 2006).

Besides the complexity of the CRL4 structure and the distinct structure of DDB1, there are flexibility and plasticity of the CRL4 complex. A large degree of rotational and torsional flexibility between BPA-BPC and BPB domains of DDB1 allows the CRL4 to establish interaction with various sized and shaped DCAF-substrates to support the polyubiquitylation chains assembly (Li *et al.*, 2006). The plasticity of CRL4 structure

also enables CRL4 to provide a large space located around DCAF-substrate complex to provide various substrates to bind to CRL4 complex and ubiquitylated (Lydeard *et al.*, 2013) as it is shown by 'open' conformation of CRL4 complex after NEDD8 conjugation (Duda *et al.*, 2008).

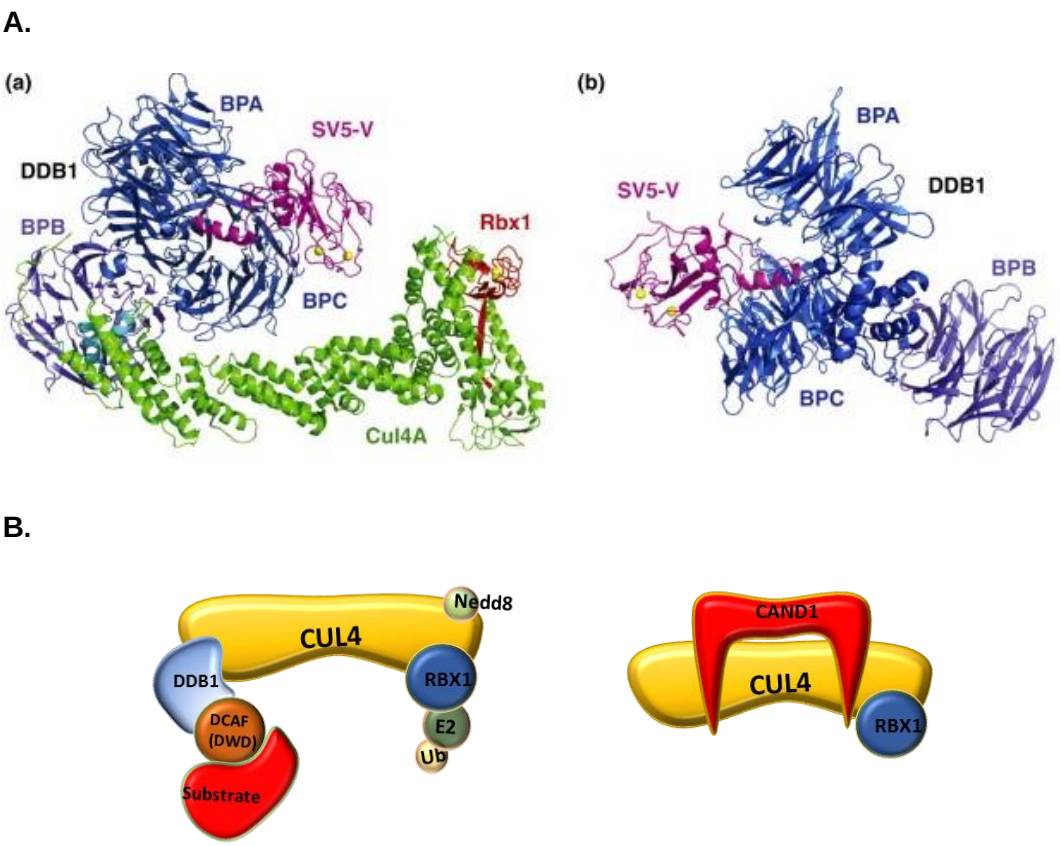

Figure 1.16. Structural assembly of human CRL4 complex. A. (a) crystal structure of CUL4A-DDB1-SV5-V complex, (b) SV5-V bipartite interaction to DDB1. (Bennett *et al.*, 2010, Lydeard *et al.*, 2013). B. schematic diagram of CRL4 complex with all components which is involved in the CRL4 regulation. DDB1, DNA damage binding protein 1; BP, beta propeller; SV5-V, simian virus 5 protein; DCAF, DDB1-cullin associated factor; DWD, aspartic acid tryptophan aspartic acid, Ub, ubiquitin; CAND1, cullin-associated Nedd8-dissociated protein 1; Rbx1, RING box protein 1.

1.5.3. Regulation of CRLs

Several events that regulate CRLs and thus modify its architecture include 1) activation by neddylation; 2) association of active neddylated forms with COP9 signalosome (CSN) complex; 3) loss of SR through proteolytic degradation; and 4) SR exchange via a cullin-associated NEDD8-dissociated protein 1 (CAND1) driven mechanism (see **Figure 1.18.**) (Bosu and Kipreos, 2008, Lydeard *et al.*, 2013).

1.5.3.1. Activation of CRLs by neddylation

NEDD8 is a ubiquitin-like protein, which shared 85% identity to ubiquitin (Veen and Ploegh, 2012). NEDD8 is covalently linked to a conserved lysine residue in the *C*-terminal domain of the winged-helix motif in cullin (Duda *et al.*, 2008) (**Figure 1.17.**). The linkage is established via an E1 NEDD8-activating enzyme (NAE)-E2 NEDD8-conjugating enzyme (Walden *et al.*, 2003). Cullin neddylation is known to be a mechanism that promotes ubiquitylation and turnover of CRLs substrate proteins *in vivo* (Soucy et al., 2009). This finding was discovered following the development of MLN4924, a small molecule NAE inhibitors (Soucy *et al.*, 2009). MLN4924 inhibits CRLs activity, and this results in the accumulation of target CRLs substrate protein (Soucy *et al.*, 2009, Nawrocki *et al.*, 2012).

The neddylation process activates CRLs, which results in the direct binding of the E2 and NEDD8 (Sakata *et al.*, 2007). Despite the rigid structure of unneddylated CRLs and catalytic cysteine residue of the Rbx1-E2, which is located only 50Å away from the substrate, the reorganisation of cullin *C*-terminal domain occurs when the NEDD8 binds to CRLs (Duda *et al.*, 2008). This reorganisation causes the RING domain of Rbx1 to change orientation, and this allows the CRLs packed structure to become loosen and mediate the ubiquitin transfer (Duda *et al.*, 2008). Upon cullin neddylation, RBX1 and its bounded E2 become closer in proximity to the lysine residue of the protein target, thus stimulating the transfer of the first ubiquitin molecule in a slow rate

(Merlet *et al.*, 2009). This first ubiquitin transfer allows flexibility of RBX1/E2-Ub heterodimer to facilitate the elongation of polyubiquitin chains (Merlet *et al.*, 2009). Considering that the regulation of CRLs includes CRLs deneddylation by the CSN complex, after the first ubiquitin transfer, the polyubiquitylation rate is increased so that the process proceeds with a faster rate than the dissociation rate (Lydeard *et al.*, 2013).

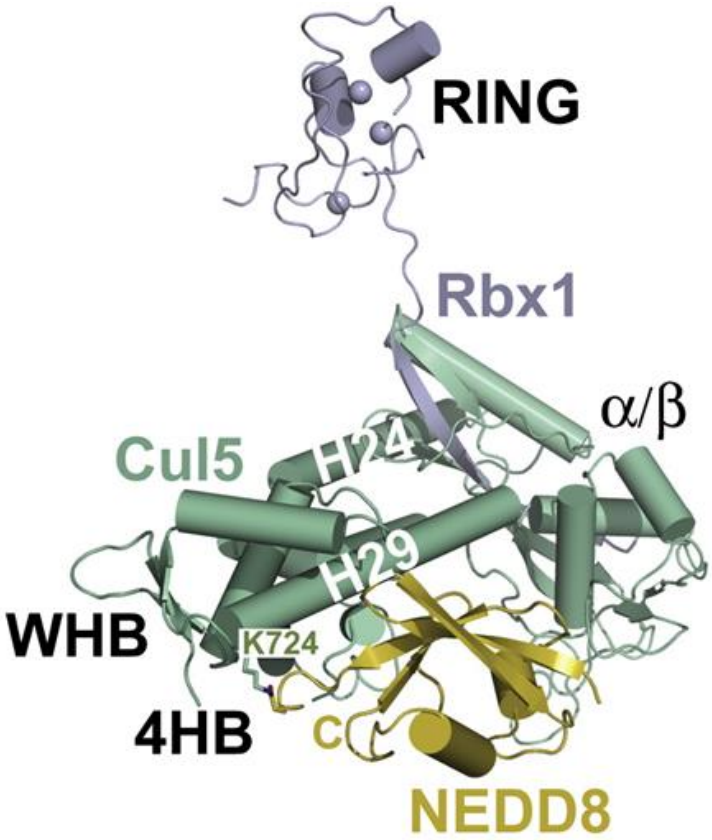

Figure 1.17. Structure of NEDD8-CUL5-Rbx1. Cartoon showing the structure of NEDD8-CUL5-Rbx1 (PDB ID: 3DPL) where NEDD8 binds to the winged-helix (consist of WHB and 4HB subdomains) of CUL5 and covalently bind to CUL5 Lysine residue (K724) at C-terminal domain (Duda *et al.*, 2008). The figure show subdomain WHB, 4HB and α/β of CUL5. RING, really interesting new gene; Rbx1, RING box protein 1; Cul, cullin; H, helix; K, lysine; C, carboxy-terminal.

1.5.3.2. Inhibition of CRLs by the CSN deneddylase

The CSN is comprised of eight subunits (CSN1-8), most of which contain PCI domains (**Figure 1.13.**) (Li and Deng, 2003). As deneddylase, the main functions of the CSN is to transiently bind the CRLs and remove NEDD8 (Li and Deng, 2003). The absence of NEDD8 means that the ubiquitin transfer is inhibited. The binding of the CSN to the CRLs can be reversed by the presence of substrates, because the substrates compete with the CSN to bind CRLs, and thus provide a control mechanism for the abundance and architecture of CRLs (Lydeard *et al.*, 2013). When the concentration of a substrate is reduced, CSN binding to the CRLs is increased, and this leads to the removal of the substrate receptor from the 'active' CRL and deneddylation (**Figure 1.18.**). Dissociation of the deneddylated form of CRL-SR from the CSN eventually allows CAND1 to bind, and the substrate then undergoes CAND1-dependent receptor exchange (Lydeard *et al.*, 2013).

1.5.3.3. CRLs remodelling by CAND1

CAND1 is considered an inhibitor of CRLs as it binds the cullin-Rbx complex, which lacks both the neddylation and the adaptor proteins (Zheng *et al.*, 2002a). The crystal structure of human CAND1 revealed that CAND1 binds to cullin by wrapping around the cullin with *N*-terminus of CAND1 binding to cullin *C*-terminus and *C*-terminus of CAND1 binding to the *N*-terminus of the cullin (**Figure 1.13.**) (Goldenberg *et al.*, 2004). CAND1 binding to cullin prevents the substrate adaptor and NEDD8 binding by blocking their binding and conjugation site, respectively. Thus, the cullin is prevented from undergoing the neddylation process (Bosu and Kipreos, 2008).

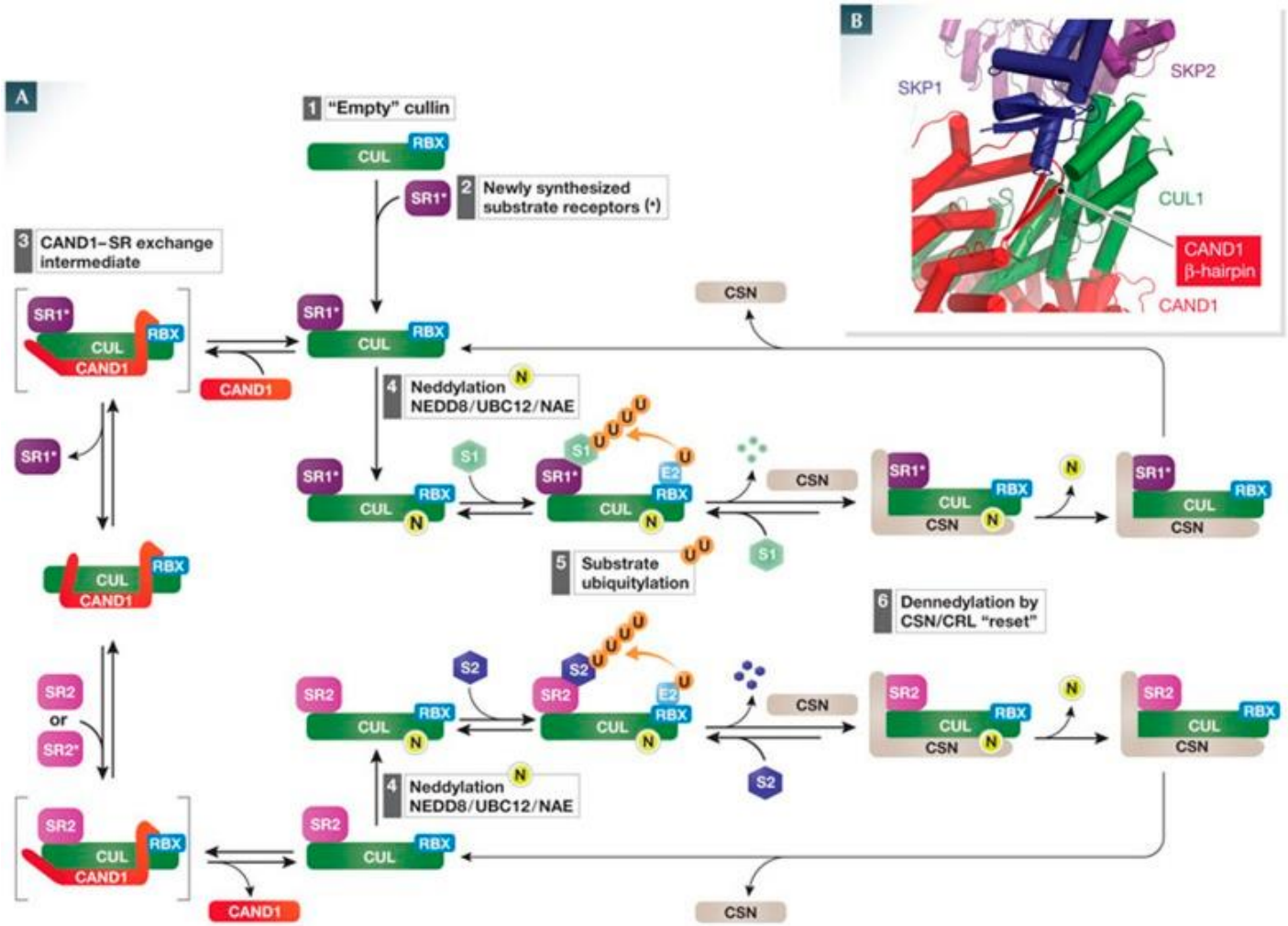

Figure 1.18. (Continued on the following page)

Figure 1.18. Regulation of CRLs by activation, deneddylation and SR exchange. Empty cullin (step1) could be interacted with SR1 (step 2) or integrated into a CAND1 complex (step 3) for exchange substrates (step 4 and 5). Along with the reduced of the substrate abundance, CSN is associated with CRLs and lead to deneddylation (step 6) followed by the dissociation of CRLs to enter the new cycles. The CAND1-exchange substrate cascade allows the exchange of substrate by dissociation of SR1 and association of SR2 based on the target substrate protein (Lydeard et al., 2013). RBX, RING box protein; CUL, cullin; SR, substrate receptor; CAND1, cullin-associated Nedd8-dissociated protein 1; S, substrate; U, ubiquitin; N, Nedd8; CSN, COP9 signalosome complex subunit; SKP, S-phase kinase-associated protein.

However, CAND1 can also be considered as a positive regulator of CRLs (Lydeard *et al.*, 2013). It was shown that CAND1 exhibits reversible function toward CRLs as it can promote SR exchange *in vitro* and its dissociation from CRLs complex can alter the steady-state distribution of receptors (Bosu and Kipreos, 2008, Bennett *et al.*, 2010, Lydeard *et al.*, 2013). It was also reported that the presence of CAND1 in the unneddylated CRL-SR complex increases the rate of SR dissociation (Pierce *et al.*, 2013). However, the neddylated form of the CRL-SR abrogated the effect of CAND1 towards the rate of SR dissociation, which corresponds with the evidence that NEDD8 was able to block the access of CAND1 binding to CRLs (**Figure 1.18.**) (Lydeard *et al.*, 2013).

1.5.4. CRLs functions and their various substrates

Based on the structure of CRLs, which is composed of cullins, adaptor proteins, and substrate receptors that target a vast array of substrates, the function of CRLs depends on the functional characteristics of the target substrates (Jackson and Xiong, 2009, Hannah and Zhou, 2015). The functions of CRLs and their substrates are summarised in Table 1.1. Most of the functions listed are for human CRLs, but several are for viral proteins, which affect humans.

Table 1.1. CRLs functions and the substrates (part 1 of 2)

CRLs	Adaptor	Substrate Receptor	Protein Substrate	Cellular and Physiological Function	References
SCF	Skp1	β-TrCP	PFKFB3	Glycolysis regulation during the cell cycle	(Tudzarova *et al.*, 2011)
SCF	Skp1	β-TrCP	β-catenin	Regulates the stability of β-catenin	(Latres *et al.*, 1999)
SCF	Skp2		$p27^{kip1}$	Promotes ubiquitin-dependent proteolysis and cell cycle progression	(O'Hagan *et al.*, 2000)
SCF	Skp1	Fbxl4	KDM4A/JMJD2A	Histone demethylase regulation	(Van Rechem *et al.*, 2011)
SCF	Skp1	β-TrCP	Securin	Cell-cycle arrest after UV irradiation	(Limón-Mortés *et al.*, 2008)
SCF	Skp1	FBXW11-NSs	Protein kinase R	Suppress viral protein synthesis Rift Valley fever virus infection	(Mudhasani *et al.*, 2016)
SCF	Skp1	Fbxl3	Cry	Regulate oscillation of the circadian clock	(Yumimoto *et al.*, 2013)
SCF	Skp2		CDT1	DNA replication control	(Li *et al.*, 2003)
SCF	Skp1	β-TrCP	DEPTOR	Enhancing cap-dependent translation	(Chen *et al.*, 2016)
CRL2	Elongin C/B	VHL	HIFα	Tumour suppression and regulation vasculogenesis	(Sufan and Ohh, 2006, Maeda *et al.*, 2008)
CRL2	Elongin C/B	PRAME	NFY promoters	Transcription regulation	(Costessi *et al.*, 2011)
CRL3	BTB	Keap1	Nrf2	Cell death by oxidative damage	(Shibata *et al.*, 2008)
CRl3	KLHL3		WNKs	Gordon' s hypertension syndrome	(Ohta *et al.*, 2013)
CRL3	KLHL21		Auroroa B	Mitosis regulation	(Maerki *et al.*, 2009)
CRL3	BTB	SPOP	Daxx	Transcription, cell cycle, and apoptosis regulation	(Kwon *et al.*, 2006)

Table 1.1. CRLs functions and the substrates (part 2 of 2)

CRLs	Adaptor	Substrate Receptor	Protein Substrate	Cellular and Physiological Function	References
CRL4	CDT2		CDT1	Prevent re-replication by encircling DNA and make a sliding	(Arias and Walter, 2006)
CRL4	DDB1	CDT2	CDT1	Histone methylation regulation	(Higa *et al.*, 2006)
CRL4	DDB1	DCAF1	Vpr	HIV Vpr cell cycle arrest	(Le Rouzic *et al.*, 2007)
CRL4	DDB1	Fbw5	TSC2	Tumour suppression regulation	(Hu *et al.*, 2008)
CRL4	DDB1		Chk1	Perturbed cell division cycle under replication stress	(Leung-Pineda *et al.*, 2009)
CRL4	DDB1	MLL1	p6-INK4a	Tumour suppressor p16 activation	(Kotake *et al.*, 2009)
CRL4	DDB1	CRBN	BK channel	Restrict BK channel activity and prevent epileptogenesis	(Liu *et al.*, 2014)
CRL4	DDB1	CRBN	CLC-1	Membrane excitability of skeletal muscle regulation	(Chen *et al.*, 2015)
CRL4	DDB1	CRBN	CK1α	Regulation of kinase in multiple myeloma	(Petzold *et al.*, 2016)
CRL4	DDB1	WDR70	DSB	Regulation H2B monoubiquitylation and facilitates Exo-1 dependent resection	(Zeng *et al.*, 2016)
CRL5	Elongin C/B	Vif	APOBEC3G	Proteasomal degradation of DNA deaminase	(Mehle *et al.*, 2004)

Hypothesis, Aims and Objectives

Hypothesis

SPAK and OSR1 phosphorylation at S-motif by WNK kinase impact their regulation.

Aims:

1. Identify the proteins that bind SPAK and OSR1 kinases in S-motif phosphorylation-dependent manner.
2. Verify the binding of these proteins to SPAK and OSR1 kinases.
3. Establish the impact of the binding of these proteins on the regulation of SPAK and OSR1 kinases.

Objectives:

1. Use pulldown assays and mass spectrometry to identify proteins that bind SPAK and OSR1 through their S-motif in a phosphorylation-dependent manner.
2. Employ protein overexpression, endogenous proteins immunoprecipitations and Western blotting to verify the binding of SPAK and OSR1 S-motif phosphorylation-dependent protein partners.
3. Use ‘in cell’ assays to understand the regulation of SPAK and OSR1 upon the binding of these proteins to SPAK and OSR1 kinases.

CHAPTER II.

MATERIALS AND METHODS

CHAPTER II. MATERIALS AND METHODS

2.1 MATERIALS

2.1.1 Cell lines

HEK293 cells were purchased from ATCC as 293 [HEK293] (ATCC®CRL-1573™). HEK293 cell is cultured as adherent cells, which is derived from human embryonic kidney cells and has epithelial morphology.

U266 cells were purchased from ECACC as U266B1 (ECACC 85051003). U266 cell is cultured as suspension cells, which is derived from human B lymphocyte cell and has lymphoblast morphology.

2.1.2 Media

2.1.2.1 Media for mammalian cell culture

HEK293 cells were cultured in DMEM-high glucose (D6429, Sigma-Aldrich) supplemented with 10% Fetal Bovine Serum (FBS) (F0804, Sigma-Aldrich) and 1% of PenStrep (Gibco™Penicillin-Streptomycin 10,000 U/mL). U266 cells were cultured in RPMI1640 (R8758, Sigma-Aldrich) supplemented with 15% FBS and 1% of Pen-Strep.

2.1.2.2 Media for bacterial culture

Bacterial media for *E. coli* DH5α is Luria-Bertani (LB) media either broth (L7275, Sigma-Aldrich) or with agar (L7025, Sigma-Aldrich) supplemented with 100 ug/mL Ampicillin (A5354, Sigma-Aldrich).

2.1.3 Chemicals and reagents

All chemicals and reagents were purchased from Sigma-Aldrich UK unless otherwise stated. Chemicals for cell treatment: dimethyl sulfoxide (DMSO) (D8418), indisulam (SMLl225), MG132 (LKT Laboratories), MLN4924 (Biovision), pomalidomide (P0018),

thalidomide (T144). Reagents for cell culture: glycerol (G5516), lipofectamine (Lipofectamine 2000, Thermo Fisher), phosphate buffered saline (PBS) (D8662), polyethyleneimine (PEI) (43896, Alfa Aesar), puromycin dihydrochloride (P8833), trypsin for cell dissociation (TrypLE™ Xpress Enzyme 1x, 12605036, ThermoFisher). Chemicals and reagents for buffers preparation: benzamidine (434760), bromophenol blue (114391), CHAPS hydrate (C3023), EDTA (A1103, Applichem), EGTA (E3889), glycine (0167, VWR Chemicals), HEPES (172570250, Acros Organic), magnesium chloride (M8266), 2-mercaptoethanol (M6250), nonidet-P40 (A1694, Applichem), phenylmethanesulfonylfluoride (PMSF) (78830), potassium chloride (P9541), potassium gluconate (P1847), sodium chloride (443827W, VWR Chemicals), SDS (4415HN, VWR Chemicals), sodium fluoride (S7920), sodium gluconate (S2054), sodium orthovanadate (S6508), sodium phosphate ($Na_2HPO_4.7H_2O$) (431478), sodium pyrophosphate (221368), sodium sulphate (239313), sucrose (A15583, Alfa Aesar), tris-HCl (22676, Affymetrix), tween-20 (P1379). Chemicals and reagents for gel electrophoresis: 30% acrylamide/bis solution 37.5:1 (#1610158, Bio-rad), agarose (J60299.18, Alfa Aesar), ammonium persulphate (APS) (215589), ethidium bromide (E1510), TEMED (T9281). Other chemicals and reagents: bovine serum albumin (BSA) (A2153), dimethyl pimelimidate (DMP) (D8388).

2.1.4 Buffers

Cell lysis buffer for mammalian cells comprises of 50 mM Tris–HCl (pH 7.5), 1 mM EGTA, 1 mM EDTA, 1% (w/v) nonidet-P40, 0.27 M sucrose, 1 mM sodium orthovanadate, 50 mM NaF, 5 mM sodium pyrophosphate, 1 mM benzamidine and 0.1 mM PMSF (benzamidine and PMSF were freshly added prior to use). Buffer A contains 50 mM Tris–HCl (pH 7.5), 0.1 mM EGTA and 0.1% (v/v) 2-mercaptoethanol. The SDS sample loading buffer was 50 mM Tris–HCl (pH 6.8), 1% (w/v) SDS, 10% (v/v) glycerol, 0.005% (w/v) bromophenol blue and freshly added of 1% (v/v) 2-mercaptoethanol. TBS-T buffer was 50 mM Tris–HCl (pH 7.5), 0.15 M NaCl and

0.25% (v/v) tween-20. Basic control buffer was prepared from 135 mM NaCl, 5 mM KCl, 1 mM $CaCl_2$/$MgCl_2$, 1 mM Na_2HPO_4/Na_2SO_4 and 15 mM HEPES (pH 7.0). Hypotonic low-chloride buffer consists of 67.5 mM sodium gluconate, 2.5 mM potassium gluconate, 0.5 mM $CaCl_2$/$MgCl_2$, 1 mM Na_2HPO_4/Na_2SO_4 and 7.5 mM sodium HEPES (pH 7.0). TBS buffer for FLAG pull-down contains 50 mM Tris-HCl, 150 mM NaCl pH7.4, and 0.1 M glycine pH 3.5. Buffers for His pull-down assay: binding buffer contains 20 mM Tris-HCl pH8.0, 100 mM NaCl, 30 mM imidazole and 10 µg/mL BSA); and washing buffer comprise of 20 mM Tris-HCl pH 8.0, 200 mM NaCl, 50 mM imidazole and 0.2% tween-20. TAE Buffer for DNA agarose gel electrophoresis: 40 mM Tris, 20 mM glacial acetic acid, 1 mM EDTA.

2.1.5 Beads for pull-down assay and immunoprecipitation

Streptavidin Sepharose® High-Performance beads (17-5113-01, GE Healthcare), Protein G-Sepharose beads (PC-G5, Generon), GST beads (Glutathione Sepharose High Performance, GE Healthcare), FLAG resin beads (Anti-FLAG M2 affinity gel, Sigma-Aldrich), HisPur Ni-NTA resin beads (Thermo Scientific).

2.1.6 Antibodies

Antibodies which were used are listed in **Table 2.1.**

Table 2.1 List of Antibodies

Antibody	Identification Code	Supplier	Conc./ Dilution
Primary antibodies:			
Anti-Aiolos	#15103	Cell Signalling Technology	1:1000
Anti-CAND1	#7433	Cell Signalling Technology	1:500
Anti-CAPERα (P14)	SC-101103	Santa Cruz Biotechnology	1:1000
Anti-CLCN1	CPA2947	Cohesion Bioscience	1:1000
Anti-CRBN	SAB1407456	Sigma-Aldrich	1:1000
Anti-CUL2	ab166917	Abcam	
Anti-CUL4A	#2699	Cell Signalling Technology	1:1000
Anti-CUL4B	C9995	Sigma-Aldrich	1:1000
Anti-DDB1 (Polyclonal antibody)	#5428	Cell Signalling Technology	1:1000
Anti-DDB1 (Monoclonal antibody)	#6988	Cell Signalling Technology	1:1000
Anti-DDDK tag antibody (equivalent to FLAG antibodies from Sigma-Aldrich) (HRP)	ab2493	Abcam	1:1000
Anti DDDDK-tag antibody (equivalent to Anti-FLAG SIGMA-ALDRICH antibody)	ab45766	Abcam	1:1000
Anti-DYKDDDDK (Polyclonal antibody)	#2368	Cell Signalling Technology	1:1000
Anti-DYKDDDDK (Monoclonal antibody)	#14793	Cell Signalling Technology	1:1000
Anti-GAPDH	#2118	Cell Signalling Technology	1:5000
Anti GST Tag Monoclonal	8-326	ThermoFisher Scientific	1:500
Anti-HA	#3724	Cell Signalling Technology	1:1000
Anti-His Monoclonal antibody	#2366	Cell Signalling Technology	1:1000
Anti 6xHis Tag Monoclonal	MA1-135	ThermoFisher Scientific	1:1000
Anti-Myc tag HRP-Conjugated	#14038	Cell Signalling Technology	1:1000
Anti-OSR1	S636B	MRC-PPU Univ. of Dundee	2 µg/mL

Antibody	Identification Code	Supplier	Conc./ Dilution
Anti-OSR1	#2281	Cell Signalling Technology	1:1000
Anti-SPAK	S551D	MRC-PPU Univ. of Dundee	2 µg/mL
Anti-SPAK	S637B	MRC-PPU Univ. of Dundee	2 µg/mL
Anti-SPAK	#2281	Cell Signalling Technology	1:1000
Anti-SPAK pS373	S670B	MRC-PPU Univ. of Dundee	2 µg/mL
Anti-Ubiquitin	#3933	Cell Signalling Technology	1:1000
Anti-WDR3	102-1161	RayBiotech	1:1000
Anti WDR6	PA5-41984	Invitrogen	1:1000
Anti-WNK1 (residue 61-661)	S079B	MRC-PPU Univ. of Dundee	2 µg/mL
Anti-WNK1 (residue 2360-2382)	S062B	MRC-PPU Univ. of Dundee	2 µg/mL
Anti-WNK1	#4979	Cell Signalling Technology	1:1000
Secondary Antibodies:			
Anti-Rabbit IgG, HRP-linked	#7074	Cell Signalling Technology	1:2500
Rabbit Anti-Sheep IgG H&L (HRP)	ab97130	Abcam	1:2500
Anti-Mouse IgG, HRP-linked	#7076	Cell Signalling Technology	1:2000

2.1.7 Peptides

The RFQV (Biotin-Ahx-SK-18 331938), AFQV (Biotin-Ahx-SK 372447), pS325-OSR1 (Biotin-Ahx-KG19 479896), S325-OSR1 (Biotin-Ahx-KG-19 479895) were purchased from GL Biochem (China). The peptides had the following sequences: RFQV (Biotin-C_6-SEEGKPQLVGRFQVTSSK), AFQV (Biotin-C_6-SEEGKPQLVGAFQVTSSK), S325-OSR1 (Biotin-C_6-KKVRRVPGSSGRLHKTEDG) aa 316-334, pS325-OSR1 (Biotin-C_6-KKVRRVPGSpSGRLHKTEDG) aa 316-334.

2.1.8 Plasmids

2.1.8.1 cDNA plasmid for mammalian protein expression

Plasmids pcDNA5D-FRT-TO-FLAG-CAND1 (DU25404), pEBG-GST-HA-OSR1 (DU44767), pCMV5-HA-Ubiquitin (DU3650), pEBG-GST empty, pcDNA5D-FRT-TO-6xHis-WDR3 (DU63480), pcDNA5D-FRT-TO-6xHis-WDR6 (DU63606), plasmids for the fragments of GST-HA-OSR1 (pEBG6P-GST-HA-OSR1 1-311 (DU6018), pEBG6P-GST-HA-OSR1 1-363 (DU6019), pEBG6P-GST-HA-OSR1 1-435 (DU6020) and pEBG6P-GST-HA OSR1 429-end (DU6586)) and pEBG6P GST-HA SPAK S373/E (DU10061) were purchased from MRC-PPU Reagents and Services, University of Dundee. pcDNA5D-FRT-TO-FLAG-CAND1 expressing Flag-CAND1 with parental plasmid pcDNA5D-FRT-TO was inserted by FLAG-CAND1 in *Not*I restriction site. pEBG-GST-HA-OSR1 containing GST-HA-OSR1 insert in pEBG6P as parent plasmid. pCMV5-HA-Ubiquitin was inserted by HA-Ub in *BamH*I restriction site as *N*-terminal insert for mammalian expression. Both pcDNA5D-FRT-TO-6xHis-WDR3 and pcDNA5D-FRT-TO-6xHis-WDR6 contain WDR3 or WDR6 insert in the *Bam*HI restriction site for mammalian expression. The GST-HA was inserted as N-terminal of OSR1 fragments in *Bam*HI restriction site of pEBG6P parental plasmids for mammalian expression. GST-HA SPAK with a mutation on serine 373 to glutamic acid was inserted in pEBG6 vector plasmid.

Plasmids pcDNA3-Myc3-CUL4A (#19951), pcDNA3-Myc3-CUL4B (#19922), pcDNA3-Flag-DDB1 (#19918), and pcDNA5-FRT/TO-Venus-Flag (#40998) as FLAG empty vector were purchased from Addgene. The gene of interest in all the plasmids were inserted in the *N*-terminal of the parental plasmid. Myc3-CUL4A was inserted in pcDNA3 *Eco*RI (5') and *Apa*l (3') cloning site. pcDNA3-Myc3-CUL4B with CMV as a promoter was inserted in pcDNA3-Myc3 as vector backbone. FLAG-DDB1 insert on pcDNA3 as parent plasmid used CMV as a promoter.

2.1.8.2 sgRNA plasmids for gene knockout by CRISPR

sgRNA plasmid pairs that were used to knock out WDR3 and WDR6 using Dual Nickase CRISPR were purchased from MRC-PPU Reagents and Services, University of Dundee. Antisense guides were cloned into the Cas9 D10A vector p335 (Amp^r) and sense guides into pBABED puro U6 (Amp^r). It comprises of pX335-WDR3 Antisense A (which will be denoted as WDR3 As A), pBABED-WDR3 Sense A (WDR3 S A), pX335-WDR3 Antisense B (WDR3 As B), pBABED-WDR3 Sense B (WDR3 S B), pX335-WDR6 Antisense A (WDR6 As A), pBABED-WDR6 Sense A (WDR6 S A), pX335-WDR6 Antisense B (WDR6 As B), pBABED-WDR6 Sense B (WDR6 S B), pX335-WDR6 Antisense C (WDR6 As C), pBABED-WDR6 Sense C (WDR6 S C). The WDR3 and WDR3 gene locus showed the sequences that were used for designing the sgRNA to create WDR3 and WDR6 knockout (see Figure 7.1 and 7.2 in Chapter VII. Appendices).

2.1.9 Primers for knockout CRISPR clone confirmation

The primers for clone confirmation as synthetic nucleotides were synthesised by Sigma-Aldrich and provided by MRC-PPU Reagents and Services, University of Dundee. The primers were designed in the location, as is shown in the sequence map of WDR3 and WDR6 locus (Figure 7.3 and 7.4 in Chapter VII. Appendices). The information about all the primers is detailed in **Table 2.2.**

Table 2.2 PCR primers for clone confirmation

Primer	Nucleotide sequences
WDR3 ex2 F (Forward primer)	5'-ACTAACCTAGTAGAACCAAGGCACC-3' (base 5510-5534)
WDR3 ex2 R (Reverse primer)	5'-ACTTGATGCTTGGCTAGCTAGACC-3' (base 5910-5933)
WDR6 ex2 C F (Forward primer)	5'-GACCAGGTCTGCTCAAGGACC-3' (base 8035-8055)
WDR6 ex2 C R (Reverse primer)	5'-GTATCAGAGAATGCCCACGAACG-3' (base 8445-8467)

2.1.10 siRNA

Human CUL4A siRNA (sc-443554), CUL4B siRNA (sc-37572), DDB1 siRNA (sc-37797), WDR3 siRNA (sc-78573), WDR6 siRNA (sc-78080), control siRNA-A (sc-37007) were purchased from Santa Cruz Biotechnology, Inc. Scrambled shRNA control (Origene TR30013) was a gift from Prof. Nicholas M. Barnes (University of Birmingham). The concentration of siRNA and shRNA were 25 pmol as recommended by the company.

2.2 METHODS

2.2.1 Mammalian Cell Culture

2.2.1.1 Cell thawing

To culture the mammalian cell lines from the frozen stocks, the following steps were performed. The vial of the frozen cell was taken out from -80 ºC to the ice. The cells were always kept in the ice to be thawed. Once the last piece of ice in the vial had melted, the cell suspension content in the vial was transferred to the T25 flask with 10 mL of complete growth media. At this step, the thawed cell could be also be pelleted by centrifugation at 1,000*g* for 5 min before the cell was resuspended in 1 mL growth media and transferred to the T25 flask. The cells were then incubated in a CO_2 incubator with 5% CO_2 at 37 ºC. On the following day, the complete growth media was later replaced with the new complete growth media, and the cells were kept in the incubator until they reached 80-90% confluency. Cell passaging was then performed by transferring the cells to T75 flasks, and the cells were kept growing to be prepared for further use after two cells passaging cycles.

2.2.1.2 Cell culture routine maintenance

Cell subculturing was performed by emptying the growth media from the T75 flask. PBS ~2-5 mL was used to wash the cell by pipetting down the buffer to the flask surface opposite to the adhered cells, and the flask was swirled to allow sufficient

wash. A 2 mL of trypsin, a cell dissociation reagent, was added to the cells after the PBS was discarded. The cells were then kept in the CO_2 incubator for 2 min to increase the dissociation rate. As much as 8 mL of complete growth media were then added to the flask to make cell suspension. A 1 mL from the total of 10 mL of cell suspension was transferred to the 15 mL of complete growth media in the new T75 flask before the cells were incubated in a CO_2 incubator.

U266 cell growth was maintained as suspension cell (~1-5x10^5 cells) in a T75 flask with constant shaking (12 rpm) in 37 °C, 5% CO_2 incubator. As a non-adherent cell, U266 cells were subcultured every 5-7 days by performing additional centrifugation and cell counting to the procedure for adherent cells. The cell suspension in the flask was transferred to the 25 mL universal centrifuge tube. After centrifugation (1,000*g* for 5 min), the growth media, as a supernatant layer, was discarded. 1 mL PBS was added to the pelleted cell, and the cells were resuspended before it was spun down and the supernatant was discarded. Another 1 mL of complete growth media was then added to washed cell pellet to generate cell suspension. Based on the cell number after cell counting, some volume of cell suspension was transferred to the T75 flask with 15 mL complete growth media, so the cell number was ~1-5x10^5 cells. The cells were then incubated in a CO_2 incubator with 5% CO_2 at 37 °C with constant shaking (12 rpm).

In order to check mycoplasma contamination, mycoplasma testing was always performed to all mammalian cell lines, which were cultured for the first time and to the cell culture every year. The test utilised PlasmoTest™ kit (InvivoGen).

2.2.1.3 Cell Freezing

Cell freezing was achieved typically for at least two vials for the first five passaging cycles from the original cell stock. After cell dissociation step (for the adherent cells) and centrifugation at 1000*g* for 5 min, the growth media was discarded. Then 2-4 mL

of freezing media, which comprised of complete growth media and 5% DMSO, was added to the pelleted cells to obtain cell suspension. As much as 1 mL cell suspension was distributed on each cryovials tube and immediately transferred to the Mr Frosty box before being stored in -80 °C freezer.

2.2.1.4 Cell Counting

Cell counting was performed using a Beckman Coulter counter machine. 100 µL from 1 mL of cell suspension was transferred to the special cuvette for the counter machine, and 10 mL of sterile isotonic water was added. The cuvette was placed in the cuvette holder in the machine, and the cell counting started after the start button was pressed. The counter calculated all the particles with the size between 9-30 µm and displayed the cell number in the monitor. The displayed number was corrected with particle/cell number from the blank (isotonic water only) in 200-fold dilution factor. The cell number was then calculated using the following formula:

$$\text{Total cell number (cells)} = \text{A x } 200 \text{ x B}$$

Where A = cell number displayed, B = volume of cell suspension (mL) and 200 is the dilution factor.

2.2.1.5 Hypotonic condition for cell culture

The hypotonic condition was applied to stimulate WNK signalling by replacing media with hypotonic low-chloride buffer pH 7.4 (Moriguchi *et al.*, 2005) for 30 min incubation in 37 °C, 5% CO_2.

2.2.2 Preparation of total protein lysates

2.2.2.1 Total protein lysates from adherent cell HEK293

Cell culture with 70-80% confluency was lysed as follows: cells were washed with PBS. A 300-400 µL lysis buffer was used on each 10 cm dishes. The cells were scraped and transferred to the Eppendorf tube and eventually spun down at 9402*g*

(10,000 rpm with radius rotor 8.4 cm) for 10 min at 4 °C. Finally, the supernatant was transferred to a new Eppendorf tube and stored at -20 °C.

2.2.2.2 Total protein lysate from non-adherent cell U266

As U266 cells were cultured as a suspension, the total protein lysates were prepared differently to those of the adherent HEK293 cells. The cell suspension was centrifuged (212*g* for 10 min) to collect the cell pellet. After the growth media was discarded, the cell pellet was washed with PBS. Following centrifugation (212*g* for 10 min), 1% Nonidet-40 cell lysis buffer was added to the cell pellet. Then, after vigorous mixing using a vortex, the cell suspension was immediately frozen in dry ice for 3 min. Subsequently, the cells were thawed at 42 ºC. This 'freeze and thaw' process was repeated four times. As a final step, centrifugation (13,539*g* for 10 min) was done to get the total protein of U266 cell lysate, which was used for further analysis.

2.2.3 Protein concentration measurement

Protein concentration was measured in 96-well plates using the Bradford Assay (Bradford, 1976). BSA with concentration of 0.125, 0.25, 0.5 and 1 mg/mL was used as protein standard. 5 µL of the standard BSA concentrations given above was used in triplicate in each protein measurement assay. Then, 2 µL of the total protein lysate in triplicate was added. The volume of protein lysate was reduced if the absorbance value was found to be higher than 0.8. Subsequently, 280 µL of Bradford reagent was added to each well that has protein and incubated for 5 min. After that, the absorbance, at 595 nm, was measured using Infinite F200 PRO Tecan® microplate reader.

The absorbance value as a reading output was then analysed to calculate the protein concentration of each sample by linear regression analysis. Initially, the mean absorbance value was calculated from the readings of the triplicate samples. The linear regression standard curve was built by plotting the absorbance as Y value and

protein BSA standard as X value in the XY-scattered chart in Microsoft Excel program. Once the linear regression curve was built, protein concentration was calculated by determining the X value from the linear regression equation $y = bx + a$ which was derived from the curve. The X value was then multiplied by its dilution factor 2.5 and, the protein concentration of each sample was provided in the mg/mL unit. The dilution factor was changed if the protein sample volume to be measured had changed as the protein concentration was determined using 5 µL sample in 280 µL Bradford Reagent. For instance, when 1 µL of the protein sample was used, the dilution factor would be 5.

2.2.4 Peptide pull-down

Buffer A pre-washed Streptavidin beads were incubated with 1 mg of HEK293 protein lysate at 4 °C for 10 min three times. After the pre-clearing step to allow the clearing of non-specific protein that could bind to the beads, the supernatant was incubated with 3 µg of peptide for 10 min on ice. The fresh new beads were then added, and incubation was performed for 5 min at 4 °C in rolling shaker. Finally, the beads were washed with lysis buffer and buffer A two times. After spinning the beads down and the supernatant was discarded, 50 µL of 1x SDS loading buffer was added. The beads in SDS loading buffer were then boiled at 95 °C for 5 min to be used for SDS-PAGE and MS analysis.

2.2.5 SDS-PAGE analysis

2.2.5.1 SDS-PAGE gel preparation

The SDS-PAGE gels were prepared in BioRad Mini Protean SDS-PAGE apparatus as 8; 10 or 12.5% bis-acrylamide gel. All the gels were denaturing bis-acrylamide gels with 1.0 or 1.5 mm thickness and contained 1% SDS. The differences in gel percentage depended on the molecular weight of the protein of interest that was being detected. The recipe for making the gels is given in Table 2.3.

Table 2.3 Gel recipes for SDS-PAGE analysis

Resolving gel (10mL)	8%	10%	12.5%
1.5M Tris-HCl pH 8.8 (mL)	2.6	2.6	2.6
dH_2O (mL)	4.6	3.8	3.2
10% SDS (µL)	100	100	100
10% APS (µL)	100	100	100
TEMED (µL)	10	10	10
30% Acrylamide/ 0.8% Bis-acrylamide (mL)	2.6	3.4	4.0

Stacking gel (10mL)	
0.5M Tris-HCl pH 6.8	2.5 mL
dH_2O	5.95 mL
10% SDS	100 µL
10% APS	100 µL
TEMED	10 µL
30% Acrylamide/ 0.8% Bis-acrylamide	1.34 mL

2.2.5.2 SDS-PAGE

The gels were placed in the gel holder and ran using the running buffer (recipes were described in Section 7.1 Chapter VII. Appendices). 20 µg of the protein sample was loaded in each well unless otherwise specified. 3 µL of protein ladder was used as standard (PageRuler Plus Prestained Ladder, ThermoFisher Pierce). The separation was run on 200 V for 45 min.

2.2.5.3 Gel Staining

Gel staining was performed using the NOVEX Colloidal Blue Staining Kit (LC6025, Invitrogen) for Bis-Tris Gels. At first, the fixing solution, which consisted of 40 mL deionised water, 50 mL methanol and 10 mL acetic acid, was prepared. The staining solution was also made by combining 55 mL deionised water, 20 mL methanol, 20 mL stainer A. The gel was then immersed in the fixing solution for 10 min at room temperature followed by shaking the gel in the staining solution without stainer B for another 10 min. To the existing staining solution, 5 mL of stainer B was added, and the gel was shaken further in the staining solution overnight. In the following day, the

staining solution was discarded and replaced by 200 mL deionised water. The gel was then shaken for at least 7 h in water to clear the background before gel imaging on a Gel Doc imaging system.

2.2.5.4 Gel Imaging

Visualisation of the protein after separation by SDS-PAGE was performed using G:Box SynGene XX6 Gel Imaging system, which was operated by GeneSys software. The gel was positioned in the transilluminator box that was covered by visible light converter screen (white screen) before the GeneSys software was started. After the software was launched, the icon of 'Gels' in the home screen followed by 'Visible Protein Gel' was selected from the drop-down list under 'Gel' menu. The 'Coomassie Blue' was selected in the Dye selection menu before moved to the next screen. If the gel positioning needs to be adjusted, then the focus, iris and zoom in the 'Lens control' menu was modified before the picture of the gel was captured and saved as TIF file in the next screen.

2.2.6 Mass Spectrophotometry analysis for protein identification

After protein separation by SDS-PAGE and gel staining using NOVEX Colloidal Blue Staining Kit (LC6025, Invitrogen), the gel was sliced on the molecular weight of protein interest. Gel slices were then washed and submitted to the Advanced Mass Spectrometry Facility in School of Bioscience University of Birmingham. After proteins were digested by trypsin, the peptides were separated by liquid chromatography which was coupled to the mass spectrometer utilising Thermo Fisher Velos Orbitrap ETD mass spectrometer equipped with nano-flow liquid chromatographic (LC) system Triversa Nanomate and nanoLC (LC-MS/MS). The peptides masses were determined from mass spectrometry, and eventually, the peptide sequences were defined through MS/MS. The detected peptide sequences were matched against the UniProt protein database. The RAW files were then analysed by Mascot algorithm

(http://www.matrixscience.com) the significant probability of identified proteins was P > 95.0% with at least two unique peptides were identified (Mehellou *et al.*, 2018).

2.2.7 Immunoprecipitation

2.2.7.1 Antibody conjugation

Anti-SPAK or OSR1 full-length antibodies were conjugated to Protein G-Sepharose beads via covalent cross-linking method using DMP with a ratio 1:1 (Thastrup *et al.*, 2012). The beads in one volume were pre-washed with PBS three times using centrifugation at 847*g*, 4 °C for 2 min. The same ratio of antibody was added to the pre-washed beads, and the mixture was then incubated for 1 h, 4 °C on rotator shaker. After completing the incubation, the mix of pre-washed beads and antibody was spun at 847*g*, 4 °C for 2 min and washed with PBS. The washing was done for three times. 1 mL of 0.1 M sodium borate pH 9.0 was added to the beads and repeated the washing by 0.1 M sodium borate pH 9.0 for three times. 1 mL of 20 mM DMP in 0.1 M sodium borate pH 9.0 was resuspended to the bead to build the covalent linkage, and the mixture was incubated at room temperature for 30 min in rotator shaker. The cross-linking process was repeated two times. Following incubation at room temperature, the mixture was spun down, and the supernatant was discarded. The antibody-conjugated beads were then resuspended with 1 mL of 50 mM Glycine pH 2.5. The mixture then was spun, and the supernatant was discarded. The washing step was repeated for another cycle before the supernatant was washed, and 1 mL PBS was added to the antibody-conjugated beads for 4 °C storage.

2.2.7.2 Immunoprecipitation by antibody-conjugated beads

Protein lysates from HEK-293 were pre-cleared by incubation with Protein G-Sepharose beads at 4 °C for 10 min three times. The supernatant then was incubated overnight in rolling shaker with 20 µL of SPAK or OSR1-Protein G-Sepharose conjugated antibody at 4 °C. Eventually, the immunoprecipitated protein was washed with CHAPS lysis buffer and buffer A (10 mM Tris/HCl (pH 8), 0.1 mM EGTA) two

times each. The collected beads were then prepared for SDS PAGE by adding 1x SDS loading buffer 150 µL and boiled 95 °C for 5 min.

2.2.8 Pull-down assay

2.2.8.1 GST Pull-down

Three times washing of GST beads by 1 mL PBS or buffer A with centrifugation 500 rpm, 1 min on 4ºC was done before use. GST pull-down employed 1 mg of total protein lysate from HEK293 cell, which was incubated overnight with 40 µL of GST beads on 4 ºC with constant shaking. The beads then were collected by centrifugation 24*g*, 1 min on 4 ºC. Subsequently, one mL CHAPS lysis buffer and buffer A were used for washing the beads twice each time. For further immunoblotting analysis application, 100 µL of 1x SDS loading buffer was added to the beads and gently mixed before boiled 95 °C for 5 min.

2.2.8.2 FLAG Pull-down

The resin beads were prepared by washing the beads with TBS buffer for three times. The beads were then equilibrated with TBS buffer before being used to pulling down 1 mg total protein lysate for overnight in 4 °C. SDS sample for immunoblotting analysis were prepared by washing the overnight incubation of the mixture of beads and protein lysate with TBS buffer three times. Finally, 2x SDS loading buffer was added and boiled for 95 °C and 5 min before it was ready to be analysed.

2.2.8.3 His Pull-down

His pull-down assay was performed using HisPur Ni-NTA resin beads. One mg of total protein lysate of HEK293 cell was incubated with 500 µL of binding buffer and 20 µL Ni-NTA resin bead at 4 °C for overnight in a rotator shaker. The beads then pelleted the next day by centrifugation 46*g* for 1 minute and washed three times using washing buffer. The beads then eluted by denaturation with 1x SDS loading buffer and boiled for 95 °C and 5 min before underwent for immunoblotting analysis.

2.2.9 Plasmid amplification and extraction

2.2.9.1 Plasmid maxi-prep

Plasmid DNA extraction from the overnight cultured cell was done according to company protocol recommendation using Qiagen Plasmid Maxi Kit (Cat. No.12163) with slight modification. Overnight bacterial culture was harvested by centrifugation 6,000 rpm using SLA-1500 rotor on Sorvall RC5B Plus centrifuge (with rotor radius 135.9 mm is equal to 5465*g*) for 15 min at 4 °C. The harvesting process was repeated for all (typically 2 litres) bacterial culture using the same 250 mL propylene centrifuge tube. The supernatant then was discarded, and the bacterial pellet was resuspended with 10 mL of Buffer P1. The cell pellet and Buffer P1 suspension then was transferred to 50 mL conical tube and added 10mL Buffer P2. The mixture then was vigorously mixed by inverting six times and incubated at room temperature for 5 min. The solution generated a colour change to blue as the LyseBlue reagent were added to Buffer P2 before use. Ten millilitres of pre-chilled Buffer P3 was added to the solution, and after the solution was mixed vigorously by inverting six times, incubation on ice for 20 min produced a colourless solution. The solution was then centrifuged to separate the cell debris at 8,000 rpm for 10min using SLA-600TC rotor (equal to 10,509*g* with rotor radius 147.0 mm). The supernatant which was separated from the debris were transferred to the QIAGEN tip which had been equilibrated with 10 mL Buffer QBT before use. After the supernatant which contains DNA was passed to enter the resin in the QIAGEN tip by gravity flow, the QIAGEN tip was washed by Buffer QC 30 mL twice. The bound DNA in the resin was then eluted by adding Buffer QF to the new 50 mL conical tube. The eluted DNA which was collected in 50 mL conical tube was then precipitated by addition of 10.5 mL (0.7 volumes) room-temperature of isopropanol. The precipitated DNA was then separated from isopropanol by centrifugation at 8,000 rpm for 30 min using SLA-600TC rotor (equal to 10,509*g* with rotor radius 147.0 mm) at 4 °C. The supernatant was then decanted very carefully so

that the DNA pellet was still intact in the tube. The pellet DNA was then washed with 5 mL of 70% ethanol and separated from pellet DNA by centrifugation at 8,000 rpm for 10 min using SLA-600TC rotor (equal to 10,509*g* with rotor radius 147.0 mm). Finally, the pellet DNA was air-dried by let them dry in an inverted open tube and then dissolved in 150 µL of sterile DNAse and RNAse free distilled water. The DNA was kept in -20 °C freezer for long term storage.

2.2.9.2 The DNA concentration and purity measurement

The DNA concentration and purification measurement applied PHERAstar FS (BMG Labtech) or NanoVue Plus (GE Healthcare Lifesciences) to determine the quality DNA. The analysis was based on the UV-Visible spectrophotometry principle. A sample of 2 µL DNA was placed in the optic in the sample plate, and the absorbance of the sample was read against the reference (distilled water) as a blank.

The output from the computer showed the DNA concentration in µg/mL. The ratio of absorbance in 260 nm/230 nm and 260 nm/280 nm were also shown to determine DNA purity. DNA is considered having high purity if the ratio of absorbance 260 nm/230 nm is 1.7-1.9 and absorbance 260 nm/230 nm is ~2.2. cDNA plasmid concentration and its absorbance, which represents its purity, were summarised in **Table 2.4.**

Table 2.4 Plasmid DNA concentration and purity

Plasmid	Concentration (µg/µL)	A260/280 ratio	A260/230 ratio
pcDNA5D-FRT/TO-FLAG-CAND1	1.1	1.9	2.3
pcDNA3-Myc3-CUL4A	0.9	1.9	2.2
pcDNA3-Myc3-CUL4B	1.0	1.8	2.3
pcDNA3-Flag-DDB1	1.1	1.8	2.1
pEBG-GST-HA-OSR1	0.7	1.9	2.3
pCMV5-HA-Ubiquitin	0.9	1.9	2.2
pcDNA5-FRT/TO- (empty FLAG)	1.1	1.9	2.3
pEBG-GST- (empty GST)	1.0	1.9	2.3
pCMV-HA (empty HA)	1.1	1.9	2.1
pcDNA3-Flag-OSR1	1.0	1.8	2.2
pcDNA3-Flag-Ubiquitin	1.0	1.8	2.1
pcDNA5D-FRT-TO-6xHis-WDR3	0.3	1.7	2.2
pcDNA5D-FRT-TO-6xHis-WDR6	0.9	1.8	2.3
pEBG6P-GST-HA-OSR1 1-311	0.1	1.7	2.4
pEBG6P-GST-HA-OSR1 1-363	1.9	1.8	2.3
pEBG6P-GST-HA-OSR1 1-435	2.1	1.8	2.3
pEBG6P-GST-HA OSR1 429-end	2.1	1.8	2.3
pEBG6P-GST-HA SPAK S373/E	0.7	1.8	2.3

2.2.10 Plasmid DNA transformation or transfection

2.2.10.1 Bacteria Transformation

Transformation of all cDNA plasmids to *E.coli* DH5α (Invitrogen) was done by heat shock at 42 ºC for 90 s. After incubation in heat shock condition, the mixture eventually was spread onto LB agar media containing ampicillin 100 µg/µL and incubated on 37 ºC for 24 h. Other plasmids which were purchased as colony transformants in a slant agar directly undergoes to the culture step. Several colonies of transformants were grown in 500 mL of LB broth containing ampicillin 100 µg/µL by incubation at 37 ºC overnight with 180 rpm shaking to increase the copy number of recombinant DNA. Plasmid DNA was ready to be extracted from overnight culture and followed by DNA concentration and purity measurement.

2.2.10.2 Mammalian DNA transfection

cDNA plasmids for mammalian expression were transiently transfected or co-transfected to HEK293 cell using PEI in free serum and free antibiotic growth media. The concentration of cDNA plasmids that were used in the transfection was 2.5 µg of DNA unless otherwise stated. The PEI (1 mg/mL) was used in volume ratio 1:1 with the volume of DNA. Transfected cells were then lysed 2-4 days post-transfection and subjected to be applied for further experiments. Level of protein overexpression was confirmed by immunoblotting using respective tag antibody.

2.2.11 siRNA Knockdown

siRNA transfection was performed on HE293 cell on ~60-80% cell confluency. Preparation of RNA-lipid complexes was initiated with a dilution of siRNA and lipofectamine in a separate 150 µL of free serum media to get a final concentration of siRNA 25 pmol (according to the manufacturer recommendation). Diluted siRNA then was added to diluted lipofectamine in 1:1 ratio. After incubation in room temperature for 5 min, 250 µL siRNA-lipid complex was added to the cell which grown in 2 mL of growth media. Analysis of protein level to confirm the knockdown was performed by immunoblotting after three days of transfection.

2.2.12 Drug treatments

2.2.12.1 MLN4924 and MG132 treatment on HEK293 cell

MLN4924 and MG132 treatments were applied on HEK293 cells with ~80% confluency. Stock compounds in the concentration of 100 mM were prepared in 100% DMSO as a solvent. Serial dilution was then carried out to generate concentrations in the range 10 – 0.1 mM. Thus, the highest final DMSO concentration in the cell was less than 1%. The cell which was treated with the compounds in the range concentration of 0.01 to 10 µM then were incubated in 37 ºC with 5% CO_2 for 1; 3; 6 or 24 h. Drug concentration for each experiment was varied (see on each figure

legends for the drug concentration that were used). WNK-SPAK/OSR1 signalling stimulation was achieved by treating the cell with the hypotonic low-chloride buffer for 30 min before cell lysis (Moriguchi *et al.*, 2005).

2.2.12.2 Treatment of Thalidomide, Pomalidomide and Indisulam in HEK293 and U266 cell

The cells with ~80-90 % confluency were cultured in 6-well plate before the treatment. For creating a hypotonic condition, growth media of the cultured cell were replaced by hypotonic low-chloride buffer and incubated for 30 min prior to treatment. All diluted concentration of compounds was prepared from 100 mM of stock compounds in DMSO 100%. A serial dilution of stock compounds was prepared to achieve the final concentration of the compounds so that the highest concentration of DMSO in the cell was 1%, which is considered do not cause cell toxicity. Drug concentration for each experiment was varied (see on each figure legends for the drug concentration that were used). After adding the drug in a volume dropwise to reach a final concentration in the cell culture, the cells then were incubated for 1; 3; 6; or 24 h. Total protein lysate was then prepared to be used for further western blot analysis.

2.2.13 Western Blotting

2.2.13.1 SDS-PAGE, Protein transfer and Ponceau staining

SDS-PAGE gel preparation and analysis was detailed in section 2.2.5. The protein which was separated then underwent transfer process to nitrocellulose membrane (Amersham 0.45 µm Nitrocellulose for Western blotting, GE Healthcare Lifesciences). The transfer was done by wet transfer method in transfer buffer (recipes was described in Section 7.1 Chapter VII. Appendices) under 100 V transfer condition for 1 h or 1 h 10 min.

2.2.13.2 Protein detection by immunoblotting

Membranes were incubated in 10% skim milk blocking buffer (see Section 7.1 Chapter VII. Appendices for recipes) for 30 min at room temperature after the transfer process. The membranes were then incubated on a primary antibody in 5% BSA or 5% skimmed milk in TBS-T overnight at 4 °C or 1 h at room temperature. After membrane washing process with TBS-T for 5 min three times, the secondary antibody respective to the specificity for the antibody species and isotype of the primary antibody, then was used to incubate the membrane. List of primary antibodies and a secondary antibody that was used in this research is described in Table 2.1. Finally, protein detection system either using the ECL® reagent (Amersham Bioscience) film processing or SynGene G:Box Chemi XX6 gel doc system imaging was performed. If the imaging process was using the film processor, the membrane was placed in the X-ray film cassette. The ECL reagent in ~1 mL per 10 x 6.5 cm membrane was added dropwise to the entire membrane surface. One layer of clear plastic was placed on top of the membrane to cover it. A gentle wipe was done to clean the ECL reagent excess and assure that the ECL reagent was fully covered the membrane surface. The X-ray film (Amersham Hyperfilm ECL – GE Healthcare) then was placed on top of the plastic layer. After a specific developing time, the film was then inserted into Film Processor machine (Konica Minolta).

For imaging process using SynGene G:Box Chemi XX6 imaging system, the membrane which was covered with a layer of clear plastic was placed in the illuminator inside the box. After the GeneSys software started and the menu ‘Blots’ was selected from Home screen display. The sample selection of ‘Chemi Blot’ was then selected either for ‘Chemi Blot (Single Image)’ or ‘Chemi Blot (Series)’ to capture multiple images. To capture a single image, after ‘Chemi Blot (Single Image)’ icon was selected, the blot membrane size (sample size) was chosen from the drop-down list depending on the membrane that was used, typically ‘Biorad blot (7x8.4cm)’. In

the dye selection menu, the chemiluminescent substrate icon ‘ECL’ was selected and followed by checking the ‘Visible marker’ box to image the protein marker before proceeding to click the green bouncing arrow to move to next screen. After the sample positioning was adjusted its focus and zoom, the green bouncing arrow was then clicked to move on to the next screen. In the capture screen, the ‘Faster Speed/High Definition’ bar was slide to the designated capture time or towards the High Definition side to get a higher quality image. The ‘Capture’ button then was pressed to capture an image. Finally, the picture was saved as a TIF file by clicking the ‘disk’ icon. In order to capture multiple images, the number of captures with each exposure time was typed in the provided box before the ‘Capture’ button was pressed.

2.2.13.3 Bands Intensity Quantification by ImageJ software

The intensity of the blot from western blot analysis, if it was required, was quantified using the ImageJ software program. The analysis was initiated by selecting ‘Rectangular selection’ tool and draw a rectangular shape outlining the surrounding of selected bands. Then it was followed by entering the command *Analyse>Gels>Select First Lane* to highlight the band of protein interest as lane ‘1’. This command was then applied for all the protein of interest bands which then denoted as lane ‘2’, lane ‘3’, and so on by using command *Analyse>Gels>Select Next Lane*. The plot profiles were then generated by typing command *Analyse>Gels>Plot Lanes*. The plots were showing curves where the width represented the density of the bands, and the height represented the darkness of the bands. For each curve, the ‘Straight lines’ tool was used to define the area of the curves by drawing the straight line in the bottom of the curve so that the measurement was taken by omitting the background. The ‘Wand’ tool was then applied to select each of the curves which generated a separated ‘Result’ window. The Result window was showing the measurement of the band's densities of the protein of interest as an area under the curve. The numbers were then exported to Microsoft Excel, and the calculation of

relative density of each band, which was normalised to the house-keeping protein such as GAPDH band was performed.

2.2.14 *In silico* analysis for protein-protein docking simulation

Simulation of protein-protein interaction between OSR1 and CRL4 components was performed using ClusPro 2.0 (Kozakov *et al.*, 2017). This free online web server for protein-protein docking performs three computational steps: 1) rigid-body docking utilises billions of global protein conformation databases, 2) clustering the 1000 lowest energy structure based on root-mean-square deviation (RMSD) to obtain the representative model clusters, 3) sorting the selected structure based on energy minimisation.

The PDB ID for OSR1 (2VWI), DDB1 (2B5M), DDB1-CUL4A-Rbx1-SMV5 (2HYE), CUL4B (4A0C) was used as input in the web page. As there is no 3D structure available for WDR3 and WDR6, a homology model for WDR3 and WDR6 were used as input. These homology models were built utilising SWISS-MODEL homology modelling (Waterhouse *et al.*, 2018). Homology model for WDR3 was built using a template 5wlc.22.A (38.10% sequence identity to Utp12 protein with Global Model Quality Estimation (GMQE) 0.63). The WDR6 homology model utilised 2ymu.1.A as the template (22.56% sequence identity to WD-40 repeat protein with GMQE 0.27). These templates were chosen due to their sequence identity percentage which was the highest among other templates. The homology model validation for WDR3 model utilising Ramachandran plot assessment results 89.95% residues in the favoured region and 2.51% residues are in the outlier region. The WDR6 model has 81.81% residue in the favoured region and 5.2% residues are in the outlier region.

Four sets cluster models were generated based on the scoring algorithms designated as balanced, electrostatic-favoured, hydrophobic-favoured and Van der Waals + electrostatic. As the properties of the complex are unknown, then the lowest energy

model clusters based on balanced coefficient sets were chosen to be visualised and analysed using PyMOL software.

2.2.15 WDR3 and WDR6 knockout by CRISPR Dual Nickase method

Dual Nickase CRISPR for WDR3 and WDR6 knockout was attempted based on Dual Nickase CRISPR protocol from MRC-PPU University of Dundee. The protocol was done in several stages, as shown in **Figure 2.1.** and described in the following paragraphs.

Stage 1. Transfection

Prior to transfection, maxi prep DNA was performed for each DNA guides using Qiagen Plasmid Maxi Kit (Cat. No.12163). The DNA concentration and purification measurement applied NanoVue Plus (GE Healthcare Lifesciences) to determine the quality DNA. Based on the quality and purity of DNA guides which is showed in Table A1.1, only cDNA plasmids WDR3 As A, WDR3 S A, WDR3 As B, WDR3 S B, WDR6 As C, and WDR6 S C were transfected to HEK293 cells with PEI method. cDNA guided pairs were transfected to the overnight culture of $1x10^6$ of HEK293 cells in 10cm dishes. Each transfection mixture, which was consisted of 1 mL serum-free DMEM, 20 µL PEI (1 mg/mL) and one µg each of sense or antisense guide plasmids, were added dropwise to the cells after 10 s of vortexing and 30 min incubation in room temperature. Transfection was also done by mixing antisense and sense guide primer pairs and 20 µL PEI in 1 mL of serum-free DMEM. The DMEM as complete growth media were then replaced by DMEM complete media containing Puromycin 2 µg/mL for clonal selection on the next day. Media replacement with DMEM growth media containing Puromycin was continued on the next 24 h to assure the selection process. On the next day, the selection process was stopped by replacing the DMEM growth media containing Puromycin with recovery media. After 24 h of recovery, the selected cells were undergoing initial screening of pool by western blot. The level of knockdown

was considered as successful when the knockdown achieved 20-80% reduction in the protein level compare to the WT.

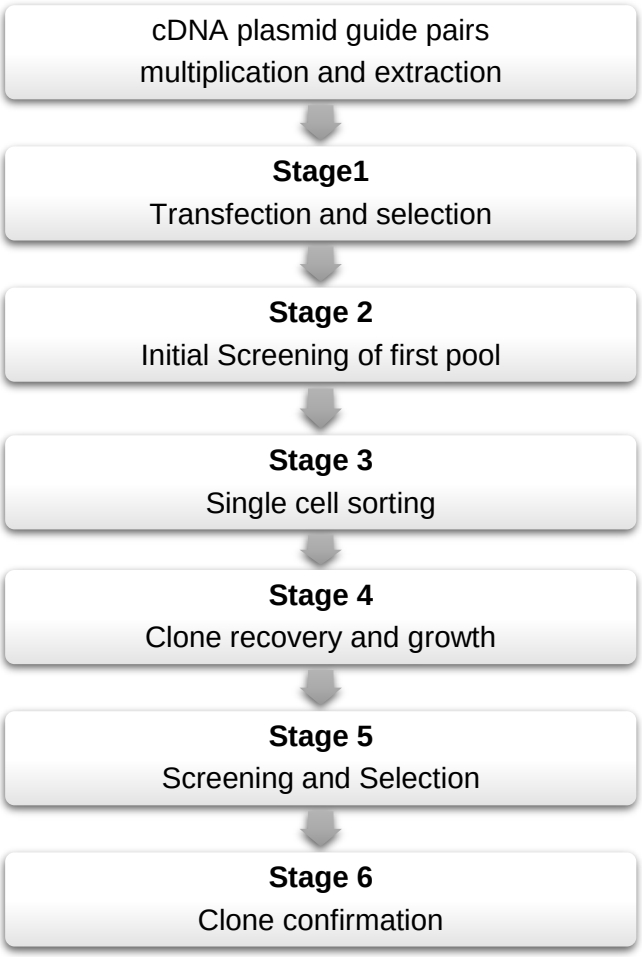

Figure 2.1. Schematic diagram of stages for WDR3 and WDR6 knock out by CRISPR dual nickase. The protocol was provided by MRC-PPU University of Dundee.

Stage 2. Initial screening of pool

The screening for the first pool of transfection was done to the unsorted plated cells by western blot to check the knockdown of the target gene compared to the wild type (WT). The selected cells ($2x10^5$ cells) from DMEM growth media containing puromycin and WT cells were lysed to extract total protein lysate using freeze and thaw method. 80 µL of lysis buffer containing 1% nonidet-40 was added to the cell pellet following centrifugation 212*g* for 10 min and washing with PBS. After vigorous

mixing using a vortex, the cell suspension immediately was being frozen in dry ice for 3 min. Subsequently, the cell was thawed on 42 ºC. This 'freeze and thaw' process was repeated for four times. Centrifugation 13,539*g* for 10 min was done to get the total protein lysate of selected cells. SDS sample for western blot analysis was then prepared by adding 20 µL of 4x SDS loading buffer and boiled for 95 °C and 5 min.

Stage 3. Single-cell sorting

As the DNA guides do not contain GFP fusion, single-cell sorting to obtain a clonal population was performed using single-cell dilution protocol instead of flow cytometry (Gross *et al.*, 2015). Single-cell dilution for selected cells was calculated to get five cells/well (25 cell/mL) on two 96-well plates. The suspension cells in a volume based on the previous calculation were mixed with pre-conditioned media. Pre-conditioned media was 0.2 µm filter sterilised media, which was collected from the growth media of healthy cells at about 48 h with no more than 70% confluency. The mixture of cells in the pre-conditioned media then was distributed in all 96 wells with a volume of 200 µL per well. The single-cell growth in each well was observed for 7-10 days with the changing yellow colour of media was used as the sign of cell growth.

Stage 4. Clone recovery and growth

The cell in a well which the colour of media was changed then was transferred to the 24-well plate in duplicate (labelled as plates A and B) to proceed to the screening stage. The transfer was done by adding 50 µL of trypsin to the well of interest in 96-well plate and pipetting 300 µL of media up and down subsequently to detach the cells. The suspension cells then were transferred to the 24-well plate A (Analysis plate). Further 1 mL of media was added to this 24-well plate and mixed well before 650 µL of suspension cell was transferred to the plate B (Clonal plate). The cells were allowed to recover and grow for another seven days before going to the next stage.

Stage 5. Screening and selection

The screening and selection were performed by western blot, followed by PCR. Western blot analysis to check the knockdown compared to the control (WT) was done from plate A according to the method in the initial screening of the first pool (stage 2). Positive clones were then prepared its genomic DNA by using GenElute Mammalian Genomic DNA Miniprep kit (Sigma-Aldrich G1N70) for clone confirmation by PCR analysis.

Stage 6. Clone confirmation

Clone confirmation was done by PCR using PCR-KOD Hot Start (Novogen). PCR mixture which consists of:

- 2.5 µL 10x Buffer
- 2.5 µL 2 mM dNTPs
- 1.5 µL 25 mM $MgSO_4$
- 0.75 µL 10 µM F Primer
- 0.75 µL 10 µM R Primer
- 1.5 µL DMSO
- 0.5 µL KOD
- 100 ng Genomic DNA
- dH20 up to 25 µL

Were used to perform PCR in condition, as shown in **Figure 2.2.** The PCR result was then analysed by DNA Agarose Gel Electrophoresis.

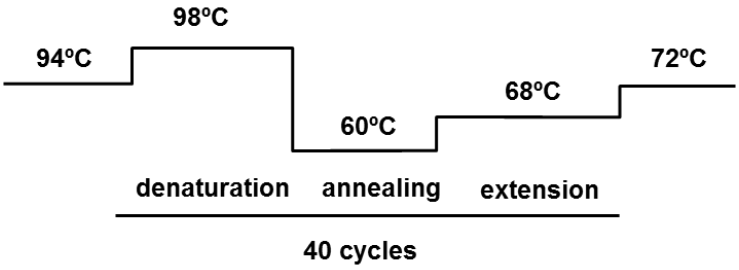

Figure 2.2. Schematic diagram of Hot Start PCR condition for clone confirmation of WDR3 and WDR6 knockout.

2.2.16 Genomic DNA Preparation

Genomic DNA template for PCR was prepared using GenElute Mammalian Genomic DNA Miniprep Kit with slight modification. HEK293 cells in a number of up to $5x10^6$ cells were harvested by centrifugation at 1000*g* for 5 min, and the media was completely removed and discarded. The cell pellet was resuspended in 200 µL 'resuspension solution' and added 20 µL 'RNase A solution' to produced RNA free genomic DNA. After 2 min incubation at room temperature, 20 µL of 'proteinase K solution' was added to the solution followed by 200 µL of 'lysis solution'. The mixture was then vortexed thoroughly (around 15 seconds) and incubated at 70 °C for 10 min. 'GenElute Miniprep binding column' was prepared by adding 500 µL of 'column preparation solution'. The flow-through liquid from the column resulted from the centrifugation at 12,000*g* for 1 min then were discarded. Following the addition of 200 µL of ethanol absolute to the cell lysate and vortexing for 10 seconds, the homogenous solution was transferred by wide bored pipette tip to the treated binding column. The column was centrifuged at 6,500*g* for 1 min, and the collection tube which contained the flow-through liquid is discarded and replaced with the new 2 mL collection tube. A 500 µL of 'wash solution' was added to the binding column to wash the bound DNA. After centrifugation at 6,500*g* for 1 min and the collection tube which contained the flow-through liquid is discarded and replaced with the new 2 mL collection tube. As the second wash step, 500 µL 'wash solution' was added to the binding column and centrifuge at 12,000*g* for 3 min to dry the binding column and free

the column from ethanol. Then, the collection tube which contained the flow-through liquid is discarded and replaced with the new 2 mL collection tube for DNA elution. A 200 µL of 'elution solution' was pipetted directly to the centre of the binding column and incubated 5 min at room temperature to increase elution efficiency before centrifugation at 6,500*g* for 1 min. The eluted DNA then was measured its concentration and determined its purity (as described in Section 2.2.8.2) and kept in -20 °C for long term storage.

2.2.17 DNA Agarose Gel Electrophoresis

2.2.17.1 Gel preparation

Agarose gel that was used for gel electrophoresis is 2% gel. The gel was prepared by dissolving 1 gram of agarose in 50 mL of 1x TAE Buffer by heating in the microwave for 1 min in maximum power. The mixture was swirled to homogenise and allowed to be cooled before 1 µL of ethidium bromide 10 mg/mL in H_2O was added. The mixture then poured into the gel cassette, and a well comb was placed before the gel was solidified. After the gel was solidified, the gel with the cassette was placed in the electrophoresis tank which was already filled with 1X TAE Buffer.

2.2.17.2 Gel loading and running

Genomic DNA or sample from DNA amplification by PCR was mixed with 3 µL of DNA loading buffer (6 g of Sucrose, up to 10 mL distilled water and one grain of Bromophenol Blue). The sample was loaded on to agarose gel alongside with the 2.5 µL of DNA ladder. The electrophoresis was run at 70 V for around 1.5 h until the bands of DNA were separated as required. The bands on the gel were then visualised using SynGene XX6 Gel Doc imaging system.

2.2.17.3 Agarose gel DNA visualisation

In order to visualise DNA from agarose gel electrophoresis, G:Box SynGene XX6 Imaging system was used. The software operation was similar to what is described in section 2.2.5.2 for visible protein visualisation. For this DNA visualisation, after the 'Gels' was selected, then 'DNA Agarose Gel' was chosen from the Sample selection menu. In the Dye selection menu 'Ethidium Bromide' was selected before proceeding to the next screen for adjusting the focus, iris and zoom and capturing the image. As the final step, the captured image was saved as a TIF file.

CHAPTER III.

RESULTS

CHAPTER III. RESULTS

3.1. NOVEL PROTEINS BINDERS TO OSR1 S325

Studying the role of SPAK/OSR1 S-motif phosphorylation was initiated by carrying out peptide affinity pull-down assays. The peptide pull-down was performed by incubating total protein lysates with the short peptides that had been conjugated to biotin. Following streptavidin-biotin pulldown, the proteins which interact with the peptide were eluted from the beads and used for further analysis. This approach is an effective strategy in identifying proteins that interact with specific sites, and it was first introduced in 2004 (Schulze and Mann, 2004) and has been applied widely since then (Vitari *et al.*, 2006, Wysocka, 2006, Villa *et al.*, 2007).

3.1.1. SDS-PAGE and MS analysis of OSR1 S325 and OSR1 pS325 peptide pull-down assay

The pursuit of understanding the function of OSR1 S325 phosphorylation by WNK kinases started by synthesising two *N*-terminally biotinylated 18-mer peptides, which correspond to amino acids 316-334 (KKVRRVPGSSGRLHKTEDG) of human OSR1, with one of them having S325 phosphorylated and the other unphosphorylated (**Figure 3.1.**). These peptides were subsequently incubated with HEK293 cell lysates and then underwent biotin-streptavidin pull-down. As controls, we used an *N*-terminally biotinylated 18-mer RFQV (SEEGKPQLVGRFQVTSSK), which is known to bind endogenous OSR1 and SPAK, and its corresponding single point mutant AFQV (SEEGKPQLVGAFQVTSSK) peptide, which does not bind SPAK and OSR1 (Vitari *et al.*, 2006). As seen in **Figure 3.2.**, RFQV peptide successfully pulled down SPAK, whereas the peptide with R to A mutation (AFQV peptide) did not pull-down SPAK. The pull-down system was shown to be effective for pulling down the protein using the short-fragment peptides.

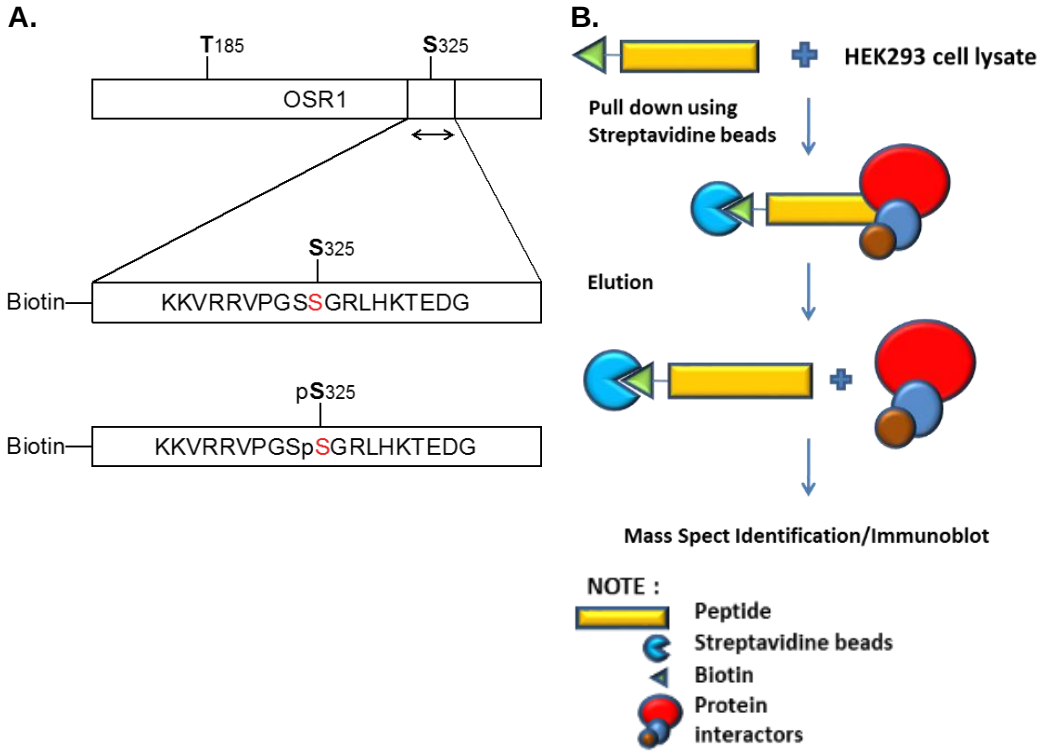

Figure 3.1. Scheme of peptide pull-down assay. (A.) Peptides comprised of 18 or 19-mer contains OSR1 S325, either unphosphorylated or phosphorylated, (B.) attracts proteins from HEK293 cell, which could form binding with the peptides. Protein identification and analysis is performed after washing and elution of the beads.

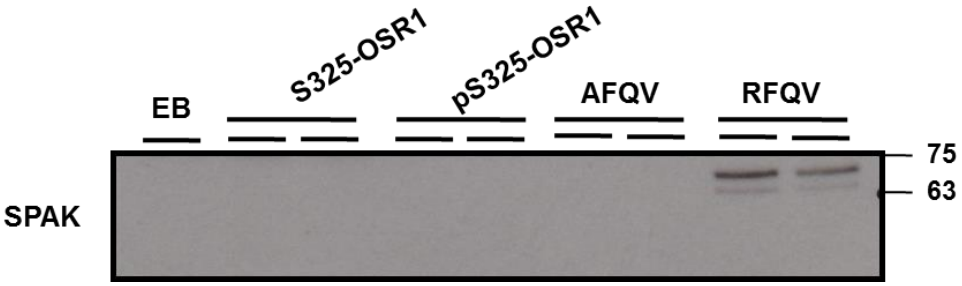

Figure 3.2. RFQV peptide pulled down SPAK protein by peptide pull-down assay. HEK293 cell lysate was subjected to pull-down assay using biotinylated peptides of 18 or 19 amino acid contained non-phospho S325, phosphorylated S325 of OSR1, RFQV and AFQV motif. Immunoblotting of SPAK was performed after peptide pull-down. SPAK was bound to RFQV peptide but not to AFQV peptide. RFQV, arginine phenylalanine glutamine valine; AFQV, alanine phenylalanine glutamine valine. Representative result from at least three independent experiments was shown.

The same peptide pull-down assay condition was then performed to pull-down and identify the protein interactor of OSR1 S325 and OSR1 pS325 peptides. The pulled down material was run on an SDS-PAGE gel and stained with Coomassie blue staining. The result showed that the material pulled down by OSR1 S325 peptide had prominent protein bands with molecular weights ~100-150 kDa, and these were not present in the OSR1 pS325 peptide sample. The gel bands with MW ~100-150 kDa then were excised and analysed by MS fingerprinting analysis (**Figure 3.3.**).

The mass spectrometry data was then analysed by the Mascot Search Algorithm to determine the Mascot score. The Mascot score represents the probability of identified peptide sequences to match those from proteins acquired from experimental data and sequences protein databases. The higher the Mascot score means the less probability that the match of identified protein occurring randomly. **Table 3.1.** displays the summary of selected proteins that bound the OSR1 S325, but not the OSR1 pS325 in the range MW ~100-150 kDa with the Mascot score above 30 (www.matrixscience.com) (for a full list of identified protein from MS fingerprinting analysis see Table 7.1 to 7.5 in Chapter VII. Appendices). The proteins DDB1, CAND1, CUL4B, WDR3, CUL4A and WDR6 were found to be identified in OSR1 S325 peptide pull-down sample and were not identified in OSR1 pS325 peptide sample. It is known that DDB1, CUL4A/B and WDR3/6 forms a complex of cullin RING E3 ubiquitin ligase CRL4 (Angers *et al.*, 2006, He *et al.*, 2006) with CAND1 as its regulator (Goldenberg *et al.*, 2004).

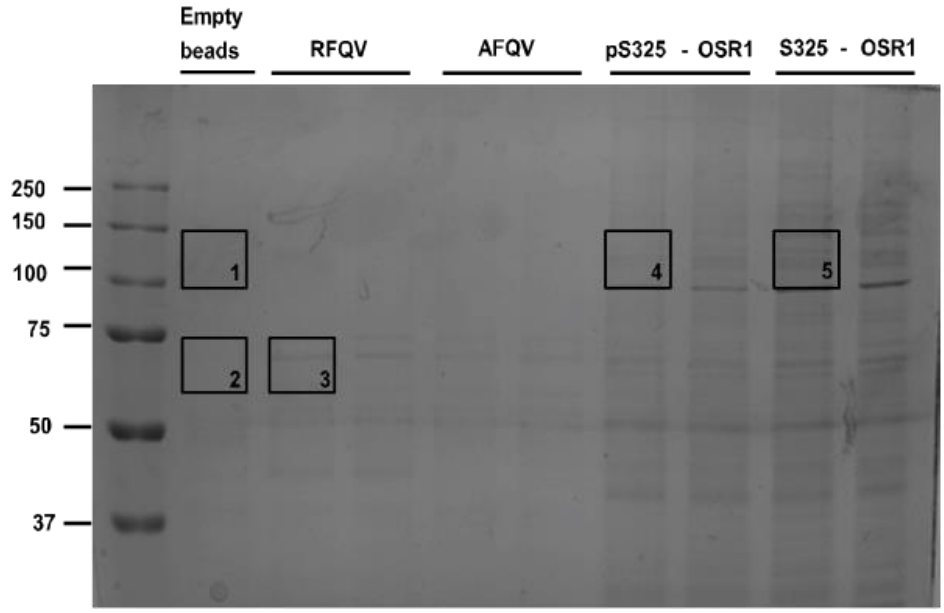

Figure 3.3. Gel image from Coomassie Blue stained gel of peptide pull-down assay for MS analysis. Subsequent to SDS PAGE protein separation, the proteins were subjected to MS analysis. The gel was excised on the respective bands in the range of molecular weight of interest ~100-150 kDa. Piece of gels were trypsinised, determined its identities on mass-spectral fingerprinting and analysed using Mascot search algorithm. Double lane on each sample showed the sample was run duplicate, except for empty beads sample. Representative result from two independent experiments was shown.

Table 3.1. Selected protein hits of MS fingerprinting from OSR1 S325 peptide pull-down

Sample No.	Protein Name		MW (kDa)	Protein Score	Accession No.
3	SPAK	Ste-20/SPS1-related proline-alanine-rich kinase	59.9	600	Q9UEW8
	OSR1	Oxidative Stress Responsive 1	58.3	89	O95747
5	DDB1	DNA damage-binding protein 1	128.1	261	Q16531
	CAND1	Cullin-associated NEDD8-dissociated protein 1	138.0	162	Q86VP6
	CUL4B	Cullin-4B	104.5	116	Q13620
	WDR3	WD repeat-containing protein 3	107.1	52	Q9UNX4
	CUL4A	Cullin-4A	88.1	46	Q13619
	WDR6	WD repeat-containing protein 6	123.6	38	Q9NNW5

Note: Accession numbers were retrieved from UniProt database

3.1.2. Binding confirmation of novel protein interactors

Based on the proteins identified in the peptide pull-down assay, initial confirmation of the binding was performed by immunoblotting the protein precipitate from peptide pull-down using CAND1, WDR3, and WDR6 antibodies. The positive control peptide, RFQV, pulled down endogenous SPAK, while its mutant peptide, AFQV, did not pull-down endogenous SPAK as expected (**Figure 3.4.**). In terms of the other proteins, CAND1, WDR3, and WDR6, they all bound the non-phosphopeptide OSR1 S325, but not its phosphorylated derivatives, in agreement with the mass spectrometry data (**Figure 3.4.**). Notably, the empty beads did not show any binding to these proteins of interest (**Figure 3.4.**). Together, this confirms the binding of CAND1, WDR3 and WDR6 to the non-phosphorylated peptide of OSR1.

As the most studied protein component of the CRL complex is cereblon (Ito *et al.*, 2010), we also probed for its binding to the OSR1 peptides. Cereblon did not appear in the mass spectrometry data because its molecular weight ~ 50-58 kDa was not included in the part of the gel, molecular weight 100-150 kDa, which was studied in this work (**Figure 3.3.**). Unfortunately, the commercially available anti-cereblon antibody was not clean and thus there was a strong background in the Western blot, though there was a hint of some binding of cereblon to the non-phospho peptide of OSR1, but not to its phosphorylated one (**Figure 3.4.**).

As seen in the bottom panel of **Figure 3.4.**, there were unexpected bands which were detected in the empty beads lane. These bands were overexposed protein bands, which showed in the same molecular weight as the bands of the standard protein. The standard protein bands could be detected on empty beads lane because the protein ladder was loaded in the same well as the empty beads in the SDS PAGE gel. Thus, as expected, there were no proteins were eluted and detected from the empty beads because the detected proteins were only the bands of the standard protein.

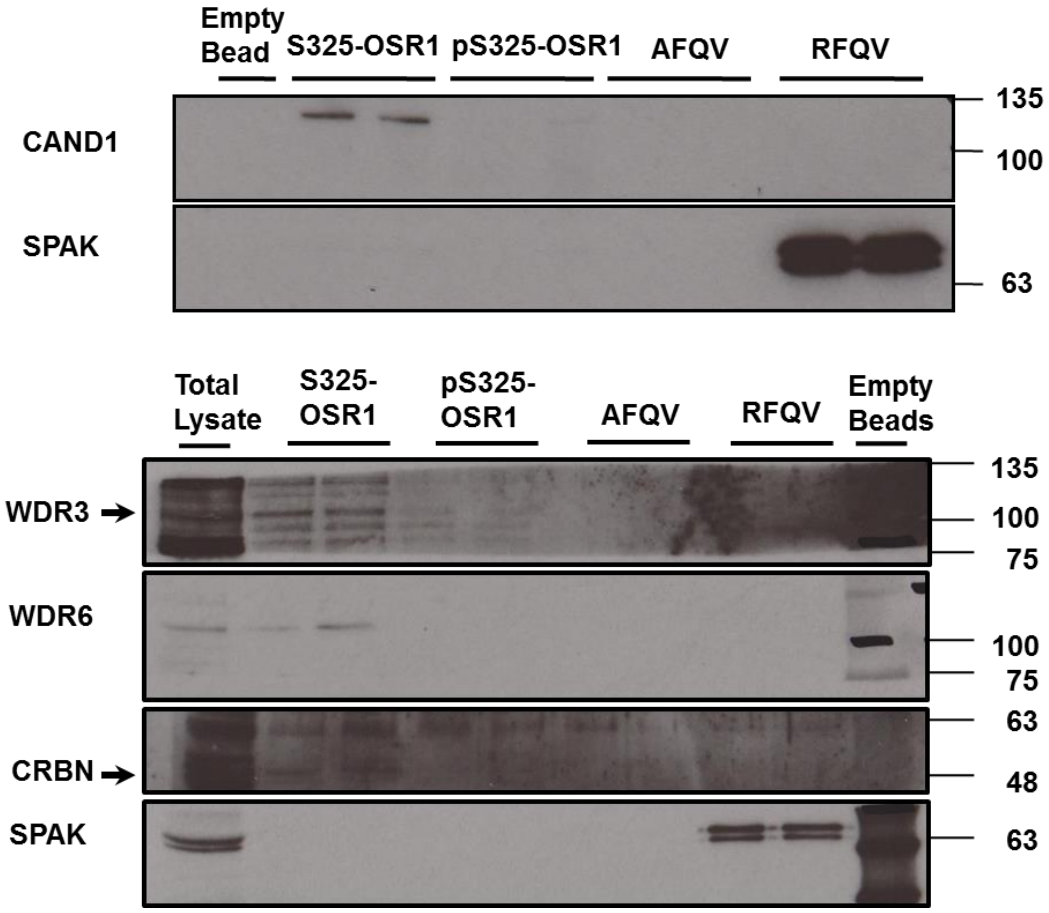

Figure 3.4. Immunoblot for novel protein binding confirmation on OSR1 S325 peptides. Immunoblotting was performed after peptide pull-down assay. Band of CAND1, WDR3, WDR6 and CRBN was observed in the non-phospho OSR1 S325 and not in the OSR1 pS325. SPAK blotting showed bands in the peptide contains RFQV motif as a positive control. Representative results from two independent experiments were shown.

Since CAND1 displayed low basal expression in HEK293 cells, CAND1 abundance was increased by FLAG-CAND1 overexpression to confirm the binding of CAND1 in resting and hypotonic conditions. FLAG-CAND1 overexpression was optimum when 5 µg of cDNA was transfected in HEK293 cells regardless of the conditions (see Table 2.4 for the cDNA concentration and purity) (**Figure 3.5.A.**).

The total protein in the amount of 1 and 0.5 mg was then applied for peptide pull-down using the unphosphorylated OSR1 S325 and the phosphorylated OSR1 pS325 peptides. The FLAG-tag immunoblotting was then performed to detect the binding of overexpressed CAND1. The results showed that using 1 mg total protein for pull-down, overexpressed CAND1 was more precipitated compared to 0.5 mg protein.

Overexpressed CAND1 were precipitated by OSR1 S325 peptide and not by OSR1 pS325 peptide (**Figure 3.5.B.**).

Immunoblotting for CUL4B was also performed to the same cell lysates to study the endogenous CUL4B binding toward OSR1 S325 and OSR1 pS325 peptides. The result shows the same result as overexpressed CAND1 (**Figure 3.5.B.**). Endogenous CUL4B were precipitated by OSR1 S325 peptide and not or in the lesser amount by OSR1 pS325 peptide. As also seen in **Figure 3.5.B.**, SPAK protein bound to RFQV peptide and there was no protein bound to AFQV motif-containing peptide and empty beads as it was expected.

CUL4B binding to the OSR1 S325 peptide, which was shown in **Figure 3.5.**, was in the presence of an abundance amount of CAND1 in the cell as the CAND1 was overexpressed. The binding might be different from the cell without CAND1 overexpression because of the cell with a high concentration of protein likely to exhibit non-physiological protein interactions (Moriya, 2015). CUL4B is a scaffold protein (Cullin subunit) of Cullin RING-ligase 4 (CRL4) complex that is essential for ubiquitylation of CRL4 substrate (Jackson and Xiong, 2009), whereas CAND1 is the inhibitor of CRL4 (Bosu and Kipreos, 2008). Therefore, overexpression of CAND1 may affect the CUL4B interaction to the OSR1 S325 peptide.

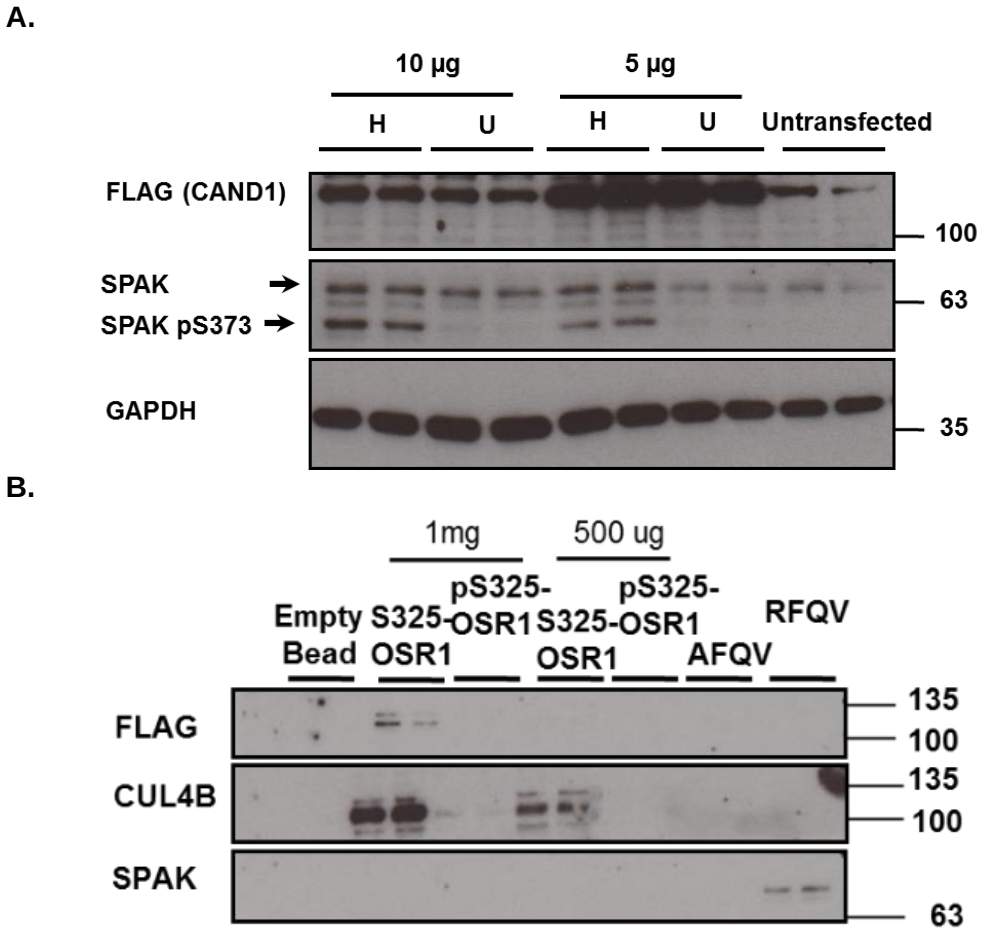

Figure 3.5. Binding confirmation of exogenous CAND1 and endogenous CUL4B to OSR1 S325 and OSR1 pS325 peptides. (A.) Overexpression of FLAG-CAND1 in HEK293 cell by transfection 5 µg and 10 µg cDNA FLAG-CAND1 with (H) or without (U) hypotonic condition. Three days post-transfection, total protein lysate was prepared for immunoblotting using Anti-FLAG antibody to confirm CAND1 expression level with GAPDH as a loading control and SPAK pS373 as a control for hypotonic stimulation. (B.) Total protein lysate (500 µg and 1 mg) from unstimulated condition then was subjected to peptide pull-down. Anti-DDDK antibody (equivalent to anti-FLAG) was used to confirm the binding of overexpressed FLAG-CAND1. SPAK antibody was used as a control to detect the binding of RFQV peptide. CUL4B antibody detected endogenous CUL4B binding to the peptides. Representative results from two independent experiments were shown.

To confirm the binding of endogenous CUL4B to SPAK/OSR1 without overexpressed CAND1, the same peptide pull-down assay using total protein lysate of untransfected HEK293 cell was carried out. CUL4B immunoblotting was performed following the peptide pull-down assay. As shown in **Figure 3.6.**, endogenous CUL4B was more precipitated by SPAK S373 (= OSR1 S325) than by SPAK pS373 peptide (= OSR1 pS325). This finding supported the result shown in **Figure 3.5.B**.

Figure 3.6. also show that no protein was precipitated by empty beads. Furthermore, as expected, the RFQV peptide could precipitate SPAK but not the AFQV peptide, although it showed in very low intensity. This low band intensity was due to the low sensitivity of the SPAK antibody as it was also shown by SPAK band in the total cell lysate.

CUL4B was precipitated by both OSR1 S325 and OSR1 pS325 peptides in different intensity under hypotonic and resting conditions. Under hypotonic conditions, the non-phospho peptide precipitated CUL4B in a slightly lesser amount than under resting conditions (**Figure 3.6.**). This indicated that WNK signalling stimulation reduced the binding of endogenous CUL4B to OSR1 S325 peptide. The CUL4B bands intensity of OSR1 pS325 peptide under hypotonic condition showed slightly stronger than untreated condition (**Figure 3.6.**). This could be due to the stronger affinity of CUL4B antibody in the immunoblot of hypotonic sample than untreated sample as it was shown from the CUL4B blot of the total cell lysate. The CUL4B blot intensity of the total cell lysate under hypotonic conditions was also slightly more intense than untreated cells.

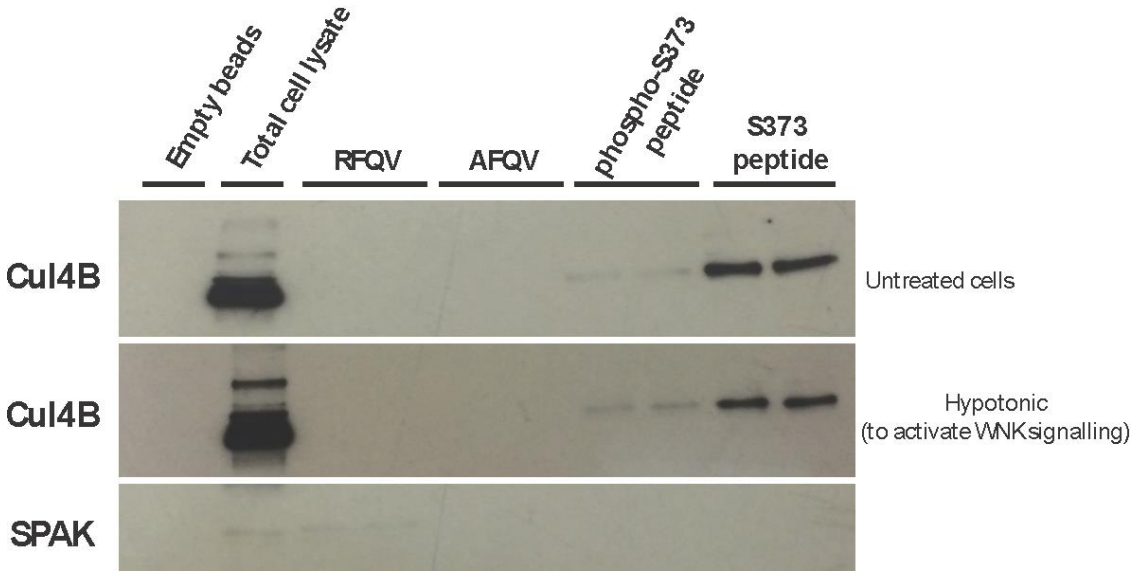

Figure 3.6. Binding confirmation of endogenous CUL4B to OSR1 S325 peptide. Total protein lysate of HEK293 cells under basal condition or treated with hypotonic low Cl^- subjected for OSR1 S325 (labelled as S373 peptide) and OSR1 pS325 (labelled as phospho-S373) peptide pull-down. CUL4B binding was detected by immunoblotting using CUL4B antibody. Immunoblotting of SPAK was used as a control for the binding of peptide-containing RFQV motif. Representative result from two independent experiments was shown.

3.2. INTERACTION OF Cullin-Ring Ligase 4 (CRL4) SUBUNIT PROTEINS WITH SPAK/OSR1

Based on the peptide pull-down assays that showed the interaction between CRL4 components and OSR1 S325 peptide, but not or lesser amount to OSR1 pS325, the confirmation of the CRL4 interaction with SPAK/OSR1 full-length protein and its truncated fragments was investigated.

3.2.1. Confirmation of CRL4 binding to SPAK/OSR1 full-length

The OSR1 peptides contain only a short fragment of OSR1, which were used as a tool to define protein interaction in the specific site of SPAK/OSR1 (Serine 325 of OSR1 or Serine 373 of SPAK). The initial finding on CRL4 binding to the OSR1 S325 peptide was needed to be further confirmed by using full-length endogenous OSR1 protein. Unlike short peptides, the binding that occurs between the full-length protein represents the protein binding in its active structure or correct protein folding as full-length proteins undergo several post-translation modifications in the cells. Thus,

evidence on CRL4 components interaction with the SPAK and OSR1 full-length protein was required.

Immunoprecipitation of endogenous SPAK and OSR1 from HEK293 cell lysates, which was followed by immunoblotting for the CRL4 components was conducted. DDB1 and CUL4B were found to bind endogenous OSR1 full-length under resting conditions more than hypotonic conditions (**Figure 3.7.A.**). This binding was also shown to occur with SPAK full-length (**Figure 3.7.C.**). These results suggested that the CRL4 components binding to SPAK/OSR1 were WNK signalling dependant. The WNK-SPAK/OSR1 signalling stimulation reduced the binding between CRL4 and SPAK/OSR1. Upon WNK-SPAK/OSR1 signalling activation, phosphorylation of SPAK/OSR1 at their *S*-motif promoted CRL4 complex dissociation from SPAK and OSR1.

The differential binding intensity between CRL4 components and OSR1 under the hypotonic and resting conditions in another OSR1 immunoprecipitation experiment could not be observed as expected (**Figure 3.7.B**). The binding of CRL4 components was expected to be stronger under the resting condition than hypotonic condition as seen in Figure 3.7.A; however the binding intensity of CRL4 to OSR1 showed no difference between the resting condition and hypotonic condition (**Figure 3.7.B.**). This unexpected result occurred may be due to the different sensitivity of the OSR1 antibodies that were conjugated to the beads for IP OSR1, as seen in **Figure 3.7.A.** and **Figure 3.7.B.**

To increase the sensitivity and specificity of the studied protein-protein interaction, we co-overexpressed GST-OSR1 or FLAG-OSR1 with FLAG-DDB1, Myc-CUL4A, or Myc-CUL4B in HEK293 cells. Upon cell lysis, the cell lysates underwent GST pull-down of the cell with overexpressed GST-OSR1 or FLAG pull-down of the cell with overexpressed FLAG-OSR1 (**Figure 3.8.**).

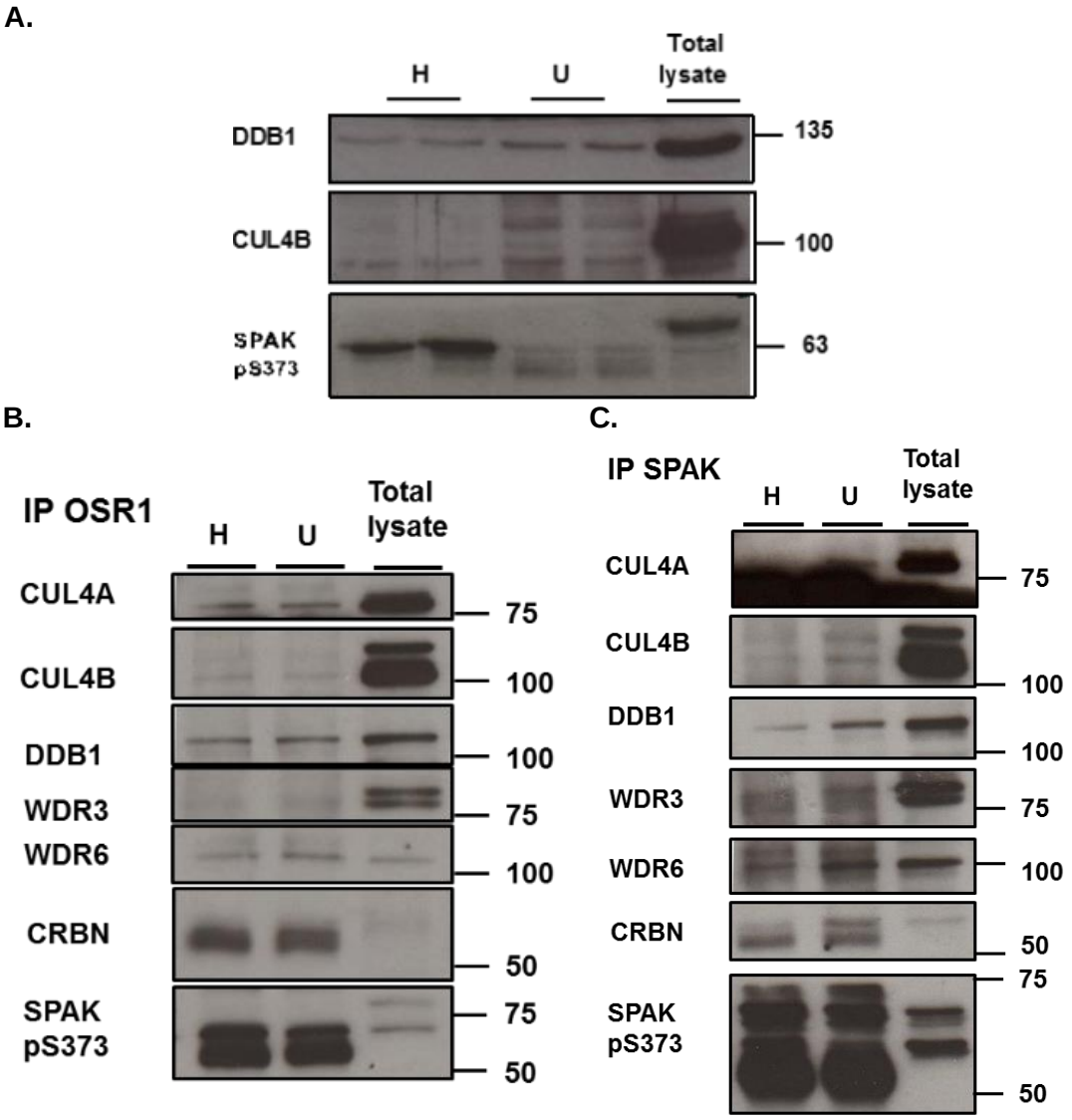

Figure 3.7. Immunoprecipitation of SPAK and OSR1. Total protein lysate of HEK293 cell (3 mg) on resting (U) or with hypotonic low-chloride stimulation (H) was incubated with anti-OSR1 (A. & B.) or Anti-SPAK (C.) conjugated beads overnight. The elute from washing step was prepared in SDS sample buffer, and 0.1 portion precipitate was immunoblotted with anti-CUL4A, CUL4B, DDB1, WDR3, WDR6 and CRBN antibodies. SPAK pS373 blot was used as a control for WNK-SPAK/OSR1 signalling activation. Total lysate of unstimulated HEK293 cell was used as a control for basal expression of the protein. Representative results from two independent experiments were shown.

Figure 3.8.A. show the FLAG immunoblot after GST pull-down of the cell lysate with co-expressed FLAG-DDB1 and GST-OSR1. The DDB1 binding to OSR1 was showed under both resting and hypotonic condition. The DDB1 binds more to OSR1 under resting conditions than hypotonic condition. As seen in the GST blot of the input, the GST-OSR1 was more overexpressed under resting condition than hypotonic

condition. This could be suggested that the different binding intensity between DDB1 and OSR1 was due to the different GST-OSR1 expression under resting and hypotonic condition. However, the difference of the band intensity between resting and hypotonic conditions on FLAG immunoblot after GST pull-down was higher (3.2 times) than the GST input (1.8 times) after it was normalised with FLAG input. Thus, the different band intensity that was observed in the FLAG immunoblot after GST pull-down was not because of the difference in GST input, but it represented the different binding between DDB1 and OSR1 that was occurred under resting and hypotonic conditions.

Supporting the evidence that the DDB1 and OSR1 binding was hypotonic dependent, the dynamics of this binding under resting condition over time is shown in **Figure 3.8.B.** GST pull-down followed by FLAG immunoblot was performed from FLAG-DDB1 and GST-OSR1 co-expressed HEK293 cells lysate with the growth media replacement overtime after hypotonic stimulation treatment. After the co-overexpression stage, the cells were left untreated or stimulated with the hypotonic buffer for 30 min. After hypotonic stimulation, there were several cultures in which the media was replaced with the growth media. The cells were then lysed after different incubation time, *i.e.* 1; 2; 3; 6; 12; 18; and 24 h. The results showed that under hypotonic condition the DDB1 binding to OSR1 was reduced (**Figure 3.8.B.** bottom panel). The DDB1 and OSR1 binding was regained when the cells were grown in the growth media (resting condition) over time. The binding under resting condition was increased at 6 and 12 h and then started to decrease after 18 h.

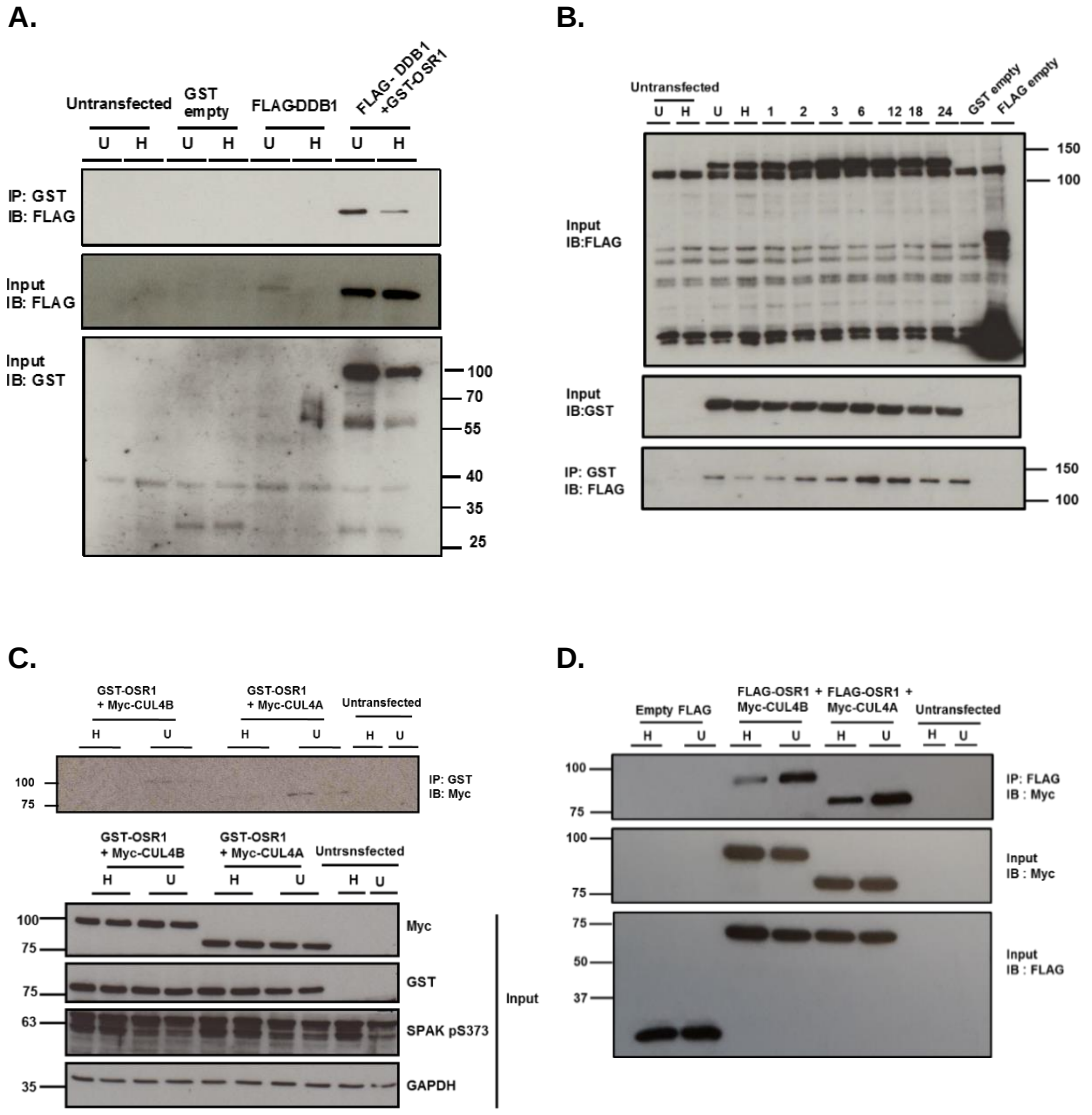

Figure 3.8. Binding confirmation of exogenous OSR1 and CRL4 components. GST pull-down from 1 mg total protein lysate of co-expressed GST-OSR1 with FLAG-DDB1 (A.) and (B.); or with Myc-CUL4A or Myc-CUL4B in HEK293 cells were immunoblotted to detect the FLAG-tag and Myc-tagged protein precipitated by GST bead (C.). (D.) FLAG-OSR1 was co-expressed with Myc-CUL4A or Myc-CUL4B, and the total protein lysate was incubated with FLAG bead to precipitate OSR1 protein interactor which was detected by Myc-tag immunoblotting. Transient transfection was employed 2.5 µg DNA of each plasmid. After 36 or (B.) 48 h of transfection, the cells were either left on the resting condition (U) or treated using hypotonic low-chloride buffer (H) for 30 min prior to cell lysis except for (B.). For (B.), after hypotonic condition treatment, the buffer was replaced by the growth media and incubated for denoted time (hours) before total protein lysate was prepared and used for GST pull-down. Representative results from two independent experiments were shown.

The interaction between CUL4A/CUL4B and OSR1 are shown in **Figure 3.8.C.** and **Figure 3.8.D**. Myc immunoblotting from the GST pull-down of cell lysate with Myc-CUL4A or Myc-CUL4B and GST-OSR1 co-overexpression was performed (**Figure 3.8.C.**). Using the CUL4A/CUL4B and OSR1 protein input for GST-pull down as shown in the top panel, the Myc immunoblot of the precipitated protein in the bottom panel confirmed the interaction between CUL4A/CUL4B and OSR1 under resting condition, but not under the hypotonic condition.

Since the precipitated proteins in the GST pull-down from the GST-OSR1 and Myc-CUL4A/Myc-CUL4B overexpression were very low, FLAG pull-down from the total cell lysate with FLAG-OSR1 co-overexpressed with Myc-CUL4A/Myc-CUL4B was performed (**Figure 3.8.D.**). Following Myc-tag immunoblot, the results clearly showed that CUL4A and CUL4B established stronger interaction with OSR1 under resting condition than hypotonic condition. In agreement with the peptide pull-down and IP assays result, the interaction between OSR1 and CRL4 components was established under the resting condition and diminished or significantly reduced under hypotonic condition.

3.2.2. CRL4 binds OSR1 kinase domain and S-motif

In order to understand where the CRL4 complex binds SPAK and OSR1, various truncated OSR1 fragments were used in studying the binding to the CRL4 complex. These OSR1 fragments were the kinase domain with (1-363) or without S-motif domain (1-311); the kinase domain with the linker sequences between S-motif domain and carboxy-terminal (CCT) domain (1-435); and the CCT domain (429-end) (**Figure 3.9.**). These proteins, bearing an *N*-terminal GST-tag, were co-overexpressed in HEK293 cells with full-length Myc-CUL4A, Myc-CUL4B, FLAG-DDB1, His-WDR3, or His-WDR6. Affinity pulldown was then performed against one tag and immunoblotting for the other protein partner tag was performed (**Figure 3.10. - 3.12.**).

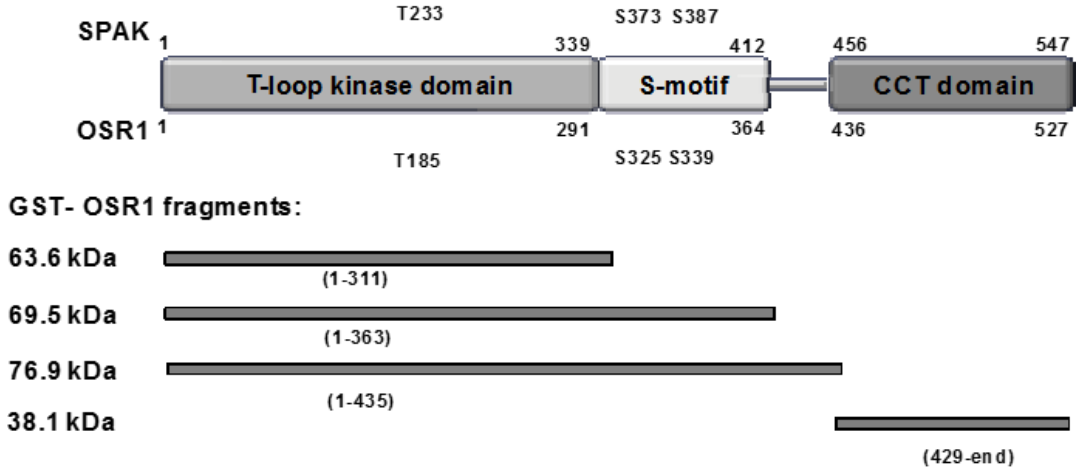

Figure 3.9. Diagram of GST-OSR1 fragments to study OSR1 domain of CRL4 subunit binding. GST-OSR1 fragments consist of *N*-terminal domain of OSR1 without S-motif domain (GST-OSR1 1-311), with S-motif domain (GST-OSR1 1-363), without CCT domain (GST-OSR1 1-435) and CCT domain only (GST-OSR1 429-end).

Figure 3.10. show the FLAG and GST immunoblot of the HEK293 total cell lysate and its GST pull-down. The cells contained co-overexpressed FLAG-DDB1 and GST-OSR1 full-length (FL) or its fragments. FLAG immunoblot of the total lysate showed that the FLAG-DDB1 was successfully overexpressed in the cell, either of its single overexpression or when it was co-overexpressed with GST-OSR1 FL and its fragments. The expression of co-expressed FLAG-DDB1 with GST-OSR1 FL, and with 1-311 showed a high expression (top panels). GST immunoblot of total lysate shown in the middle panels of **Figure 3.10.** showed that the GST-OSR1 FL and its fragments were successfully overexpressed, except fragment 429-end that did not express at all. The GST-OSR1 1-363 and 1-435 were indeed showed low expression, the same as shown in FLAG immunoblot. Notably, these low expressed proteins under resting condition exhibit more pronounce expression than in under hypotonic condition.

The bottom panels of **Figure 3.10.** show the FLAG immunoblot of GST pull-down from the co-expressed proteins. From this figure, it showed that DDB1 was confirmed to

bind to OSR1 FL, OSR1 1-311 and OSR1 1-435. The binding of DDB1 to OSR1 429-end, which represent OSR1 CCT domain, could not be observed as the fragments OSR1 429-end could not be expressed (see left middle panel). Cell lysate without any transfected plasmids and transfected with the plasmid containing GST or FLAG empty vector were used as a control in this experiment. There were no bands which were detected on this cell lysate sample as expected.

Notably, the DDB1 binding was not showed in fragment OSR1 1-363. Considering that the binding was established in the fragment OSR1 1- 435, so it was expected that the binding should occur in the fragments OSR1 1-363. The absence of the expected bands can be explained by low expression of the protein input GST-OSR1 1-363 (see the middle panel). The low expression of the protein input means that the protein which might establish interaction with the OSR1 also in low amount, if it is the case, hence it was required higher sensitivity antibody for protein detection. If the argument of low expression of the protein input was not the case, and the interaction was not present, then it can be speculated that there is a steric hindrance in the region between aa 311-363 of OSR1 which weaken the DDB1 binding to fragments OSR1 1-363.

Thus, it can be concluded that the binding of DDB1 was established in the kinase domain of OSR1. However, the interaction of DDB1 in OSR1 *C*-terminal domain could not be concluded from this experiment as the OSR1 fragment 429-end could not be overexpressed. Notably, DDB1 binds more to GST-OSR1 full-length, fragments 1-311, and fragments 1-435 under resting condition than in the hypotonic condition.

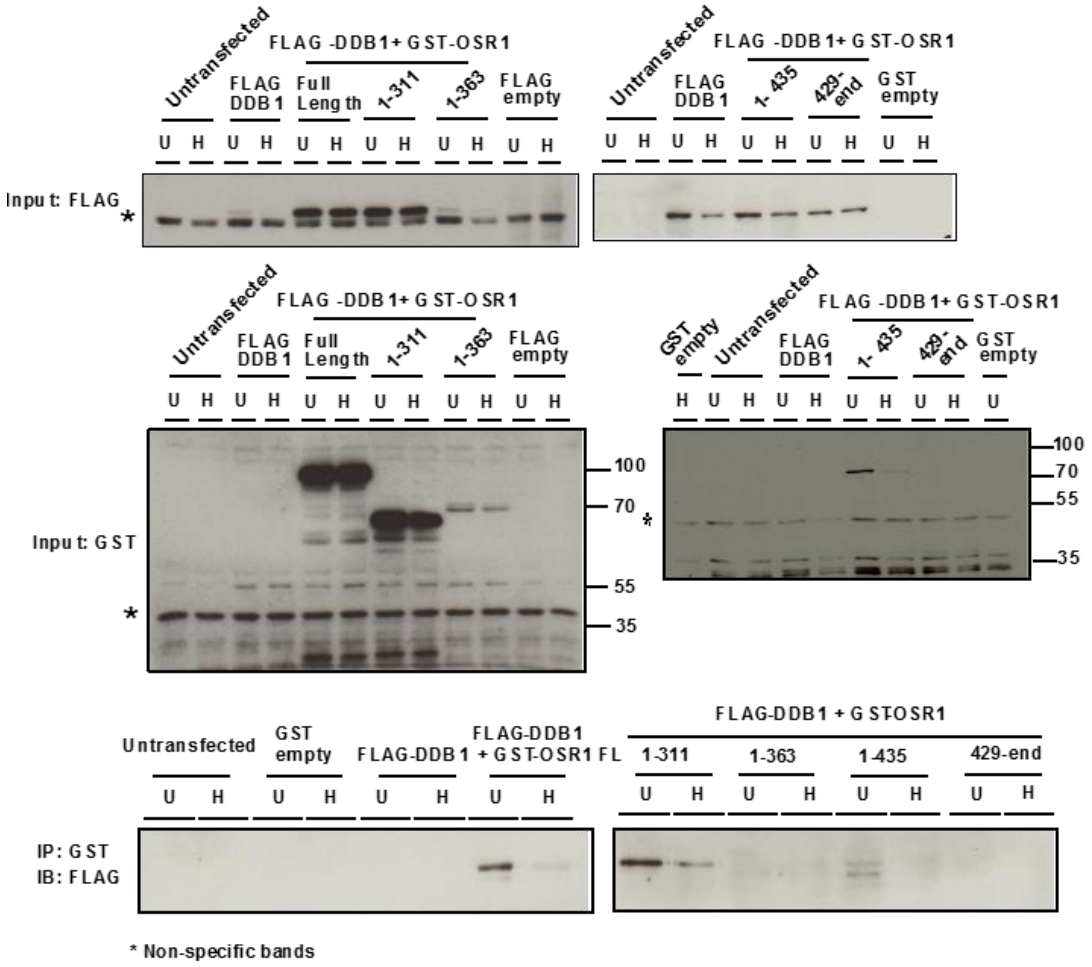

Figure 3.10. DDB1 binding to OSR1 regions. FLAG-DDB1 and GST-OSR1 full-length (FL) (MW ~99 kDa); GST-OSR1 1-311 (~64 kDa); GST-OSR1 1-363 (~70 kDa); GST-OSR1 1-435 (~77 kDa); or GST-OSR1 429-end (~38 kDa) fragments were co-expressed in HEK293 cells. GST pull-down assay was performed from total protein lysate, which was prepared three days post-transfection under resting (U) and hypotonic (H) condition. Immunoblotting using anti-FLAG tag antibody was done to confirm the DDB1 binding to OSR1 fragments. Representative results from two independent experiments were shown.

Figure 3.11. display the GST immunoblot of the HEK293 total cell lysate and His pull-down from co-overexpressed His-WDR3 (**Figure 3.11.A.**) and His-WDR6 (**Figure 3.11.B.**) with GST-OSR1 full-length (FL) or its fragments. GST immunoblot of the total lysate showed that His-WDR3, which was co-overexpressed with GST-OSR1 FL and its fragment was successfully overexpressed (**Figure 3.11.A.**) although the expression of co-expressed His-WDR3 with GST-OSR1 429-end showed low expression (top panel **Figure 3.11.A.**).

The bottom panel of **Figure 3.11.A.** show the GST immunoblot of His pull-down from the co-expressed proteins. In this figure, WDR3 was confirmed to bind to OSR1 FL, OSR1 1-311, OSR1 1-363 and OSR1 1-435. The weaker binding between WDR3 with OSR1 fragments 1-435 than with 1-311 and 1-363 was observed. However, the binding between WDR3 and OSR1 429-end, which represent OSR1 *C*-terminal domain, could not be observed. Cell lysate without any transfected plasmids and transfected with the plasmid containing GST empty vector were used as a control in this experiment. There were no bands which were detected on these cell lysate sample as expected.

In **Figure 3.11.B.**, GST immunoblot of the HEK293 total cell lysate showed that His-WDR6, which was co-overexpressed with GST-OSR1 FL or its fragment was successfully overexpressed in the cell (top panel **Figure 3.11.B.**). The bottom panel shows the GST immunoblot of His pull-down from the co-expressed proteins. In this figure, WDR6 was confirmed to bind to OSR1 FL, OSR1 1-311, and OSR1 1-363. The weaker binding between WDR3 with OSR1 1-363 than with OSR1 1-311 was observed. Notably, the WDR6 binding to OSR1 1-435, and to OSR1 429-end, which represent OSR1 *C*-terminal domain, could not be observed. The same set of controls as the His-WDR3 experiments were used. There were also no bands which were detected on these controls as expected.

Thus, based on the result of the WDR3 and WDR6 binding to OSR1 fragments, it indicated that the interaction between WDR3 and WDR6 with OSR1 occurred in the kinase domain. It also suggested that the linker sequence between 363-435 of OSR1 responsible for decreasing or abolishing the interaction between WDR3/WDR6 and OSR1.

Notably, the interaction between WDR3/WDR6 with OSR1 was affected by the hypotonic condition, although the differential binding under resting and hypotonic condition showed inconsistency among the sample.

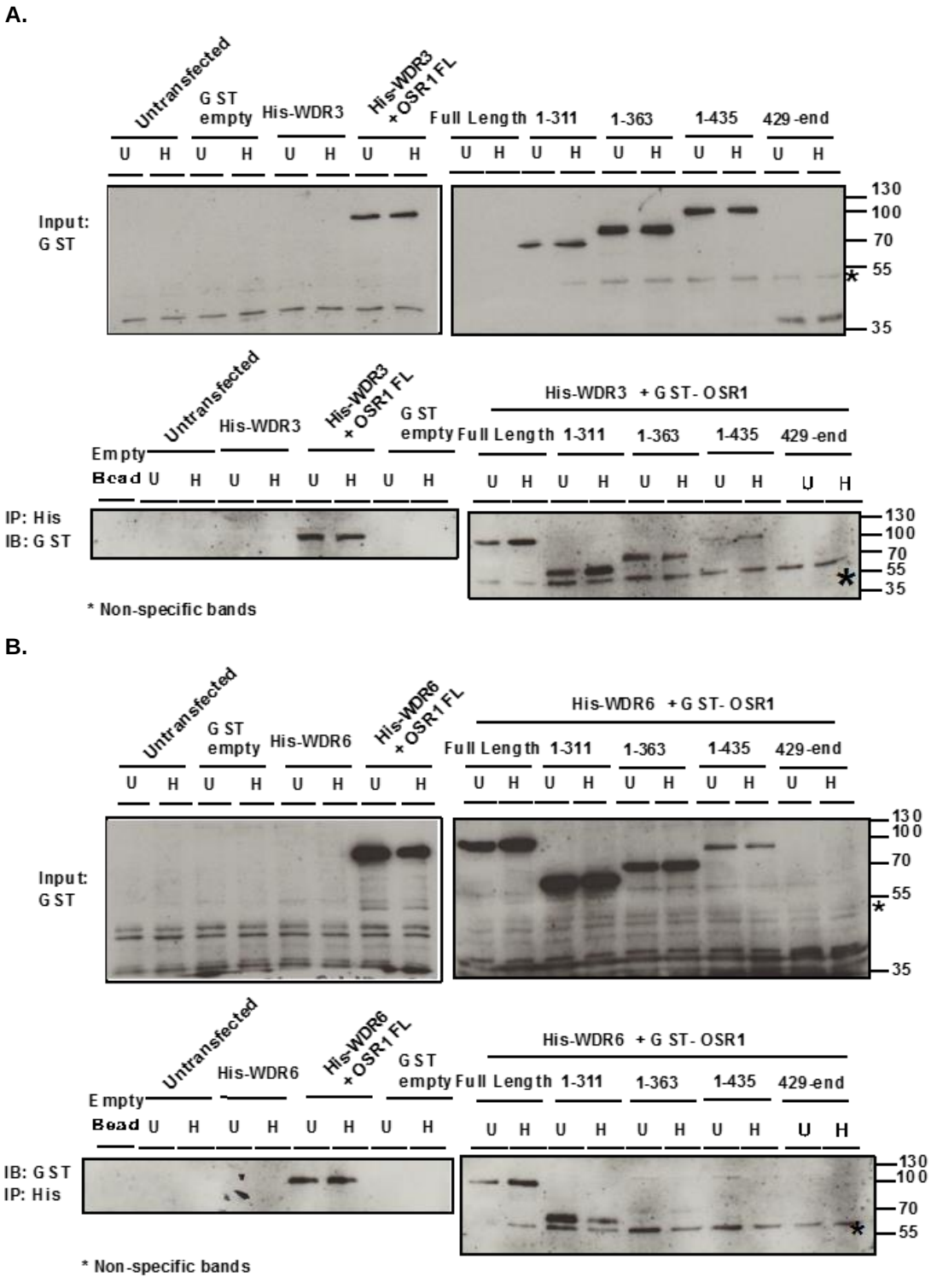

Figure 3.11. WDR3 and WDR6 binding to OSR1 regions. (A.) His-WDR3 or (B.) His-WDR6 and GST-OSR1 full-length (FL) (MW ~99 kDa); GST-OSR1 1-311 (~64 kDa); GST-OSR1 1-363 (~70 kDa); GST-OSR1 1-435 (~77 kDa); or GST-OSR1 429-end (~38 kDa) fragments were co-expressed in HEK293 cells. His pull-down assay using Ni-NTA beads was performed from total protein lysate, which was prepared three days post-transfection under resting (U) and hypotonic (H) condition. Immunoblotting using anti-GST tag antibody was done to confirm the WDR3 and WDR6 binding to OSR1 domain. Representative results from two independent experiments were shown.

Figure 3.12. show the GST and Myc-tag immunoblot of the total lysate and their GST pull-down of co-overexpressed Myc-CUL4A and Myc-CUL4B with GST-OSR1 full-length (FL) or its fragments in HEK293 cells. GST and Myc-tag immunoblot of the total lysate showed that Myc-CUL4A along with GST-OSR1 FL and its fragment was successfully overexpressed (top panel **Figure 3.12.A.**). However, non-specific bands in GST immunoblot were detected with MW around 100 kDa. Unfortunately, these non-specific bands were merged with the GST-OSR1 full-length band (MW ~99 kDa). These non-specific bands were constantly appeared whenever GST immunoblot was performed in Myc-CUL4A or Myc-CUL4B overexpression. However, the merging of non-specific bands with GST-OSR1 full-length band was not shown in the GST immunoblot on Myc-CUL4B (MW ~120kDa) overexpression as it was easily differentiated by its MW (top panel **Figure 3.12.B.**).

The bottom panel of **Figure 3.12.A.** shows the Myc-tag immunoblot of GST pull-down from the co-expressed proteins. In this figure, CUL4A was confirmed to bind to OSR1 FL and other GST-OSR1 fragments except fragment 1-311. CUL4A binds more to OSR1 FL under resting condition than under hypotonic condition. The stronger interaction under resting condition than hypotonic condition was also observed between CUL4A and OSR1 fragments (1-363 and 1-435). However, the interaction between CUL4A and fragments 429-end was showed reversely. The CUL4A binds to OSR1 429-end under hypotonic condition more than resting condition.

Even though the non-specific bands, which were observed in the Myc-CUL4A total lysate need to be taken into consideration, the interaction between CUL4A and OSR1 was not affected by the non-specific bands. As seen in **Figure 3.12.A.**, the CUL4A that can be pulled down by GST beads was showing different intensity among fragments. Cell lysate without any transfected plasmids and transfected with the plasmid containing GST empty vector were used as a control in this experiment. There were no bands which were detected on these cell lysate sample as expected.

The result for Myc-CUL4B co-expression with GST-OSR1 FL and its fragments (**Figure 3.12.B.**) showed a similar result to the Myc-CUL4A experiment. GST and Myc-tag immunoblot of the total lysate showed that Myc-CUL4B and GST-OSR1 FL and its fragments were successfully overexpressed (top panel **Figure 3.12.B.**). Myc-tag immunoblot of GST pull-down from the co-expressed proteins is shown in the bottom panel of **Figure 3.12.B.** In this figure, CUL4B was confirmed to bind to OSR1 FL and other GST-OSR1 fragments. CUL4B binds to OSR1 FL in the same intensity regardless of the condition. The interaction between CUL4B and OSR1 fragments 1-311 and 1-435 was stronger under resting condition than hypotonic condition. The interaction between CUL4B and fragments 1-363 and 429-end was showed reversely, the interaction under hypotonic condition was stronger than resting condition.

To be noted, the same explanation regarding the non-specific bands that was appeared as **Figure 3.12.A.** was also proposed for the result shown in **Figure 3.12.B.** It indicated that GST created interaction with Myc-tag protein in our system with unknown mechanism (e.g. nucleic acid bridging or other superficial interactions). As negatively charged molecules, DNA/RNA can adhere to basic surfaces of proteins, thus can mediate the interaction between immobilised bait protein with the protein target. Adding micrococcal nuclease (S7 nuclease), which cleaved the DNA/RNA strands was proved to be a solution to this problem (Nguyen and Goodrich, 2006). However, from the technical point of view, the problem could also be solved by replacing 1) the tagged protein (Myc-tag) to another tag protein or 2) the beads other than GST-beads to be used for pulling down the Myc-tag protein. Unfortunately, the replacement could not be done due to time and technical constraint.

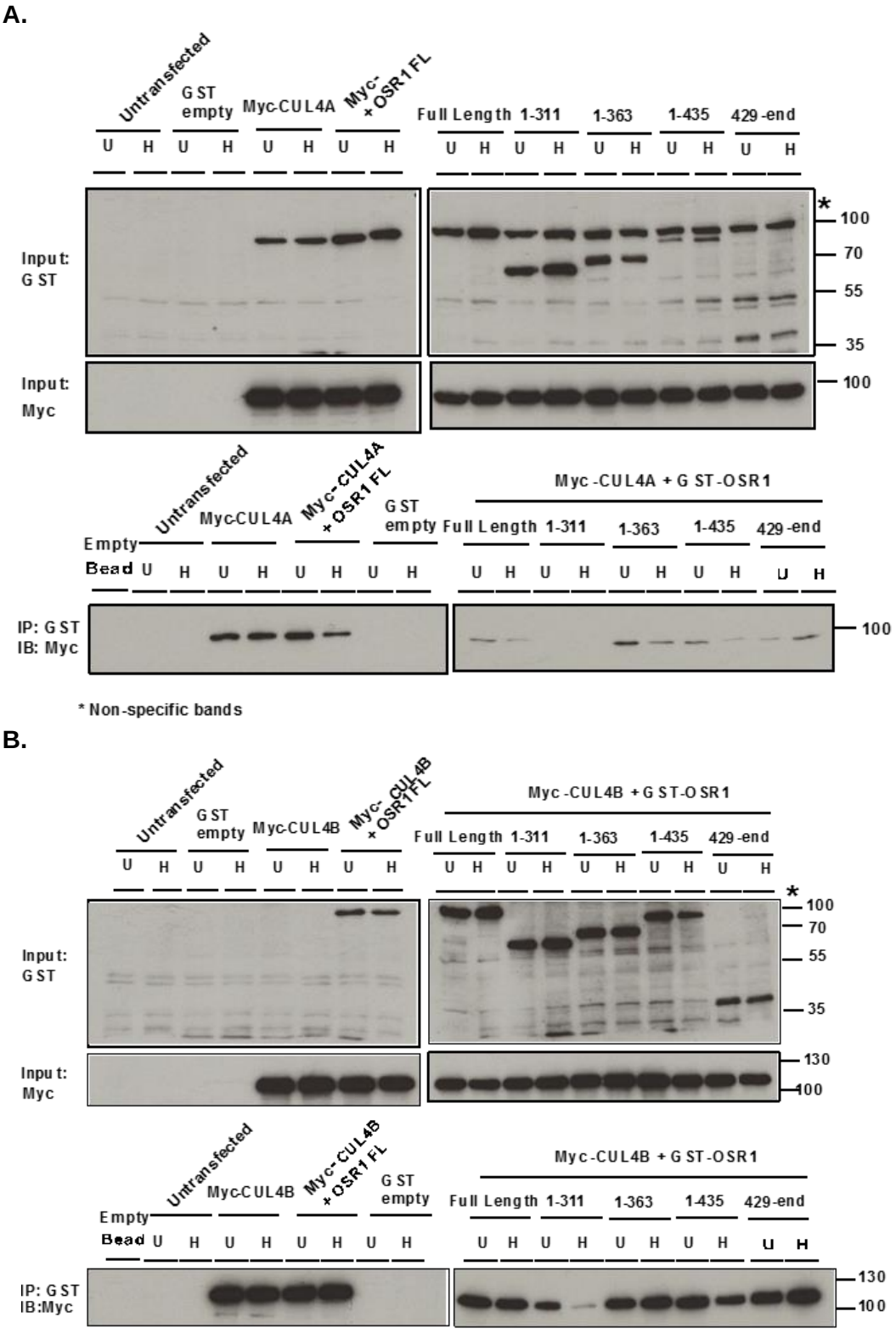

Figure 3.12. CUL4A and CUL4B binding to OSR1 regions. A. Myc-CUL4A or **B.** Myc-CUL4B and GST-OSR1 full-length (FL) (MW 99 kDa); GST-OSR1 1-311 (64 kDa); GST-OSR1 1-363 (70 kDa); GST-OSR1 1-435 (77 kDa); or GST-OSR1 429-end (38 kDa) fragments were co-expressed in HEK293 cells. GST pull-down assay was performed from total protein lysate, which was prepared 3 days post-transfection under resting (U) and hypotonic (H) condition. Immunoblotting using anti-Myc tag antibody was done to confirm CUL4A and CUL4B binding to OSR1 domain. Representative results from two independent experiments were shown.

3.2.3. Interaction between CRL4 components

His pull-down assays were performed under the resting condition on the HEK293 cells with co-expression of His-WDR3 or His-WDR6 and FLAG-DDB1, Myc-CUL4A or Myc-CUL4B to investigate the interaction between these CRL4 components as an addition to their interaction with OSR1. As shown in **Figure 3.13.A.**, Myc-tag and FLAG immunoblot of total cell lysate showed the successful overexpression of Myc-CUL4A, Myc-CUL4B and FLAG-DDB1 with His-WDR3; Myc-CUL4A/CUL4B with His-WDR6, but not FLAG-DDB1 with His-WDR6. These overexpressed protein inputs were then used for His pull-down. The result after Myc immunoblot showed that CUL4A and CUL4B interacted with WDR3 or WDR6. Even though very weak intensity band was observed after FLAG immunoblot from His-pull down, DDB1 also established interaction with WDR3.

Since the FLAG-DDB1 co-expression with His-WDR6 could not be obtained, the co-expression of FLAG-DDB1 with His-WDR3 and His-WDR6 were repeated to undergo another His pull-down. **Figure 3.13.B.** show that FLAG-DDB1 was successfully expressed. FLAG immunoblot of His pull-down demonstrated the interaction between DDB1 and WDR3/6, although the non-specific band was appeared on FLAG-DDB1 sample and in the total protein lysate.

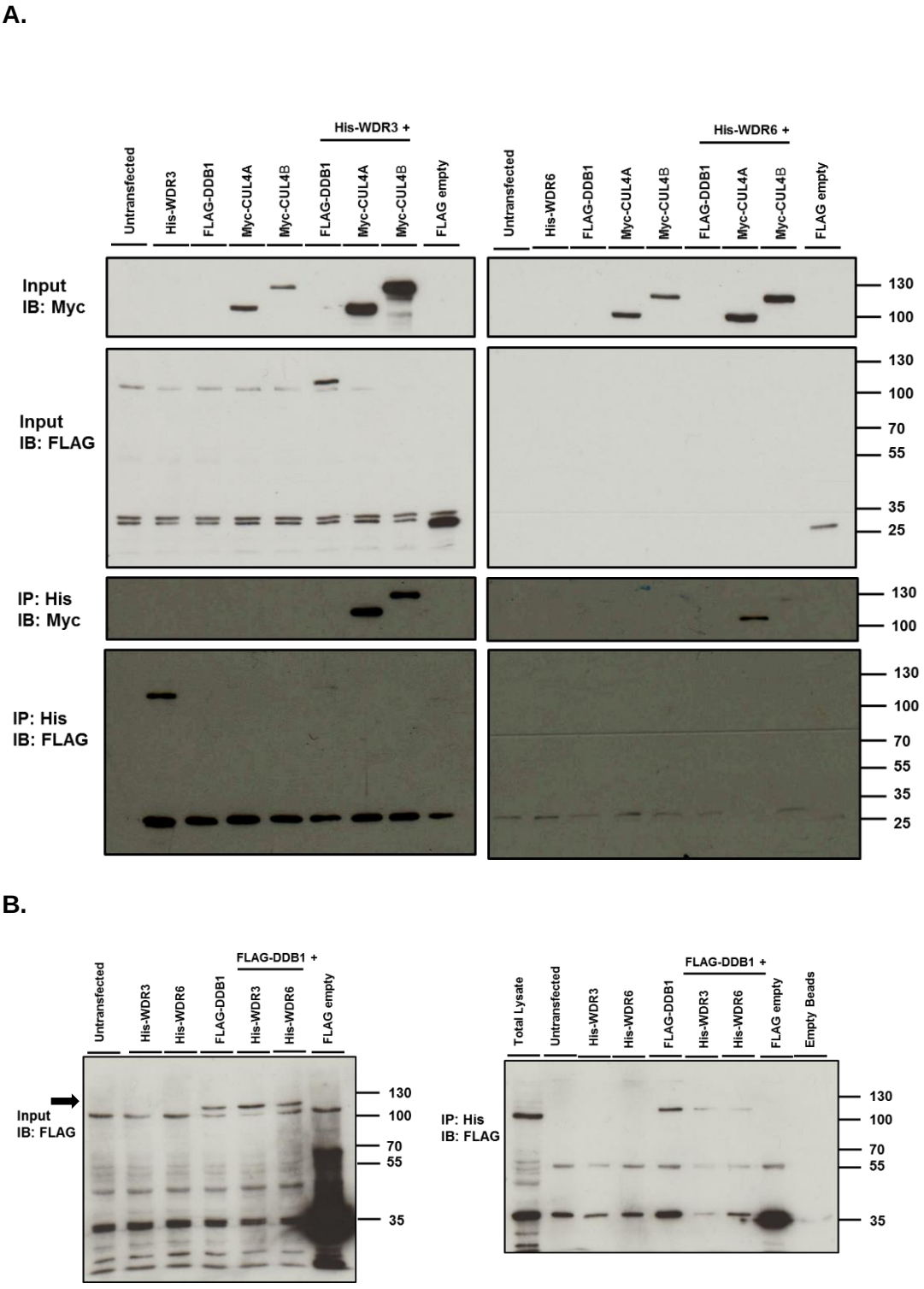

Figure 3.13. CRL4 component established interaction with another CRL4 component. (A.) His pull-down assay was performed on HEK293 with His-WDR3 or His-WDR6 and Myc-CUL4A, Myc CUL4B, or FLAG-DDB1 co-expression. Immunoblot using Myc-tag and FLAG-tag antibody detected the interaction between WDR3-CUL4A, WDR6-CUL4A, WDR3-DDB1 and WDR6-DDB1. The same experiment was done on (B.) but immunoblotting only for FLAG-DDB1 with His-WDR3/6 co-expression**.** Representative results from two independent experiments were shown.

To understand how the interaction between CRL4 components with OSR1 was established, visualisation of the interaction was then performed using protein-protein docking software ClusPro 2.0 under default mode. The protein interaction model was developed based on the crystal structure of DDB1-CUL4A-Rbx1-SMV5 (PDB ID: 2HYE) (**Figure 3.14.A.**). The validated homology model of WDR3 and WDR6 then was docked to predict the interaction between CUL4A-DDB1-WDR3 and CUL4A-DDB1-WDR6. The generated models of these interactions then were chosen based on the models in which WDR3 and WDR6 were docked to the big pocket between beta-propeller A (BPA) and beta-propeller C (BPC) of DDB1 (Angers *et al.*, 2006). It has been reported that WDR3 and WDR6 are WDRs protein family, which its DXR box domain bind to the BPA-BPC of DDB1 (Hu *et al.*, 2004). The chosen models of CUL4A-DDB1-WDR3 and CUL4A-DDB1-WDR6 complex were then docked with the OSR1 kinase domain (2VWI) (**Figure 3.14.B. and C.**) and the visualisation of OSR1 interaction with CRL4 complex was obtained. Highly homology sequences of the *N*-terminal domain of CUL4A and CUL4B, especially in the sequence where the DDB1 is bound (N406-N640) suggested that the interaction of CUL4B-DDB1-WDR3/WDR6-OSR1 could be represented as CUL4A-DDB1-WDR3/WDR6-OSR1.

A.

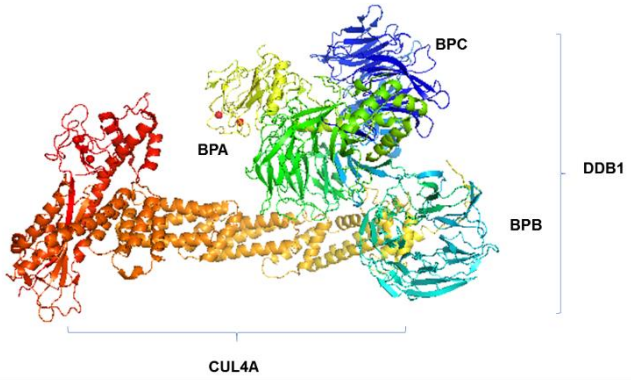

B.

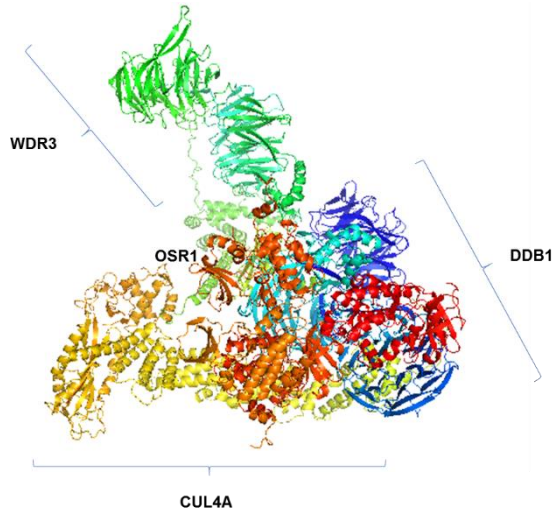

C.

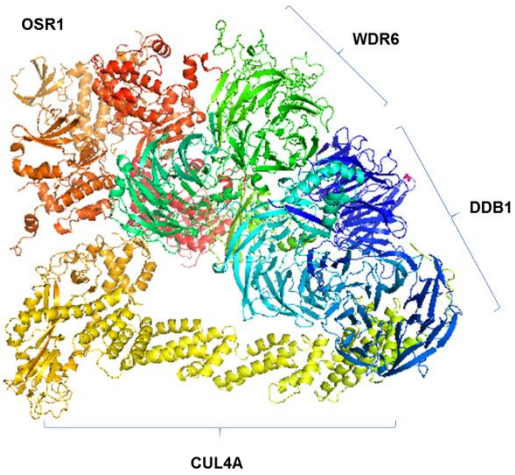

Figure 3.14. Visualisation of protein interaction prediction between CRL4 complex with OSR1. (A.) Crystal structure of DDB1-CUL4A-Rbx1-SMV5 (2HYE) was used to dock the homolog model of WDR3 or WDR6 and OSR1 (2VWI) structure, subsequently using protein-protein docking software ClusPro 2.0. The best model was chosen to present the predicted interaction of (B.) CUL4A-DDB1-WDR3-OSR1 and (C.) CUL4A-DDB1-WDR6-OSR1.

3.3. SPAK/OSR1 UBIQUITYLATION AND DEGRADATION UPON CRL4 INHIBITION

3.3.1. siRNA CUL4A and siRNA CUL4B silencing toward SPAK and OSR1 degradation

Small interfering RNA (siRNA) and short hairpin RNA (shRNA) are tools to silence or knockdown target gene (Fire *et al.*, 1998). siRNA is the most commonly used RNA interference (RNAi) to produce a short-term silencing of protein-coding genes. siRNA is introduced in the cytoplasm as a single-stranded RNA (21-25 nucleotide) which could bind to a complementary target sequence in mRNA then undergoes for cleaving and degrading the mRNA. This degradation eventually blocks protein expression leading to reduced protein level and finally a knockdown. shRNA is a double-stranded form of RNAi with a hairpin loop which is created after transduction or transfection of DNA construct into the nucleus. Regard to its origin, shRNA exhibits superiority compares to siRNA. Its production inside the cell allows shRNA avoiding the RNA degradation in the cytoplasm. Moreover, shRNA can be produced by the self-machinery of the target cell, so the silence or knockdown gene can be obtained continuously (Rao *et al.*, 2009). The schematic figure for siRNA and shRNA mechanism is illustrated in **Figure 3.15.**

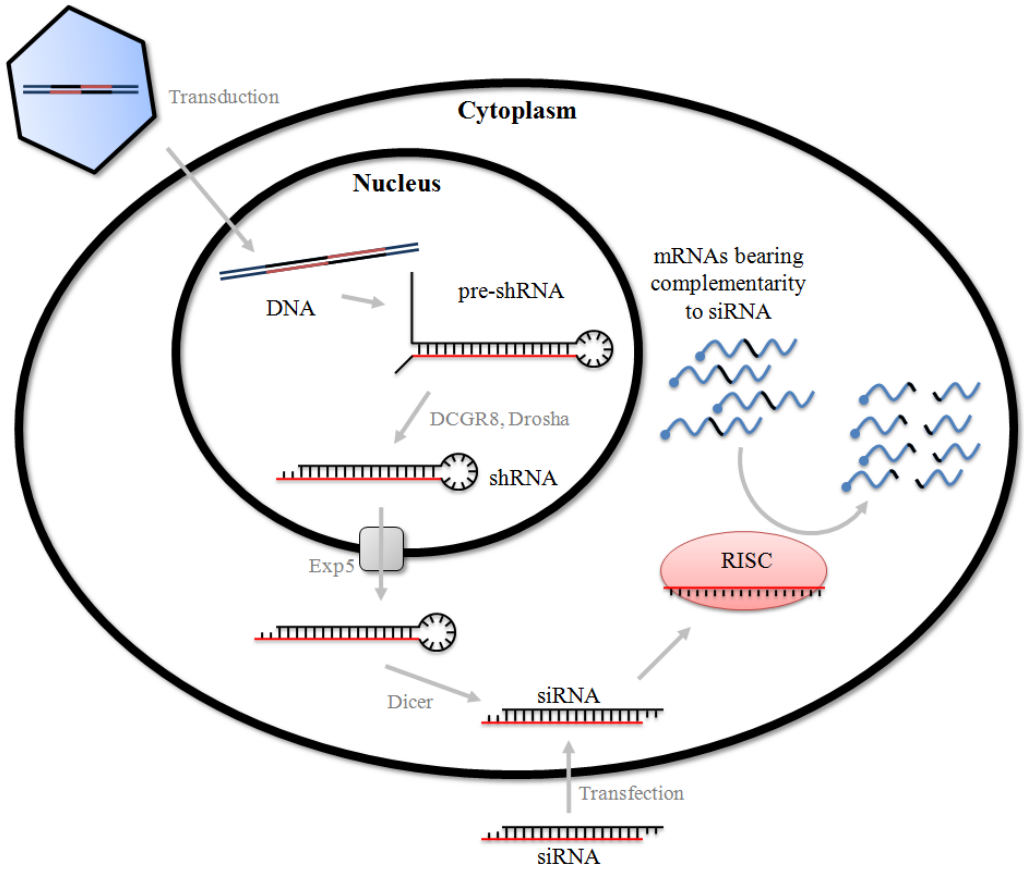

Figure 3.15. Mechanism of RNAi to silence a gene. After being introduced to the cell by transduction or transfection and expressed in the nucleus, shRNA is exported out from nucleus by Exportin-5 to cytoplasm. Association of shRNA with Dicer remove the loop sequence, and it starts to be processed like siRNA. siRNA is directly introduced into the cytoplasm as short duplexes and recognised by Dicer. After association with RISC (RNA-induced silencing complex) and the removal of one of the RNA strands, they bind to the complementary sequence of target mRNAs and lead to its degradation (O'Keefe, 2013).

The role of CRL4 on SPAK/OSR1 degradation was further investigated by silencing the CUL4A, CUL4B, both CUL4A and CUL4B, and DDB1 gene and detected the SPAK and OSR1 expression level by immunoblotting. Delivery of siRNA CUL4A and siRNA CUL4B into HEK293 cell was facilitated by cationic liposome, *i.e.* lipofectamine. Lipofectamine forms a complex with a nucleic acid, which carries a net negative charge in normal physiological conditions. The positively charged complex of Lipofectamine and nucleic acid allowing the complex of nucleic acid- liposome to be inserted to the cell. It is widely known that lipofectamine is a transfection agent that provides high transfection efficiency (Dalby *et al.*, 2004).

In order to achieve high transfection efficiency, optimum RNAi transfection condition is obliged to be set (Denning *et al.*, 2013). siRNA CUL4A and siRNA CUL4B transfection using a different concentration of lipofectamine, *e.g.* 6 and 9 µL in a total of 300 µL of siRNA and lipid mixture were performed to obtain optimum transfection condition. As shown in **Figure 3.16.A.** and **Figure 3.16.B.**, CUL4A and CUL4B gene knockdown were successfully achieved on both concentrations of lipofectamine. It also showed that DDB1 was not knocked down by siRNA CUL4A and CUL4B, which means that the siRNA system knocked down the target gene specifically. These CUL4A and CUL4B knockdowns, however, did not alter SPAK and OSR1 protein expression. Untransfected cell and cell with scramble RNA (scRNA) were used as a control for the siRNA system.

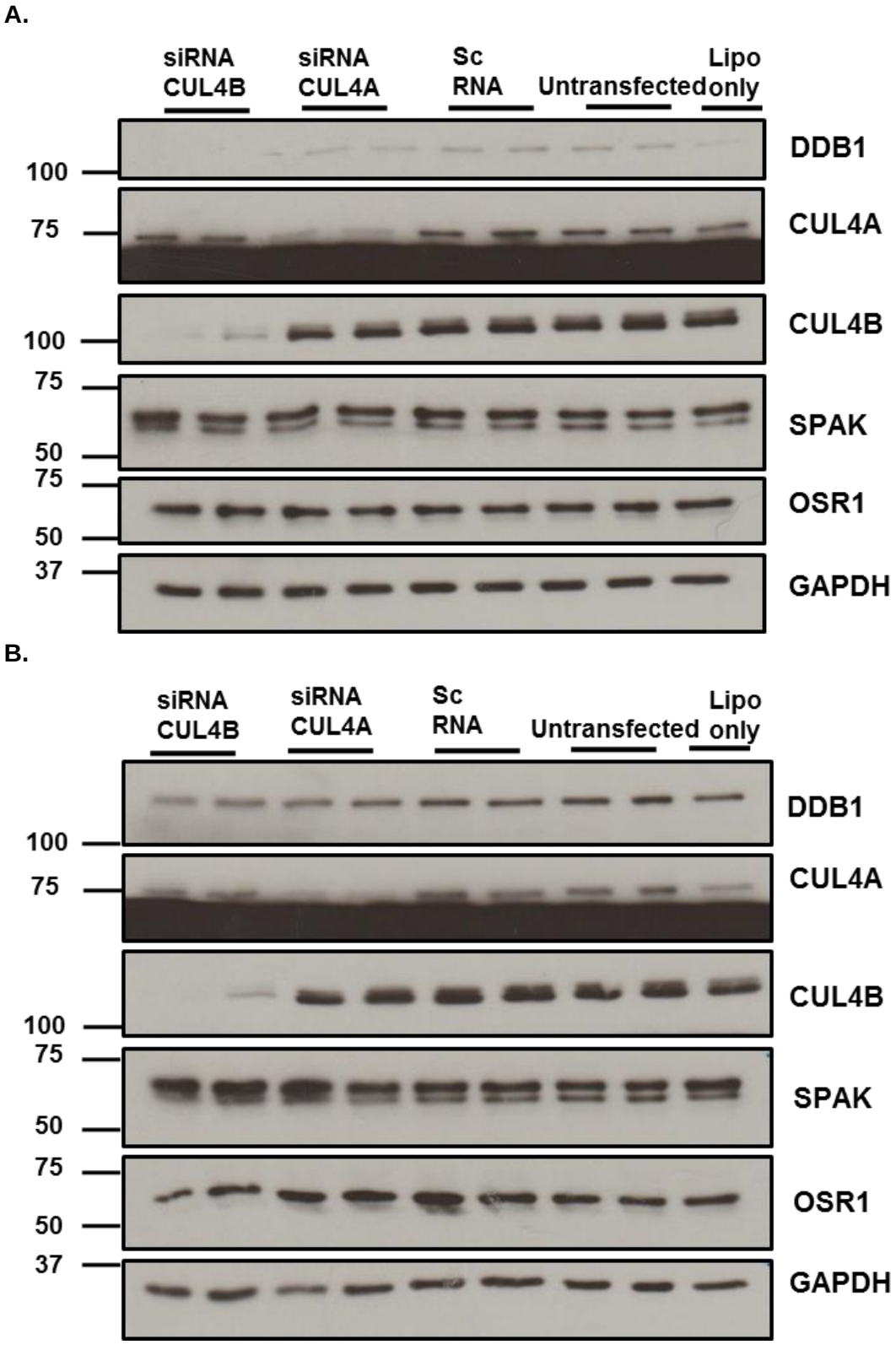

Figure 3.16. **siRNA knockdown of CUL4A or CUL4B showed no effect on SPAK and OSR1 expression**. Immunoblot was carried out three days post-transfection of 25 pmol siRNAs transfection using (A.) 6 and (B.) 9 µL lipofectamine to HEK293 cell. The dark blot under the CUL4A bands was the blotting membrane of another protein in high exposure. Representative results from two independent experiments were shown.

The absence of alteration on SPAK and OSR1 expression after siRNA CUL4A and siRNA CUL4B knockdown did not support the temporary hypothesis of the role CUL4A/B to promote SPAK/OSR1 degradation. These steady expression of SPAK and OSR1 after CUL4A and CUL4B knockdown could be explained by two reasons: First, CUL4A and CUL4B, which both present in HEK293 cell and showed interaction with SPAK and OSR1, may works complementary. Although CUL4A and CUL4B are structurally similar, they exhibit several distinct and overlapping functions. They share 82% identity, which differs only 149 amino acids extension at *N*-terminus of CUL4B to facilitates nuclear localisation (Hannah and Zhou, 2015). Thus, knocking down one of CUL4A or CUL4B which has overlapping functions, does not alter their functions to degrade a protein. The absence of CUL4A as E3 ubiquitin ligase in the cell could be replaced by CUL4B to degrade the substrate protein and *vice versa*.

The second reason, even though CUL4A and CUL4B established direct interaction with SPAK and OSR1, CUL4A/CUL4B are having the function as protein scaffold in CRL4 complex. They facilitate other CRL4 components that directly bind to and exhibit direct function on SPAK and OSR1 degradation, *e.g.* DDB1, WDR3, WDR6 or CRBN. Thus, knocking down the CUL4A or CUL4B does not enough to stop the other components to be functioned on OSR1 ubiquitylation or degradation.

To prove the first hypothesis, both CUL4A and CUL4B were double knocked down. As shown in **Figure 3.17.A.**, double knockdown of CUL4A and CUL4B blot exhibited weaker intensity of both CUL4A and CUL4B compare to its single knockdown, the wild type (untransfected), and the cell with scRNA. However, double knockdown of CUL4A and CUL4B did not exhibit any differences in SPAK and OSR1 expression. Thus, it was temporary concluded that the complementary function of CUL4A and CUL4B as E3 ubiquitin ligase did not directly promote SPAK and OSR1 degradation.

Then, in order to answer the second reason, which hypothesised that CUL4A and or CUL4B are having a function as a protein scaffold of CRL4 E3 ubiquitin ligase

complex, DDB1 knockdown was performed. shRNA DDB1 was employed for achieving efficient DDB1 gene knockdown. However, the attempt to knockdown DDB1 gene using shRNA was not successful (see **Figure 3.17.B.**). DDB1 expression was not reduced after shRNA DDB1 were transfected to HEK293 cell utilised lipofectamine. Even, it exhibited a more intense band compared to the scRNA control. Moreover, GAPDH as loading control also showed an unexpected reduction on shRNA DDB1 transfected cell. It indicated that shRNA DDB1 alter the expression of non-specific proteins in the cell.

Transfection methods used in our shRNA DDB1 transfection (Lipofectamine) was not the best choice for shRNA DDB1 delivery to the nucleus. Transduction of shRNA using lentiviral particle is widely used and considered as the efficient gene-delivery vehicles for shRNA. Unfortunately, due to the limited facilities to perform lentiviral-mediated transduction of shRNA, the shRNA DDB1 knockdown experiment could not be carried out. The work then was proceeded to study the role of protein subunits of CRL4 on SPAK and OSR1 ubiquitylation and degradation using small molecule inhibitors for protein degradation, which is described in the next sections.

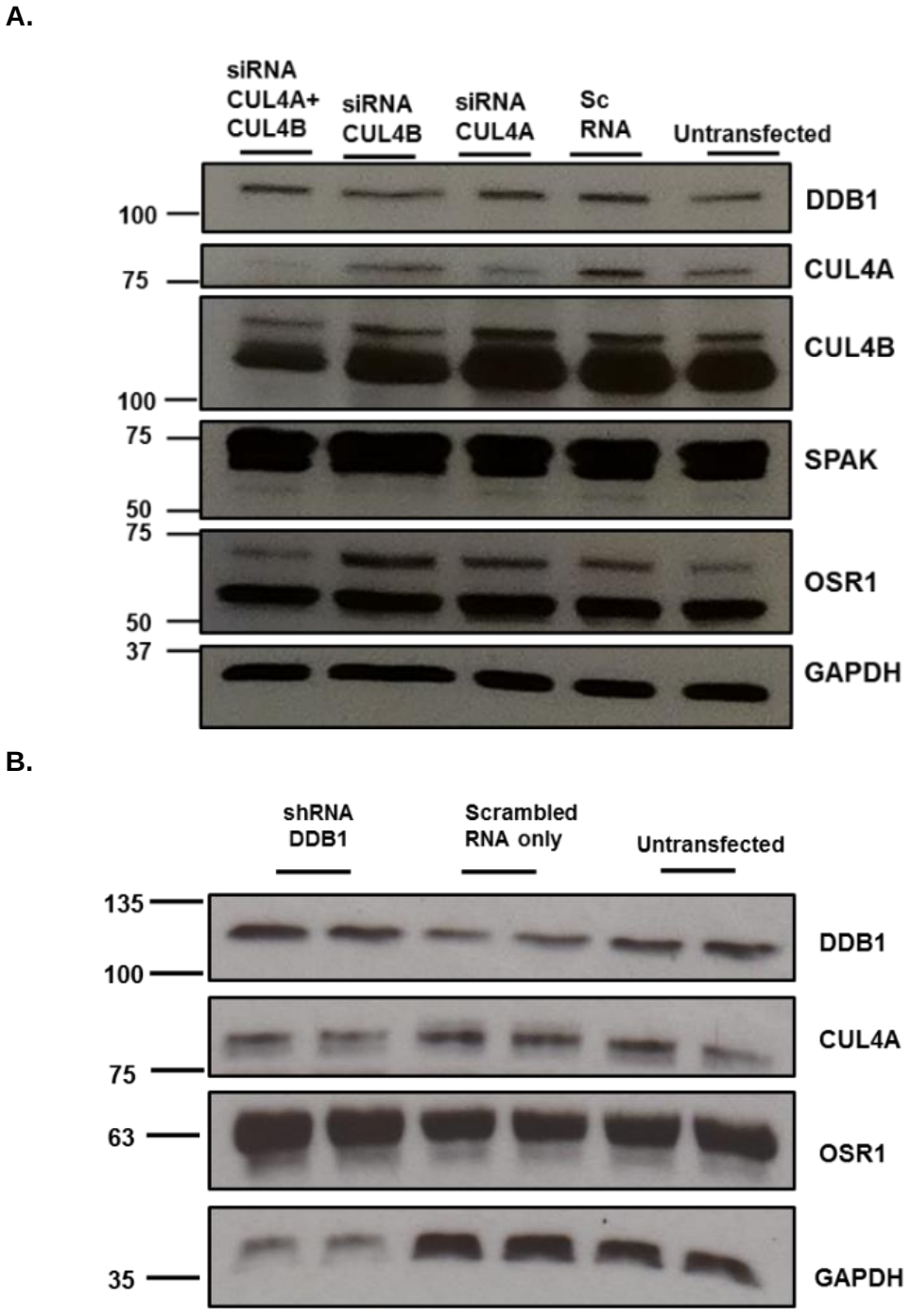

Figure 3.17. siRNA double knockdown of CUL4A and CUL4B and shRNA DDB1. (A.) Double knockdown of CUL4A and CUL4B did not alter SPAK and OSR1 expression. Immunoblot was carried out three days post-transfection of 25 pmol siRNAs on HEK293 cell. Scramble RNA (scRNA) was used as a negative control. (B.) shRNA DDB1 knockdown on HEK293 cell. Gene knockdown of DDB1 was unable to decrease or abolish DDB1 expression as expected. shRNA DDB1 plasmid was transfected to HEK293 cell using lipofectamine. Immunoblotting analysis was conducted three days post-transfection. Representative results from two independent experiments were shown.

3.3.2. Effect of MLN4924 and MG132 on ubiquitylation and degradation of endogenous and overexpressed SPAK and OSR1

Protein degradation by CRL4 is a protein degradation mechanism via ubiquitylation activation, which requires neddylation by Nedd8 (Jackson and Xiong, 2009). Nedd8 (a ubiquitin-like protein) binds to cullin and activate the binding of ubiquitin protein to a ubiquitin-activation enzyme (E1). Ubiquitin is subsequently transferred to E2, a ubiquitin conjugation protein, which complexes with E3 ubiquitin ligase. This E3 ubiquitin ligase recognises protein substrates, which then be ubiquitinated and finally degraded (see details in **Figure 1.9.**).

Several compounds are known to target protein ubiquitylation and degradation. MLN4924 ((1S,2S,4R)-4-(4-[(1S)-2,3-dihydro-1H-inden-1ylamino]7H-pyrrolo[2,3-d] pyrimidin-7-yl)-2-hydroxycyclopentyl) methyl sulphamate) is a selective inhibitor of NEDD8-activating enzyme (NAE) (Soucy *et al.*, 2009). Since Nedd8 is required for CRL4 activation, the inhibition of NAE prevents CRL4 to degrade the target substrate. MLN4924 is widely used in the experiments as a negative confirmation that substrate degradation occurs via ubiquitylation (Liu *et al.*, 2014, Keuss *et al.*, 2016).

Another compound, MG132 is a proteasome inhibitor which is widely known to inhibit protein degradation. MG132 (carbobenzoxyl-leucinyl-leucinyl-leuc-inal-H) is a peptide aldehyde, which blocks the 26S proteasome complex to perform proteolysis (Lee and Goldberg, 1998). MG132 was considered as early proteasome inhibitor to be identified and studied as a potential cancer therapeutic target (Teicher and Tomaszewski, 2015). Later studies utilised MG132 as a negative control for protein degradation confirmation in various experiments (Liu *et al.*, 2014, Nguyen *et al.*, 2017). Unlike MLN4924, MG132 unable to negatively confirm the ubiquitylation-mediated protein degradation. MG132 inhibition occurs when the protein is in ubiquitinated form and ready to be cleaved by 26S proteasome into small peptides inside its canonical structure (Bedford *et al.*, 2010) (**Figure 3.18.**).

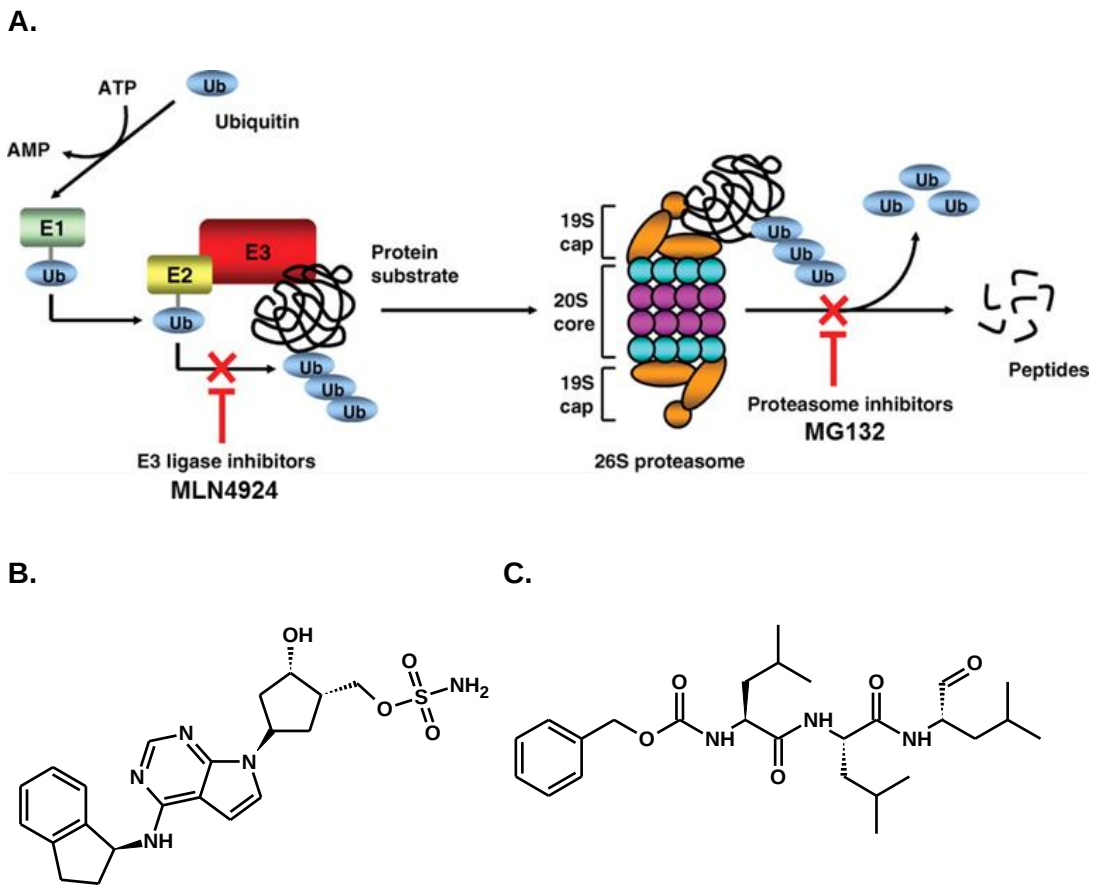

Figure 3.18. Mechanism of MLN4924 and MG132 to inhibit protein degradation. (A.) MLN4924 inhibition target is in the protein ubiquitylation process, thus protein unable to be ubiquitinated and further be degraded. MG132 targets the 26S proteasome function, thus ubiquitinated protein which is ready to proceed to be degraded is being inhibited. (B.) Structure of MLN4924 and (C.) MG132 (retrieved from (Yu and Kem, 2010) with slight modification).

MLN4924 and MG132 were applied to study the ubiquitylation and degradation on the endogenous and overexpressed SPAK and OSR1. The investigation was performed to confirm whether: 1) the ubiquitylation and or degradation occurs as a result of SPAK and OSR1 binding to CRL4, and 2) CRL4 involves in the ubiquitylation and or degradation of SPAK and OSR1.

MLN4924 in a series of concentration ranging from 0.01 to 10 µM was incubated in HEK293 cells for 6 hours. The cells were left untreated or stimulated with the hypotonic buffer for 30 min before cell lysis. CRL4 components (CUL4A, CUL4B, WDR3, WDR6 and CRBN), SPAK and OSR1 immunoblotting were performed. SPAK

pS373 immunoblotting was also carried out as a control for hypotonic stimulation. As shown in **Figure 3.19.**, MLN4924 treatment on HEK293 under resting and hypotonic condition resulted in the different effect on the expression of cullins proteins: CUL2, CUL4A and CUL4B. There was no difference in CUL4A expression after MLN4924 treatment both under resting and hypotonic condition. Whereas, CUL4B expression started to increase from 0.1 µM of MLN4924 on both conditions (**Figure 3.19.A.**).

Other cullin protein that was used as a control for MLN4924 treatment in this experiment was cullin 2 (CUL2). CUL2 is a highly neddylated Cullin protein. This neddylation occurs as a result of the binding of its substrate-recognition module to the substrates (Merlet *et al.*, 2009, Keuss *et al.*, 2016). Neddylated form of CUL2 can be observed in the SDS gel as a band with higher molecular weight than CUL2 band. **Figure 3.19.A.** show that neddylated form of CUL2 was abolished after the cell was treated with 1 µM MLN4924 under resting condition. Whereas, under hypotonic condition, the neddylated form of CUL2 was started to decrease at 0.01 µM of MLN4924 treatment. The ability to inhibit neddylated form of CUL2 suggested that the range concentrations of MLN4924 for 6 h incubation was sufficient to inhibit neddylation process. However, the neddylated form of CUL4A and CUL4B could not be observed.

MLN4924 treatment altered the expression of DDB1. The DDB1 protein band intensity exhibited a slightly reduced after 1 µM of MLN4924 treatment, both under resting and hypotonic condition (**Figure 3.19.B.**). However, treatment of MLN4924 did not result any differences in WDR3, WDR6, SPAK and OSR1 expression. It indicated that inhibition of NAE likely to affect more on some of the CRL4 components (CUL4B and DDB1) and did not affect SPAK and OSR1 expression level.

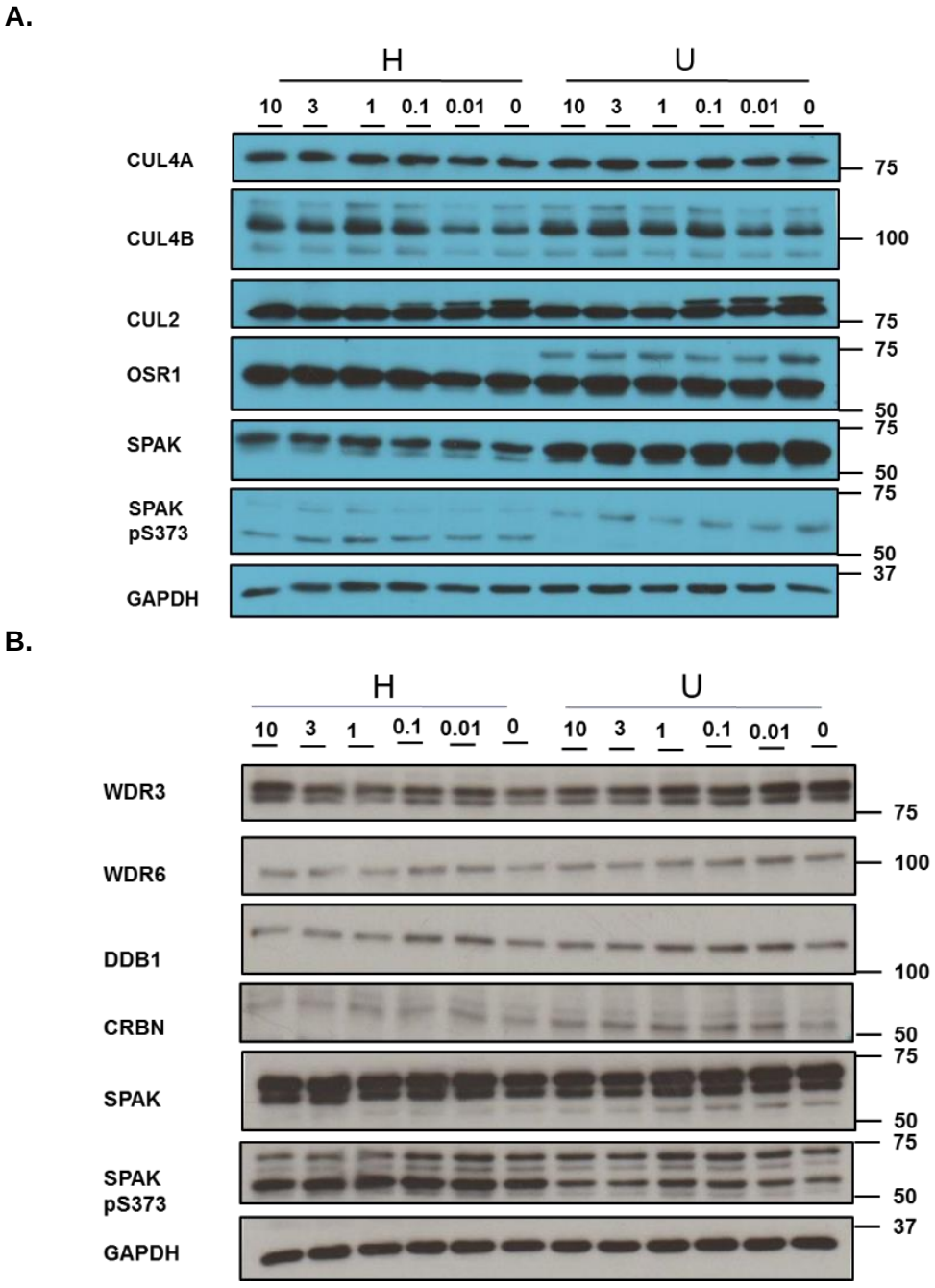

Figure 3.19. Expression of CRL4 subunits, SPAK and OSR1 after MLN4924 treatment. Different concentrations ranging from 0.01-10 µM of Neddylation-activation enzyme inhibitor MLN4924 was incubated for 6 h with HEK293 cell under resting and hypotonic condition. Immunoblotting of (A.) CUL4A; CUL4B; CUL2; SPAK and OSR1 as well as (B.) WDR3; WDR6; DDB1; CRBN; and SPAK was performed to detect their expression level. SPAK pS373 blot was used as a control for hypotonic condition, and GAPDH was used as a loading control. Representative results from two independent experiments were shown.

To demonstrate detail observation of SPAK and OSR1 ubiquitylation and or degradation, we overexpressed GST-OSR1 and subsequently treat the HEK293 cell with 10 μM MG132 and MLN4924 for 24 h under resting and hypotonic stimulated condition. On the overexpressed GST-OSR1 cell, the neddylated form of CUL2 was abolished in the presence of MLN4924 (**Figure 3.20.**). As accordance with the previous result shown in **Figure 3.19.A.**, CUL4B expression was also increased after MLN4924 treatment under resting and stimulated condition. The increased bands intensity of CRBN and GST-tag protein were also observed after MLN4924 treatment. SPAK pS373 immunoblot, which was used as a control for hypotonic stimulation showed stronger band intensity under the hypotonic condition as expected. GAPDH was used as a loading control.

An increase in CUL4B expression after MG132 treatment was exhibited under the resting condition (**Figure 3.20.**). This increase was also shown by endogenous SPAK and OSR1 on both conditions, resting and hypotonic condition. Ubiquitinated protein after MG132 treatment under both resting and hypotonic condition was exhibited the highest intensity compared to the controls and that of MLN4924 treatment. However, the immunoblot using anti-ubiquitin antibody from HEK293 total lysate with OSR1 over-expressed only was not able to provide specific evidence whether the OSR1 was ubiquitinated or degraded. The detected ubiquitinated protein after MG132 treatment as shown in **Figure 3.20.** represented all ubiquitinated proteins in the cell. Thus, it could not be concluded as ubiquitinated OSR1.

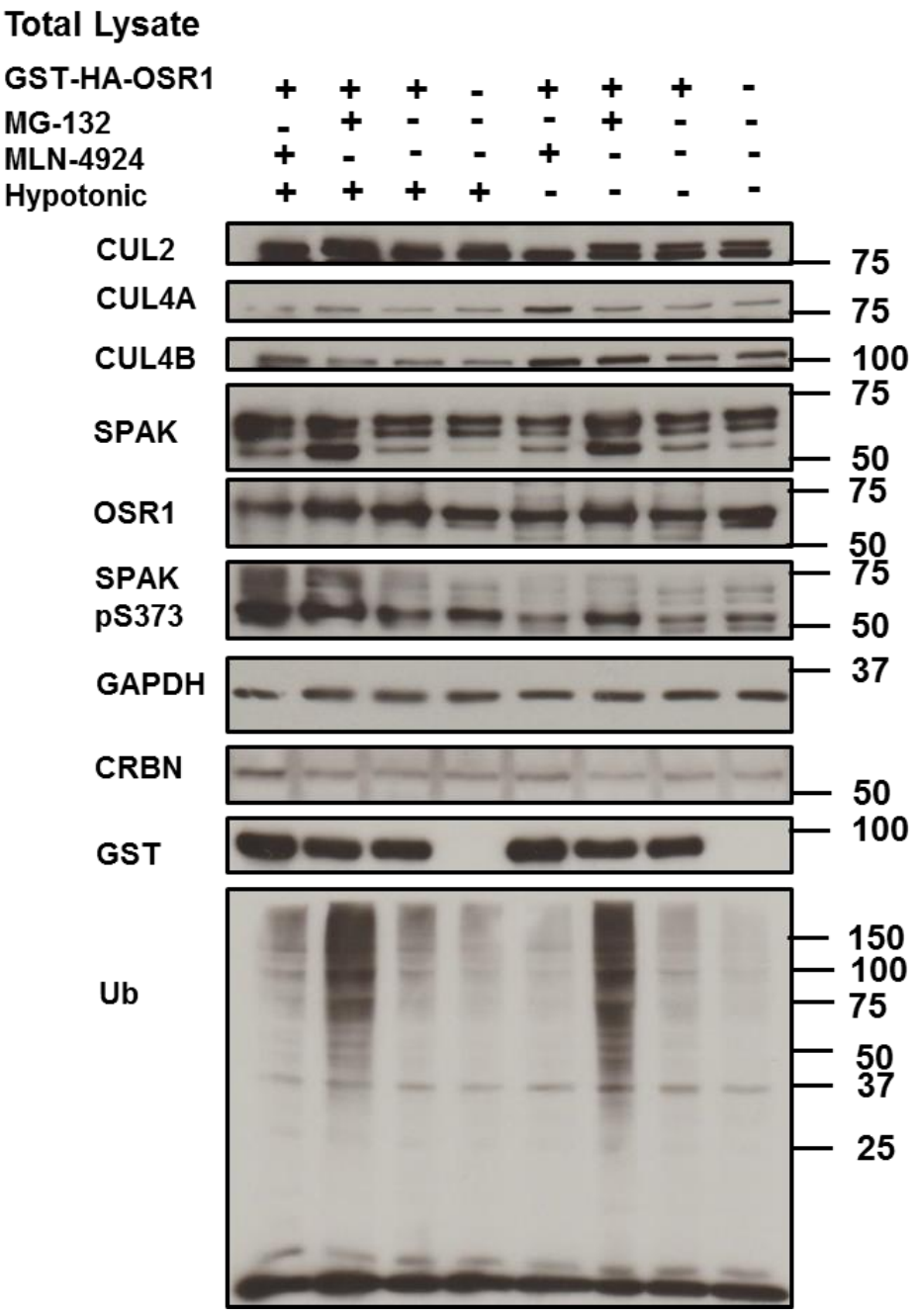

Figure 3.20. Expression of CRL4 subunits, SPAK and OSR1 after MLN4924 and MG132 treatment with overexpressed OSR1. CRL4 components expression of HEK293 cell with GST-HA-OSR1 overexpressed on HEK293 total protein lysate after treatment with MG132 10 μM and MLN4924 10 μM for 24h under the resting condition and hypotonic stimulation. Immunoblotting used denoted antibodies to detect each protein expression level. Representative result from two independent experiments was shown.

To provide more evidence on OSR1 ubiquitylation or degradation specifically, HA-Ubiquitin was co-expressed with GST-OSR1 (**Figure 3.21.**). Subsequently, the cells were treated with 10 μM MG132 for 24 h and 1 μM MLN4924 for 6 h under resting and hypotonic stimulated condition. The total cell lysates were then used for GST pull-down, and immunoblotting was performed. The result on the total lysate immunoblot showed that neddylated form of CUL2 was reduced under MLN4924 treatment. An increase of CUL4A and CUL4B expression after MLN4924 treatment was shown on both conditions, resting and hypotonic condition (**Figure 3.21.A.**). It also showed that the expression of CRBN and GST exhibited no differences in all treatments. HA immunoblotting which represented ubiquitinated proteins under MG132 treatment on either unstimulated or stimulated condition was the strongest intensity compared to any other conditions. SPAK pS373 immunoblot, which was used as a control for hypotonic stimulation showed more intense blot under the hypotonic condition as expected. GAPDH was used as a loading control.

As shown in **Figure 3.21.B.**, GST pull-down from co-expressed GST-OSR1 and HA-Ub resulted in more intensity of all sample on HA blot under hypotonic condition than resting condition. Under the hypotonic condition, there was no difference between HA-Ub blot of the untreated cell and the cell with MG132 or MLN4924 treatments. Interestingly, in resting condition, the intensity of HA blot after MG132 treatment demonstrated as the highest compared to the untreated cell and MLN4924 treatment. The result also suggested that OSR1 is ubiquitinated under the resting condition in which the CRL4 complex establishes the interaction with OSR1 (**Figure 3.21.B.**). Hypotonic condition, which WNK-signalling is stimulated, dissociates the interaction. Thus, ubiquitinated OSR1 could not be observed under hypotonic condition, even when the ubiquitylation and degradation process was inhibited by MG132 treatment.

The increase of HA blot intensity under resting condition after MG132 treatment and its steady expression after MLN4924 treatment suggested that MLN4924 is a perfect

negative confirmation of ubiquitylation. MLN4924 as an inhibitor of Nedd-8 activator enzyme prevent the protein from being ubiquitinated so that immunoblotting of ubiquitinated protein could not be detected or detected in low level.

However, important to note that the GST-OSR1, which was co-expressed with HA-Ub was also having HA-tag fused to OSR1 as GST-HA-OSR1. The same tag protein in both co-expressed proteins caused a bias result as HA immunoblotting represented both HA-OSR1 and HA-Ub.

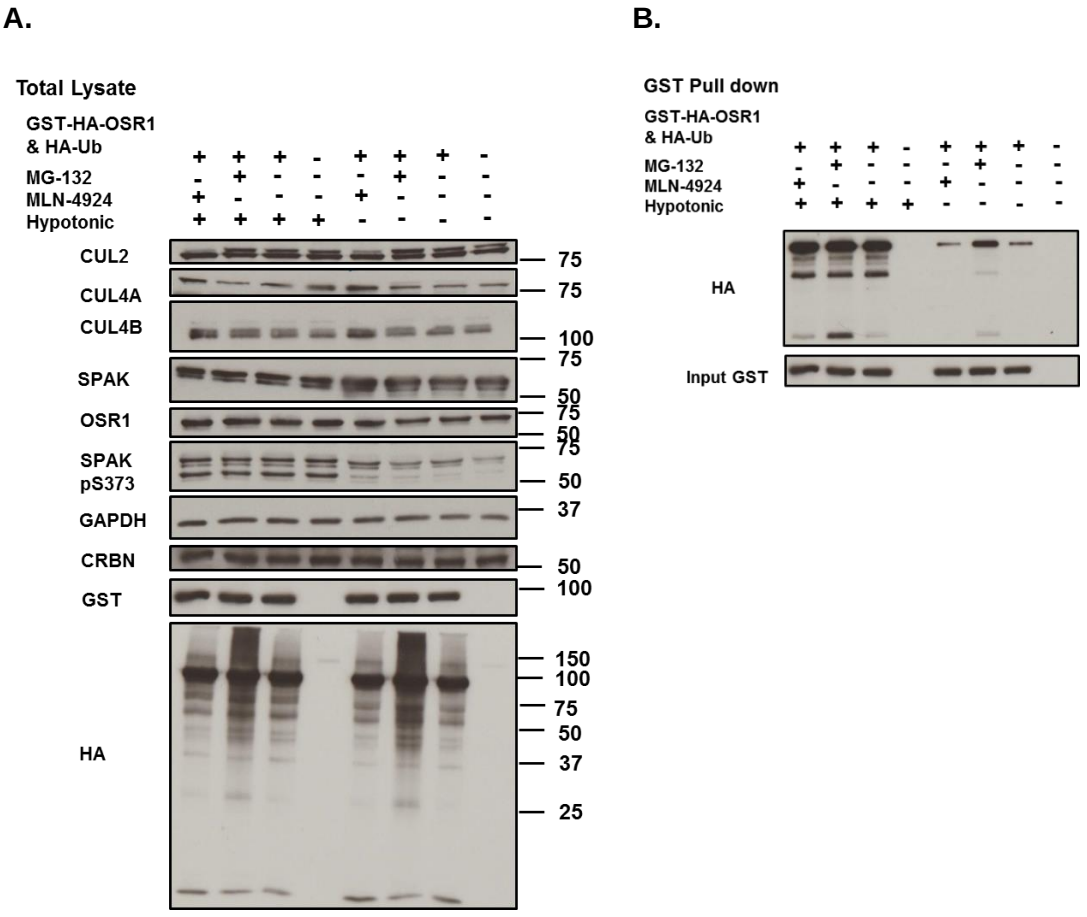

Figure 3.21. Expression of CRL4 subunits, SPAK and OSR1 after MLN4924 and MG132 treatment with co-expressed GST-OSR1 and HA-Ubiquitin. (A.) CRL4 components expression of HEK293 cell with GST-HA-OSR1 and HA-Ub co-expressed in HEK293 with the treatment of 10 µM MG132 for 24 h and 1 µM MLN4924 for 6 h under the resting condition and hypotonic stimulation. (B.) The total protein lysate was used for GST-pull-down. Immunoblotting using denoted antibodies was performed to detect each protein expression level. Representative results from two independent experiments were shown.

The same set of experiments were then performed to avoid bias by over-expressing FLAG-tagged of OSR1 as FLAG-OSR1 (**Figure 3.22.**), and co-expressed FLAG-OSR1 with HA-Ub (**Figure 3.23.**) in HEK293 cells. Following FLAG-OSR1 overexpression, the cells were treated with 10 µM MG132 for 24 h and 1 µM MLN4924 for 6 h under resting and hypotonic stimulated condition. The total cell lysates were then analysed by immunoblotting. The result showed that FLAG-OSR1 was successfully over-expressed (**Figure 3.22.**). The neddylated form of CUL2 was reduced under MLN4924 treatment, whereas CUL4A, CUL4B and DDB1 expression were not affected by MLN4924 on both conditions resting and hypotonic condition. MG132 treatment showed no effect on the CUL4A, CUL4B and DDB1 expression on both condition as well. Endogenous SPAK and OSR1 were showed an increase after MG132 treatment under hypotonic condition. It also showed that the HA immunoblot, which represented ubiquitinated proteins, has the strongest intensity under MG132 treatment on either resting or hypotonic stimulated condition compared to any other conditions. SPAK pS373 immunoblot, which was used as a control for hypotonic stimulation showed more pronounce expression under the hypotonic condition as expected. GAPDH was used as a loading control.

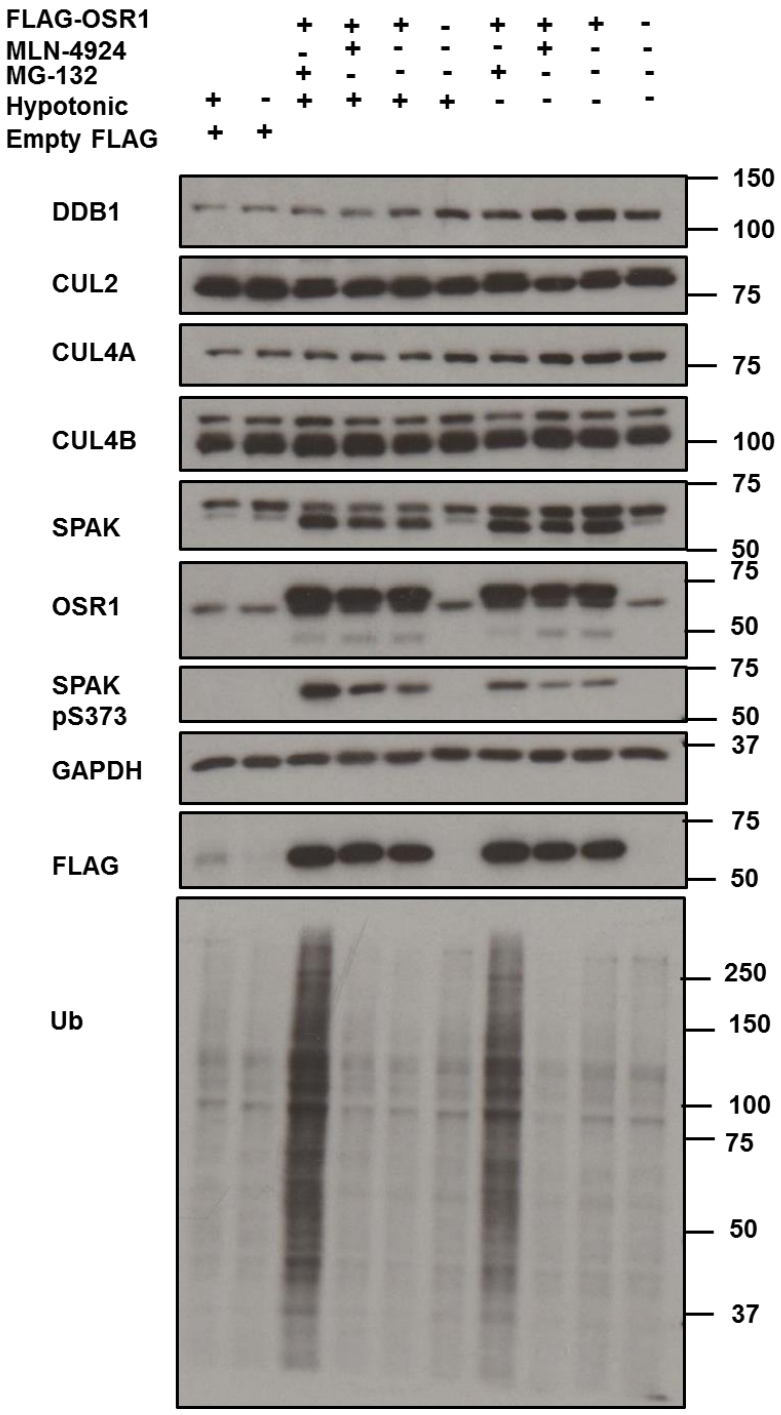

Figure 3.22. Expression of CRL4 subunits, SPAK and OSR1 after MLN4924 and MG132 treatment with overexpression of FLAG-OSR1. CRL4 components expression of HEK293 cell with FLAG-OSR1 overexpressed in HEK293 with the treatment of 10 μM MG132 for 24 h and 1 μM MLN4924 for 6 h under the resting condition and hypotonic stimulation. Immunoblotting using denoted antibodies was performed to detect each protein expression level. Representative result from two independent experiments was shown.

Figure 3.23.A. show the expression of CRL4 components, SPAK and OSR1 after MLN4924 and MG132 treatment from FLAG-OSR1 and HA-Ub overexpressed HEK293 cells. As shown in **Figure 3.23.A.**, FLAG-OSR1 and HA-Ub were successfully co-expressed. The neddylated form of CUL2 was reduced under MLN4924 treatment, whereas CUL4A, CUL4B and DDB1 expression were not affected by MLN4924 under both resting and hypotonic conditions. MG132 treatment showed no effect on the CUL4A, CUL4B and DDB1 expression on both resting and hypotonic conditions as well. Endogenous SPAK and OSR1 bands showed more pronounced intensity after MG132 treatment than MLN4924 treatment, which was more clearly observed under hypotonic condition.

Moreover, HA immunoblot, which represented ubiquitinated proteins, exhibited the highest expression under MG132 treatment condition compared to any other treatments under either resting or hypotonic conditions (**Figure 3.23.A.**). SPAK pS373 immunoblot, which was used as a control for hypotonic stimulation showed more pronounced intensity under the hypotonic than resting condition as expected. GAPDH in this experiment was used as a loading control.

As shown in **Figure 3.23.B.**, HA immunoblot from FLAG pull-down exhibited more ubiquitinated OSR1 after MG132 treatment under resting condition than hypotonic condition. This result supported the evidence that OSR1 degradation was inhibited by MG132, which showed stronger ubiquitinated OSR1 bands intensity under resting condition than hypotonic condition. It indicated that under resting condition, there was a factor that could promote OSR1 ubiquitylation and or degradation in which its activity was decreased by the hypotonic condition.

Further confirmation for investigation on OSR1 ubiquitylation could be done by Tandem-repeated Ubiquitin-Binding Entities (TUBE) pull-down assay (Hjerpe *et al.*, 2009). The Ubiquitin-Associated domain (4x UBA) protein, which is immobilized on the bead, could be used for pulling-down ubiquitinated protein. Thus, OSR1

immunoblotting analysis could be performed to detect more enriched ubiquitinated OSR1 protein from the precipitate (Emmerich and Cohen, 2015). We attempted to express the protein Ubiquilin containing 4X UBA domain in BL21 bacteria and perform protein purification. Unfortunately, the protein could not be expressed due to the major technical constraint, although the condition for the protein expression and induction has been optimised (see Figure 7.15 in Chapter VII. Appendices).

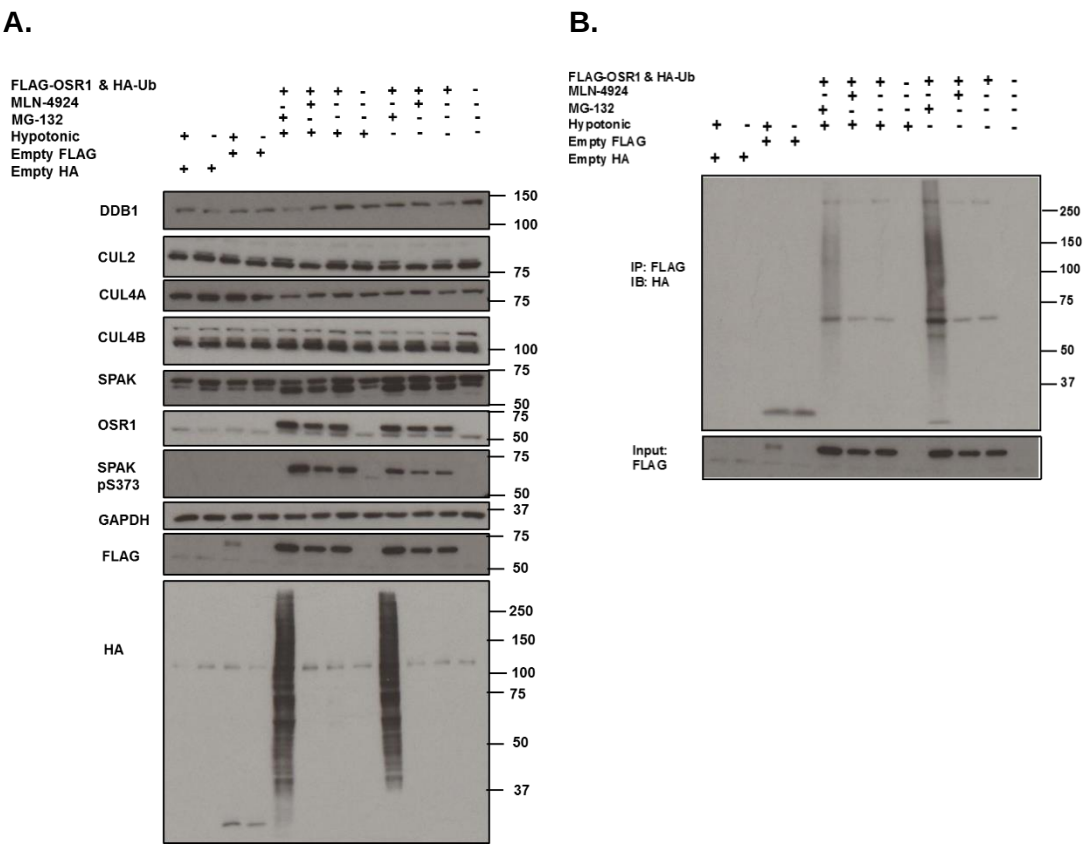

Figure 3.23. Expression of CRL4 subunits, SPAK and OSR1 after MLN4924 and MG132 treatment with co-expressed FLAG-OSR1 and HA-Ubiquitin. (A.) CRL4 components expression of HEK293 cell with FLAG-OSR1 and HA-Ubiquitin co-expressed in HEK293 with the treatment of MG132 10 µM for 24 h and MLN4924 1 µM for 6h under resting condition and hypotonic stimulation. (B.) The total protein lysate was then used for FLAG-pull down. Immunoblotting using denoted antibodies was performed to detect each protein expression level. Representative results from two independent experiments were shown.

3.4. CRL4 COMPLEX SUBUNITS ROLE ON SPAK/OSR1 UBIQUITYLATION AND DEGRADATION

3.4.1 Role of CRBN on SPAK/OSR1 ubiquitylation and degradation

Thalidomide was widely consumed around 50 years ago for reducing morning sickness in pregnant women, but it was found to cause congenital disability, including teratogenicity. The later study discovered that thalidomide possessed the anti-angiogenic activity and increased immune surveillance by targeting cereblon (CRBN). Thus, it is recently used for multiple myeloma cancer treatment (Ito *et al.*, 2010). CRBN, which forms E3 ubiquitin ligase complex with DDB1 and CUL4 protein is also targeted by other Immunomodulatory imide Drugs (IMiDs), which are thalidomide derivatives; lenalidomide and pomalidomide (Lopez-Girona *et al.*, 2012). The binding of IMiDs to CRBN-DDB1-CUL4A, causing a CRL activation that triggers their substrate degradation (Krönke *et al.*, 2014).

Considering that 1) OSR1 degradation was inhibited by MG132 as a result of its binding with the CRL4 complex as indicated by the results shown in **Figure 3.20.** to **3.23.**, and 2) there were three DCAF proteins (CRBN, WDR3, and WDR6) in CRL4 complex which could bind to non-phospho peptide OSR1 S325. Thus, the question on which DCAF subunits binds to OSR1 has emerged. In order to answer this question, several small molecules belong to IMiDs class, i.e. thalidomide and pomalidomide (see **Figure 3.24.** for their structure) were employed to investigate the role of CRBN on SPAK and OSR1 degradation on HEK293 cell and U266 cell.

Pomalidomide treatment was applied to U266 cell objected to being used in the system as a positive control. U266 cell is a non-adherent multiple myeloma cell line, which expressing IKZF3 (aiolos) protein, an endogenous substrate for CRBN-DDB1-CUL4 complex (Krönke *et al.*, 2014). Immunoblot of aiolos could provide information that the cell was susceptible to pomalidomide in the range concentration which was

applied in the experiment. The cells were also treated with indisulam (the structure is showed in **Figure 3.24.C.**), a small molecule activator of CRL4 complex, which involves DCAF15 as DCAF subunit instead of CRBN (Uehara *et al.*, 2017). Thus, the investigation on the question of whether SPAK and or OSR1 degradation by CRL4 was CRBN dependent or via other DCAF subunits can be answered.

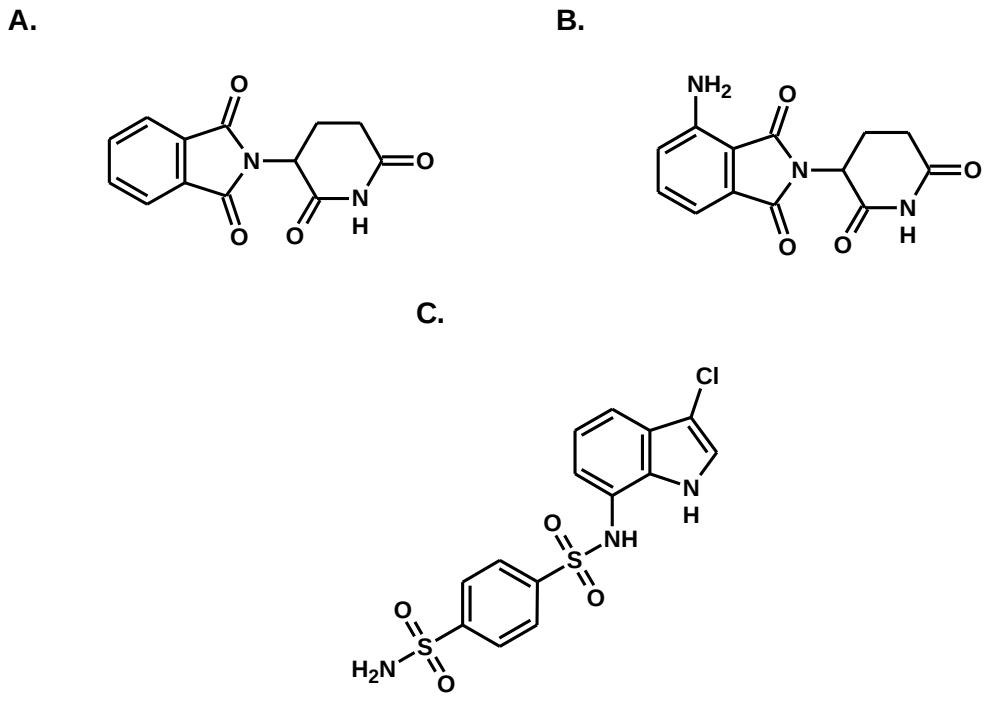

Figure 3.24. Chemical structure of small molecules of CRLs regulator. (A.) Thalidomide, (B.) Pomalidomide, and (C.) Indisulam

3.4.1.1 Thalidomide and Pomalidomide treatment on HEK293 cells

Thalidomide was applied for the treatment of HEK293 cells in a series concentration ranging from 0.01 to 50 µM for 1 and 3 h. Immunoblots of CRL4 components, SPAK, OSR1, aiolos, and GAPDH as a loading control were performed. The result showed that aiolos expression was decreased with the increase of thalidomide concentration on 1 h and 3 h incubation, even though the signal was very weak (**Figure 3.25.**). CRBN immunoblot, however, could not show clear blot due to the antibody sensitivity

issue. WDR3 expression was decreased by increasing the concentration of thalidomide in 1 h incubation, but there were no changes in its expression after 3 h incubation. However, WDR6 expression could not be observed in 1 h incubation. Thus, the lack of differential expression level from CUL4A, CUL4B, SPAK and OSR1 after thalidomide treatment may be due to the incubation time that was too short. Three hours incubation of thalidomide probably was not long enough to trigger changes in the expression level of these proteins.

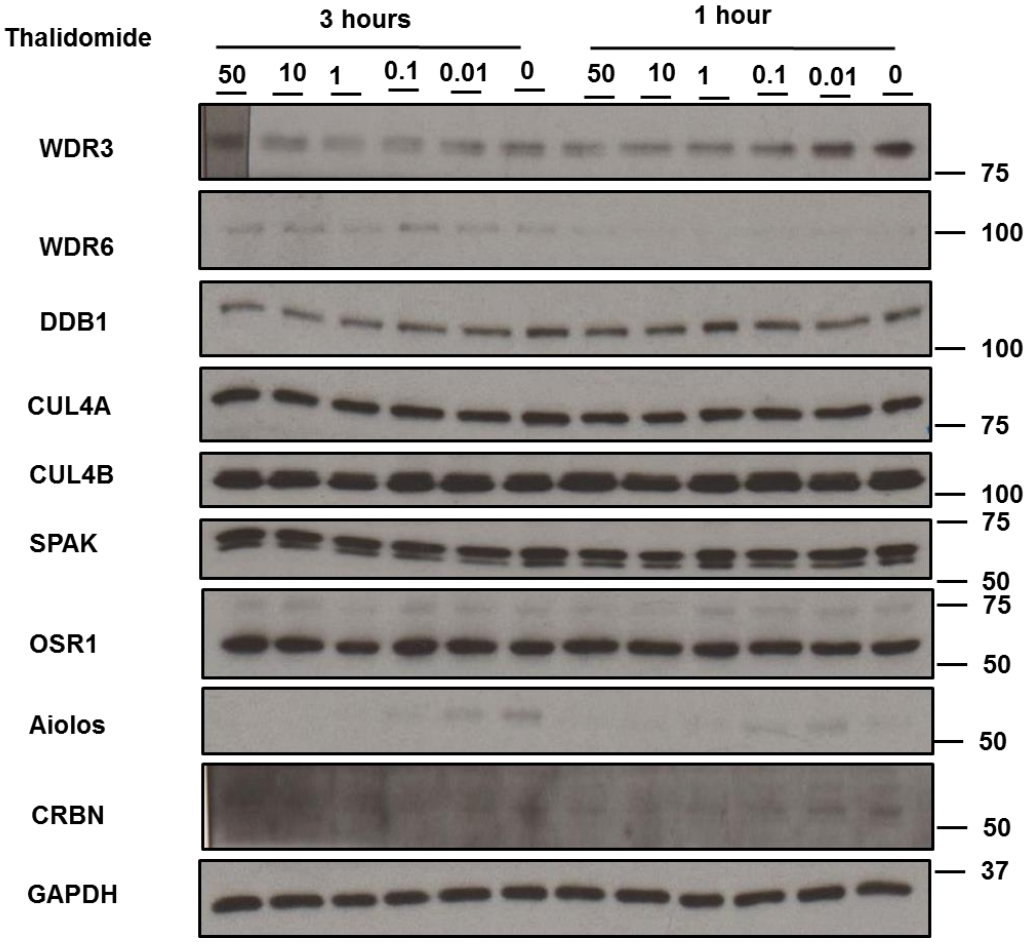

Figure 3.25. Expression of CRL4 subunits, SPAK, OSR1 and aiolos on HEK293 cell after 1 and 3 h thalidomide treatment. Thalidomide was incubated in HEK293 cell culture for 1 and 3 h in different serial concentration (µM) before the total protein lysate was prepared and analysed by immunoblotting. Immunoblotting of all denoted antibodies was performed with GAPDH as a loading control. Representative result from two independent, triplicate experiments was shown.

Longer incubation time for thalidomide as well as pomalidamide (6 h) treatment was then performed (**Figure 3.26.**). The longer incubation time, however, did not cause any changes on SPAK and OSR1 expression level. WDR3 expression was likely to decrease, which was started from 10 and 50 µM of thalidomide and pomalidomide, respectively. Furthermore, the WDR6 expression showed an increase at 30 and 10 µM of thalidomide and pomalidomide treatment, respectively. However, there were no changes in the expression of other proteins. Aiolos expression could not be detected in this experiment, as aiolos expression in HEK293 cell was known to be very low (http://www.proteinatlas.org/ENSG00000161405-IKZF3/cell, 2017).

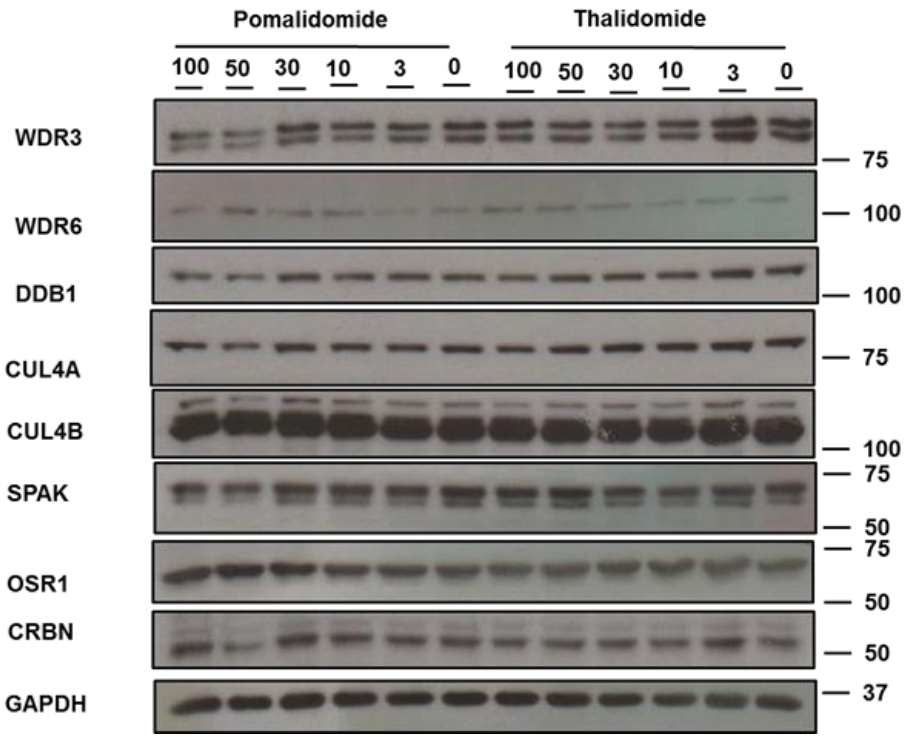

Figure 3.26. Expression of CRL4 subunits, SPAK, and OSR1 on HEK293 cell after 6 h thalidomide and pomalidomide treatment. Pomalidomide and thalidomide were incubated in HEK293 cell culture for 6 h in different serial concentration (µM) before the total protein lysate was prepared and analysed by immunoblotting. Immunoblotting of all denoted antibodies was performed with GAPDH as a loading control. Representative result from two independent, triplicate experiments was shown.

To overcome the low protein expressions, we increased the concentration of OSR1 protein exogenously by overexpressing GST-OSR1 in HEK293 cell. GST-OSR1 overexpressed HEK293 cell then was treated with pomalidomide for 6 h in the concentration of 1; 3; 10; 50; and 100 µM under resting and hypotonic condition. Aiolos expression with two bands on molecular weight 58 and ~70 kDa were observed (**Figure 3.27.**). Based on the ~70 kDa band of aiolos, which represented the phosphorylated form of aiolos (http://www.abcam.com/ikzf3-antibody-ab64400.html, 2017), the highest aiolos expression was observed in the cell without pomalidomide treatment. The phosphorylated aiolos expression started to decrease from 1 µM pomalidomide treatment. In contrast, as shown in the lower MW of aiolos band (58 kDa), the increase of aiolos expression was clearly exhibited started from 1 µM of pomalidomide treatment under both resting and hypotonic condition. However, pomalidomide treatment under resting and hypotonic condition did not alter any expression level of any other proteins (WDR6, DDB1, CUL4A, CUL4B, SPAK, and OSR1).

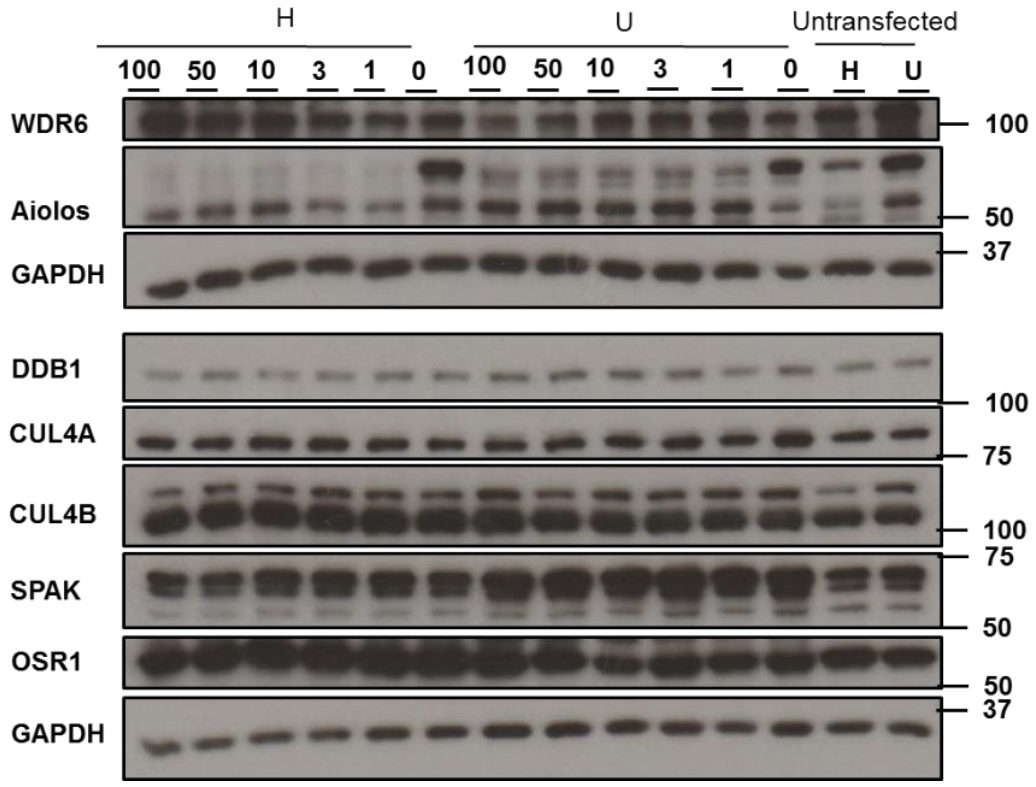

Figure 3.27. Expression of CRL4 subunits, SPAK, OSR1, and aiolos on HEK293 cell after 6 h of pomalidomide treatment. Pomalidomide was incubated in GST-OSR1 overexpressed of HEK293 cell for 6 h in different serial concentration (μM) and being left under resting condition (U) or treated with hypotonic buffer (H) before the total protein lysate was prepared and analysed by immunoblotting. The cell without any plasmid transfection (untransfected) was used as transfection control. Immunoblotting of all denoted antibodies was performed with GAPDH as a loading control. Representative result from two independent, triplicate experiments was shown.

3.4.1.2 Pomalidomide treatment on U266 cells

Low expression of aiolos, an endogenous substrate for CUL4-DDB1-CRBN complex, in HEK293 cell, caused the results hard to be concluded. Aiolos expression function as control positive for the experiments. Thus, the U266 cell line that profoundly expresses aiolos instead of HEK293 cell (http://www.proteinatlas.org/ENSG00000161405-IKZF3/cell, 2017) was used.

Before proceeding to the experiment with U266 cell lines, confirmation to ensure that the U266 cells exhibited the same system as HEK293 cells was carried out. To confirm the CRL4 components binding to SPAK and OSR1 in U266 cells,

immunoprecipitation of SPAK and OSR1 were performed. It was clearly showed that CRL4 components bound to SPAK and OSR1 under unstimulated more than the hypotonic condition in U266 cells (Figure 7.6. in Chapter VII. Appendices). This result was in accordance with the results of immunoprecipitation in HEK293 cells (see Figure 3.7.).

The U266 cells then were treated with pomalidomide under resting condition for 6 h in the concentration of 0.1; 1; 3; 20; 30 and 50 µM. Immunoblotting to detect DCAF proteins (WDR3, WDR6 and CRBN), aiolos, SPAK, and GAPDH as loading control were performed (**Figure 3.28.**). The result showed that increasing concentration of pomalidomide leads to the decrease of aiolos and SPAK expression. An increase of WDR6 expression was also observed with the increase of pomalidomide treatment. Noteworthy, decreasing of SPAK expression was ended at 30 µM of pomalidomide treatment and it started to show an increase at concentration 50 µM.

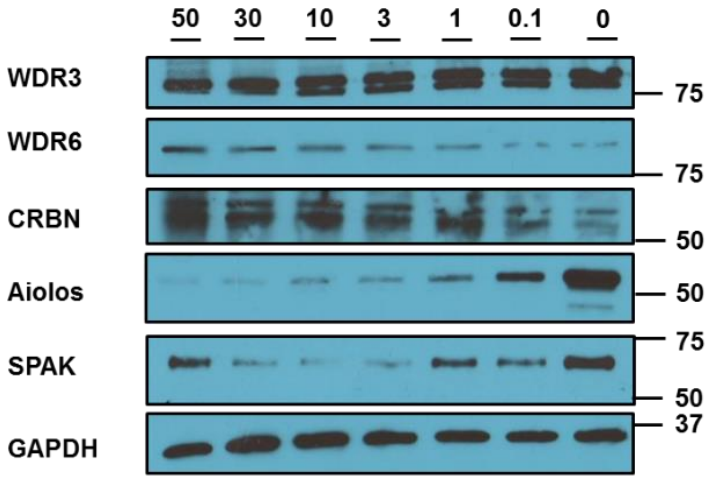

Figure 3.28. Expression of CRL4 protein subunits (WDR3, WDR6 and CRBN) and its substrate after pomalidomide treatment. Pomalidomide in different concentration (µM) was incubated for 6 h in U266 cells (~1x10^6 cells) under basal condition. Immunoblotting utilising respective antibodies was performed afterwards. GAPDH was used as a loading control. Representative result from two independent, triplicate experiments was shown.

In order to investigate the difference between CRL4 subunits, SPAK and OSR1 expression after pomalidomide treatment under resting and hypotonic condition, the same serial concentration of pomalidomide was incubated on U266 cells for 6 h. After the cells were treated with pomalidomide, the cells then being left untreated (resting condition) or treated with low chloride hypotonic buffer (hypotonic condition) before cell lysis. **Figure 3.29.** show that hypotonic stimulation affected the expression of all detected proteins after pomalidomide treatment. It was showed on the immunoblot of Erk1/2 and GAPDH as a loading control, there was an obvious decreasing expression on the hypotonic condition. The decreased expression after pomalidomide treatment was also observed in other proteins. Treatment with pomalidomide as an addition to the hypotonic low-chloride buffer treatment on U266 cells might trigger cell stress. As non-adherent cells with sphere form, U266 cells might develop cell membrane disruption upon treatment with hypotonic low-chloride buffer.

A contrary result, which was depicted by these two experiments (see **Figure 3.28.** and **Figure 3.29.**), might be due to the cell number that was used. In the first experiment (**Figure 3.28.**), the number of cells that were used was five times higher than the second experiment (**Figure 3.29.**). Besides this 'technical' reason, it also suggested that CRBN as DCAF subunit in CRL4 complex it is not involved in SPAK and OSR1 ubiquitylation/degradation as IMiDs are selectively bound only to CRBN (Ito *et al.*, 2010).

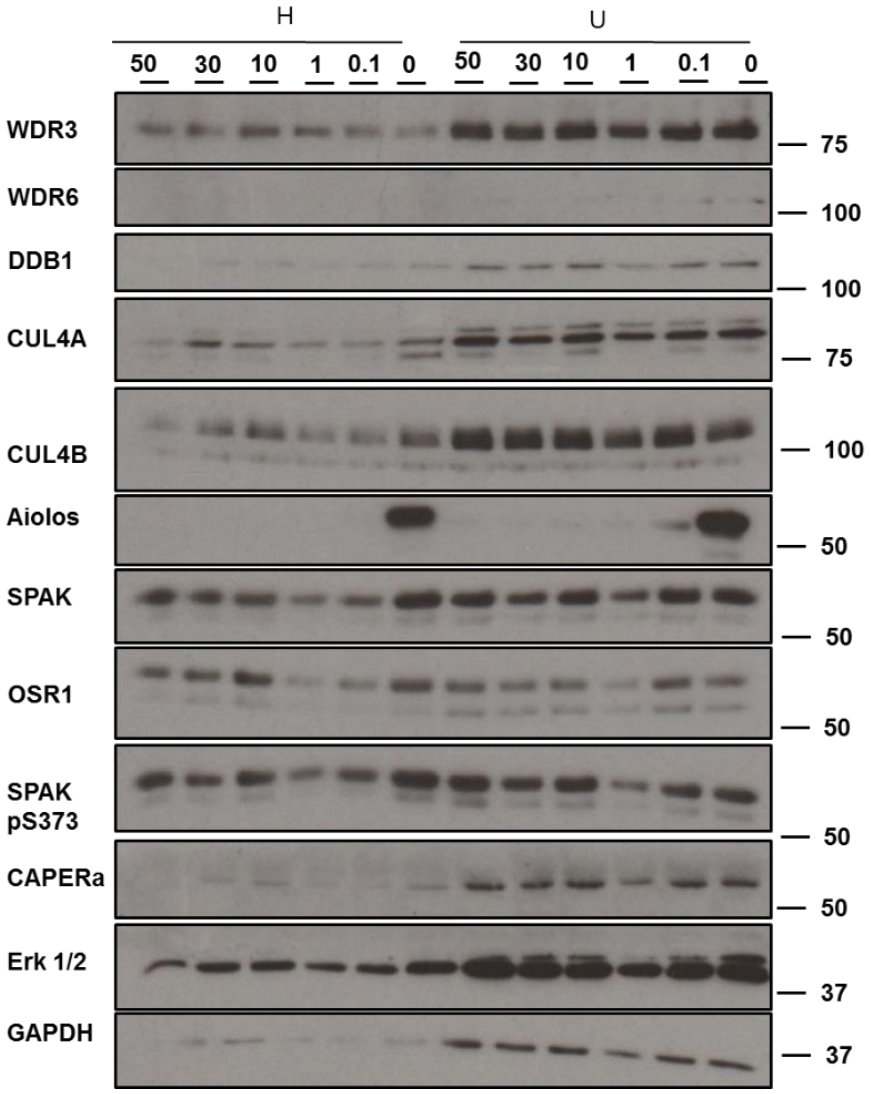

Figure 3.29. Expression of CRL4 protein subunits (WDR3, WDR6 and CRBN) and its substrate after pomalidomide treatment under resting and hypotonic condition. Pomalidomide in different concentration (µM) was incubated for 6 h in U266 cells (~2x10^5 cells) under resting and hypotonic stimulated condition. Immunoblotting utilising respective antibodies was performed afterwards. GAPDH was used as a loading control. Representative result from two independent, triplicate experiments was shown.

3.4.1.3 Indisulam treatment on U266 cells

To study further whether other DCAF proteins are involved in SPAK/OSR1 degradation, indisulam was applied for the treatment of U266 cells. Indisulam act as an activator of CRL4 complex with DCAF15 as its substrate receptor. CRL4 complex with DCAF15 is involved in its substrate, CAPERα, degradation (Uehara *et al.*, 2017).

The U266 cells were treated with indisulam in the concentration of 0.01; 0.1; 1; 3; and 10 µM for 24 h. After 24 h, the cells were being left under resting condition or stimulated with the hypotonic buffer for 40 min before cell lysate preparation and immunoblotting were performed. The result showed that under resting condition, as expected, CAPERα expression was reduced along with the increasing concentration of indisulam (**Figure 3.30.**). The steady expression of SPAK and OSR1 were exhibited on all given concentration of indisulam on both conditions. Notably, the expression of other proteins (WDR3, WDR6, DDB1, CUL4A and CUL4B) were decreased started from 0.1 µM of indisulam under resting condition. However, these decreases were also observed on GAPDH as a loading control, which was more profound under hypotonic condition. Thus, it suggested that the decrease of the protein expression was not due to indisulam effect on the protein level and indisulam may be toxic to the cell, which can lower the total protein expression.

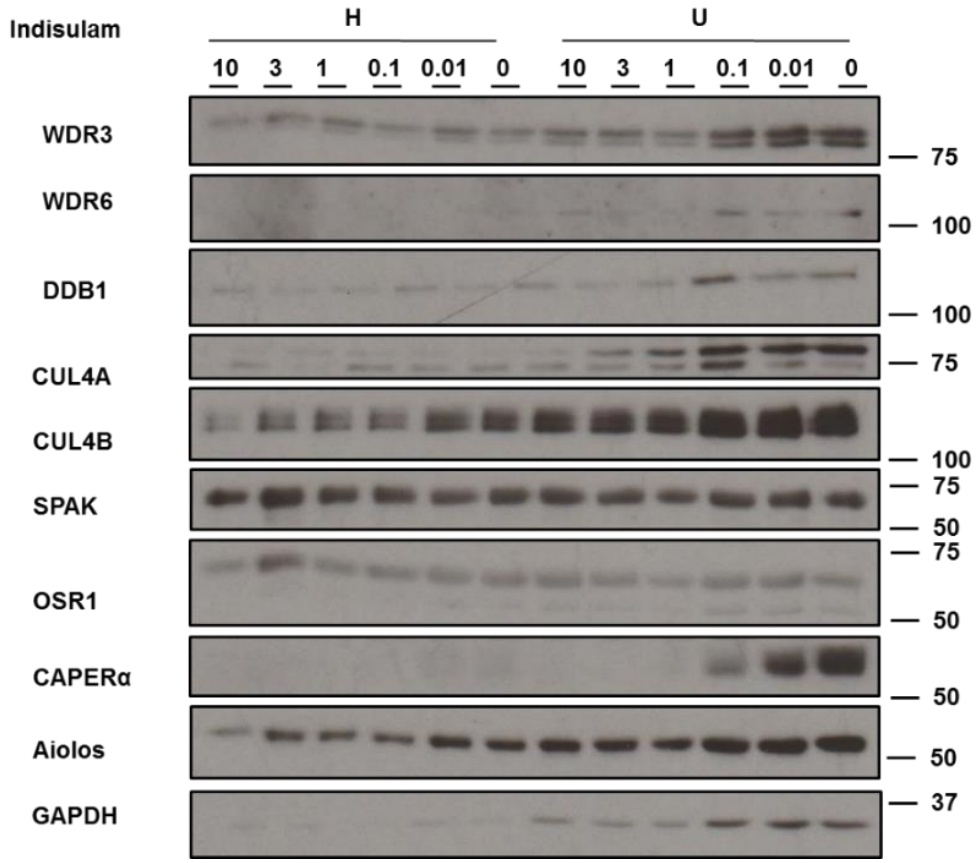

Figure 3.30. Expression of CRL4 subunits, SPAK, OSR1, aiolos and CAPERa after indisulam treatment. Indisulam in different concentration (µM) was incubated with U266 cell (~8x10^4 cell) for 24 h under resting and hypotonic stimulated condition. Immunoblotting utilising respective antibodies was performed afterwards. GAPDH was used as a loading control. Representative result from two independent, triplicate experiments were shown.

Considering that the expression of all protein was reduced significantly under hypotonic condition, which was also observed in the previous experiments with pomalidomide treatment, it was assumed that the reduction of protein expression might be caused by the cell was under stress condition. In order to overcome this stress condition, another experiment with the same set of indisulam concentration with the higher cell number (~1x10^5 cells) was conducted (**Figure 3.31.**). Since the GAPDH as a loading control in the previous experiment was being affected by indisulam treatment under hypotonic condition (see **Figure 3.30.**), another loading control protein was used. Considering that indisulam is a compound which affects the cell cycle progression, β-actin, an extracellular matrix (ECM) protein, which is not involved in cell cycle or cell proliferation was chosen as a loading control.

Figure 3.31. show that SPAK and OSR1 expression were not affected by indisulam treatment regardless of the condition. In general, except SPAK and OSR1, the expression of all proteins (WDR3, CUL4A, CUL4B and aiolos) was decreased under hypotonic stimulation. This decrease was also showed by β-actin and Erk1/2 as a loading control. It was clearly indicated that the cell number which was used in these experiments still could not cope with the stress caused by the hypotonic condition and indisulam treatment. Thus, another experiment that used higher cell number, perhaps at least $1x10^6$ cell/well, need to be accomplished. Unfortunately, CAPERα expression could not be observed at all due to mishandling on antibody storage. It was speculated that the unchanging expression of SPAK and OSR1 upon indisulam treatment was because the DCAF15 was not a subunit of CRL4 that plays a role in SPAK and OSR1 ubiquitylation and degradation.

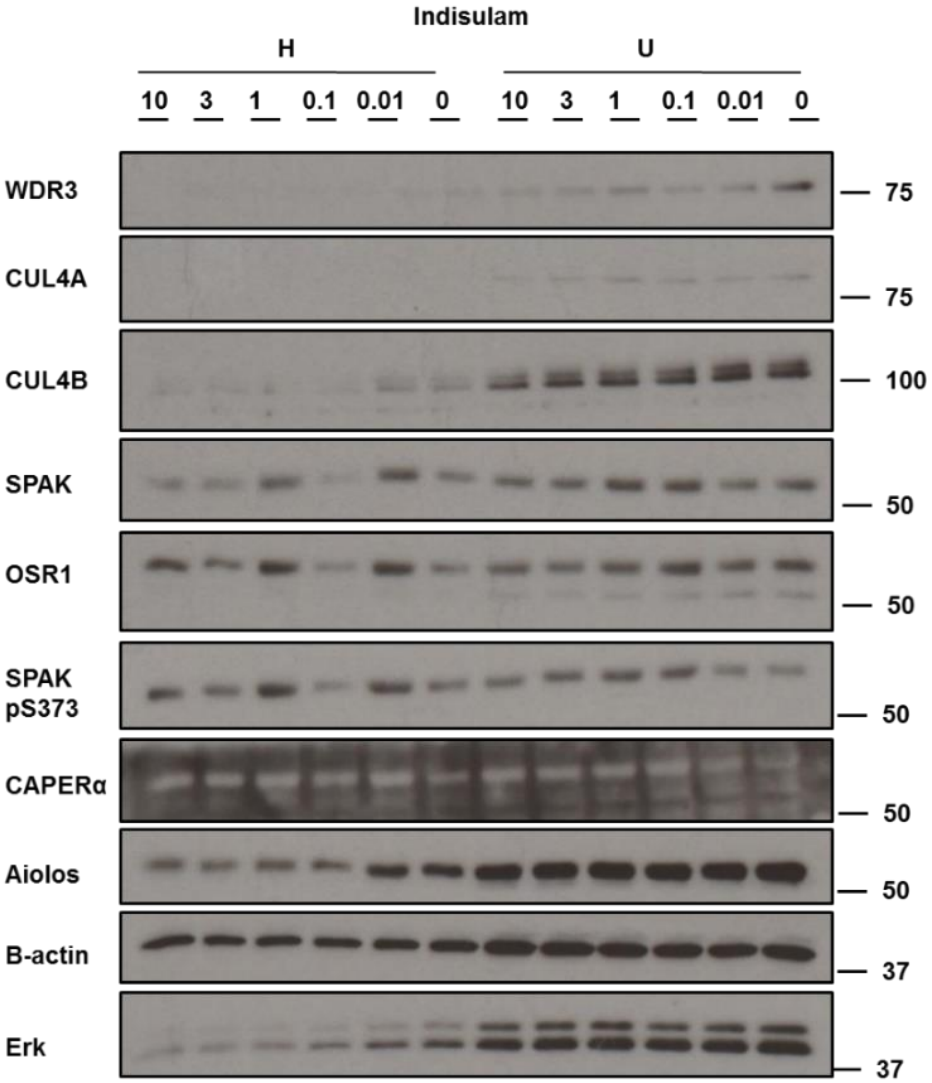

Figure 3.31. Expression of CRL4 subunits, SPAK, OSR1, aiolos and CAPERα after indisulam treatment. Indisulam in different concentration (µM) was incubated with U266 cells (~1x10^5 cell) for 24 h under resting and hypotonic stimulated condition. Immunoblotting utilising respective antibodies was performed afterwards. β-actin and Erk1/2 were used as a loading control. Representative result from two independent, triplicate experiments was shown.

3.4.2 Role of DDB1 and WDR3/WDR6 on SPAK/OSR1 ubiquitylation and degradation

3.4.2.1 Generation of WDR3 and WDR6 KO clone by CRISPR

Clustered regularly interspaced short palindromic repeat (CRISPR) was first discovered in *E. coli* 30 years ago by Yoshida Ishino with unknown function due to the lack of sufficient DNA sequence data. This enigmatic function finally started to be uncovered by the discovery of CRISPR in Archaea, specifically in *Haloferax mediterranei*. The finding of the CRISPR in two of three domains promoted the research of its importance, which then Mojica and others in the year 2013 reported the discovery of CRISPR function in the immune system. In the same time, there are several genes responsible for DNA repair mechanism that were identified strictly associated with CRISPR, denoted as Cas (CRISPR-associated) genes. The CRISPR-Cas system was later found to function together as acquired immune system to protect bacteria against viruses and plasmids, similar to the system of RNA interference (RNAi) of eukaryotic cells (Ishino *et al.*, 2018).

Despite underappreciated CRISPR sequences and functions discoveries at those times, recent technology is widely applying CRISPR-Cas9 system for genome editing. The RNA-guided Cas9 nucleases from bacterial CRISPR-Cas systems promote targeted double-stranded DNA breaks in eukaryotic cells, which results in non-homologous end joining (NHEJ) or homology-directed repair (HDR) pathways for the cellular repair mechanism. These cellular repair mechanisms can be exploited to stimulate error-prone or defined alterations. However, this system can lead to undesirable potential off-target double-strand DNA breaks and indel formation. Thus, the technology to combine the CRISPR-Cas9 system with D10A mutant nickase was developed to increase the specificity. The combination involves a pair of offset sgRNAs complementary to opposite strands of the target site. Thus, the ‘nicking’ process leads to site-specific double-strand break and NHEJ (Ran *et al.*, 2013) (see

Figure 3.32.). The advantage of its high specificity of this system, the CRISPR-Cas9 by dual nickase was applied for knocking out WDR3 and WDR6. The WDR3 and WDR6 KO clones then were used to study its effect on SPAK and OSR1 protein ubiquitylation/degradation.

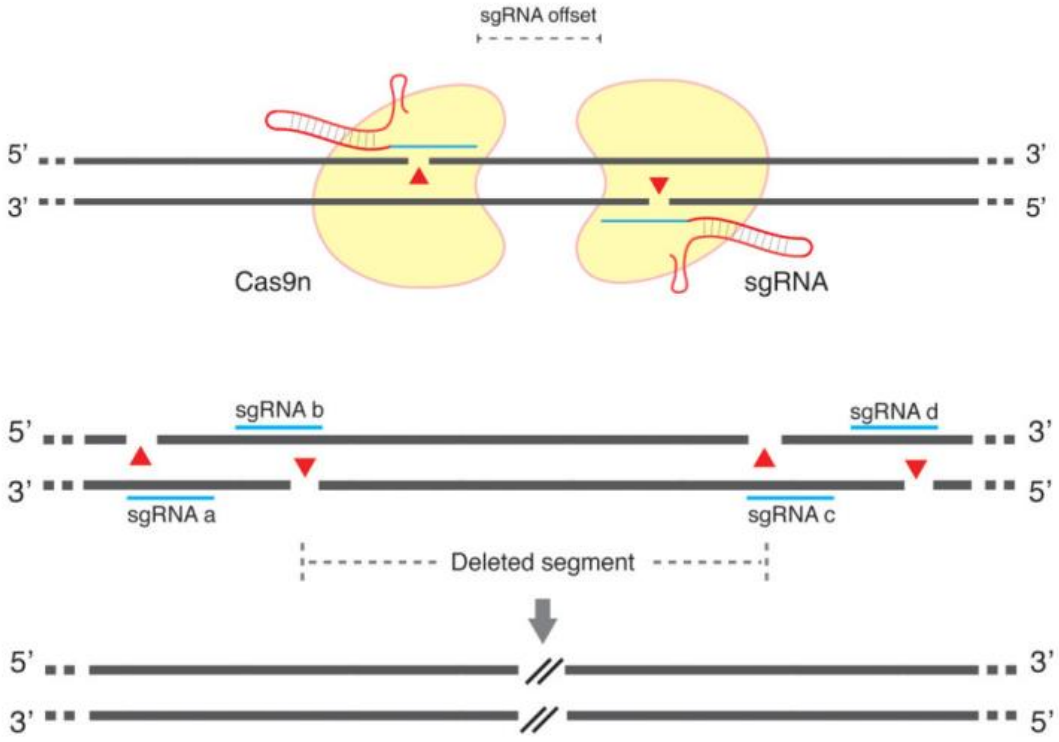

Figure 3.32. Genome editing using the CRISPR system by dual nickase Cas9 guided primer pairs. A schematic diagram describes DNA double-strand breaks using a pair of Cas9 D10A nickases (Cas9n). The D10A mutation allows Cas9 to cleave only the strand complementary to sgRNA. Thus, a pair of sgRNA-Cas9n complexes can nick double strands together (Ran *et al.*, 2013).

Stage 1. Transfection

Prior to transfection, DNA plasmid multiplication and extraction of the cDNA plasmid guide pairs resulted in the concentration and purity as listed in Table 3.2. The DNA concentration of pBABED-WDR6 Sense A and pBABED-WDR6 Sense B was very low. The absorbance ratio of 260/280 and 260/230, which less than 1.7 and 2.0 respectively suggested that DNA contain RNA and protein impurities. Thus, the plasmid guide pairs of WDR6 As A and WDR6 S A, as well as WDR6 As B and WDR6 S B were not included for transfection.

Transfection was done with two different amounts of PEI (1 mg/mL). The first mixture was a mixture of each guide pair with 20µL of PEI for each pair (denoted WDR3 A, WDR3 B followed by 1, 2 or 3 showing the plate number). The second one was a mixture of two guide primer pairs with total 20 µL PEI (denoted as WDR3 AII, WDR3 BII and WDR6 CII). These two modifications were objected to investigate whether the cells were survived with the total amount PEI of 40 µL, as PEI in a certain amount is known to be toxic to the cell (Breunig *et al.*, 2007, Kafil and Omidi, 2011).

Table 3.2 cDNA plasmid used for WDR3 and WDR KO

Plasmid	Concentration (µg/ µL)	A260/280 ratio	A260/230 ratio
pX335-WDR3 Antisense A	1.18	1.80	2.20
pBABED-WDR3 Sense A	0.38	1.80	2.20
pX335-WDR3 Antisense B	1.32	1.80	2.15
pBABED-WDR3 Sense B	0.41	1.80	2.22
pX335-WDR6 Antisense A	0.95	1.80	2.25
pBABED-WDR6 Sense A	0.01*	1.60*	1.44*
pX335-WDR6 Antisense B	1.27	1.80	2.22
pBABED-WDR6 Sense B	0.04*	1.64*	1.85*
pX335-WDR6 Antisense C	1.27	1.80	2.22
pBABED-WDR6 Sense C	1.62	1.78	2.18

Note: * the cDNA plasmids were in low concentration and purity, they were not included in the further steps

Stage 2. Initial screening of pool

Initial screening for WDR3 and WDR6 KO was done by western blot analysis to all of the unsorted transfected cells (in the number of 2x10^5 cells), *i.e* WDR3 A1, WDR3 A2, WDR3 A3, WDR3 B1, WDR3 B2, WDR3 B3, WDR6 C1, WDR6 C2, WDR6 C3, WDR3 AII, WDR3 BII, and WDR6 CII (data not shown). Top four pools, which showed the high knockdown percentage of WDR3 from all the WDR3 pools then were selected to proceed to the next stages. However, only WDR6 CII pools were showed WDR6 knockdown, so this pool then was used for further steps (**Figure 3.33.**).

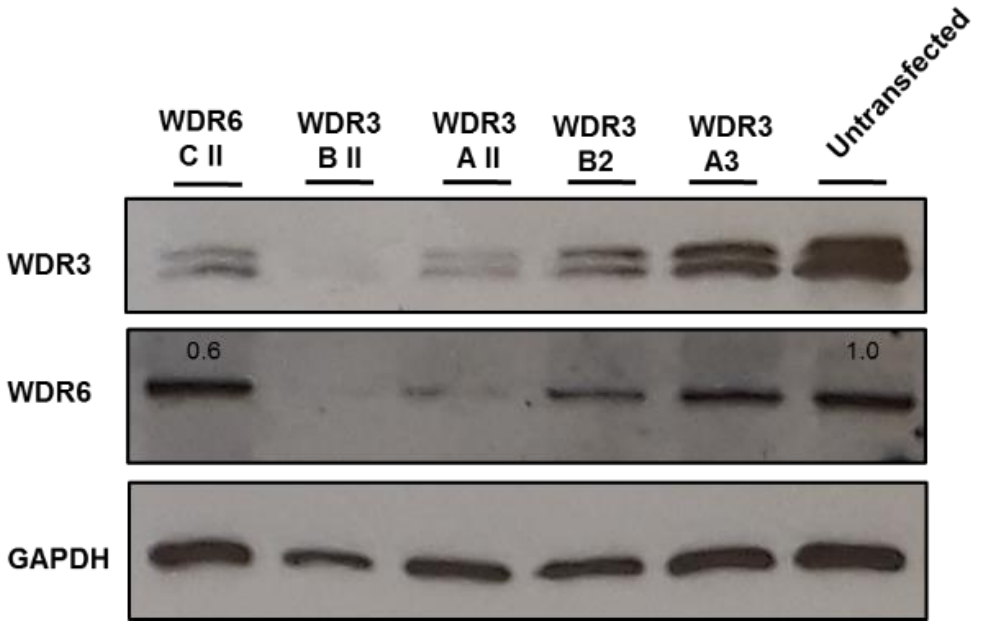

Figure 3.33. Immunoblot of first pool transfected clone of WDR3 and WDR6 knockout by CRISPR. As much as 2x10^5 cells were lysed by freeze and thaw method. Cell lysis was conducted using 80 µL of 1% Nonidet-40 Lysis Buffer. A 20 µL of 4XSDS sample buffer was added and boiled at 90ºC for 5 min prior to SDS-PAGE. Intensity band ratio between the respective band and untransfected sample is showed on WDR6 KO. Quantification was normalised against the highest intensity of the GAPDH band using ImageJ. Result from a single experiment was shown.

Stage 3. Single-cell sorting

Based on the initial screening of the first pool, then selected pools proceeded to the single-cell sorting. Since there was no GFP fusion protein in any of the guide primer pairs that were transfected, the alternative method for single-cell sorting, *i.e.* single cell dilution method was chosen. All the wells, which exhibited the sign of cell growth, by a yellow colour change on the DMEM media were identified and counted. A number of the wells, which showed cell growth that was obtained from the cell dilution in two of 96-well plate is displayed in Table 3.3.

Table 3.3 Number of clone growth by single-cell dilution

Pool	Clone *g*rowth (well) / total well
WDR3 A3	64/222
WDR3 B2	10/240
WDR3 AII	5/232
WDR3 BII	6/240
WDR6 CII	7/216

Stage 4. Clone recovery and growth

Each of the clone obtained from the single-cell sorting then was recovered and grown in the 24-well plate. **Figure 3.34.** show the change of media colour in some wells in the 24-well plate after recovery for 7-10 days. The growth rate for each clone in this stage was varied. Thus, the clones were undergoing recovery and growth for a further week.

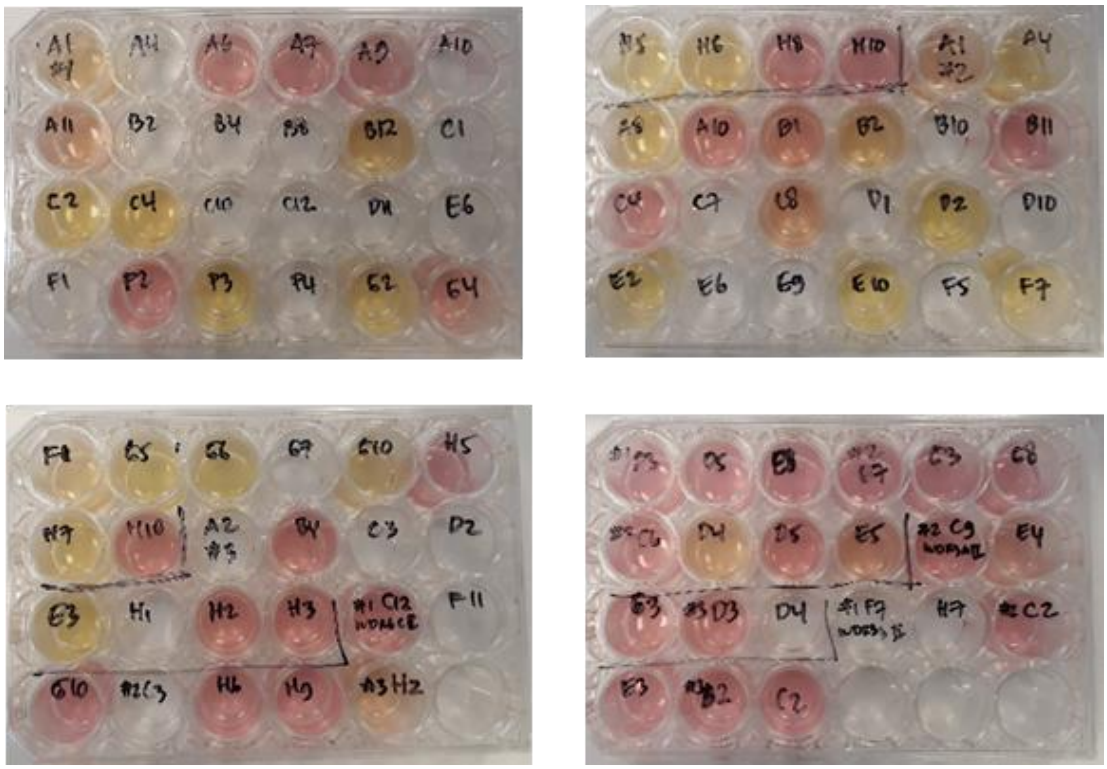

Figure 3.34. Clone of WDR3 and WDR6 KO selected from single-cell sorting. Clone recovery and growth was done in 24-well plate for 7-10 days. The picture was taken on seven days of incubation, and empty wells showed the clone was already prepared for screening and selection.

Stage 5. Screening and selection

After the full period of clone recovery and growth was achieved, the clones which showed the sign of growth proceeded to the next step. The total protein lysate was prepared and applied for western blot to check the WDR3 and WDR6 knockdown compared to the WT. **Figure 3.35.** show that all clones were having WDR3 or WDR6 knockdown with different percentage compared to WT. The GAPDH bands as a loading control in clone A4 was lost probably due to the knockdown of WDR3, which affected the expression of GAPDH. Even though the GAPDH blot of WT also showed slightly more intense than the rest of the sample, the lost expression of the WDR3 and WDR6 in some clones indicated that WDR3 and WDR6 were knocked down. Genomic DNA from these clones and some other clones were then prepared to be used for clone confirmation by PCR.

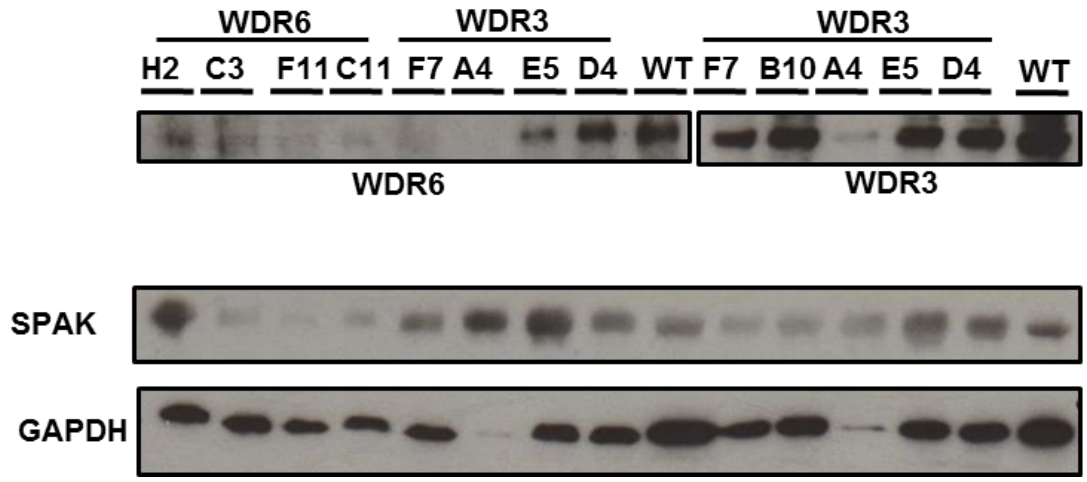

Figure 3.35. Immunoblot of WDR3 and WDR6 KO clones obtained from recovery and growth stage. Total protein lysate from each clone was prepared on SDS loading buffer and separated by SDS-PAGE. Anti-WDR3 (1:1000) and Anti-WDR6 (1:1000) with anti-IgG Rabbit antibody (1:2500) were used to check the knockdown of WDR3 and WDR6 on each clone. GAPDH was used as a loading control. Result from a single experiment was shown.

Stage 6. Clone confirmation

Confirmation of WDR3 or WDR6 KO by PCR employed primers in the location where the 'nicked' sequence was deleted. The PCR product where there was no deletion, as for WT, were expected to have a product with the length of 423 bp**. Figure 3.36.** show the PCR product of WT in the expected length (~420 bp). However, the PCR products with no deletion were also demonstrated by all WDR3 KO clones (A4, B2, B4, B8, C1, C10, E6, B10, H1, F7 and H7). Clone E5 of WDR3 KO in **Figure 3.36.B.** was showed similar PCR product with WT. Clone D4 of WDR3 KO resulted in 4 PCR products with different length to WT (~400; ~450; ~500 and ~550bp).

WDR6 ex2 KO primers amplified the region of WT in the length of 434bp (**Figure 3.36.B.**). Clone F11 and C3 resulted in 3 PCR product with the length ~380; ~400 and ~450bp which could be differentiated from the WT. Interestingly, clone C11 of WDR6 KO resulted in a PCR product in shorter length (~250 bp). These different PCR products between clone D4 of WDR3 KO, clone F11; clone C3 and clone C11 of WDR6 KO indicated insertion and deletion (indel) in the DNA sequence. This indel,

however, should be confirmed further by genotyping by DNA sequencing. The DNA sequence analysis also very useful to confirm the double allele (homozygous or heterozygous) knockout. Unfortunately, due to the time and technical constraint, genotyping by DNA sequencing analysis could not be performed.

A.

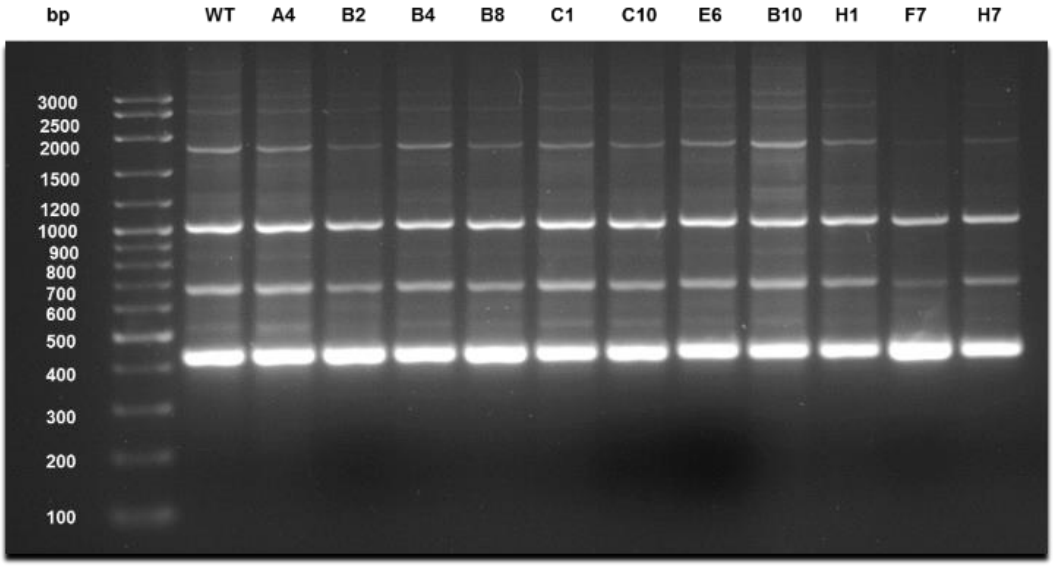

B.

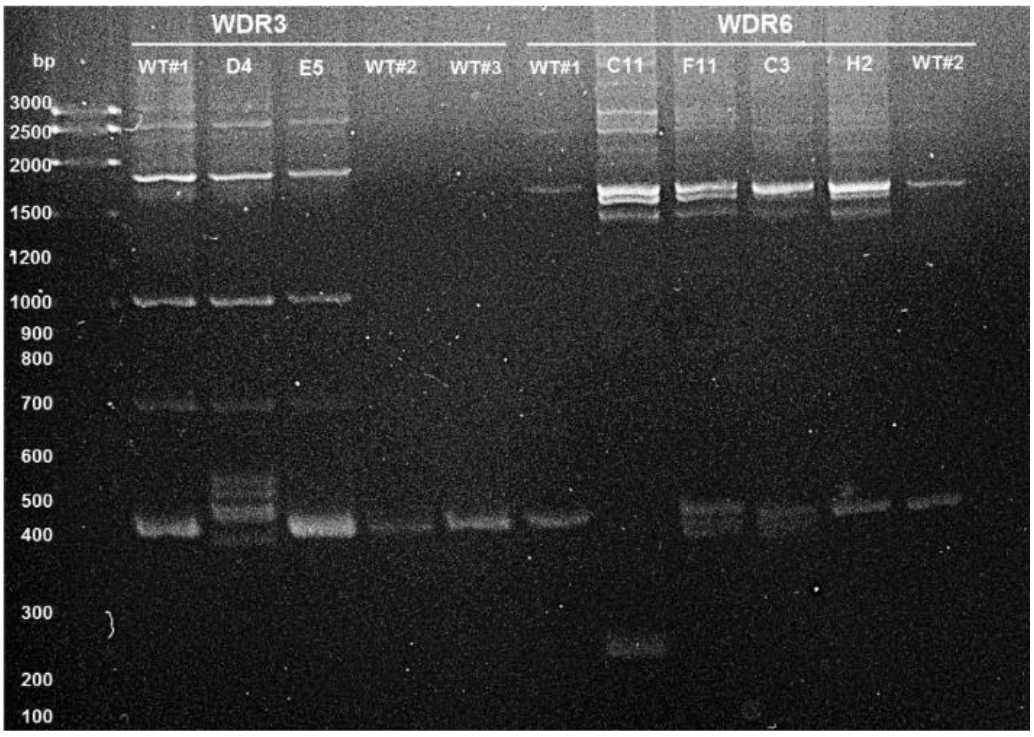

Figure 3.36. Agarose gel electrophoresis of PCR products for (A.) WDR3 KO and (B.) WDR6 KO clone confirmation. The lane denoted as WT was used as a control for all clones in each lane.

3.4.2.2 Effect of WDR3 and WDR6 KO clones on SPAK/OSR1 ubiquitylation and degradation

Based on the DNA agarose gel electrophoresis from PCR confirmation and without further analysis of DNA sequencing analysis, the immunoblotting of selected WDR3 KO and WDR6 KO clone was performed (**Figure 3.37.**). Clone A4 and D4 of WDR3 KO and clone C11 of WDR6 KO were selected. Clone D4 of WDR3 KO and clone C11 of WDR6 KO was selected as they were exhibited different DNA profile with the WT. Clone A4 of WDR3 KO was chosen as a control to that clone D4, as clone A4 showed the same DNA profile as wildtype (see **Figure 3.36.**).

WDR3 expression was significantly reduced in WDR3 KO clones. This reduction was following the slight increase of SPAK and OSR1 protein expression level (**Figure 3.37.**). The decreased of WDR3 expression on the WDR3 KO clones compared to the WT, which both clones showed different DNA fragment profiles, indicating the possibility of the off-target KO, which could affect the WDR3 expression. Thus, the increase of SPAK and OSR1 expression level could be concluded as a bias positive result of the WDR3 KO. If the KO clones were confirmed as positive unbiassed WDR3 KO clones by DNA sequencing, then the increasing level of SPAK and OSR1 expression indicated the inability of SPAK being recruited by WDR3, which subsequently was prevented from being ubiquitinated and degraded.

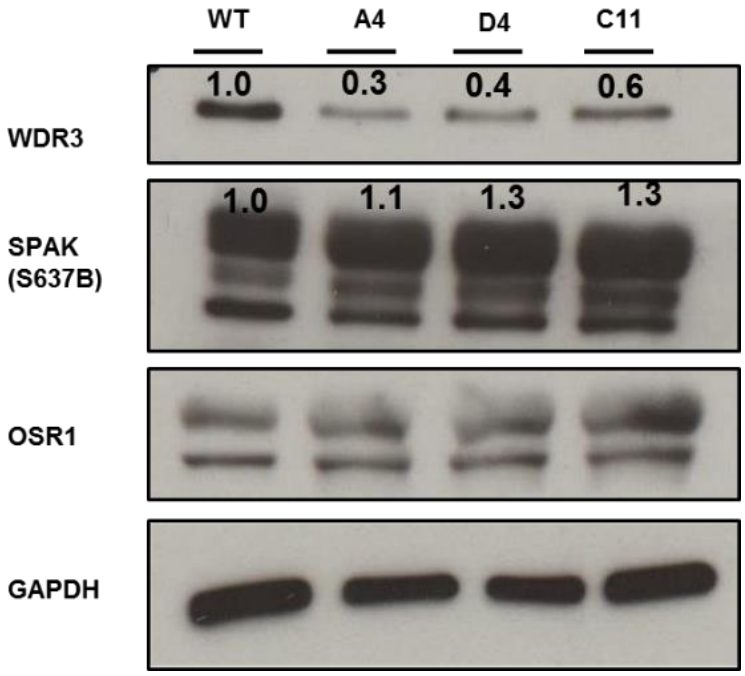

Figure 3.37. SPAK and OSR1 protein expression and on WDR3 KO and WDR6 KO. Immunoblotting of SPAK, OSR1 and WDR3 was performed on WDR3 ex2 KO clone A4; D4 and WDR6 ex2 KO clone C11 passage 14 under basal condition. WDR6 blot was not shown. GAPDH was used as a loading control. Bands intensity was quantified using ImageJ analysis. Representative result from two independent experiments was shown.

3.4.2.3 Effect of siRNA of DDB1, WDR3 and WDR6 knockdown on SPAK/OSR1 ubiquitylation and degradation

As the knockout of WDR3 and WDR6 clones by CRISPR could not proceeded to the genotyping analysis by DNA sequencing. Thus, the DDB1, WDR3 and WDR6 were transiently silenced by siRNA. The siRNA DDB1, WDR3, and WDR6 were conducted to explore the effect of the DDB1, WDR3 and WDR6 gene silence on SPAK/OSR1 ubiquitylation and degradation.

As shown in **Figure 3.38.**, DDB1 was effectively silenced. The knockdown of DDB1 increased the OSR1 protein expression level independent from the treatment of proteasome inhibitor, MG132, and NAE inhibitor, MLN4924. It suggested that knocking down the DDB1, an adaptor protein of CRL4, prevent the OSR1 to be recruited to CRL4 complex, so the OSR1 was prevented to be degraded.

Ubiquitin immunoblot revealed that MG132 treatment increased the ubiquitinated protein total in the cell, which showed a remarkable stronger intensity of bands on DDB1 knockdown cell than WT (**Figure 3.38.**). It suggested that total protein degradation via proteasomal degradation was inhibited by MG132. The DDB1 also contributed to the total protein degradation as the knockdown of DDB1 showing more accumulated ubiquitinated protein compare to WT.

Additionally, SPAK protein band intensity level on both wildtype and siRNA DDB1 showed weaker intensity after MG132 treatment and stronger intensity after MLN4924 treatment than the untreated cell. Thus, DDB1 knockdown prevents SPAK degradation via neddylation which showed by SPAK accumulation in the cell after MLN4924 treatment. Unfortunately, the mentioned above explanation about DDB1 could not be applied for WDR3 and WDR6, as there were no changes on ubiquitin immunoblot when the cells were WDR3 and WDR6 silenced (see Figure 7.5 on Chapter VII. Appendices).

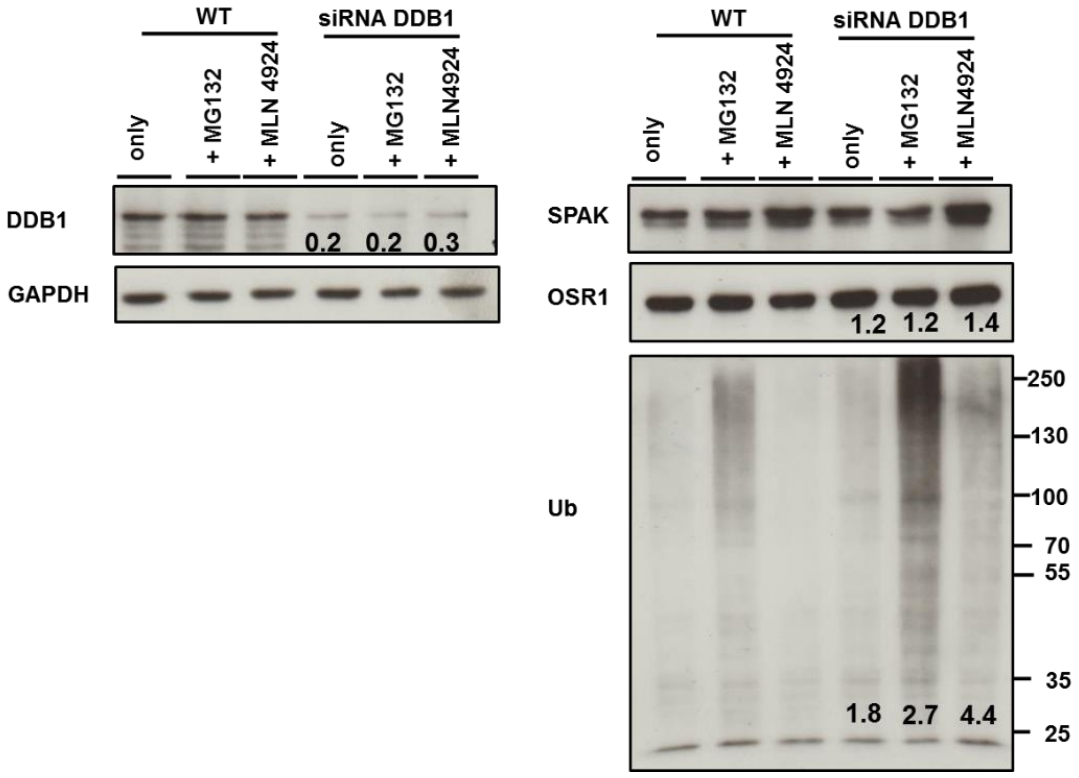

Figure 3.38. DDB1 plays a role in SPAK and OSR1 ubiquitylation and degradation. DDB1 knockdown was performed by siRNA. The cell was treated with 10 µM MG132 for 24 h, and 1 µM of MLN4924 for 6 h before the total protein lysate of both wildtype and siRNA DDB1 cell was used for immunoblotting using DDB1; SPAK; OSR1 and ubiquitin antibody to confirm the DDB1 silencing. GAPDH immunoblot was used as a loading control. The number under each band represented the ratio between respective bands under siRNA DDB1 and WT. Representative results from two independent experiments were shown.

CHAPTER IV.

DISCUSSION

CHAPTER IV. DISCUSSION

The kinase activity of SPAK/OSR1 relies on its catalytic carboxyl-terminal (CCT) domain (Villa *et al.*, 2007). The activation occurs as a result of its phosphorylation in the activation loop (T185 of OSR1). In addition to the phosphorylation in the T-activation loop, in the PF1 region of SPAK and OSR1 lays two serine residues which can be phosphorylated by its upstream kinases (WNKs). However, the function of phosphorylation at this serine motif (S-motif), specifically OSR1 S325, remains unknown (Vitari *et al.*, 2006). Thus, the discovery of novel proteins, which interact with the serine residues in the S-motif of SPAK and OSR1 is crucial to define their regulation in the WNK-SPAK/OSR1 signalling pathway.

The role of Cullin-RING ubiquitin ligases (CRLs) in the WNK-SPAK/OSR1 signalling pathway is not well reported in the literature. Kelch-like 2 (KLHL2) and KLHL3 interact with WNK1 at residues 490-626, which then ubiquitylate, and degrade WNK1 (Takahashi *et al.*, 2013). The complex of CUL3 and its BTB protein showing interactions and degradation of WNK isoforms and mutation of E3 ligase disrupts the interaction and promotes hypertension (Ohta *et al.*, 2013, Andérica-Romero *et al.*, 2014). This thesis reports the finding of novel protein interactors of SPAK and OSR1 in the S-motif domain, *i.e.* an E3 ubiquitin ligase complex CRL4, and the regulation of SPAK and OSR1 by ubiquitylation in relation to the WNK-SPAK/OSR1 signalling pathway.

The key findings of this thesis are summarised as follows; **1)** The CRL4, an E3 ubiquitin ligase complex, was identified as the novel interactor of OSR1 S325 based on MS fingerprint analysis. This CRL4 was confirmed to be bound to OSR1 S325 peptide under resting condition in which the WNK/SPAK-OSR1 signalling pathway is unstimulated (**Figure 3.1.** to **3.6.** and **Table 3.1.**); **2)** The binding between CRL4 and OSR1 was also confirmed on the OSR1 full-length protein by immunoprecipitation of

its endogenous and over-expressed protein under resting condition (**Figure 3.7.** and **3.8.**); **3)** The CRL4 binding has been confirmed to occur in the OSR1 kinase domain and its S-motif (**Figure 3.9.** to **3.12.**). Interestingly, the components of CRL4 complex, DDB1, WDR3 and WDR6 was also confirmed to establish interaction with CUL4A and CUL4B, the scaffold protein of CRL4 complex (**Figure 3.13.** and **3.14.**); **4)** The binding of CRL4 result in the OSR1 ubiquitylation and most likely its degradation (**Figure 3.15.** to **3.22.**); and **5)** The WDR3/WDR6, not CRBN, is the DCAF protein of CRL4 complex that is responsible for OSR1 ubiquitylation (**Figure 3.25.** to **3.38.**).

Based on the key findings of this thesis, the discussion sections are grouped to three parts. Part one discusses the binding of CRL4 complex to SPAK/OSR1, which refer to key findings number 1), 2), and 3). The second part discusses the effect of the CRL4 complex binding toward OSR1 ubiquitylation and likely its degradation, which refer to key findings number 4) and 5). Then, the final part of this chapter discusses the insight about the possible functions of CRL4 binding to OSR1 beyond the OSR1 ubiquitylation and degradation.

4.1 THE BINDING OF CRL4 COMPLEX TO SPAK/OSR1

Based on the MS fingerprinting analysis from OSR1 S325 peptide pull-down, Cullin-RING ubiquitin ligase 4 (CRL4) subunits were shown to be bound to non-phospho OSR1 S325 peptide (**Table 3.1.**). Controlling a vast variety of cellular processes, CRLs are a group of ubiquitin ligases that are widely studied. As a complex of subunits, CRLs consist of a cullin, a RING H2 finger protein (Rbx protein), a substrate-recognition subunit (SRS) and an adaptor subunit (Angers *et al.*, 2006). Among five cullins observed in metazoans, CUL1, CUL2, CUL3, CUL4 and CUL5 (Nayak *et al.*, 2002), Cullin 4 (CUL4A/B) was found to interact with non-phospho OSR1 S325 peptide (**Figure 3.4 to Figure 3.6.**). DNA damage binding protein (DDB1), WD-repeat protein (WDR3/6) and CAND1, which are the subunits of the CRL complex, were identified by the MS analysis from the peptide pull-down assay (**Table 3.1.**). In

western blot analysis, these CRL4 component proteins and CRBN were detected bound to non-phospho OSR1 S325 peptide but not to its phosphorylated peptide. DDB1 in the CRL4 complex is an adaptor protein that links the scaffold proteins CUL4A/B and WDR3/6 or CRBN, which act as SRS in the CRL4 complex (He *et al.*, 2006) (**Figure 1.15.**).

As addition to the binding of the CRL4 component protein to OSR1 S325 peptide, the binding of CRL4 components to SPAK and OSR1 full-length was also confirmed by immunoprecipitation (**Figure 3.7.**). The protein, which was precipitated by a short fragment peptide from peptide pull-down assay only establish a partial physical interaction with the peptide. The protein interactors, which were precipitated from peptide pull-down by short fragment 18-19 mer peptides establish an interaction that might different from the actual protein-protein interaction *in vivo*. The interaction between protein and peptide could not describe the protein-protein interaction in their active folding structure and other post-translational modifications which affect the binding. Interaction of CRL4 protein subunits with SPAK and OSR1 full-length, which was confirmed by immunoprecipitation, proves that their binding can be considered as a physiological protein-protein interaction.

The interaction between CRL4 subunits with SPAK and OSR1 occurred in phosphorylation-dependent manners (**Figure 3.8**). Hypotonic conditions stimulate the WNK-SPAK/OSR1 signalling pathway, which leads to SPAK and OSR1 phosphorylation. This phosphorylation leads to the CRL4 complex dissociation from SPAK and OSR1. Hence, when the cell is in an unstimulated state, the CRL4 complex binds with SPAK and OSR1.

Replacement of hypotonic buffer with the growth media in several different time durations exhibited the stronger binding of CRL4 components to OSR1 (see **Figure 3.8.B**), meaning that the dissociation of CRL4 complex from OSR1 was happening due to OSR1 phosphorylation. When the cell is in a resting condition and the

phosphorylation has been gradually terminated, the CRL4 regains the interaction with OSR1.

Phosphorylation is generally known to increase the binding affinity and activity of two proteins. It is demonstrated by the phosphorylation of WNK which cause SPAK and OSR1 association and activation (Thastrup *et al.*, 2012, Alessi *et al.*, 2014). However, phosphorylation can also decrease the binding affinity between proteins which is showed in the dissociation of Smad2 from its kinase (Wu *et al.*, 2001) as a result of a negative control mechanism (Nishi *et al.*, 2011). Thus, the dissociation between two proteins could happen as a result of phosphorylation in a manner similar to the dissociation of CRL4 complexes from SPAK and OSR1 which occurs when the protein kinase is phosphorylated.

The OSR1 fragments, which represent different binding domains of OSR1, precipitated CRL4 components in the kinase and S-motif domain of OSR1 (**Figure 3.10. to 3.12.**). However, the OSR1 fragments that were used for precipitating CRL4 units did not include the fragment which contains only S-motif domain where it lies in the PF1 domain of OSR1. The use of an OSR1 fragment which contains only the S-motif domain would be able to identify the interaction between CRL4 complex and OSR1 exclusively in the S-motif domain to support the finding of S325-OSR1 peptide pull-down assay as previously mentioned. OSR1 fragments which contain S-motif domains only, *e.g.* OSR1 aa 242-363, would allow a robust finding of CRL4 units interaction with OSR1 as it eliminates the possibility of associated events in the OSR1 kinase domain; mainly phosphorylation in the T-loop, or other events, which would affect the interaction.

The interaction between DDB1, which was firmly established with OSR1 fragment 1-435 but very weak with fragments 1-363 (**Figure 3.10**), could be explained by the steric hindrance. It has been speculated that there could be a steric hindrance in the OSR1 region between 311-363, which prevents or weakens the binding of DDB1. It

was reported that a scaffold protein MO25 binds to SPAK/OSR1 in S339 of OSR1 (S387 of SPAK) which increases the activity of SPAK/OSR1 to phosphorylate NKCC1. The binding of the MO25 in Serine 339 of OSR1 occurs in the basal condition, and its affinity is increased once the phosphorylation of OSR1 S339 is stimulated with a hypotonic buffer (Filippi *et al.*, 2011, Mehellou *et al.*, 2018). Thus, the steric hindrance, which prevents or weakens the DDB1 binding to this OSR1 311-363 region, is probably a MO25 protein that bound to S339 OSR1 (**Figure 4.1.**). To prove the assumption that MO25 binds to the OSR1 311-363 region, a pull-down assay using OSR1 fragments 311-363 and immunoblotting with anti-MO25 antibody, as well as anti-DDB1 antibodies could be performed. It would be convincing evidence to prove this hypothesis if the MO25 band then could be detected but not DDB1.

The interaction of CRL4 subunits with OSR1 was unlikely to occur in the *C*-terminal domain (PF2 domain) of OSR1, as shown in **Figure 3.10.** to **3.12**. In the PF2 domain of OSR1 (434-527) lies the binding domain for KCC3 and NKKCs (Piechotta *et al.*, 2002, Vitari *et al.*, 2006), the downstream proteins of SPAK and OSR1 in the WNK signalling pathway. Thus, the interaction between CRL4 subunits may not occur in the PF2 domain of OSR1, where the KCC3 and NKCCs would bind (see **Figure 4.1.**). It would be crucial evidence if the immunoprecipitated protein from OSR1 fragments 429 - end pull-down assay could be detected as KCC3 or NKCCs proteins by western blotting using KCC3, NKCC1 or NKCC2 antibodies to show their interaction with OSR1 in the 429 - end region.

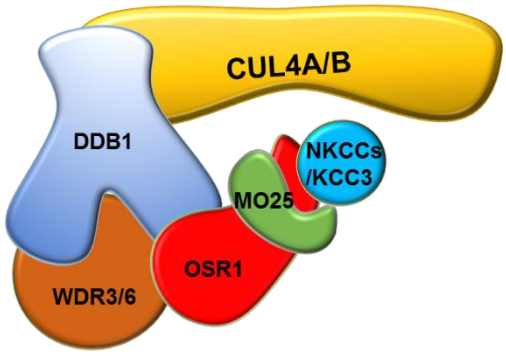

Figure 4.1. Schematic diagram of proposed CRL4 complex binding with OSR1 in the presence of MO25 and NKCCs/KCC3 protein. The binding of DDB1 is weakened in OSR1 311-363 where the MO25 is bound. The PF2 domain of OSR1 lies the region where NKCCs are bound. Thus, CRL4 components could not interact with OSR1 in the 429-end region.

The direct binding between CRL4 subunits; WDR3/WDR6 to DDB1 and WDR3/WDR6 to CUL4A/B (**Figure 3.13.**) revealed that WDR3/WDR6 are the DCAF subunits of our novel CRL4 complex. These DCAF subunits bind to DDB1 and establish interactions with the scaffold protein CUL4A/B as well. Based on the crystal structure of CRL4 complex which consists of DDB1-CUL4A-Rbx-SMV1 (PDB ID: 2HYE) (see **Figure 3.14.A.**), WDR family proteins could establish interactions with DDB1 between BPA and BPC pocket of DDB1 *via* its DXR domain (Higa *et al.*, 2006). WDR3 and WDR6 homolog proteins likely established a direct interaction with CUL4A/4B as it was visualised in one of the models from the WDR3/6 homolog protein docking into DDB1-CUL4A-Rbx-SMV1 structure (see **Figure 3.14.B. and C.**).

In the predicted OSR1-CRL4 complex structure showed the CRL4 complex, with a total molecular weight of around 300 kDa, embracing the OSR1 protein. The OSR1 was interacted by sitting in the ‘pocket’ of the ‘shoe horse’-like structure of the N-terminal domain of CUL4A/B and DDB1-WDR3/WDR6 (see **Figure 3.14.B., 3.14.C.** and **4.1.**). Even though the chosen model was generated using default mode setting on ClusPro 2.0 and likely showed preferential subjectivity, the visualisation of the possible interaction could help to describe the proposed interaction between CRL4 complex and OSR1. The validation of the protein-protein docking, including omitting

the SMV1 component from the DDB1-CUL4A-Rbx-SMV1 crystal structure and masking the known binding domain of other proteins, would perhaps provide more accurate visualisation. Indeed, protein crystallisation to depict the structure of the OSR1-CRL4 complex is vital work to be done. Additionally, several point mutations in the essential residues for the binding between the OSR1 and CRL4 complex components would be beneficial to strengthen the evidence of their interactions. Surface Plasmon Resonance (SPR) assays to determine the kinetics of the binding between the proteins is also another essential work which could uncover the binding affinity of each protein so that the CRL4 complex components which are most likely to interact with OSR1 could be determined, *e.g*. CUL4A-DDB1-WDR3; CUL4B-DDB1-WDR3; CUL4A-DDB1-WDR3; or CUL4B-DDB1-WDR6.

4.2 THE ROLE OF CRL4 COMPLEX ON OSR1 UBIQUITYLATION AND DEGRADATION

The novel finding of the interaction between OSR1 and CRL4 is a real breakthrough in the field of WNK-SPAK/OSR1 signalling cascade research. The binding between OSR1 and CRL4 required the study on the regulation of SPAK and OSR1 kinases as the result of its binding with the CRL4 complex. Considering that a kinase interacts with an E3 ubiquitin ligase, so the functional study as a result of this interaction is highly important to be carried out. Either OSR1 regulation of its ubiquitylation/degradation by CRL4 complex or, *vice versa*, CRL4 complex components may be phosphorylated by OSR1. These two regulations are in accordance to the prediction of ubiquitylation site both in SPAK and OSR1 (see **Figure 7.7. and 7.8.** in the Appendices) as well as phosphorylation site prediction in all CRL4 components (see **Figure 7.9. to 7.13.** in the Appendices).

The CRL4 complex as an E3 ubiquitin ligase, which plays a critical role in protein ubiquitylation and degradation, was found to establish a binding with OSR1 under

resting conditions. Thus, a hypothesis, that CRL4 ubiquitylates and eventually degrades SPAK and OSR1 when CRL4 binds to SPAK and OSR1 in unstimulated condition was proposed (**Figure 4.2.**). Under hypotonic conditions, where the WNK-SPAK/OSR1 signalling is stimulated, and SPAK and OSR1 are in a phosphorylated form, the CRL4 complex is dissociated from the SPAK and OSR1 and thus the ubiquitylation and degradation does not occur and leads to the accumulation of SPAK and OSR1. In the WNK-SPAK/OSR1 signalling pathway, NCC protein (the downstream protein of SPAK and OSR1) is reported to exhibit a similar mechanism to the ubiquitylation of SPAK and OSR1 in resting conditions where the protein is unphosphorylated. The phosphorylation of the NCC protein, which caused the reduction of the ubiquitinated NCC protein, was reported by a group of researchers from Japan (Hossain Khan *et al.*, 2012).

Single CUL4A and CUL4B knockdown or its double knockdown by siRNA under basal conditions were unable to show the increase of the SPAK and OSR1 level (**Figure 3.17. and 3.18.**). The expected accumulation of SPAK and OSR1 levels was hypothesised as a result of the inhibition of CUL4A or CUL4B to degrade SPAK and OSR1. As previously mentioned, the high homology of the CUL4A and CUL4B, which are both only structurally different by the truncation of 149 aa in the N-terminal domain of CUL4B (Hannah and Zhou, 2015), make them possible to work complementary to interact with the OSR1. However, the possibility of their complementary function was challenged by a steady level of SPAK and OSR1 when both CUL4A and CUL4B was knocked down. This phenomenon leads to the hypothesis that CUL4A and CUL4B as a scaffold protein in the CRL4 complex may not be the sole agent that is necessary for SPAK or OSR1 degradation.

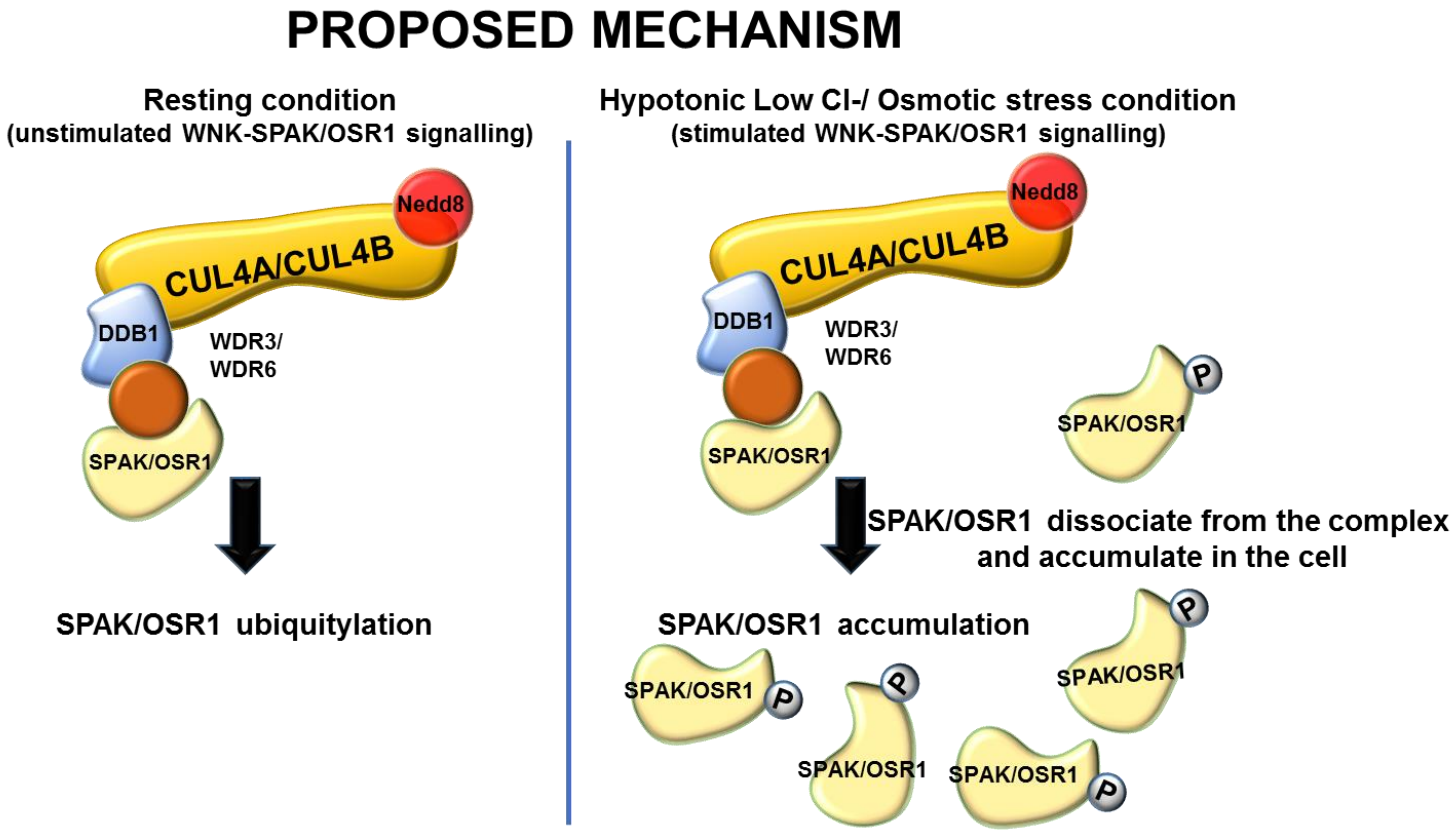

Figure 4.2. Proposed mechanism of CRL4 binding to SPAK and OSR1. Under the resting/basal condition, CRL4 complex binds to SPAK and OSR1 and promote ubiquitylation and degradation. The hypotonic condition which stimulates WNK-SPAK/OSR1 signalling dissociates the CRL4 complex from SPAK and OSR1.

The next attempt to knock down the other components of the CRL4 complex, *i.e.* WDR3 and WDR6 (**Figure 7.5**), by siRNA also did not result in any observed changes in the expression level of SPAK and OSR1. The lack of SPAK or OSR1 protein level changes may be due to the unreliability of the transient siRNA approach to knockdown WDR3 and WDR6. Unfortunately, the attempt to produce more reliable WDR3 and WDR6 knock out by CRISPR was also unsuccessful (**Figure 3.36. and 3.37.**). However, siRNA knockdown of DDB1 (**Figure 3.38.**) resulted in a slight increase of OSR1 levels. This accumulation of OSR1 levels suggested that DDB1, as an adaptor protein of CRL4 complexes, plays a role in OSR1 degradation. The OSR1 level which could only be observed as a slight increase in DDB1 knockdown may be due to the necessity of CRL4 which can only function to degrade OSR1 if it works as the whole unit of CRL4 complex machinery. Thus, the OSR1 or SPAK degradation could be observed as a significant increase in protein levels when all of the CRL4 components are knocked down. Due to the possibility of the cell that could not cope with the stress of having five exogenous plasmid transfections, then the point mutation on residue/s which are essential for the CRL4 binding to OSR1 as well as OSR1 degradation is likely to be the best approach to link the CRL4 complex with the OSR1 degradation.

Furthermore, the slight increase in OSR1 levels after DDB1 knockdown may also be due to the cell survival mechanism. Considering that OSR1 is essential for the activation of a series of ion co-transporter proteins and plays a role in cellular ion homeostasis, OSR1 accumulation perturbs the balance of intra and extracellular ion concentration, which is potentially toxic for the cells. Thus, the cells perhaps having an unknown mechanism to counter the imbalance cellular ion concentration which utilises the OSR1 protein so the accumulation of OSR1 is reduced.

CRLs, as E3 Ubiquitin Ligases, require the NEDD8 on the ubiquitylation and degradation of its protein substrate (Vittal *et al.*, 2015). Thus, utilisation of the inhibitors which have a mechanism of action in the inhibition of protein degradation

via 26S proteasomal degradation (MG132) and neddylation (MLN4924) process is beneficial to uncover the role and the mechanism of CRL4 complex toward OSR1 ubiquitylation and degradation.

The SPAK and OSR1 levels in the cells after NAE inhibitor MLN4924 treatment did not exhibit any changes in the protein levels when it was compared to the untreated cell. However, when the cell was treated with a proteasomal degradation inhibitor, MG132, the ubiquitinated protein remarkably increased (**Figure 3.23.**) (Emmerich and Cohen, 2015). As expected, the inhibition of 26S proteasome to degrade OSR1 by MG132 allowed the OSR1 to be ubiquitinated but prevented to be degraded. Whereas, on the immunoblotting using anti-ubiquitin antibody, neither the ubiquitinated nor degraded protein could be observed under MLN4924 (an inhibitor of NEDD8 activating enzyme) treatment as the protein was prevented being ubiquitinated and degraded further. Thus, the OSR1 degradation, which was observed in the resting condition when the CRL4 complex binds to SPAK/OSR1, could not be concluded *via* the inhibition of neddylation processes. Immunoblotting using anti-NEDD8 antibody from the cells after MG132 and MLN4924 treatment would provide evidence that the OSR1 ubiquitylation and degradation by CRL4 complex is neddylation dependant.

CRL4 which forms a complex has been found to have a vast variety of DCAF proteins which target specifically to a particular substrate (Jackson and Xiong, 2009). As one of the widely known and investigated DCAF proteins, CRBN, was detected in our precipitated protein from pull-down assays (**Figure 3.25. to 3.29.**). However, based on several approaches that were conducted applying thalidomide and pomalidomide (CUL4A-DDB1-CRBN activator) to the cells, it was confirmed that CRBN was not a DCAF protein in the CRL4 complex that binds to OSR1. The investigation of whether other DCAF proteins may play a role in the interaction of CRL4 and OSR1 was also performed utilising indisulam, a DCAF15 activator. The result demonstrated that there

was no SPAK or OSR1 protein level change on the cell after indisulam treatment (**Figure 3.30. and 3.31.**). It means that the DCAF15 was also not the DCAF protein in our CRL4-OSR1 interaction. Thus, it is suggested that WDR3 or WDR6 is the DCAF protein in the CRL4 complex as it was also identified in MS analysis from peptide pull-down assay.

Interestingly, even though WDR3 and WDR6 are the DCAFproteins which associate CUL4A or CUL4B and DDB1, they seemed to have no direct role in the ubiquitylation and degradation of OSR1 (**Figure 7.5.**). DDB1 protein was likely responsible for the OSR1 ubiquitylation and degradation (**Figure 3.38.**). DDB1 knockdown exhibited the increase of OSR1 protein levels as well as the ubiquitinated OSR1 when it was compared to the wild type. With the DDB1 knockdown, the OSR1 is prevented from being degraded, so the abundance of OSR1 in the cell is high. Thus, it increases the OSR1 abundance, which could be ubiquitinated (see **Figure 4.3.**).

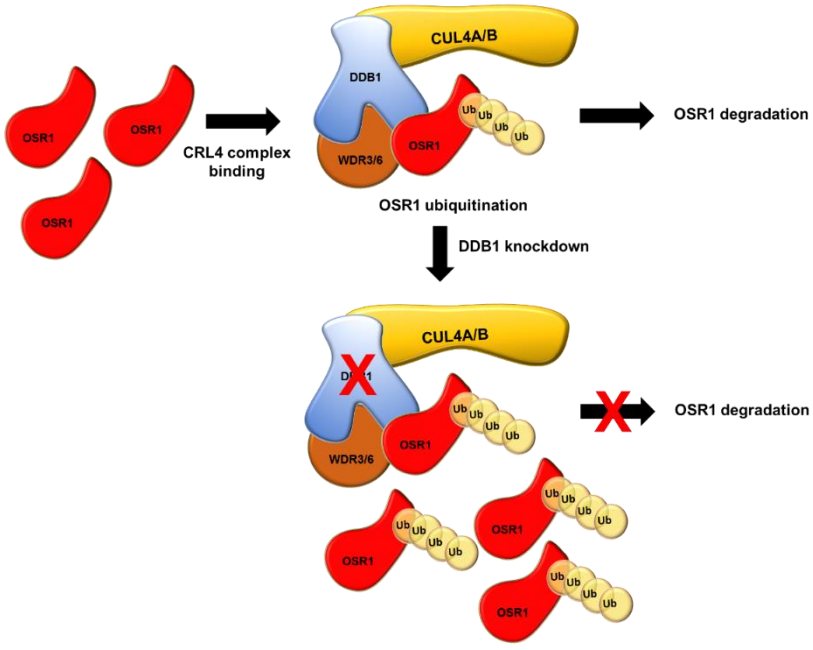

Figure 4.3. The role of DDB1 in OSR1 ubiquitylation and degradation. In WT cell, the binding CRL4 complex to OSR1 promotes the ubiquitylation and degradation of OSR1. The DDB1 knockdown prevents OSR1 degradation, so it increases the OSR1 abundance in the cells, which then increase the level of ubiquitinated OSR1.

4.3 BEYOND THE OSR1 UBIQUITYLATION AND DEGRADATION BY CRL4

The detected CAND1 protein in MS analysis from OSR1 S325peptide pull-down, which also confirmed its binding to OSR1 full-length protein, raises an important question regarding the role of CAND1 in the CRL4-OSR1 system. CAND1 is known as 1.) a CRL4 inhibitor (Flick and Kaiser, 2013), as well as acting as 2.) Substrate Receptor Exchange Factor (SREF) (Lydeard *et al.*, 2013, Pierce *et al.*, 2013). CAND1 inhibits the substrate ubiquitylation as the CAND1 cause 'a steric clash' for adaptor proteins and substrate recognition subunit to bind to CUL4 (Goldenberg *et al.*, 2004). Without the adaptor protein and SRS, the CRL4 complex would not be able to ubiquitinate and degrade the CRL4 substrate.

Regarding the function of SREF, CAND1 mediates the CRL4 to exchange its substrate receptor with the new substrate receptor, which can target another specific substrate in the cell. The second function, CAND1 as SREF, is more likely fit to the CRL4 system discussed in this thesis. CAND1 was immunoprecipitated together with the adaptor protein DDB1 and substrate recognition subunit WDR3 and WDR6. If CAND1 was immunoprecipitated without the adaptor protein and substrate recognition subunit then perhaps CAND1 functions as a CRL4 inhibitor. However, the newly exchanged putative substrate could not be defined by the experiments which were conducted as there was no single article reported the protein substrate of DDB1-WDR3/WDR6 from the identified protein resulted from the MS analysis (**Table 7.1.** in Appendices). It can only be speculated that the CAND1 binding to CRL4 possibly exchanges the CUL4-DDB1-WDR3/6 substrate OSR1 to STK11 (LKB1) protein kinase. This speculation is based only on the article reported so far, which demonstrated the binding between WDR6 and STK11 kinase (Xie *et al.*, 2007) as the STK11 was not identified in the MS analysis of peptide pull-down assay.

The presence of CAND1 which was also bound to the CUL4A/B-DDB1-WDR3/6 complex suggested that the MS analysis might have captured and identified the

complex at the transition state between CAND1 or DDB1-WDR3/WDR6 binding to CUL4A/B. The binding between DDB1-WDR3/WDR6 and CUL4A/B or the binding between CAND1 and CUL4A/B may be a reversible process of assembly and disassembly (Merlet *et al.*, 2009).

Phosphorylation of CRL4 components by OSR1 is one of the areas that was highlighted to be explored in this thesis. An emerging, important, yet long-established topic derived from this thesis suggests crosstalk between ubiquitylation and phosphorylation (Hunter, 2007). As shown in the phosphorylation prediction site in **Figures 7.9.** to **Figure 7.13.**, there are possibilities that CRL4 components can be phosphorylated by OSR1, especially in their serine/ threonine residues. The subunit of a CRL4 complex was reported to be phosphorylated by another kinase. Cdt1, a substrate receptor of the CRL4 complex, can be phosphorylated by checkpoint kinase ATR (Sakaguchi *et al.*, 2012). Immunoblotting using p-Ser/Thr antibodies of pulled down protein from co-expressed OSR1 to detect phosphorylation in CRL4 components or *in vitro* kinase assays of the CRL4 components phosphorylation are two approaches which could be done to test this hypothesis. Small molecule inhibitors of WNK (*e.g.* WNK463) (Yamada *et al.*, 2016) or of SPAK and OSR1 (e.g. Rafoxanide, Closantel) (AlAmri *et al.*, 2017a) can be used as a control for the system.

As a perspective, this thesis successfully showed that the novel OSR1 S325 interactor, CRL4 complex with defined subunits, promoted SPAK and OSR1 ubiquitylation and likely their degradation upon their binding with CRL4 complex in the unstimulated WNK-SPAK/OSR1 signalling pathway. The findings are very important fundamental knowledge for unmasking the regulation of SPAK and OSR1 by CRL4 in controlling cellular ion homeostasis.

Uncovering several events following protein phosphorylation apart from ubiquitylation which was widely discussed in this thesis, such as protein subcellular localisation and another physiological functionality study, *e.g.* patch-clamp electrophysiology assay,

are the prominent future directions for the research that are derived from this thesis. Completion of future work needs to be achieved to provide more robust and rigorous data, so the full picture of how the CRL4 complex regulates OSR1 in association with ion homeostasis or other physiological consequences upon OSR1 regulation can be obtained to enhance understanding of ion imbalance-related diseases.

CHAPTER V.

CONCLUSION

CHAPTER V. CONCLUSION

5.1. SUMMARY OF FINDINGS

Activation of the WNK-SPAK/OSR1 signalling pathway leads to the activation of its downstream kinases, SPAK and OSR1 by phosphorylation. This SPAK/OSR1 activation leads to the phosphorylation of further downstream ion co-transporter proteins, NCCs and KCCs. Phosphorylation of SPAK/OSR1 by WNKS occurs in several sites, including T233, S387, S373 of SPAK and T185, S339, S325 of OSR1. The first two phosphorylation sites, T185 of OSR1 (or T233 of SPAK) and S339 (or S387 of SPAK) are known for having a role in SPAK/OSR1 catalytic activity by T-loop phosphorylation and MO25 binding domain which increases SPAK/OSR1 activity, respectively.

The role of phosphorylation at S325 OSR1 (or S373 of SPAK) which remains unclear leading to the important question on the role of S325 OSR1 (or S373 SPAK) phosphorylation in the WNK-SPAK/OSR1 signalling pathway in the regards of its role in controlling cellular ion homeostasis.

Thus, this thesis reported several experiments which were performed to answer the essential question about the role of S325 OSR1 in relation to WNK-SPAK/OSR1 signalling and provided data in several aspects as follows:

1. Novel proteins binding to serine 325 OSR1 peptide (Section 3.1 of Chapter III).
2. Interaction of Cullin-RING ligase 4 (CRL4) subunit proteins with SPAK and OSR1 (Section 3.2 of Chapter III).
3. SPAK and OSR1 ubiquitylation and degradation upon CRL4 inhibition (Section 3.3 of Chapter III), which include the inhibition of CRL4 using small molecule inhibitors siRNA, and gene KO by CRISPR.

4. CRL4 complex subunits role in SPAK and OSR1 ubiquitylation and degradation (Section 3.4 of Chapter III), which includes the role of CRBN, DDB1, WDR3 and WDR6 in SPAK and OSR1 ubiquitylation and degradation.

As there was no previous report about the role of phosphorylation in serine 325 OSR1, peptide pull-down assay using non-phospho S325 OSR1 peptide and its phosphorylated peptide was performed to figure out the protein interactors of this serine residue. This thesis identified for the first time that the CRL4 complex, an E3 ubiquitin ligase complex, establish the interaction with non-phospho OSR1 S325 peptide but not to the OSR1 pS325 peptide (Section 3.1).

The interaction of the CRL4 complex with OSR1 S325 peptide was later confirmed for its binding to full-length of OSR1 under unstimulated conditions, where WNK-SPAK/OSR1 signalling is not active (Section 3.2). Activation of WNK-SPAK/OSR1 signalling leads to phosphorylation of OSR1 S325 and dissociation of the CRL4 complex binding. To investigate the essential binding domain of OSR1 which interacts with the CRL4 complex, we found that CRL4 components were bound to kinase and S-motif domains but not to *C*-terminal domain of OSR1 (Section 3.2).

The interaction which was exhibited by CRL4 components with other components within the CRL4 complex, apart from their binding to OSR1, suggested the proposed model of CRL4 complex interaction with OSR1. This thesis reported the predictive model of interaction of CRL4 and OSR1 by docking the DDB1-CUL4A-Rbx-SMV1 with WDR3/WDR6 and subsequentially with OSR1 using ClusPro 2.0. The model of interaction predicted that CRL4 complex is embracing OSR1 so that OSR1 is sitting in the ‘pocket’ between CUL4A/B and DDB1-WDR3/WDR6, which is bound to the *N*-terminal domain of CUL4A/B.

The investigation on the function of the CRL4 complex interaction, an E3 ubiquitin ligase, with OSR1 under resting condition was performed by using inhibitors, MLN4924 (NEDD8-activating enzyme inhibitor) and MG132 (proteasome inhibitor),

as well as siRNA to knockdown CRL4 components (Section 3.3). The attempt was also carried out to knockout WDR3/WDR6 KO by CRISPR although it was unsuccessful in obtaining on-target knock out clone (Section 3.3). This thesis reported for the first time that CRL4 complex binding to OSR1 is responsible for OSR1 ubiquitylation and most likely degradation.

The CRL4 components DDB1, not WDR3 nor WDR6, was likely acting as a crucial component for OSR1 degradation (Section 3.4). The widely known and investigated CRL4 complex substrate adaptors, CRBN and DCAF15, were explored and studied in this thesis for its possibility to play a role in OSR1 ubiquitylation and degradation. As expected, it was proved that both CRBN and DCA15 did not show such a role in our CRL4 and OSR1 interaction systems (Section 3.4).

5.2. FUTURE WORKS

The work performed and discussed in this thesis has led to a number of questions which can be answered by further experimental investigation. This thesis showed that CAND1 was confirmed to establish interaction with OSR1. Therefore, the exact role and how CAND1 regulates CRL4 complexes with regard to their binding to OSR1 in the context of WNK-SPAK/OSR1 signalling remains to be elucidated. The effect of CRL4 complex-OSR1 interactions on downstream proteins of SPAK/OSR1 in WNK-SPAK/OSR1 signalling (NCCs and KCCs proteins) is also an interesting question to be studied to relate CRL4 complex-OSR1 interactions in cellular ion homeostasis.

To explore more details on how the interaction is established between CRL4 complexes and OSR1, further experimental work on SPR for binding affinity determination and point mutation studies are essential to be carried out. The binding affinity between CRL4 components will provide valuable information on the protein components which interact as a CRL4 complex. Then, the more robust protein-protein docking simulations with the support of a molecular dynamic study to identify the putative essential binding residue is needed to carry out further point mutational

analysis. Moreover, solving the crystal structure on how CRL4 complex establishes the interaction with OSR1 will depict the full picture of the CRL4-OSR1 interaction.

Several functional studies (*in vitro* and *in vivo*) as a consequence of CRL4-OSR1 interactions will add beneficial information to uncover the molecular mechanism of CRL4-OSR1 regulation. These functional studies include *in vitro* ubiquitylation assays, *in vitro* kinase assays, patch clamp electrophysiology assays and animal studies which will then place the OSR1 regulation by CRL4 as a valuable piece of knowledge in the WNK-SPAK/OSR1 signalling pathway in relation to human ion-related diseases.

Independent from ion homeostasis-related physiology, investigations on how CRL4 regulates SPAK/OSR1 in cancer is also interesting. Interaction of WDR6 with LKB1, a tumor suppressor kinase and master of the upstream activator of AMPK protein kinase, is key to unlocking the role of CRL4-DDB1-WDR3 in vast array of cancers.

It is agreed that protein subcellular localisation is one of the events which occurs as a result of protein-protein interactions. Beyond the ubiquitylation, phosphorylation and ion transport studies, exploration of how CRL4-OSR1 interactions may also affect subcellular protein localisation is also necessary to support the functional studies as well as how the protein is degraded (*i.e.* if it is localised to lysosome for lysosomal degradation).

5.3 CONCLUDING REMARKS

CRL4 complex (CUL4A/B-DDB1-WDR3/6) exhibited interaction with OSR1 under unstimulated WNK-SPAK/OSR1 kinase signalling pathway. CRL4 complex component binding to OSR1 was proven to play a role in the OSR1 ubiquitylation and likely in its degradation.

CHAPTER VI.

REFERENCES

CHAPTER VI. REFERENCES

Ahmad, K. F., Engel, C. K. & Prive, G. G. 1998. Crystal structure of the BTB domain from PLZF. *Proc Natl Acad Sci U S A,* 95**,** 12123-12128.

Akutsu, M., Dikic, I. & Bremm, A. 2016. Ubiquitin chain diversity at a glance. *Journal of Cell Science,* 129**,** 875-880.

Alamri, M. A., Kadri, H., Alderwick, L. J., Jeeves, M. & Mehellou, Y. 2018. The Photosensitising Clinical Agent Verteporfin Is an Inhibitor of SPAK and OSR1 Kinases. *Chembiochem,* 19**,** 2072-2080.

Alamri, M. A., Kadri, H., Alderwick, L. J., Simpkins, N. S. & Mehellou, Y. 2017a. Rafoxanide and Closantel Inhibit SPAK and OSR1 Kinases by Binding to a Highly Conserved Allosteric Site on Their C-terminal Domains. *ChemMedChem,* 12**,** 639-645.

Alamri, M. A., Kadri, H., Dhiani, B. A., Mahmood, S., Elzwawi, A. & Mehellou, Y. 2017b. WNK-Signaling Inhibitors as Potential New Antihypertensive Drugs. *Chem Med Chem*.

Alessi, D. R., Zhang, J., Khanna, A., Hochdörfer, T., Shang, Y. & Kahle, K. T. 2014. The WNK-SPAK/OSR1 pathway: Master regulator of cation-chloride cotransporters. *Science Signaling,* 7**,** re3-re3.

Andérica-Romero, A. C., Escobar, L., Padilla-Flores, T. & Pedraza-Chaverri, J. 2014. Insights in cullin 3/WNK4 and its relationship to blood pressure regulation and electrolyte homeostasis. *Cellular Signalling,* 26**,** 1166-1172.

Angers, S., Li, T., Yi, X., Maccoss, M. J., Moon, R. T. & Zheng, N. 2006. Molecular architecture and assembly of the DDB1-CUL4A ubiquitin ligase machinery. *Nature,* 443.

Anselmo, A. N., Earnest, S., Chen, W., Juang, Y.-C., Kim, S. C., Zhao, Y. & Cobb, M. H. 2006. WNK1 and OSR1 regulate the Na(+), K(+), 2Cl(−) cotransporter in HeLa cells. *Proceedings of the National Academy of Sciences of the United States of America,* 103**,** 10883-10888.

Arias, E. E. & Walter, J. C. 2006. PCNA functions as a molecular platform to trigger Cdt1 destruction and prevent re-replication. *Nature Cell Biology,* 8**,** 84.

Bedford, L., Paine, S., Sheppard, P. W., Mayer, R. J. & Roelofs, J. 2010. Assembly, Structure and Function of the 26S proteasome. *Trends in Cell Biology,* 20**,** 391-401.

Begum, G., Yuan, H., Kahle, K. T., Li, L., Wang, S., Shi, Y., Shmukler, B. E., Yang, S.-S., Lin, S.-H., Alper, S. L. & Sun, D. 2015. Inhibition of WNK3 Kinase Signaling Reduces Brain Damage and Accelerates Neurological Recovery After Stroke. *Stroke,* 46**,** 1956-1965.

Bennett, E. J., Rush, J., Gygi, S. P. & Harper, J. W. 2010. Dynamics of cullin-RING ubiquitin ligase network revealed by systematic quantitative proteomics. *Cell,* 143.

Berndsen, C. E. & Wolberger, C. 2014. New insights into ubiquitin E3 ligase mechanism. *Nature Structural &Amp; Molecular Biology,* 21**,** 301.

Biedermann, S. & Hellmann, H. 2011. WD40 and CUL4-based E3 ligases: lubricating all aspects of life. *Trends in Plant Science,* 16**,** 38-46.

Bosu, D. R. & Kipreos, E. T. 2008. Cullin-RING ubiquitin ligases: global regulation and activation cycles. *Cell Division,* 3**,** 1-13.

Boudeau, J., Baas, A. F., Deak, M., Morrice, N. A., Kieloch, A., Schutkowski, M., Prescott, A. R., Clevers, H. C. & Alessi, D. R. 2003. MO25α/β interact with STRADα/β enhancing their ability to bind, activate and localize LKB1 in the cytoplasm. *The EMBO Journal,* 22**,** 5102-5114.

Boyden, L. M., Choi, M., Choate, K. A., Nelson-Williams, C. J., Farhi, A., Toka, H. R., Tikhonova, I. R., Bjornson, R., Mane, S. M., Colussi, G., Lebel, M., Gordon, R. D., Semmekrot, B. A., Poujol, A., Välimäki, M. J., De Ferrari, M. E., Sanjad, S. A., Gutkin, M., Karet, F. E., Tucci, J. R., Stockigt, J. R., Keppler-Noreuil, K. M., Porter, C. C., Anand, S. K., Whiteford, M. L., Davis, I. D., Dewar, S. B., Bettinelli, A., Fadrowski, J. J., Belsha, C. W., Hunley, T. E., Nelson, R. D., Trachtman, H., Cole, T. R. P., Pinsk, M., Bockenhauer, D., Shenoy, M., Vaidyanathan, P., Foreman, J. W., Rasoulpour, M., Thameem, F., Al-Shahrouri, H. Z., Radhakrishnan, J., Gharavi, A. G., Goilav, B. & Lifton, R. P. 2012. Mutations in kelch-like 3 and cullin 3 cause hypertension and electrolyte abnormalities. *Nature,* 482**,** 98.

Bradford, M. M. 1976. A rapid and sensitive method for the quantitation of microgram quantities of protein utilizing the principle of protein-dye binding. *Anal Biochem,* 72**,** 248-254.

Breunig, M., Lungwitz, U., Liebl, R. & Goepferich, A. 2007. Breaking up the correlation between efficacy and toxicity for nonviral gene delivery. *Proceedings of the National Academy of Sciences,* 104**,** 14454-14459.

Chen, L., Liu, T., Tu, Y., Rong, D. & Cao, Y. 2016. Cul1 promotes melanoma cell proliferation by promoting DEPTOR degradation and enhancing cap-dependent translation. *Oncology reports,* 35**,** 1049-1056.

Chen, W., Yazicioglu, M. & Cobb, M. H. 2004. Characterization of OSR1, a Member of the Mammalian Ste20p/Germinal Center Kinase Subfamily. *Journal of Biological Chemistry,* 279**,** 11129-11136.

Chen, Y.-A., Peng, Y.-J., Hu, M.-C., Huang, J.-J., Chien, Y.-C., Wu, J.-T., Chen, T.-Y. & Tang, C.-Y. 2015. The Cullin 4A/B-DDB1-Cereblon E3 Ubiquitin Ligase Complex Mediates the Degradation of CLC-1 Chloride Channels. *Scientific Reports,* 5**,** 10667.

Chiga, M., Rafiqi, F. H., Alessi, D. R., Sohara, E., Ohta, A., Rai, T., Sasaki, S. & Uchida, S. 2011. Phenotypes of pseudohypoaldosteronism type II caused by the WNK4 D561A missense mutation are dependent on the WNK-OSR1/SPAK kinase cascade. *Journal of Cell Science,* 124**,** 1391-1395.

Chipperfield, A. R. & Harper, A. A. 2000. Chloride in smooth muscle. *Prog Biophys Mol Biol,* 74**,** 175-221.

Cope, G., Golbang, A. & O'shaughnessy, K. M. 2005. WNK kinases and the control of blood pressure. *Pharmacology & Therapeutics,* 106**,** 221-231.

Costessi, A., Mahrour, N., Tijchon, E., Stunnenberg, R., Stoel, M. A., Jansen, P. W., Sela, D., Martin-Brown, S., Washburn, M. P., Florens, L., Conaway, J. W., Conaway, R. C. & Stunnenberg, H. G. 2011. The tumour antigen PRAME is a subunit of a Cul2 ubiquitin ligase and associates with active NFY promoters. *The EMBO Journal,* 30**,** 3786-3798.

Dalby, B., Cates, S., Harris, A., Ohki, E. C., Tilkins, M. L., Price, P. J. & Ciccarone, V. C. 2004. Advanced transfection with Lipofectamine 2000 reagent: primary neurons, siRNA, and high-throughput applications. *Methods,* 33**,** 95-103.

Dan, I., Watanabe, N. M. & Kusumi, A. 2001. The Ste20 group kinases as regulators of MAP kinase cascades. *Trends in Cell Biology,* 11**,** 220-230.

Delaloy, C., Lu, J., Houot, A.-M., Disse-Nicodeme, S., Gasc, J.-M., Corvol, P. & Jeunemaitre, X. 2003. Multiple Promoters in the WNK1 Gene: One Controls Expression of a Kidney-Specific Kinase-Defective Isoform. *Molecular and Cellular Biology,* 23**,** 9208-9221.

Delpire, E. & Gagnon, Kenneth b. E. 2008. SPAK and OSR1: STE20 kinases involved in the regulation of ion homoeostasis and volume control in mammalian cells. *Biochemical Journal,* 409**,** 321-331.

Denning, W., Das, S., Guo, S., Xu, J., Kappes, J. C. & Hel, Z. 2013. Optimization of the Transductional Efficiency of Lentiviral Vectors: Effect of Sera and Polycations. *Molecular Biotechnology,* 53**,** 308-314.

Deshaies, R. J. & Joazeiro, C. a. P. 2009. RING Domain E3 Ubiquitin Ligases. *Annual Review of Biochemistry,* 78**,** 399-434.

Duda, D. M., Borg, L. A., Scott, D. C., Hunt, H. W., Hammel, M. & Schulman, B. A. 2008. Structural insights into NEDD8 activation of cullin-RING ligases: conformational control of conjugation. *Cell,* 134.

Duda, D. M., Scott, D. C., Calabrese, M. F., Zimmerman, E. S., Zheng, N. & Schulman, B. A. 2011. Structural regulation of cullin-RING ubiquitin ligase complexes. *Current Opinion in Structural Biology,* 21**,** 257-264.

Dzhala, V. I., Talos, D. M., Sdrulla, D. A., Brumback, A. C., Mathews, G. C., Benke, T. A., Delpire, E., Jensen, F. E. & Staley, K. J. 2005. NKCC1 transporter facilitates seizures in the developing brain. *Nat Med,* 11**,** 1205-1213.

Emmerich, C. H. & Cohen, P. 2015. Optimising methods for the preservation, capture and identification of ubiquitin chains and ubiquitylated proteins by immunoblotting. *Biochemical and Biophysical Research Communications,* 466**,** 1-14.

Feigin, V. L., Nichols, E., Alam, T., Bannick, M. S., Beghi, E., Blake, N., Culpepper, W. J., Dorsey, E. R., Elbaz, A., Ellenbogen, R. G., Fisher, J. L., Fitzmaurice, C., Giussani, G., Glennie, L., James, S. L., Johnson, C. O., Kassebaum, N. J., Logroscino, G., Marin, B., Mountjoy-Venning, W. C., Nguyen, M., Ofori-Asenso, R., Patel, A. P., Piccininni, M., Roth, G. A., Steiner, T. J., Stovner, L. J., Szoeke, C. E. I., Theadom, A., Vollset, S. E., Wallin, M. T., Wright, C., Zunt, J. R., Abbasi, N., Abd-Allah, F., Abdelalim, A., Abdollahpour, I., Aboyans, V., Abraha, H. N., Acharya, D., Adamu, A. A., Adebayo, O. M., Adeoye, A. M., Adsuar, J. C., Afarideh, M., Agrawal, S., Ahmadi, A., Ahmed, M. B., Aichour, A. N., Aichour, I., Aichour, M. T. E., Akinyemi, R. O., Akseer, N., Al-Eyadhy, A., Al-Shahi Salman, R., Alahdab, F., Alene, K. A., Aljunid, S. M., Altirkawi, K., Alvis-Guzman, N., Anber, N. H., Antonio, C. a. T., Arabloo, J., Aremu, O., Ärnlöv, J., Asayesh, H., Asghar, R. J., Atalay, H. T., Awasthi, A., Ayala Quintanilla, B. P., Ayuk, T. B., Badawi, A., Banach, M., Banoub, J. a. M., Barboza, M. A., Barker-Collo, S. L., Bärnighausen, T. W., Baune, B. T., Bedi, N., Behzadifar, M., Behzadifar, M., Béjot, Y., Bekele, B. B., Belachew, A. B., Bennett, D. A., Bensenor, I. M., Berhane, A., Beuran, M., Bhattacharyya, K., Bhutta, Z. A., Biadgo, B., Bijani, A., Bililign, N., Bin Sayeed, M. S., Blazes, C. K., Brayne, C., Butt, Z. A., Campos-Nonato, I. R., Cantu-Brito, C., Car, M., et al. 2019. Global, regional, and national burden of neurological disorders, 1990–2016: a systematic analysis for the Global Burden of Disease Study 2016. *The Lancet Neurology,* 18**,** 459-480.

Filippi, B. M., De Los Heros, P., Mehellou, Y., Navratilova, I., Gourlay, R., Deak, M., Plater, L., Toth, R., Zeqiraj, E. & Alessi, D. R. 2011. MO25 is a master regulator of SPAK/OSR1 and MST3/MST4/YSK1 protein kinases. *The EMBO Journal,* 30**,** 1730-1741.

Fire, A., Xu, S., Montgomery, M. K., Kostas, S. A., Driver, S. E. & Mello, C. C. 1998. Potent and specific genetic interference by double-stranded RNA in Caenorhabditis elegans. *Nature,* 391**,** 806-811.

Flick, K. & Kaiser, P. 2013. Set them free: F-box protein exchange by Cand1. *Cell Res,* 23**,** 870-871.

Freiman, R. N. & Tjian, R. 2003. Regulating the regulators: lysine modifications make their mark. *Cell,* 112**,** 11-17.

Gagnon, K. B. & Delpire, E. 2012. Molecular Physiology of SPAK and OSR1: Two Ste20-Related Protein Kinases Regulating Ion Transport. *Physiological reviews,* 92**,** 1577-1617.

Gagnon, K. B., England, R. & Delpire, E. 2006. Volume sensitivity of cation-Cl- cotransporters is modulated by the interaction of two kinases: Ste20-related proline-alanine-rich kinase and WNK4. *Am J Physiol Cell Physiol,* 290**,** C134-142.

Glover, M., Zuber, A. M. & O'shaughnessy, K. M. 2011. Hypertension, Dietary Salt Intake, and the Role of the Thiazide-Sensitive Sodium Chloride Transporter NCCT. *Cardiovascular Therapeutics,* 29**,** 68-76.

Glykys, J., Dzhala, V., Egawa, K., Kahle, K. T., Delpire, E. & Staley, K. 2017. Chloride Dysregulation, Seizures, and Cerebral Edema: A Relationship with Therapeutic Potential. *Trends Neurosci,* 40**,** 276-294.

Goldenberg, S. J., Cascio, T. C., Shumway, S. D., Garbutt, K. C., Liu, J., Xiong, Y. & Zheng, N. 2004. Structure of the Cand1-Cul1-Roc1 complex reveals regulatory mechanisms for the assembly of the multisubunit cullin-dependent ubiquitin ligases. *Cell,* 119**,** 517-528.

Gross, A., Schoendube, J., Zimmermann, S., Steeb, M., Zengerle, R. & Koltay, P. 2015. Technologies for Single-Cell Isolation. *International journal of molecular sciences,* 16**,** 16897-16919.

Hadchouel, J., Ellison, D. H. & Gamba, G. 2016. Regulation of Renal Electrolyte Transport by WNK and SPAK-OSR1 Kinases. *Annual Review of Physiology,* 78**,** 367-389.

Hannah, J. & Zhou, P. 2015. Distinct and overlapping functions of the cullin E3 ligase scaffolding proteins CUL4A and CUL4B. *Gene,* 573**,** 33-45.

He, Y. J., Mccall, C. M., Hu, J., Zeng, Y. & Xiong, Y. 2006. DDB1 functions as a linker to recruit receptor WD40 proteins to CUL4-ROC1 ubiquitin ligases. *Genes Dev,* 20.

Hershko, A., Heller, H., Elias, S. & Ciechanover, A. 1983. Components of ubiquitin-protein ligase system. Resolution, affinity purification, and role in protein breakdown. *J Biol Chem,* 258**,** 8206-8214.

Higa, L. A., Wu, M., Ye, T., Kobayashi, R., Sun, H. & Zhang, H. 2006. CUL4–DDB1 ubiquitin ligase interacts with multiple WD40-repeat proteins and regulates histone methylation. *Nature Cell Biology,* 8**,** 1277.

Higa, L. A. & Zhang, H. 2007. Stealing the spotlight: CUL4-DDB1 ubiquitin ligase docks WD40-repeat proteins to destroy. *Cell Division,* 2**,** 1-9.

Hjerpe, R., Aillet, F., Lopitz-Otsoa, F., Lang, V., England, P. & Rodriguez, M. S. 2009. Efficient protection and isolation of ubiquitylated proteins using tandem ubiquitin-binding entities. *EMBO reports,* 10**,** 1250-1258.

Hossain Khan, M. Z., Sohara, E., Ohta, A., Chiga, M., Inoue, Y., Isobe, K., Wakabayashi, M., Oi, K., Rai, T., Sasaki, S. & Uchida, S. 2012. Phosphorylation of Na–Cl cotransporter by OSR1 and SPAK kinases regulates its ubiquitination. *Biochemical and Biophysical Research Communications,* 425**,** 456-461.

Hotton, S. K. & Callis, J. 2008. Regulation of Cullin RING Ligases. *Annual Review of Plant Biology,* 59**,** 467-489.

Howard, H. C., Mount, D. B., Rochefort, D., Byun, N., Dupre, N., Lu, J., Fan, X., Song, L., Riviere, J.-B., Prevost, C., Horst, J., Simonati, A., Lemcke, B., Welch, R., England, R., Zhan, F. Q., Mercado, A., Siesser, W. B., George, A. L., Mcdonald, M. P., Bouchard, J.-P., Mathieu, J., Delpire, E. & Rouleau, G. A. 2002. The K-Cl cotransporter KCC3 is mutant in a severe peripheral neuropathy associated with agenesis of the corpus callosum. *Nat Genet,* 32**,** 384-392.

Http://Www.Abcam.Com/Ikzf3-Antibody-Ab64400.Html 2017.

Http://Www.Proteinatlas.Org/Ensg00000161405-Ikzf3/Cell. 2017. Available: http://www.proteinatlas.org/ENSG00000161405-IKZF3/cell [Accessed 2017].

Hu, J., Mccall, C. M., Ohta, T. & Xiong, Y. 2004. Targeted ubiquitination of CDT1 by the DDB1-CUL4A-ROC1 ligase in response to DNA damage. *Nat Cell Biol,* 6.

Hu, J., Zacharek, S., He, Y. J., Lee, H., Shumway, S., Duronio, R. J. & Xiong, Y. 2008. WD40 protein FBW5 promotes ubiquitination of tumor suppressor TSC2 by DDB1–CUL4–ROC1 ligase. *Genes & Development,* 22**,** 866-871.

Huang, D. T., Ayrault, O., Hunt, H. W., Taherbhoy, A. M., Duda, D. M., Scott, D. C., Borg, L. A., Neale, G., Murray, P. J., Roussel, M. F. & Schulman, B. A. 2009. E2-RING expansion of the NEDD8 cascade confers specificity to cullin modification. *Mol Cell,* 33**,** 483-495.

Huang, H., Song, S., Banerjee, S., Jiang, T., Zhang, J., Kahle, K. T., Sun, D. & Zhang, Z. 2019. The WNK-SPAK/OSR1 Kinases and the Cation-Chloride Cotransporters as Therapeutic Targets for Neurological Diseases. *Aging and disease,* 10**,** 626-636.

Hunter, T. 2007. The Age of Crosstalk: Phosphorylation, Ubiquitination, and Beyond. *Molecular Cell,* 28**,** 730-738.

Ishino, Y., Krupovic, M. & Forterre, P. 2018. History of CRISPR-Cas from Encounter with a Mysterious Repeated Sequence to Genome Editing Technology. *Journal of Bacteriology,* 200**,** e00580-00517.

Ito, T., Ando, H., Suzuki, T., Ogura, T., Hotta, K., Imamura, Y., Yamaguchi, Y. & Handa, H. 2010. Identification of a Primary Target of Thalidomide Teratogenicity. *Science,* 327**,** 1345-1350.

Jackson, S. & Xiong, Y. 2009. CRL4s: the CUL4-RING E3 ubiquitin ligases. *Trends in Biochemical Sciences,* 34**,** 562-570.

Kadri, H., Alamri, M. A., Navratilova, I. H., Alderwick, L. J., Simpkins, N. S. & Mehellou, Y. 2017. Towards the Development of Small-Molecule MO25 Binders as Potential Indirect SPAK/OSR1 Kinase Inhibitors. *Chembiochem,* 18**,** 460-465.

Kafil, V. & Omidi, Y. 2011. Cytotoxic impacts of linear and branched polyethylenimine nanostructures in a431 cells. *BioImpacts : BI,* 1**,** 23-30.

Kahle, K. T., Barnett, S. M., Sassower, K. C. & Staley, K. J. 2009. Decreased seizure activity in a human neonate treated with bumetanide, an inhibitor of the Na(+)-K(+)-2Cl(-) cotransporter NKCC1. *J Child Neurol,* 24**,** 572-576.

Kahle, K. T., Wilson, F. H., Leng, Q., Lalioti, M. D., O'connell, A. D., Dong, K., Rapson, A. K., Macgregor, G. G., Giebisch, G., Hebert, S. C. & Lifton, R. P. 2003. WNK4 regulates the balance between renal NaCl reabsorption and K+ secretion. *Nat Genet,* 35**,** 372-376.

Kamura, T., Maenaka, K., Kotoshiba, S., Matsumoto, M., Kohda, D., Conaway, R. C., Conaway, J. W. & Nakayama, K. I. 2004. VHL-box and SOCS-box domains determine binding specificity for Cul2-Rbx1 and Cul5-Rbx2 modules of ubiquitin ligases. *Genes Dev,* 18**,** 3055-3065.

Kamura, T., Sato, S., Haque, D., Liu, L., Kaelin, W. G., Jr., Conaway, R. C. & Conaway, J. W. 1998. The Elongin BC complex interacts with the conserved SOCS-box motif present in members of the SOCS, ras, WD-40 repeat, and ankyrin repeat families. *Genes & Development,* 12**,** 3872-3881.

Keuss, M. J., Thomas, Y., Mcarthur, R., Wood, N. T., Knebel, A. & Kurz, T. 2016. Characterization of the mammalian family of DCN-type NEDD8 E3 ligases. *Journal of Cell Science,* 129**,** 1441-1454.

Kikuchi, E., Mori, T., Zeniya, M., Isobe, K., Ishigami-Yuasa, M., Fujii, S., Kagechika, H., Ishihara, T., Mizushima, T., Sasaki, S., Sohara, E., Rai, T. & Uchida, S. 2015. Discovery of Novel SPAK Inhibitors That Block WNK Kinase Signaling to Cation Chloride Transporters. *Journal of the American Society of Nephrology,* 26**,** 1525-1536.

Kipreos, E. T., Lander, L. E., Wing, J. P., He, W. W. & Hedgecock, E. M. 1996. cul-1 is required for cell cycle exit in C. elegans and identifies a novel gene family. *Cell,* 85**,** 829-839.

Kitada, T., Asakawa, S., Hattori, N., Matsumine, H., Yamamura, Y., Minoshima, S., Yokochi, M., Mizuno, Y. & Shimizu, N. 1998. Mutations in the parkin gene cause autosomal recessive juvenile parkinsonism. *Nature,* 392**,** 605-608.

Komander, D. 2009. The emerging complexity of protein ubiquitination. *Biochemical Society Transactions,* 37**,** 937-953.

Kotake, Y., Zeng, Y. & Xiong, Y. 2009. DDB1-CUL4 and MLL1 Mediate Oncogene-Induced p16^{INK4a} Activation. *Cancer Research,* 69**,** 1809-1814.

Kozakov, D., Hall, D. R., Xia, B., Porter, K. A., Padhorny, D., Yueh, C., Beglov, D. & Vajda, S. 2017. The ClusPro web server for protein-protein docking. *Nat Protoc,* 12**,** 255-278.

Krönke, J., Udeshi, N. D., Narla, A., Grauman, P., Hurst, S. N., Mcconkey, M., Svinkina, T., Heckl, D., Comer, E., Li, X., Ciarlo, C., Hartman, E., Munshi, N., Schenone, M., Schreiber, S. L., Carr, S. A. & Ebert, B. L. 2014. Lenalidomide Causes Selective Degradation of IKZF1 and IKZF3 in Multiple Myeloma Cells. *Science,* 343**,** 301-305.

Kwon, J. E., La, M., Oh, K. H., Oh, Y. M., Kim, G. R., Seol, J. H., Baek, S. H., Chiba, T., Tanaka, K., Bang, O. S., Joe, C. O. & Chung, C. H. 2006. BTB Domain-containing Speckle-type POZ Protein (SPOP) Serves as an Adaptor of Daxx for Ubiquitination by Cul3-based Ubiquitin Ligase. *Journal of Biological Chemistry,* 281**,** 12664-12672.

Latres, E., Chiaur, D. & Pagano, M. 1999. The human F box protein β-Trcp associates with the Cul1/Skp1 complex and regulates the stability of β-catenin. *Oncogene,* 18**,** 849.

Le Rouzic, E., Belaïdouni, N., Estrabaud, E., Morel, M., Rain, J.-C., Transy, C. & Margottin-Goguet, F. 2007. HIV1 Vpr Arrests the Cell Cycle by Recruiting DCAF1/VprBP, a Receptor of the Cul4-DDB1 Ubiquitin Ligase. *Cell Cycle,* 6**,** 182-188.

Lee, D. H. & Goldberg, A. L. 1998. Proteasome inhibitors: valuable new tools for cell biologists. *Trends in Cell Biology,* 8**,** 397-403.

Leiserson, W. M., Harkins, E. W. & Keshishian, H. 2000. Fray, a Drosophila serine/threonine kinase homologous to mammalian PASK, is required for axonal ensheathment. *Neuron,* 28**,** 793-806.

Leung-Pineda, V., Huh, J. & Piwnica-Worms, H. 2009. DDB1 Targets Chk1 to the Cul4 E3 Ligase Complex in Normal Cycling Cells and in Cells Experiencing Replication Stress. *Cancer Research,* 69**,** 2630-2637.

Li, L. & Deng, X. W. 2003. The COP9 signalosome: an alternative lid for the 26S proteasome? *Trends Cell Biol,* 13**,** 507-509.

Li, T., Chen, X., Garbutt, K. C., Zhou, P. & Zheng, N. 2006. Structure of DDB1 in complex with a paramyxovirus V protein: viral hijack of a propeller cluster in ubiquitin ligase. *Cell,* 124**,** 105-117.

Li, W., Bengtson, M. H., Ulbrich, A., Matsuda, A., Reddy, V. A., Orth, A., Chanda, S. K., Batalov, S. & Joazeiro, C. A. 2008. Genome-wide and functional annotation of human E3 ubiquitin ligases identifies MULAN, a mitochondrial E3 that regulates the organelle's dynamics and signaling. *PLoS One,* 3**,** e1487.

Li, X., Zhao, Q., Liao, R., Sun, P. & Wu, X. 2003. The SCFSkp2 Ubiquitin Ligase Complex Interacts with the Human Replication Licensing Factor Cdt1 and Regulates Cdt1 Degradation. *Journal of Biological Chemistry,* 278**,** 30854-30858.

Limón-Mortés, M. C., Mora-Santos, M., Espina, Á., Pintor-Toro, J. A., López-Román, A., Tortolero, M. & Romero, F. 2008. UV-induced degradation of securin is mediated by SKP1-CUL1-βTrCP E3 ubiquitin ligase. *Journal of Cell Science,* 121**,** 1825-1831.

Lin, S.-H., Yu, I. S., Jiang, S.-T., Lin, S.-W., Chu, P., Chen, A., Sytwu, H.-K., Sohara, E., Uchida, S., Sasaki, S. & Yang, S.-S. 2011. Impaired phosphorylation of Na(+)-K(+)-2Cl(−) cotransporter by oxidative stress-responsive kinase-1 deficiency manifests hypotension and Bartter-like syndrome. *Proceedings of the National Academy of Sciences of the United States of America,* 108**,** 17538-17543.

Liu, J., Ye, J., Zou, X., Xu, Z., Feng, Y., Zou, X., Chen, Z., Li, Y. & Cang, Y. 2014. CRL4ACRBN E3 ubiquitin ligase restricts BK channel activity and prevents epileptogenesis. *Nat Commun,* 5.

Lopez-Girona, A., Mendy, D., Ito, T., Miller, K., Gandhi, A. K., Kang, J., Karasawa, S., Carmel, G., Jackson, P., Abbasian, M., Mahmoudi, A., Cathers, B., Rychak, E., Gaidarova, S., Chen, R., Schafer, P. H., Handa, H., Daniel, T. O., Evans, J. F. & Chopra, R. 2012. Cereblon is a direct protein target for immunomodulatory and antiproliferative activities of lenalidomide and pomalidomide. *Leukemia,* 26**,** 2326-2335.

Louis-Dit-Picard, H., Barc, J., Trujillano, D., Miserey-Lenkei, S., Bouatia-Naji, N., Pylypenko, O., Beaurain, G., Bonnefond, A., Sand, O., Simian, C., Vidal-Petiot, E., Soukaseum, C., Mandet, C., Broux, F., Chabre, O., Delahousse, M., Esnault, V., Fiquet, B., Houillier, P., Bagnis, C. I., Koenig, J., Konrad, M., Landais, P., Mourani, C., Niaudet, P., Probst, V., Thauvin, C., Unwin, R. J., Soroka, S. D., Ehret, G., Ossowski, S., Caulfield International Consortium for Blood Pressure, M., Bruneval, P., Estivill, X., Froguel, P., Hadchouel, J., Schott, J.-J. & Jeunemaitre, X. 2012. KLHL3 mutations cause familial hyperkalemic hypertension by impairing ion transport in the distal nephron. *Nature Genetics,* 44**,** 609.

Lydeard, J. R., Schulman, B. A. & Harper, J. W. 2013. Building and remodelling Cullin–RING E3 ubiquitin ligases. *EMBO reports,* 14**,** 1050-1061.

Maeda, Y., Suzuki, T., Pan, X., Chen, G., Pan, S., Bartman, T. & Whitsett, J. A. 2008. CUL2 Is Required for the Activity of Hypoxia-inducible Factor and Vasculogenesis. *Journal of Biological Chemistry,* 283**,** 16084-16092.

Maerki, S., Olma, M. H., Staubli, T., Steigemann, P., Gerlich, D. W., Quadroni, M., Sumara, I. & Peter, M. 2009. The Cul3–KLHL21 E3 ubiquitin ligase targets Aurora B to midzone microtubules in anaphase and is required for cytokinesis. *The Journal of Cell Biology,* 187**,** 791-800.

Mahrour, N., Redwine, W. B., Florens, L., Swanson, S. K., Martin-Brown, S., Bradford, W. D., Staehling-Hampton, K., Washburn, M. P., Conaway, R. C. & Conaway, J. W. 2008. Characterization of cullin-box sequences that direct recruitment of Cul2-Rbx1 and Cul5-Rbx2 modules to elongin BC-based ubiquitin ligases. *J Biol Chem.*

Manning, G., Whyte, D. B., Martinez, R., Hunter, T. & Sudarsanam, S. 2002. The Protein Kinase Complement of the Human Genome. *Science,* 298**,** 1912-1934.

Mccormick, J. A. & Ellison, D. H. 2011. The WNKs: atypical protein kinases with pleiotropic actions. *Physiological reviews,* 91**,** 177-219.

Mccormick, J. A., Mutig, K., Nelson, J. H., Saritas, T., Hoorn, E. J., Yang, C.-L., Rogers, S., Curry, J., Delpire, E., Bachmann, S. & Ellison, D. H. 2011. A SPAK isoform switch modulates renal salt transport and blood pressure. *Cell metabolism,* 14**,** 352-364.

Mcdowell, G. S. & Philpott, A. 2013. Non-canonical ubiquitylation: Mechanisms and consequences. *The International Journal of Biochemistry & Cell Biology,* 45**,** 1833-1842.

Mehellou, Y., Alamri, M. A., Dhiani, B. A. & Kadri, H. 2018. C-terminal phosphorylation of SPAK and OSR1 kinases promotes their binding and activation by the scaffolding protein MO25. *Biochem Biophys Res Commun,* 503**,** 1868-1873.

Mehle, A., Goncalves, J., Santa-Marta, M., Mcpike, M. & Gabuzda, D. 2004. Phosphorylation of a novel SOCS-box regulates assembly of the HIV-1 Vif-Cul5 complex that promotes APOBEC3G degradation. *Genes & Development,* 18**,** 2861-2866.

Merlet, J., Burger, J., Gomes, J.-E. & Pintard, L. 2009. Regulation of cullin-RING E3 ubiquitin-ligases by neddylation and dimerization. *Cellular and Molecular Life Sciences,* 66**,** 1924-1938.
Metzger, M. B., Hristova, V. A. & Weissman, A. M. 2012. HECT and RING finger families of E3 ubiquitin ligases at a glance. *J Cell Sci,* 125**,** 531-537.
Meyer, J. W., Flagella, M., Sutliff, R. L., Lorenz, J. N., Nieman, M. L., Weber, C. S., Paul, R. J. & Shull, G. E. 2002. Decreased blood pressure and vascular smooth muscle tone in mice lacking basolateral Na+-K+-2Cl− cotransporter. *American Journal of Physiology-Heart and Circulatory Physiology,* 283**,** H1846-H1855.
Min, X., Lee, B. H., Cobb, M. H. & Goldsmith, E. J. 2004. Crystal structure of the kinase domain of WNK1, a kinase that causes a hereditary form of hypertension. *Structure,* 12**,** 1303-1311.
Moniz, S., Verissimo, F., Matos, P., Brazao, R., Silva, E., Kotevelets, L., Chastre, E., Gespach, C. & Jordan, P. 2007. Protein kinase WNK2 inhibits cell proliferation by negatively modulating the activation of MEK1/ERK1/2. *Oncogene,* 26**,** 6071-6081.
Moore, T. M., Garg, R., Johnson, C., Coptcoat, M. J., Ridley, A. J. & Morris, J. D. H. 2000. PSK, a Novel STE20-like Kinase Derived from Prostatic Carcinoma That Activates the c-Jun N-terminal Kinase Mitogen-activated Protein Kinase Pathway and Regulates Actin Cytoskeletal Organization. *Journal of Biological Chemistry,* 275**,** 4311-4322.
Mori, T., Kikuchi, E., Watanabe, Y., Fujii, S., Ishigami-Yuasa, M., Kagechika, H., Sohara, E., Rai, T., Sasaki, S. & Uchida, S. 2013. Chemical library screening for WNK signalling inhibitors using fluorescence correlation spectroscopy. *Biochemical Journal,* 455**,** 339-345.
Moriguchi, T., Urushiyama, S., Hisamoto, N., Iemura, S.-I., Uchida, S., Natsume, T., Matsumoto, K. & Shibuya, H. 2005. WNK1 Regulates Phosphorylation of Cation-Chloride-coupled Cotransporters via the STE20-related Kinases, SPAK and OSR1. *Journal of Biological Chemistry,* 280**,** 42685-42693.
Moriya, H. 2015. Quantitative nature of overexpression experiments. *Molecular Biology of the Cell,* 26**,** 3932-3939.
Mudhasani, R., Tran, J. P., Retterer, C., Kota, K. P., Whitehouse, C. A. & Bavari, S. 2016. Protein kinase R degradation is essential for Rift Valley fever virus infection and is regulated by SKP1-CUL1-F-box (SCF) FBXW11-NSs E3 ligase. *PLoS pathogens,* 12**,** e1005437.
Murthy, M., Kurz, T. & O'shaughnessy, K. M. 2017. WNK signalling pathways in blood pressure regulation. *Cellular and Molecular Life Sciences,* 74**,** 1261-1280.
Na, T., Wu, G., Zhang, W., Dong, W. J. & Peng, J. B. 2013. Disease-causing R1185C mutation of WNK4 disrupts a regulatory mechanism involving calmodulin binding and SGK1 phosphorylation sites. *Am J Physiol Renal Physiol,* 304**,** F8-f18.
Naito, S., Ohta, A., Sohara, E., Ohta, E., Rai, T., Sasaki, S. & Uchida, S. 2010. Regulation of WNK1 kinase by extracellular potassium. *Clinical and Experimental Nephrology,* 15**,** 195-202.
Nawrocki, S. T., Griffin, P., Kelly, K. R. & Carew, J. S. 2012. MLN4924: a novel first-in-class inhibitor of NEDD8-activating enzyme for cancer therapy. *Expert opinion on investigational drugs,* 21**,** 1563-1573.
Nayak, S., Santiago, F. E., Jin, H., Lin, D., Schedl, T. & Kipreos, E. T. 2002. The Caenorhabditis elegans Skp1-Related Gene Family. *Current Biology,* 12**,** 277-287.
Ncd-Rfc, N. R. F. C. 2016. Worldwide trends in blood pressure from 1975 to 2015: A pooled analysis of 1479 population-based measurement studies with 19·1 million participants. World Health Organization.

Nguyen, T. N. & Goodrich, J. A. 2006. Protein-protein interaction assays: eliminating false positive interactions. *Nature methods,* 3**,** 135-139.
Nguyen, T. V., Li, J., Lu, C.-C., Mamrosh, J. L., Lu, G., Cathers, B. E. & Deshaies, R. J. 2017. p97/VCP promotes degradation of CRBN substrate glutamine synthetase and neosubstrates. *Proceedings of the National Academy of Sciences,* 114**,** 3565-3571.
Nishi, H., Hashimoto, K. & Panchenko, A. R. 2011. Phosphorylation in protein-protein binding: effect on stability and function. *Structure (London, England : 1993),* 19**,** 1807-1815.
O'hagan, R. C., Ohh, M., David, G., De Alboran, I. M., Alt, F. W., Kaelin, W. G. & Depinho, R. A. 2000. Myc-enhanced expression of Cul1 promotes ubiquitin-dependent proteolysis and cell cycle progression. *Genes & Development,* 14**,** 2185-2191.
O'keefe, E. P. 2013. siRNAs and shRNAs: Tools for Protein Knockdown by Gene Silencing. *MATER METHODS,* 3**,** 197.
Ohta, A., Schumacher, F.-R., Mehellou, Y., Johnson, C., Knebel, A., Macartney, Thomas j., Wood, Nicola t., Alessi, Dario r. & Kurz, T. 2013. The CUL3–KLHL3 E3 ligase complex mutated in Gordon's hypertension syndrome interacts with and ubiquitylates WNK isoforms: disease-causing mutations in KLHL3 and WNK4 disrupt interaction. *Biochemical Journal,* 451**,** 111-122.
Pacheco-Alvarez, D., Cristobal, P. S., Meade, P., Moreno, E., Vazquez, N., Munoz, E., Diaz, A., Juarez, M. E., Gimenez, I. & Gamba, G. 2006. The Na+:Cl- cotransporter is activated and phosphorylated at the amino-terminal domain upon intracellular chloride depletion. *J Biol Chem,* 281**,** 28755-28763.
Pao, K.-C., Wood, N. T., Knebel, A., Rafie, K., Stanley, M., Mabbitt, P. D., Sundaramoorthy, R., Hofmann, K., Van Aalten, D. M. F. & Virdee, S. 2018. Activity-based E3 ligase profiling uncovers an E3 ligase with esterification activity. *Nature,* 556**,** 381-385.
Petroski, M. D. & Deshaies, R. J. 2005. Function and regulation of cullin-RING ubiquitin ligases. *Nat Rev Mol Cell Biol,* 6.
Petzold, G., Fischer, E. S. & Thomä, N. H. 2016. Structural basis of lenalidomide-induced CK1α degradation by the CRL4CRBN ubiquitin ligase. *Nature,* 532**,** 127.
Piala, A. T., Moon, T. M., Akella, R., He, H., Cobb, M. H. & Goldsmith, E. J. 2014. Chloride Sensing by WNK1 Involves Inhibition of Autophosphorylation. *Science Signaling,* 7**,** ra41-ra41.
Piechotta, K., Garbarini, N., England, R. & Delpire, E. 2003. Characterization of the Interaction of the Stress Kinase SPAK with the Na-K-2Cl Cotransporter in the Nervous System. *Journal of Biological Chemistry,* 278**,** 52848-52856.
Piechotta, K., Lu, J. & Delpire, E. 2002. Cation Chloride Cotransporters Interact with the Stress-related Kinases Ste20-related Proline-Alanine-rich Kinase (SPAK) and Oxidative Stress Response 1 (OSR1). *Journal of Biological Chemistry,* 277**,** 50812-50819.
Pierce, N. W., Lee, J. E., Liu, X., Sweredoski, M. J., Graham, R. L. J., Larimore, E. A., Rome, M., Zheng, N., Clurman, B. E., Hess, S., Shan, S.-O. & Deshaies, R. J. 2013. Cand1 Promotes Assembly of New SCF Complexes through Dynamic Exchange of F Box Proteins. *Cell,* 153**,** 206-215.
Rafiqi, F. H., Zuber, A. M., Glover, M., Richardson, C., Fleming, S., Jovanovic, S., Jovanovic, A., O'shaughnessy, K. M. & Alessi, D. R. 2010. Role of the WNK-activated SPAK kinase in regulating blood pressure. *EMBO Mol Med,* 2**,** 63-75.
Ran, F. A., Hsu, Patrick d., Lin, C.-Y., Gootenberg, Jonathan s., Konermann, S., Trevino, A. E., Scott, David a., Inoue, A., Matoba, S., Zhang, Y. & Zhang, F. 2013. Double Nicking by RNA-Guided CRISPR Cas9 for Enhanced Genome Editing Specificity. *Cell,* 154**,** 1380-1389.

Rao, D. D., Vorhies, J. S., Senzer, N. & Nemunaitis, J. 2009. siRNA vs. shRNA: Similarities and differences. *Advanced Drug Delivery Reviews,* 61**,** 746-759.
Richardson, C. & Alessi, D. R. 2008. The regulation of salt transport and blood pressure by the WNK-SPAK/OSR1 signalling pathway. *Journal of Cell Science,* 121**,** 3293-3304.
Richardson, C., Rafiqi, F. H., Karlsson, H. K. R., Moleleki, N., Vandewalle, A., Campbell, D. G., Morrice, N. A. & Alessi, D. R. 2008. Activation of the thiazide-sensitive Na+-Cl– cotransporter by the WNK-regulated kinases SPAK and OSR1. *Journal of Cell Science,* 121**,** 675-684.
Riley, B. E., Lougheed, J. C., Callaway, K., Velasquez, M., Brecht, E., Nguyen, L., Shaler, T., Walker, D., Yang, Y., Regnstrom, K., Diep, L., Zhang, Z., Chiou, S., Bova, M., Artis, D. R., Yao, N., Baker, J., Yednock, T. & Johnston, J. A. 2013. Structure and function of Parkin E3 ubiquitin ligase reveals aspects of RING and HECT ligases. *Nat Commun,* 4**,** 1982.
Rinehart, J., Vázquez, N., Kahle, K. T., Hodson, C. A., Ring, A. M., Gulcicek, E. E., Louvi, A., Bobadilla, N. A., Gamba, G. & Lifton, R. P. 2011. WNK2 Kinase Is a Novel Regulator of Essential Neuronal Cation-Chloride Cotransporters. *Journal of Biological Chemistry,* 286**,** 30171-30180.
Rotin, D. & Kumar, S. 2009. Physiological functions of the HECT family of ubiquitin ligases. *Nat Rev Mol Cell Biol,* 10**,** 398-409.
Sakaguchi, H., Takami, T., Yasutani, Y., Maeda, T., Morino, M., Ishii, T., Shiomi, Y. & Nishitani, H. 2012. Checkpoint Kinase ATR Phosphorylates Cdt2, a Substrate Receptor of CRL4 Ubiquitin Ligase, and Promotes the Degradation of Cdt1 following UV Irradiation. *PLoS One,* 7**,** e46480.
Sakata, E., Yamaguchi, Y., Miyauchi, Y., Iwai, K., Chiba, T., Saeki, Y., Matsuda, N., Tanaka, K. & Kato, K. 2007. Direct interactions between NEDD8 and ubiquitin E2 conjugating enzymes upregulate cullin-based E3 ligase activity. *Nat Struct Mol Biol,* 14**,** 167-168.
Schulze, W. X. & Mann, M. 2004. A Novel Proteomic Screen for Peptide-Protein Interactions. *Journal of Biological Chemistry,* 279**,** 10756-10764.
Shibata, S., Zhang, J., Puthumana, J., Stone, K. L. & Lifton, R. P. 2013. Kelch-like 3 and Cullin 3 regulate electrolyte homeostasis via ubiquitination and degradation of WNK4. *Proceedings of the National Academy of Sciences,* 110**,** 7838-7843.
Shibata, T., Ohta, T., Tong, K. I., Kokubu, A., Odogawa, R., Tsuta, K., Asamura, H., Yamamoto, M. & Hirohashi, S. 2008. Cancer related mutations in NRF2 impair its recognition by Keap1-Cul3 E3 ligase and promote malignancy. *Proceedings of the National Academy of Sciences,* 105**,** 13568-13573.
Simon, D. B., Karet, F. E., Hamdan, J. M., Pietro, A. D., Sanjad, S. A. & Lifton, R. P. 1996a. Bartter's syndrome, hypokalaemic alkalosis with hypercalciuria, is caused by mutations in the Na-K-2Cl cotransporter NKCC2. *Nat Genet,* 13**,** 183-188.
Simon, D. B., Nelson-Williams, C., Johnson Bia, M., Ellison, D., Karet, F. E., Morey Molina, A., Vaara, I., Iwata, F., Cushner, H. M., Koolen, M., Gainza, F. J., Gitelman, H. J. & Lifton, R. P. 1996b. Gitelman's variant of Barter's syndrome, inherited hypokalaemic alkalosis, is caused by mutations in the thiazide-sensitive Na-Cl cotransporter. *Nat Genet,* 12**,** 24-30.
Skaar, J. R., Florens, L., Tsutsumi, T., Arai, T., Tron, A., Swanson, S. K., Washburn, M. P. & Decaprio, J. A. 2007. PARC and CUL7 form atypical cullin RING ligase complexes. *Cancer Res,* 67**,** 2006-2014.
Skowyra, D., Craig, K. L., Tyers, M., Elledge, S. J. & Harper, J. W. 1997. F-box proteins are receptors that recruit phosphorylated substrates to the SCF ubiquitin-ligase complex. *Cell,* 91**,** 209-219.
Soucy, T. A., Smith, P. G., Milhollen, M. A., Berger, A. J., Gavin, J. M., Adhikari, S., Brownell, J. E., Burke, K. E., Cardin, D. P., Critchley, S., Cullis, C. A.,

Doucette, A., Garnsey, J. J., Gaulin, J. L., Gershman, R. E., Lublinsky, A. R., Mcdonald, A., Mizutani, H., Narayanan, U., Olhava, E. J., Peluso, S., Rezaei, M., Sintchak, M. D., Talreja, T., Thomas, M. P., Traore, T., Vyskocil, S., Weatherhead, G. S., Yu, J., Zhang, J., Dick, L. R., Claiborne, C. F., Rolfe, M., Bolen, J. B. & Langston, S. P. 2009. An inhibitor of NEDD8-activating enzyme as a new approach to treat cancer. *Nature,* 458**,** 732-736.

Spratt, D. E., Walden, H. & Shaw, G. S. 2014. RBR E3 ubiquitin ligases: new structures, new insights, new questions. *Biochem J,* 458**,** 421-437.

Sufan, R. I. & Ohh, M. 2006. Role of the NEDD8 modification of Cul2 in the sequential activation of ECV complex. *Neoplasia,* 8**,** 956-963.

Takahashi, D., Mori, T., Nomura, N., Khan, M. Z., Araki, Y., Zeniya, M., Sohara, E., Rai, T., Sasaki, S. & Uchida, S. 2014. WNK4 is the major WNK positively regulating NCC in the mouse kidney. *Biosci Rep,* 34.

Takahashi, D., Mori, T., Wakabayashi, M., Mori, Y., Susa, K., Zeniya, M., Sohara, E., Rai, T., Sasaki, S. & Uchida, S. 2013. KLHL2 interacts with and ubiquitinates WNK kinases. *Biochemical and Biophysical Research Communications,* 437**,** 457-462.

Tamari, M., Daigo, Y. & Nakamura, Y. 1999. Isolation and characterization of a novel serine threonine kinase gene on chromosome 3p22-21.3. *J Hum Genet,* 44**,** 116-120.

Tang, Z., Li, B., Bharadwaj, R., Zhu, H., Ozkan, E., Hakala, K., Deisenhofer, J. & Yu, H. 2001. APC2 Cullin protein and APC11 RING protein comprise the minimal ubiquitin ligase module of the anaphase-promoting complex. *Mol Biol Cell,* 12**,** 3839-3851.

Taylor, C. A., An, S.-W., Kankanamalage, S. G., Stippec, S., Earnest, S., Trivedi, A. T., Yang, J. Z., Mirzaei, H., Huang, C.-L. & Cobb, M. H. 2018. OSR1 regulates a subset of inward rectifier potassium channels via a binding motif variant. *Proceedings of the National Academy of Sciences,* 115**,** 3840-3845.

Teicher, B. A. & Tomaszewski, J. E. 2015. Proteasome inhibitors. *Biochemical Pharmacology,* 96**,** 1-9.

Thastrup, Jacob o., Rafiqi, Fatema h., Vitari, Alberto c., Pozo-Guisado, E., Deak, M., Mehellou, Y. & Alessi, Dario r. 2012. SPAK/OSR1 regulate NKCC1 and WNK activity: analysis of WNK isoform interactions and activation by T-loop trans-autophosphorylation. *Biochemical Journal,* 441**,** 325-337.

Touyz, R. M., Alves-Lopes, R., Rios, F. J., Camargo, L. L., Anagnostopoulou, A., Arner, A. & Montezano, A. C. 2018. Vascular smooth muscle contraction in hypertension. *Cardiovasc Res,* 114**,** 529-539.

Tudzarova, S., Colombo, S. L., Stoeber, K., Carcamo, S., Williams, G. H. & Moncada, S. 2011. Two ubiquitin ligases, APC/C-Cdh1 and SKP1-CUL1-F (SCF)-β-TrCP, sequentially regulate glycolysis during the cell cycle. *Proceedings of the National Academy of Sciences,* 108**,** 5278-5283.

Uehara, T., Minoshima, Y., Sagane, K., Sugi, N. H., Mitsuhashi, K. O., Yamamoto, N., Kamiyama, H., Takahashi, K., Kotake, Y., Uesugi, M., Yokoi, A., Inoue, A., Yoshida, T., Mabuchi, M., Tanaka, A. & Owa, T. 2017. Selective degradation of splicing factor CAPER[alpha] by anticancer sulfonamides. *Nat Chem Biol,* 13**,** 675-680.

Ushiro, H., Tsutsumi, T., Suzuki, K., Kayahara, T. & Nakano, K. 1998. Molecular Cloning and Characterization of a Novel Ste20-Related Protein Kinase Enriched in Neurons and Transporting Epithelia. *Archives of Biochemistry and Biophysics,* 355**,** 233-240.

Van Rechem, C., Black, J. C., Abbas, T., Allen, A., Rinehart, C. A., Yuan, G.-C., Dutta, A. & Whetstine, J. R. 2011. The SKP1-Cul1-F-box and Leucine-rich Repeat Protein 4 (SCF-FbxL4) Ubiquitin Ligase Regulates Lysine Demethylase 4A (KDM4A)/Jumonji Domain-containing 2A (JMJD2A) Protein. *Journal of Biological Chemistry,* 286**,** 30462-30470.

Veen, A. G. V. D. & Ploegh, H. L. 2012. Ubiquitin-Like Proteins. *Annual Review of Biochemistry,* 81**,** 323-357.
Vidal-Petiot, E., Elvira-Matelot, E., Mutig, K., Soukaseum, C., Baudrie, V., Wu, S., Cheval, L., Huc, E., Cambillau, M., Bachmann, S., Doucet, A., Jeunemaitre, X. & Hadchouel, J. 2013. WNK1-related Familial Hyperkalemic Hypertension results from an increased expression of L-WNK1 specifically in the distal nephron. *Proc Natl Acad Sci U S A,* 110**,** 14366-14371.
Villa, F., Goebel, J., Rafiqi, F. H., Deak, M., Thastrup, J., Alessi, D. R. & Van Aalten, D. M. F. 2007. Structural insights into the recognition of substrates and activators by the OSR1 kinase. *EMBO reports,* 8**,** 839-845.
Vitari, A. C., Deak, M., Morrice, N. A. & Alessi, D. R. 2005. The WNK1 and WNK4 protein kinases that are mutated in Gordon's hypertension syndrome phosphorylate and activate SPAK and OSR1 protein kinases. *Biochemical Journal,* 391**,** 17-24.
Vitari, A. C., Thastrup, J., Rafiqi, F. H., Deak, M., Morrice, N. A., Karlsson, H. K. R. & Alessi, D. R. 2006. Functional interactions of the SPAK/OSR1 kinases with their upstream activator WNK1 and downstream substrate NKCC1. *Biochemical Journal,* 397**,** 223-231.
Vittal, V., Stewart, M. D., Brzovic, P. S. & Klevit, R. E. 2015. Regulating the Regulators: Recent Revelations in the Control of E3 Ubiquitin Ligases. *Journal of Biological Chemistry,* 290**,** 21244-21251.
Vitvitsky, V. M., Garg, S. K., Keep, R. F., Albin, R. L. & Banerjee, R. 2012. Na+ and K+ ion imbalances in Alzheimer's disease. *Biochim Biophys Acta,* 1822**,** 1671-1681.
Walden, H., Podgorski, M. S., Huang, D. T., Miller, D. W., Howard, R. J., Minor, D. L., Jr., Holton, J. M. & Schulman, B. A. 2003. The structure of the APPBP1-UBA3-NEDD8-ATP complex reveals the basis for selective ubiquitin-like protein activation by an E1. *Mol Cell,* 12**,** 1427-1437.
Waterhouse, A., Rempfer, C., Heer, F. T., Studer, G., Tauriello, G., Bordoli, L., Bertoni, M., Gumienny, R., Lepore, R., Bienert, S., De beer, T. A p. & Schwede, T. 2018. SWISS-MODEL: homology modelling of protein structures and complexes. *Nucleic Acids Research,* 46**,** W296-W303.
Wenzel, D. M., Lissounov, A., Brzovic, P. S. & Klevit, R. E. 2011. UBCH7 reactivity profile reveals parkin and HHARI to be RING/HECT hybrids. *Nature,* 474**,** 105-108.
Wilson, F. H., Disse-Nicodème, S., Choate, K. A., Ishikawa, K., Nelson-Williams, C., Desitter, I., Gunel, M., Milford, D. V., Lipkin, G. W., Achard, J.-M., Feely, M. P., Dussol, B., Berland, Y., Unwin, R. J., Mayan, H., Simon, D. B., Farfel, Z., Jeunemaitre, X. & Lifton, R. P. 2001. Human Hypertension Caused by Mutations in WNK Kinases. *Science,* 293**,** 1107-1112.
Wu, J.-W., Hu, M., Chai, J., Seoane, J., Huse, M., Li, C., Rigotti, D. J., Kyin, S., Muir, T. W., Fairman, R., Massagué, J. & Shi, Y. 2001. Crystal Structure of a Phosphorylated Smad2: Recognition of Phosphoserine by the MH2 Domain and Insights on Smad Function in TGF-β Signaling. *Molecular Cell,* 8**,** 1277-1289.
Wysocka, J. 2006. Identifying novel proteins recognizing histone modifications using peptide pull-down assay. *Methods (San Diego, Calif.),* 40**,** 339-343.
Xie, X., Wang, Z. & Chen, Y. 2007. Association of LKB1 with a WD-repeat protein WDR6 is implicated in cell growth arrest and $p27^{Kip1}$ induction. *Mol Cell Biochem,* 301**,** 115-122.
Xu, B.-E., English, J. M., Wilsbacher, J. L., Stippec, S., Goldsmith, E. J. & Cobb, M. H. 2000. WNK1, a Novel Mammalian Serine/Threonine Protein Kinase Lacking the Catalytic Lysine in Subdomain II. *Journal of Biological Chemistry,* 275**,** 16795-16801.

Xu, B.-E., Min, X., Stippec, S., Lee, B.-H., Goldsmith, E. J. & Cobb, M. H. 2002. Regulation of WNK1 by an Autoinhibitory Domain and Autophosphorylation. *Journal of Biological Chemistry,* 277**,** 48456-48462.

Yamada, K., Park, H.-M., Rigel, D. F., Dipetrillo, K., Whalen, E. J., Anisowicz, A., Beil, M., Berstler, J., Brocklehurst, C. E., Burdick, D. A., Caplan, S. L., Capparelli, M. P., Chen, G., Chen, W., Dale, B., Deng, L., Fu, F., Hamamatsu, N., Harasaki, K., Herr, T., Hoffmann, P., Hu, Q.-Y., Huang, W.-J., Idamakanti, N., Imase, H., Iwaki, Y., Jain, M., Jeyaseelan, J., Kato, M., Kaushik, V. K., Kohls, D., Kunjathoor, V., Lasala, D., Lee, J., Liu, J., Luo, Y., Ma, F., Mo, R., Mowbray, S., Mogi, M., Ossola, F., Pandey, P., Patel, S. J., Raghavan, S., Salem, B., Shanado, Y. H., Trakshel, G. M., Turner, G., Wakai, H., Wang, C., Weldon, S., Wielicki, J. B., Xie, X., Xu, L., Yagi, Y. I., Yasoshima, K., Yin, J., Yowe, D., Zhang, J.-H., Zheng, G. & Monovich, L. 2016. Small-molecule WNK inhibition regulates cardiovascular and renal function. *Nature Chemical Biology,* 12**,** 896.

Yang, S. S., Lo, Y. F., Wu, C. C., Lin, S. W., Yeh, C. J., Chu, P., Sytwu, H. K., Uchida, S., Sasaki, S. & Lin, S. H. 2010. SPAK-knockout mice manifest Gitelman syndrome and impaired vasoconstriction. *J Am Soc Nephrol,* 21**,** 1868-1877.

Yoshida, S., Araki, Y., Mori, T., Sasaki, E., Kasagi, Y., Isobe, K., Susa, K., Inoue, Y., Bomont, P., Okado, T., Rai, T., Uchida, S. & Sohara, E. 2018. Decreased KLHL3 expression is involved in the pathogenesis of pseudohypoaldosteronism type II caused by cullin 3 mutation in vivo. *Clin Exp Nephrol,* 22**,** 1251-1257.

Yu, X. & Kem, D. C. 2010. Proteasome inhibition during myocardial infarction. *Cardiovascular Research,* 85**,** 312-320.

Yumimoto, K., Muneoka, T., Tsuboi, T. & Nakayama, K. I. 2013. Substrate Binding Promotes Formation of the Skp1-Cul1-Fbxl3 (SCFFbxl3) Protein Complex. *Journal of Biological Chemistry,* 288**,** 32766-32776.

Zagórska, A., Pozo-Guisado, E., Boudeau, J., Vitari, A. C., Rafiqi, F. H., Thastrup, J., Deak, M., Campbell, D. G., Morrice, N. A., Prescott, A. R. & Alessi, D. R. 2007. Regulation of activity and localization of the WNK1 protein kinase by hyperosmotic stress. *The Journal of Cell Biology,* 176**,** 89-100.

Zeng, M., Ren, L., Mizuno, K. I., Nestoras, K., Wang, H., Tang, Z., Guo, L., Kong, D., Hu, Q., He, Q., Du, L., Carr, A. M. & Liu, C. 2016. CRL4Wdr70 regulates H2B monoubiquitination and facilitates Exo1-dependent resection. *Nature Communications,* 7**,** 11364.

Zeniya, M., Sohara, E., Kita, S., Iwamoto, T., Susa, K., Mori, T., Oi, K., Chiga, M., Takahashi, D., Yang, S. S., Lin, S. H., Rai, T., Sasaki, S. & Uchida, S. 2013. Dietary salt intake regulates WNK3-SPAK-NKCC1 phosphorylation cascade in mouse aorta through angiotensin II. *Hypertension,* 62**,** 872-878.

Zeqiraj, E., Filippi, B. M., Deak, M., Alessi, D. R. & Van Aalten, D. M. F. 2009. Structure of the LKB1-STRAD-MO25 complex reveals an allosteric mechanism of kinase activation. *Science (New York, N.Y.),* 326**,** 1707-1711.

Zheng, J., Yang, X., Harrell, J. M., Ryzhikov, S., Shim, E. H., Lykke-Andersen, K., Wei, N., Sun, H., Kobayashi, R. & Zhang, H. 2002a. CAND1 binds to unneddylated CUL1 and regulates the formation of SCF ubiquitin E3 ligase complex. *Mol Cell,* 10.

Zheng, N., Schulman, B. A., Song, L., Miller, J. J., Jeffrey, P. D., Wang, P., Chu, C., Koepp, D. M., Elledge, S. J., Pagano, M., Conaway, R. C., Conaway, J. W., Harper, J. W. & Pavletich, N. P. 2002b. Structure of the Cul1–Rbx1–Skp1–F boxSkp2 SCF ubiquitin ligase complex. *Nature,* 416**,** 703-709.

Zheng, N. & Shabek, N. 2017. Ubiquitin Ligases: Structure, Function, and Regulation. *Annual Review of Biochemistry,* 86**,** 129-157.

Zhuang, M., Calabrese, M. F., Liu, J., Waddell, M. B., Nourse, A., Hammel, M., Miller, D. J., Walden, H., Duda, D. M., Seyedin, S. N., Hoggard, T., Harper, J. W., White, K. P. & Schulman, B. A. 2009. Structures of SPOP-substrate complexes: insights into molecular architectures of BTB-Cul3 ubiquitin ligases. *Mol Cell,* 36**,** 39-50.

Zimmerman, E. S., Schulman, B. A. & Zheng, N. 2010. Structural assembly of cullin-RING ubiquitin ligase complexes. *Current Opinion in Structural Biology,* 20**,** 714-721.

CHAPTER VII.

APPENDICES

CHAPTER VII. APPENDICES

7.1. REAGENT AND BUFFERS RECIPES

7.1.1. Reagent and buffers recipe for Western blot

RUNNING BUFFER (1x):

For 10 L;	Tris base	30.3 g
	SDS powder	10 g
	Glycine	144.3 g

TRANSFER BUFFER (1x):

For 10 L;	Tris base	58.2 g
	Glycine	29.3 g

(Add methanol in final conc. 20% prior to use)

TBS (1x):

For 10 L;	Add	Tris base	60 g
		NaCl	87.69 g

to 9 L of dH_20 and adjust pH 8.3 (with concentrated HCl – if using 37% fumed HCl, it needs 25 ml--), then complete to 10 L with dH_2O

TBS-T (1x):

For 1 L TBS : add 2.5 ml Tween20

Blocking Buffer : 10 % milk in TBS-T

7.1.2 Reagent and buffers recipe for DNA agarose gel electrophoresis

TAE buffer (50X):

For 1 L;	Tris base	242 g
	(Dissolve in 800 ml dH_2O)	
	Add Acetic acid glacial	100 ml
	500 mM EDTA (pH 8.0)	57.1 ml
	Add dH_2O up to	1 L

7.2. NOVEL PROTEIN BINDERS TO OSR1 325 PEPTIDE

Table 7.1 List of identified protein from MS analysis of empty beads (100-150 kDa)

Sample1: Empty Beads (100-150 kDa)				
No	**Protein name**		**MW (KDa)**	**Protein Score**
1	K1C19_HUMAN	Keratin, type I cytoskeletal 19	44.1	144
2	K2C1_HUMAN	Keratin, type II cytoskeletal 1	66.2	123
3	K22E_HUMAN	Keratin, type II cytoskeletal 2 epidermal	65.7	114
4	ACTB_HUMAN	Actin, cytoplasmic 1	42.0	92
5	K2C1B_HUMAN	Keratin, type II cytoskeletal 1b	62.1	85
6	K1C18_HUMAN	Keratin, type I cytoskeletal 18	48.0	83
7	K1C10_HUMAN	Keratin, type I cytoskeletal 10	59.0	64
8	K2C6B_HUMAN	Keratin, type II cytoskeletal 6B	60.3	54
9	H2A2A_HUMAN	Histone H2A type 2-A	140.9	48
10	K1C9_HUMAN	Keratin, type I cytoskeletal 9	62.3	46
11	H2A1B_HUMAN	Histone H2A type 1-B/E	141.3	43
12	SHRM3_HUMAN	Protein Shroom3	218.3	40
13	FETUA_HUMAN	Alpha-2-HS-glycoprotein	n/a	39
14	ACTBM_HUMAN	Putative beta-actin-like protein 3	42.3	38
15	K1C15_HUMAN	Keratin, type I cytoskeletal 15	49.4	38
16	K1C14_HUMAN	Keratin, type I cytoskeletal 14	51.9	38
17	K2C6A_HUMAN	Keratin, type II cytoskeletal 6A	60.3	33
18	K1H1_HUMAN	Keratin, type I cuticular Ha1	48.6	31
19	K1H2_HUMAN	Keratin, type I cuticular Ha2	n/a	31
20	KRT38_HUMAN	Keratin, type I cuticular Ha8	n/a	31
21	K1C13_HUMAN	Keratin, type I cytoskeletal 13	49.9	30
22	IF4A1_HUMAN	Eukaryotic initiation factor 4A-I		<30
23	VIME_HUMAN	Vimentin		<30
24	KRT84_HUMAN	Keratin, type II cuticular Hb4		<30
25	K2C79_HUMAN	Keratin, type II cytoskeletal 79		<30
26	KRT85_HUMAN	Keratin, type II cuticular Hb5		<30
27	ALBU_HUMAN	Serum albumin		<30
28	MUC16_HUMAN	Mucin-16		<30
29	TNIP2_HUMAN	TNFAIP3-interacting protein 2		<30
30	ACTBL_HUMAN	Beta-actin-like protein 2		<30
31	S10A6_HUMAN	Protein S100-A6		<30
32	SIGL6_HUMAN	Sialic acid-binding Ig-like lectin 6		<30

Sample1: Empty Beads (100-150 kDa)				
No	**Protein name**		**MW (KDa)**	**Protein Score**
33	EF1A1_HUMAN	Elongation factor 1-alpha 1		<30

Table 7.2 List of identified protein from MS analysis of empty beads (63-75 kDa)

Sample 2: Empty Beads (63-75 kDa)				
No	**Protein name**		**MW (KDa)**	**Protein Score**
1	K2C1_HUMAN	Keratin, type II cytoskeletal 1	66.2	1319
2	K1C10_HUMAN	Keratin, type I cytoskeletal 10	59.0	720
3	K1C9_HUMAN	Keratin, type I cytoskeletal 9	62.3	568
4	K22E_HUMAN	Keratin, type II cytoskeletal 2 epidermal	65.7	472
5	K2C6C_HUMAN	Keratin, type II cytoskeletal 6C	60.3	383
6	K2C6B_HUMAN	Keratin, type II cytoskeletal 6B	60.3	359
7	K2C5_HUMAN	Keratin, type II cytoskeletal 5	62.6	322
8	HS71A_HUMAN	Heat shock 70 kDa protein 1A	70.3	258
9	K1C14_HUMAN	Keratin, type I cytoskeletal 14	51.9	239
10	HNRPM_HUMAN	Heterogeneous nuclear ribonucleoprotein M	77.7	217
11	K1C16_HUMAN	Keratin, type I cytoskeletal 16	51.6	176
12	HS71L_HUMAN	Heat shock 70 kDa protein 1-like	70.7	163
13	PABP1_HUMAN	Polyadenylate-binding protein 1	70.8	150
14	PABP4_HUMAN	Polyadenylate-binding protein 4	71.1	148
15	K2C1B_HUMAN	Keratin, type II cytoskeletal 1b	62.1	146
16	HSP76_HUMAN	Heat shock 70 kDa protein 6	71.4	142
17	K2C75_HUMAN	Keratin, type II cytoskeletal 75	59.8	136
18	K2C79_HUMAN	Keratin, type II cytoskeletal 79	59.1	128
19	K1C13_HUMAN	Keratin, type I cytoskeletal 13	49.9	127
20	K22O_HUMAN	Keratin, type II cytoskeletal 2 oral	66.4	114
21	K1C15_HUMAN	Keratin, type I cytoskeletal 15	49.4	104
22	XRCC6_HUMAN	X-ray repair cross-complementing protein 6	70.1	96
23	HSP7C_HUMAN	Heat shock cognate 71 kDa protein	71.1	95
24	K2C3_HUMAN	Keratin, type II cytoskeletal 3	64.5	83
25	K1C17_HUMAN	Keratin, type I cytoskeletal 17	48.4	81
26	HSP72_HUMAN	Heat shock-related 70 kDa protein 2	70.3	73
27	TRY1_HUMAN	Trypsin-1	27.1	71
28	TRY6_HUMAN	Putative trypsin-6	27.1	70
29	DDX17_HUMAN	Probable ATP-dependent RNA helicase DDX17	80.9	67
30	PLAK_HUMAN	Junction plakoglobin	82.4	67
31	LCN1_HUMAN	Lipocalin-1	19.4	61

Sample 2: Empty Beads (63-75 kDa)				
No	**Protein name**		**MW (KDa)**	**Protein Score**
32	CMC2_HUMAN	Calcium-binding mitochondrial carrier protein Aralar2	74.5	58
33	GRP78_HUMAN	78 kDa glucose-regulated protein	72.4	57
34	NDUS1_HUMAN	NADH-ubiquinone oxidoreductase 75 kDa subunit, mitochondrial	80.4	50
35	K2C4_HUMAN	Keratin, type II cytoskeletal 4	57.6	48
36	ALBU_HUMAN	Serum albumin	71.3	47
37	K1C24_HUMAN	Keratin, type I cytoskeletal 24	55.6	47
38	PIP_HUMAN	Prolactin-inducible protein	16.8	46
39	PAP1L_HUMAN	Polyadenylate-binding protein 1-like	69.0	44
40	K1C27_HUMAN	Keratin, type I cytoskeletal 27	50.4	44
41	FILA2_HUMAN	Filaggrin-2	249.3	43
42	EPN4_HUMAN	Clathrin interactor 1	68.3	43
43	DESP_HUMAN	Desmoplakin	334.0	43
44	CYTA_HUMAN	Cystatin-A	11.0	41
45	SHRM3_HUMAN	Protein Shroom3	218.3	40
46	KRT84_HUMAN	Keratin, type II cuticular Hb4	65.9	39
47	K2C8_HUMAN	Keratin, type II cytoskeletal 8	53.7	39
48	K1C19_HUMAN	Keratin, type I cytoskeletal 19	44.1	38
49	K2C74_HUMAN	Keratin, type II cytoskeletal 74	58.2	38
50	KAPCA_HUMAN	cAMP-dependent protein kinase catalytic subunit alpha	40.7	37
51	PABP3_HUMAN	Polyadenylate-binding protein 3	70.2	36
52	RS27A_HUMAN	Ubiquitin-40S ribosomal protein S27a	18.3	36
53	K2C78_HUMAN	Keratin, type II cytoskeletal 78	57.6	35
54	KRT82_HUMAN	Keratin, type II cuticular Hb2	58.0	35
55	K2C7_HUMAN	Keratin, type II cytoskeletal 7	51.4	35
56	KPRP_HUMAN	Keratinocyte proline-rich protein	67.2	34
57	CP135_HUMAN	Centrosomal protein of 135 kDa	133.9	33
58	KRT85_HUMAN	Keratin, type II cuticular Hb5	n/a	33
59	PKP1_HUMAN	Plakophilin-1	84.1	32
60	CCD40_HUMAN	Coiled-coil domain-containing protein 40	130.4	31
61	NEST_HUMAN	Nestin	n/a	31
62	KRT37_HUMAN	Keratin, type I cuticular Ha7	n/a	30
63	KT33B_HUMAN	Keratin, type I cuticular Ha3-II		<30
64	KRT38_HUMAN	Keratin, type I cuticular Ha8		<30

Sample 2: Empty Beads (63-75 kDa)				
No	**Protein name**		**MW (KDa)**	**Protein Score**
65	NFAC4_HUMAN	Nuclear factor of activated T-cells, cytoplasmic 4		<30
66	K2C71_HUMAN	Keratin, type II cytoskeletal 71		<30
67	GFAP_HUMAN	Glial fibrillary acidic protein		<30
68	VIME_HUMAN	Vimentin		<30
69	Z324A_HUMAN	Zinc finger protein 324A		<30
70	IF2B1_HUMAN	Insulin-like growth factor 2 mRNA-binding protein 1		<30
71	NFH_HUMAN	Neurofilament heavy polypeptide		<30
72	SCLT1_HUMAN	Sodium channel and clathrin linker 1		<30
73	CO1A1_HUMAN	Collagen alpha-1(I) chain		<30
74	K1C39_HUMAN	Keratin, type I cytoskeletal 39		<30
75	SPEF2_HUMAN	Sperm flagellar protein 2		<30
76	GPT2L_HUMAN	G patch domain-containing protein 2-like		<30
77	C1QT3_HUMAN	Complement C1q tumor necrosis factor-related protein 3		<30
78	TOM70_HUMAN	Mitochondrial import receptor subunit TOM70		<30
79	POGZ_HUMAN	Pogo transposable element with ZNF domain		<30
80	LACRT_HUMAN	Extracellular glycoprotein lacritin		<30
81	FXR1_HUMAN	Fragile X mental retardation syndrome-related protein 1		<30
82	AQP4_HUMAN	Aquaporin-4		<30
83	CCNB2_HUMAN	G2/mitotic-specific cyclin-B2		<30

Table 7.3 List of identified protein from MS analysis of RFQV peptide

Sample 3: RFQV				
No	**Protein name**		**MW (KDa)**	**Protein Score**
1	K2C1_HUMAN	Keratin, type II cytoskeletal 1	66.2	1585
2	GRP78_HUMAN	78 kDa glucose-regulated protein	72.4	1356
3	HS71A_HUMAN	Heat shock 70 kDa protein 1A	70.3	1135
4	K22E_HUMAN	Keratin, type II cytoskeletal 2 epidermal	65.7	1125
5	HSP7C_HUMAN	Heat shock cognate 71 kDa protein	71.1	1085
6	K1C9_HUMAN	Keratin, type I cytoskeletal 9	62.3	838
7	K1C10_HUMAN	Keratin, type I cytoskeletal 10	59.0	835
8	STK39_HUMAN	STE20/SPS1-related proline-alanine-rich protein kinase	60.0	600
9	HS71L_HUMAN	Heat shock 70 kDa protein 1-like	70.7	600
10	HSP72_HUMAN	Heat shock-related 70 kDa protein 2	70.3	534
11	HSP76_HUMAN	Heat shock 70 kDa protein 6	71.4	448
12	K2C5_HUMAN	Keratin, type II cytoskeletal 5	62.6	378
13	K2C6A_HUMAN	Keratin, type II cytoskeletal 6A	60.3	377
14	HNRPM_HUMAN	Heterogeneous nuclear ribonucleoprotein M	77.7	371
15	PABP1_HUMAN	Polyadenylate-binding protein 1	70.8	336
16	IF2B1_HUMAN	Insulin-like growth factor 2 mRNA-binding protein 1	63.8	330
17	K2C6B_HUMAN	Keratin, type II cytoskeletal 6B	60.3	300
18	CKAP4_HUMAN	Cytoskeleton-associated protein 4	66.1	266
19	K1C14_HUMAN	Keratin, type I cytoskeletal 14	51.9	266
20	PABP4_HUMAN	Polyadenylate-binding protein 4	71.1	202
21	XRCC6_HUMAN	X-ray repair cross-complementing protein 6	70.1	193
22	K2C1B_HUMAN	Keratin, type II cytoskeletal 1b	62.1	173
23	K1C16_HUMAN	Keratin, type I cytoskeletal 16	51.6	173
24	K2C79_HUMAN	Keratin, type II cytoskeletal 79	58.1	167
25	ALBU_HUMAN	Serum albumin	71.3	164
26	PABP3_HUMAN	Polyadenylate-binding protein 3	70.2	141
27	K2C75_HUMAN	Keratin, type II cytoskeletal 75	59.8	141
28	K22O_HUMAN	Keratin, type II cytoskeletal 2 oral	66.4	134
29	K1C13_HUMAN	Keratin, type I cytoskeletal 13	49.9	129
30	NUCL_HUMAN	Nucleolin	76.6	128

Sample 3: RFQV				
No	**Protein name**		**MW (KDa)**	**Protein Score**
31	RPN1_HUMAN	Dolichyl-diphosphooligosaccharide--protein glycosyltransferase subunit 1	68.6	118
32	G3BP1_HUMAN	Ras GTPase-activating protein-binding protein 1	52.1	118
33	GRP75_HUMAN	Stress-70 protein, mitochondrial	73.9	109
34	K2C3_HUMAN	Keratin, type II cytoskeletal 3	64.5	105
35	IF2B3_HUMAN	Insulin-like growth factor 2 mRNA-binding protein 3	64.0	102
36	K1C15_HUMAN	Keratin, type I cytoskeletal 15	49.4	98
37	PARP1_HUMAN	Poly [ADP-ribose] polymerase 1	113.8	93
38	OXSR1_HUMAN	Serine/threonine-protein kinase OSR1	58.3	89
39	K1C17_HUMAN	Keratin, type I cytoskeletal 17	48.4	86
40	K2C8_HUMAN	Keratin, type II cytoskeletal 8	53.7	81
41	AIFM1_HUMAN	Apoptosis-inducing factor 1, mitochondrial	67.1	81
42	PIP_HUMAN	Prolactin-inducible protein	16.8	76
43	ATD3B_HUMAN	ATPase family AAA domain-containing protein 3B	58.2	72
44	K2C74_HUMAN	Keratin, type II cytoskeletal 74	59.5	72
45	K2C73_HUMAN	Keratin, type II cytoskeletal 73	50.4	69
46	PABP5_HUMAN	Polyadenylate-binding protein 5	62.5	69
47	K1C27_HUMAN	Keratin, type I cytoskeletal 27	56.5	68
48	YTHD2_HUMAN	YTH domain-containing family protein 2	73.7	65
49	K2C72_HUMAN	Keratin, type II cytoskeletal 72	57.6	63
50	SDHA_HUMAN	Succinate dehydrogenase [ubiquinone] flavoprotein subunit, mitochondrial	249.3	61
51	K2C78_HUMAN	Keratin, type II cytoskeletal 78	57.6	60
52	FILA2_HUMAN	Filaggrin-2	76.1	58
53	K2C4_HUMAN	Keratin, type II cytoskeletal 4	51.4	58
54	SYRC_HUMAN	Arginine--tRNA ligase, cytoplasmic	44.1	58
55	K2C7_HUMAN	Keratin, type II cytoskeletal 7	66.2	58
56	K1C19_HUMAN	Keratin, type I cytoskeletal 19	55.6	57
57	IF2B2_HUMAN	Insulin-like growth factor 2 mRNA-binding protein 2	73.6	55
58	K1C24_HUMAN	Keratin, type I cytoskeletal 24	61.0	54
59	DDX3X_HUMAN	ATP-dependent RNA helicase DDX3X	46.6	53
60	NUPL1_HUMAN	Nucleoporin p58/p45	61.0	54

Sample 3: RFQV				
No	**Protein name**		**MW (KDa)**	**Protein Score**
61	ATD3C_HUMAN	ATPase family AAA domain-containing protein 3C	46.6	53
62	DDX17_HUMAN	Probable ATP-dependent RNA helicase DDX17	81.0	51
63	CMC2_HUMAN	Calcium-binding mitochondrial carrier protein Aralar2	74.5	51
64	LC1L1_HUMAN	Putative lipocalin 1-like protein 1	18.1	51
65	GFAP_HUMAN	Glial fibrillary acidic protein	49.9	51
66	DESP_HUMAN	Desmoplakin	334.0	49
67	KT33B_HUMAN	Keratin, type I cuticular Ha3-II	47.3	49
68	HNRPQ_HUMAN	Heterogeneous nuclear ribonucleoprotein Q	69.8	49
69	CMC1_HUMAN	Calcium-binding mitochondrial carrier protein Aralar1	75.1	47
70	K1C12_HUMAN	Keratin, type I cytoskeletal 12	53.6	46
71	KRT84_HUMAN	Keratin, type II cuticular Hb4	65.9	46
72	DCD_HUMAN	Dermcidin	11.4	46
73	DDX5_HUMAN	Probable ATP-dependent RNA helicase DDX5	69.6	43
74	PLAK_HUMAN	Junction plakoglobin	82.4	41
75	KPRP_HUMAN	Keratinocyte proline-rich protein	67.2	41
76	KRT85_HUMAN	Keratin, type II cuticular Hb5	n/a	41
77	VIME_HUMAN	Vimentin	n/a	41
78	EF1A1_HUMAN	Elongation factor 1-alpha 1	50.4	41
79	TBA1A_HUMAN	Tubulin alpha-1A chain	50.8	40
80	HNRPR_HUMAN	Heterogeneous nuclear ribonucleoprotein R	71.2	39
81	KRT81_HUMAN	Keratin, type II cuticular Hb1	56.8	38
82	KRT83_HUMAN	Keratin, type II cuticular Hb3	55.9	38
83	TRI32_HUMAN	E3 ubiquitin-protein ligase TRIM32	73.5	38
84	KIF2B_HUMAN	Kinesin-like protein KIF2B	n/a	36
85	TAF1L_HUMAN	Transcription initiation factor TFIID subunit 1-like	n/a	36
86	PALM3_HUMAN	Paralemmin-3	n/a	36
87	NHLC2_HUMAN	NHL repeat-containing protein 2	80.2	35
88	U17L1_HUMAN	Ubiquitin carboxyl-terminal hydrolase 17-like protein 1	60.7	35
89	NEST_HUMAN	Nestin	177.8	34
90	CROCC_HUMAN	Rootletin	228.8	34

Sample 3: RFQV				
No	**Protein name**		**MW (KDa)**	**Protein Score**
91	RM47_HUMAN	39S ribosomal protein L47, mitochondrial	29.6	34
92	CO9_HUMAN	Complement component C9	64.6	34
93	SHRM3_HUMAN	Protein Shroom3	218.3	33
94	PSPC1_HUMAN	Paraspeckle component 1	58.8	32
95	TRY1_HUMAN	Trypsin-1	27.1	32
96	K2C80_HUMAN	Keratin, type II cytoskeletal 80	51.0	31
97	CE350_HUMAN	Centrosome-associated protein 350	58.0	30
98	KRT82_HUMAN	Keratin, type II cuticular Hb2	165.3	30
99	RSF1_HUMAN	Remodeling and spacing factor 1	n/a	30
100	ABL1_HUMAN	Tyrosine-protein kinase ABL1	96.3	30
101	ABCF1_HUMAN	ATP-binding cassette sub-family F member 1	35.4	30
102	PTF1A_HUMAN	Pancreas transcription factor 1 subunit alpha	61.1	30
103	TCPG_HUMAN	T-complex protein 1 subunit gamma		<30
104	CNTP2_HUMAN	Contactin-associated protein-like 2		<30
105	LZTR1_HUMAN	Leucine-zipper-like transcriptional regulator 1		<30
106	KI21B_HUMAN	Kinesin-like protein KIF21B		<30
107	ATPB_HUMAN	ATP synthase subunit beta, mitochondrial		<30
108	ARNT_HUMAN	Aryl hydrocarbon receptor nuclear translocator		<30
109	ARNT2_HUMAN	Aryl hydrocarbon receptor nuclear translocator 2		<30
110	CH60_HUMAN	60 kDa heat shock protein, mitochondrial		<30
111	ZMY11_HUMAN	Zinc finger MYND domain-containing protein 11		<30
112	AL2SB_HUMAN	Amyotrophic lateral sclerosis 2 chromosomal region candidate gene 12 protein		<30
113	TRHY_HUMAN	Trichohyalin		<30
114	OXDA_HUMAN	D-amino-acid oxidase		<30
115	DOCK5_HUMAN	Dedicator of cytokinesis protein 5		<30
116	ANXA2_HUMAN	Annexin A2		<30
117	DSG1_HUMAN	Desmoglein-1		<30
118	NFH_HUMAN	Neurofilament heavy polypeptide		<30

Sample 3: RFQV				
No	**Protein name**		**MW (KDa)**	**Protein Score**
119	LR74B_HUMAN	Leucine-rich repeat-containing protein 74B		<30
120	NUP88_HUMAN	Nuclear pore complex protein Nup88		<30
121	PICAL_HUMAN	Phosphatidylinositol-binding clathrin assembly protein		<30
122	ZNRF3_HUMAN	E3 ubiquitin-protein ligase ZNRF3		<30
123	CK091_HUMAN	Uncharacterized protein C11orf91		<30
124	METK2_HUMAN	S-adenosylmethionine synthase isoform type-2		<30
125	FUS_HUMAN	RNA-binding protein FUS		<30
126	OSMR_HUMAN	Oncostatin-M-specific receptor subunit beta		<30
127	EPN4_HUMAN	Clathrin interactor 1		<30
128	MVD1_HUMAN	Diphosphomevalonate decarboxylase		<30
129	NAL13_HUMAN	NACHT, LRR and PYD domains-containing protein 13		<30
130	GCN1L_HUMAN	Translational activator GCN1		<30
131	CP135_HUMAN	Centrosomal protein of 135 kDa		<30
132	WDR87_HUMAN	WD repeat-containing protein 87		<30
133	ZA2G_HUMAN	Zinc-alpha-2-glycoprotein		<30
134	GIN1_HUMAN	Gypsy retrotransposon integrase-like protein 1		<30
135	SYK_HUMAN	Lysine--tRNA ligase		<30
136	FA47B_HUMAN	Protein FAM47B		<30
137	ABCE1_HUMAN	ATP-binding cassette sub-family E member 1		<30
138	KANK2_HUMAN	KN motif and ankyrin repeat domain-containing protein 2		<30
139	ITA7_HUMAN	Integrin alpha-7		<30
140	RHG36_HUMAN	Rho GTPase-activating protein 36		<30
141	H2B1D_HUMAN	Histone H2B type 1-D		<30
142	H2B1A_HUMAN	Histone H2B type 1-A		<30
143	FRPD1_HUMAN	FERM and PDZ domain-containing protein 1		<30
144	TAF4_HUMAN	Transcription initiation factor TFIID subunit 4		<30
145	CPXM2_HUMAN	Inactive carboxypeptidase-like protein X2		<30
146	PAR14_HUMAN	Poly [ADP-ribose] polymerase 14		<30
147	ACOC_HUMAN	Cytoplasmic aconitate hydratase		<30

Sample 3: RFQV				
No	**Protein name**		**MW (KDa)**	**Protein Score**
148	TDR12_HUMAN	Putative ATP-dependent RNA helicase TDRD12		<30

Table 7.4 List of identified protein from MS analysis of OSR1 pS325 peptide

Sample 4: OSR1 pS325				
No	**Protein name**		**MW (KDa)**	**Protein Score**
1	K2C1_HUMAN	Keratin, type II cytoskeletal 1	66.2	123
2	HS71A_HUMAN	Heat shock 70 kDa protein 1A	70.3	115
3	HSP76_HUMAN	Heat shock 70 kDa protein 6	71.4	115
4	K1C19_HUMAN	Keratin, type I cytoskeletal 19	44.1	99
5	ACTB_HUMAN	Actin, cytoplasmic 1	42.0	81
6	K1C10_HUMAN	Keratin, type I cytoskeletal 10	59.0	53
7	HSP7C_HUMAN	Heat shock cognate 71 kDa protein	71.1	44
8	K2C8_HUMAN	Keratin, type II cytoskeletal 8	53.7	44
9	K2C4_HUMAN	Keratin, type II cytoskeletal 4	57.6	44
10	K2C6B_HUMAN	Keratin, type II cytoskeletal 6B	62.1	42
11	K2C1B_HUMAN	Keratin, type II cytoskeletal 1b	48.0	42
12	K1C18_HUMAN	Keratin, type I cytoskeletal 18	218.3	39
13	SHRM3_HUMAN	Protein Shroom3	62.3	38
14	K1C9_HUMAN	Keratin, type I cytoskeletal 9	14.1	36
15	H2A2A_HUMAN	Histone H2A type 2-A	42.3	32
16	ACTBL_HUMAN	Beta-actin-like protein 2	71.3	30
17	ACTBM_HUMAN	Putative beta-actin-like protein 3		<30
18	ALBU_HUMAN	Serum albumin		<30
19	K1C28_HUMAN	Keratin, type I cytoskeletal 28		<30
20	K1C24_HUMAN	Keratin, type I cytoskeletal 24		<30
21	KRT37_HUMAN	Keratin, type I cuticular Ha7		<30
22	GLYL3_HUMAN	Glycine N-acyltransferase-like protein 3		<30
23	RHG28_HUMAN	Rho GTPase-activating protein 28		<30
24	K22E_HUMAN	Keratin, type II cytoskeletal 2 epidermal		<30
25	ASAP2_HUMAN	Arf-GAP with SH3 domain, ANK repeat and PH domain-containing protein 2		<30
26	OPRM_HUMAN	Mu-type opioid receptor		<30
27	EF1A1_HUMAN	Elongation factor 1-alpha 1		<30

Table 7.5 List of identified protein from MS analysis of OSR1 S325 peptide

Sample 5: OSR1 S325				
No	**Protein name**		**MW (KDa)**	**Protein Score**
1	K2C1_HUMAN	Keratin, type II cytoskeletal 1	66.2	1697
2	NUCL_HUMAN	Nucleolin	76.6	1047
3	K1C9_HUMAN	Keratin, type I cytoskeletal 9	62.3	1028
4	SP16H_HUMAN	FACT complex subunit SPT16	120.4	1020
5	K22E_HUMAN	Keratin, type II cytoskeletal 2 epidermal	65.7	698
6	K1C10_HUMAN	Keratin, type I cytoskeletal 10	59.0	685
7	DHX9_HUMAN	ATP-dependent RNA helicase A	142.2	621
8	ABCF1_HUMAN	ATP-binding cassette sub-family F member 1	96.3	516
9	EIFCL_HUMAN	Eukaryotic translation initiation factor 3 subunit C-like protein	106.1	505
10	DESP_HUMAN	Desmoplakin	334.0	484
11	K2C5_HUMAN	Keratin, type II cytoskeletal 5	62.6	483
12	PARP1_HUMAN	Poly [ADP-ribose] polymerase 1	113.8	479
13	SYIC_HUMAN	Isoleucine--tRNA ligase, cytoplasmic	145.7	450
14	HNRPU_HUMAN	Heterogeneous nuclear ribonucleoprotein U	91.3	441
15	SF3B3_HUMAN	Splicing factor 3B subunit 3	136.6	418
16	MOV10_HUMAN	Putative helicase MOV-10	114.5	373
17	SYLC_HUMAN	Leucine--tRNA ligase, cytoplasmic	135.6	339
18	RTF1_HUMAN	RNA polymerase-associated protein RTF1 homolog	80.5	328
19	U5S1_HUMAN	116 kDa U5 small nuclear ribonucleoprotein component	110.3	314
20	SPT5H_HUMAN	Transcription elongation factor SPT5	121.3	312
21	PLAK_HUMAN	Junction plakoglobin	82.4	305
22	K1C14_HUMAN	Keratin, type I cytoskeletal 14	51.8	303
23	CD11B_HUMAN	Cyclin-dependent kinase 11B	92.8	287
24	K2C6B_HUMAN	Keratin, type II cytoskeletal 6B	60.3	281
25	SFPQ_HUMAN	Splicing factor, proline- and glutamine-rich	76.2	281
26	NOP2_HUMAN	Probable 28S rRNA (cytosine(4447)-C(5))-methyltransferase	89.6	279
27	K2C1B_HUMAN	Keratin, type II cytoskeletal 1b	62.1	263
28	DDB1_HUMAN	DNA damage-binding protein 1	128.1	261
29	AT2A2_HUMAN	Sarcoplasmic/endoplasmic reticulum calcium ATPase 2	116.3	260
30	SF3B2_HUMAN	Splicing factor 3B subunit 2	100.3	250
31	K2C6C_HUMAN	Keratin, type II cytoskeletal 6C	60.3	235

Sample 5: OSR1 S325				
No	**Protein name**		**MW (KDa)**	**Protein Score**
32	CAPR1_HUMAN	Caprin-1	78.5	233
33	DHX30_HUMAN	Putative ATP-dependent RNA helicase DHX30	134.9	224
34	MBB1A_HUMAN	Myb-binding protein 1A	149.7	224
35	SMC2_HUMAN	Structural maintenance of chromosomes protein 2	136.1	210
36	K1C16_HUMAN	Keratin, type I cytoskeletal 16	51.6	207
37	COPA_HUMAN	Coatomer subunit alpha	139.8	203
38	DDX23_HUMAN	Probable ATP-dependent RNA helicase DDX23	95.9	198
39	SYMC_HUMAN	Methionine--tRNA ligase, cytoplasmic	102.2	192
40	SNUT1_HUMAN	U4/U6.U5 tri-snRNP-associated protein 1	90.4	191
41	CALL5_HUMAN	Calmodulin-like protein 5	158.8	189
42	SF3B1_HUMAN	Splicing factor 3B subunit 1	146.5	183
43	LEO1_HUMAN	RNA polymerase-associated protein LEO1	75.5	176
44	TIF1B_HUMAN	Transcription intermediary factor 1-beta	90.3	176
45	K1C17_HUMAN	Keratin, type I cytoskeletal 17	48.4	176
46	HNRL1_HUMAN	Heterogeneous nuclear ribonucleoprotein U-like protein 1	96.2	175
47	VIGLN_HUMAN	Vigilin	142.0	174
48	HTSF1_HUMAN	HIV Tat-specific factor 1	86.4	172
49	PRP6_HUMAN	Pre-mRNA-processing factor 6	107.7	169
50	EIF3A_HUMAN	Eukaryotic translation initiation factor 3 subunit A	166.9	166
51	CAND1_HUMAN	Cullin-associated NEDD8-dissociated protein 1	138.0	162
52	CKAP5_HUMAN	Cytoskeleton-associated protein 5	227.1	162
53	SART3_HUMAN	Squamous cell carcinoma antigen recognized by T-cells 3	110.7	161
54	SRPK1_HUMAN	SRSF protein kinase 1	75.0	157
55	ARHG2_HUMAN	Rho guanine nucleotide exchange factor 2	112.4	155
56	HDGR2_HUMAN	Hepatoma-derived growth factor-related protein 2	74.3	153
57	SYEP_HUMAN	Bifunctional glutamate/proline--tRNA ligase	172	148
58	BRD2_HUMAN	Bromodomain-containing protein 2	88.3	146
59	HNRL2_HUMAN	Heterogeneous nuclear ribonucleoprotein U-like protein 2	85.6	144
60	AP3B1_HUMAN	AP-3 complex subunit beta-1	121.8	143
61	K2C78_HUMAN	Keratin, type II cytoskeletal 78	57.6	142
62	DHX29_HUMAN	ATP-dependent RNA helicase DHX29	156.2	141

Sample 5: OSR1 S325				
No	**Protein name**		**MW (KDa)**	**Protein Score**
63	ILF3_HUMAN	Interleukin enhancer-binding factor 3	95.7	138
64	IWS1_HUMAN	Protein IWS1 homolog	92.0	137
65	F120A_HUMAN	Constitutive coactivator of PPAR-gamma-like protein 1	123.0	136
66	NOLC1_HUMAN	Nucleolar and coiled-body phosphoprotein 1	73.6	135
67	K2C75_HUMAN	Keratin, type II cytoskeletal 75	59.8	134
68	TCOF_HUMAN	Treacle protein	152.2	134
69	SPB1_HUMAN	pre-rRNA processing protein FTSJ3	96.9	134
70	AT2A1_HUMAN	Sarcoplasmic/endoplasmic reticulum calcium ATPase 1	111.5	133
71	CTR9_HUMAN	RNA polymerase-associated protein CTR9 homolog	134.3	132
72	EIF3B_HUMAN	Eukaryotic translation initiation factor 3 subunit B	92.8	132
73	SK2L2_HUMAN	Superkiller viralicidic activity 2-like 2	118.8	128
74	COPB2_HUMAN	Coatomer subunit beta'	103.3	127
75	RAD50_HUMAN	DNA repair protein RAD50	154.8	127
76	UBP10_HUMAN	Ubiquitin carboxyl-terminal hydrolase 10	87.7	126
77	YTDC2_HUMAN	Probable ATP-dependent RNA helicase YTHDC2	161.6	125
78	K2C79_HUMAN	Keratin, type II cytoskeletal 79	58.1	124
79	CDC5L_HUMAN	Cell division cycle 5-like protein	92.4	121
80	K2C8_HUMAN	Keratin, type II cytoskeletal 8	53.7	120
81	K1C15_HUMAN	Keratin, type I cytoskeletal 15	49.4	118
82	CUL4B_HUMAN	Cullin-4B	104.5	116
83	NOG2_HUMAN	Nucleolar GTP-binding protein 2	83.8	115
84	EXOSX_HUMAN	Exosome component 10	101.6	111
85	SMC1A_HUMAN	Structural maintenance of chromosomes protein 1A	143.8	110
86	OAS3_HUMAN	2'-5'-oligoadenylate synthase 3	122.9	109
87	K22O_HUMAN	Keratin, type II cytoskeletal 2 oral	66.4	109
88	K1C13_HUMAN	Keratin, type I cytoskeletal 13	49.9	108
89	AT2A3_HUMAN	Sarcoplasmic/endoplasmic reticulum calcium ATPase 3	115.4	108
90	WASH7_HUMAN	WASH complex subunit 7	137.3	104
91	CCAR2_HUMAN	Cell cycle and apoptosis regulator protein 2	103.5	101
92	CYTA_HUMAN	Cystatin-A	110	101
93	SRPK2_HUMAN	SRSF protein kinase 2	78.2	101

Sample 5: OSR1 S325				
No	**Protein name**		**MW (KDa)**	**Protein Score**
94	MCM3_HUMAN	DNA replication licensing factor MCM3	91.5	100
95	NSUN2_HUMAN	tRNA (cytosine(34)-C(5))-methyltransferase	87.2	99
96	EMAL4_HUMAN	Echinoderm microtubule-associated protein-like 4	109.9	98
97	K2C7_HUMAN	Keratin, type II cytoskeletal 7	51.4	98
98	DHX57_HUMAN	Putative ATP-dependent RNA helicase DHX57	157.1	98
99	ALBU_HUMAN	Serum albumin	71.3	97
100	K2C4_HUMAN	Keratin, type II cytoskeletal 4	57.6	96
101	FLII_HUMAN	Protein flightless-1 homolog	146.1	96
102	KIF23_HUMAN	Kinesin-like protein KIF23	111.0	95
103	DSG1_HUMAN	Desmoglein-1	114.7	93
104	SRRT_HUMAN	Serrate RNA effector molecule homolog	101.1	90
105	RENT1_HUMAN	Regulator of nonsense transcripts 1	125.6	88
106	NEMF_HUMAN	Nuclear export mediator factor NEMF	123.3	86
107	K2C74_HUMAN	Keratin, type II cytoskeletal 74	58.2	84
108	K2C73_HUMAN	Keratin, type II cytoskeletal 73	59.5	84
109	LARP1_HUMAN	La-related protein 1	123.8	83
110	CTDP1_HUMAN	RNA polymerase II subunit A C-terminal domain phosphatase	105.3	82
111	KDM1A_HUMAN	Lysine-specific histone demethylase 1A	93.4	79
112	FILA2_HUMAN	Filaggrin-2	249.3	77
113	STRUM_HUMAN	WASH complex subunit strumpellin	135.1	72
114	RFC1_HUMAN	Replication factor C subunit 1	128.7	72
115	BOP1_HUMAN	Ribosome biogenesis protein BOP1	84.3	69
116	DDX24_HUMAN	ATP-dependent RNA helicase DDX24	96.9	69
117	CBPC1_HUMAN	Cytosolic carboxypeptidase 1	139.8	68
118	MA7D1_HUMAN	MAP7 domain-containing protein 1	93.2	68
119	PNISR_HUMAN	Arginine/serine-rich protein PNISR	92.5	67
120	RBM27_HUMAN	RNA-binding protein 27	119.1	67
121	K2C3_HUMAN	Keratin, type II cytoskeletal 3	64.5	66
122	ENOA_HUMAN	Alpha-enolase	47.5	65
123	RS27A_HUMAN	Ubiquitin-40S ribosomal protein S27a	18.3	64
124	K1C27_HUMAN	Keratin, type I cytoskeletal 27	50.4	64
125	K1C25_HUMAN	Keratin, type I cytoskeletal 25	49.9	64
126	K1C28_HUMAN	Keratin, type I cytoskeletal 28	51.2	64

Sample 5: OSR1 S325				
No	**Protein name**		**MW (KDa)**	**Protein Score**
127	GEMI4_HUMAN	Gem-associated protein 4	121.7	63
128	EF1A1_HUMAN	Elongation factor 1-alpha 1	50.4	63
129	NADAP_HUMAN	Kanadaptin	89.5	62
130	DSC1_HUMAN	Desmocollin-1	101.4	61
131	GFAP_HUMAN	Glial fibrillary acidic protein	49.9	61
132	UBP2L_HUMAN	Ubiquitin-associated protein 2-like	114.6	60
133	AFF4_HUMAN	AF4/FMR2 family member 4	127.8	60
134	KRT82_HUMAN	Keratin, type II cuticular Hb2	58.0	60
135	K1C24_HUMAN	Keratin, type I cytoskeletal 24	55.6	59
136	RBM28_HUMAN	RNA-binding protein 28	86.2	58
137	SRRM2_HUMAN	Serine/arginine repetitive matrix protein 2	300.2	54
138	HERC5_HUMAN	E3 ISG15--protein ligase HERC5	118.2	54
139	K2C80_HUMAN	Keratin, type II cytoskeletal 80	51.0	53
140	KIF1B_HUMAN	Kinesin-like protein KIF1B	205.8	53
141	KIF1C_HUMAN	Kinesin-like protein KIF1C	123.7	53
142	KIF1A_HUMAN	Kinesin-like protein KIF1A	192.5	53
143	KI13B_HUMAN	Kinesin-like protein KIF13B	204.0	53
144	RBP2_HUMAN	E3 SUMO-protein ligase RanBP2	362.4	53
145	RGPD5_HUMAN	RANBP2-like and GRIP domain-containing protein 5/6	200.1	53
146	RGPD3_HUMAN	RanBP2-like and GRIP domain-containing protein 3	198.7	53
147	RGPD4_HUMAN	RanBP2-like and GRIP domain-containing protein 4	198.6	53
148	RGPD2_HUMAN	RANBP2-like and GRIP domain-containing protein 2	198.7	53
149	TOP1_HUMAN	DNA topoisomerase 1	91.1	53
150	SYVC_HUMAN	Valine--tRNA ligase	141.6	52
151	WDR3_HUMAN	WD repeat-containing protein 3	107.1	52
152	RL14_HUMAN	60S ribosomal protein L14	23.5	52
153	CLASR_HUMAN	CLK4-associating serine/arginine rich protein	77.3	51
154	ENOG_HUMAN	Gamma-enolase	n/a	50
155	RRP12_HUMAN	RRP12-like protein	145.0	49
156	H13_HUMAN	Histone H1.3	22.3	49
157	H12_HUMAN	Histone H1.2	21.3	49
158	H14_HUMAN	Histone H1.4	21.8	49

Sample 5: OSR1 S325				
No	**Protein name**		**MW (KDa)**	**Protein Score**
159	RPOM_HUMAN	DNA-directed RNA polymerase, mitochondrial	140.3	49
160	TSR1_HUMAN	Pre-rRNA-processing protein TSR1 homolog	92.1	49
161	DDX20_HUMAN	Probable ATP-dependent RNA helicase DDX20	93.0	47
162	PWP2_HUMAN	Periodic tryptophan protein 2 homolog	103.4	47
163	CUL4A_HUMAN	Cullin-4A	88.1	46
164	ZFR_HUMAN	Zinc finger RNA-binding protein	118.1	45
165	K1C26_HUMAN	Keratin, type I cytoskeletal 26	52.6	45
166	K1C12_HUMAN	Keratin, type I cytoskeletal 12	53.6	45
167	PRDX1_HUMAN	Peroxiredoxin-1	22.3	45
168	RL29_HUMAN	60S ribosomal protein L29	17.8	44
169	ANR28_HUMAN	Serine/threonine-protein phosphatase 6 regulatory ankyrin repeat subunit A	114.6	44
170	NCKP1_HUMAN	Nck-associated protein 1	130.0	44
171	BAG6_HUMAN	Large proline-rich protein BAG6	119.8	43
172	G3P_HUMAN	Glyceraldehyde-3-phosphate dehydrogenase	36.2	43
173	MA7D3_HUMAN	MAP7 domain-containing protein 3	98.7	42
174	POP1_HUMAN	Ribonucleases P/MRP protein subunit POP1	116.3	41
175	TOP2A_HUMAN	DNA topoisomerase 2-alpha	175.0	41
176	POTEE_HUMAN	POTE ankyrin domain family member E	122.9	40
177	ACTB_HUMAN	Actin, cytoplasmic 1	42.0	40
178	CC112_HUMAN	Coiled-coil domain-containing protein 112	53.6	39
179	SHRM3_HUMAN	Protein Shroom3	218.3	39
180	MSH2_HUMAN	DNA mismatch repair protein Msh2	105.4	39
181	NAT10_HUMAN	N-acetyltransferase 10	116.6	39
182	FHAD1_HUMAN	Forkhead-associated domain-containing protein 1	162.7	38
183	PDS5A_HUMAN	Sister chromatid cohesion protein PDS5 homolog A	152.3	38
184	PUM1_HUMAN	Pumilio homolog 1	127.1	38
185	POF1B_HUMAN	Protein POF1B	68.9	38
186	WDR6_HUMAN	WD repeat-containing protein 6	123.6	38
187	NRDE2_HUMAN	Protein NRDE2 homolog	133.8	37
188	SCRN3_HUMAN	Secernin-3	n/a	37
189	CAH12_HUMAN	Carbonic anhydrase 12	n/a	37
190	PININ_HUMAN	Pinin	81.7	37

Sample 5: OSR1 S325				
No	**Protein name**		**MW (KDa)**	**Protein Score**
191	LAR4B_HUMAN	La-related protein 4B	80.9	37
192	MAP4_HUMAN	Microtubule-associated protein 4	121.4	37
193	AT131_HUMAN	Manganese-transporting ATPase 13A1	134.5	37
194	SPTA1_HUMAN	Spectrin alpha chain, erythrocytic 1	n/a	36
195	ATX2L_HUMAN	Ataxin-2-like protein	113.6	36
196	CLCN1_HUMAN	Chloride channel protein 1	109.6	36
197	NFH_HUMAN	Neurofilament heavy polypeptide	112.6	36
198	TF3C3_HUMAN	General transcription factor 3C polypeptide 3	102.0	36
199	DHX16_HUMAN	Putative pre-mRNA-splicing factor ATP-dependent RNA helicase DHX16	119.9	35
200	ELOA1_HUMAN	Transcription elongation factor B polypeptide 3	90.3	35
201	SYGP1_HUMAN	Ras/Rap GTPase-activating protein SynGAP	n/a	35
202	SND1_HUMAN	Staphylococcal nuclease domain-containing protein 1	102.6	35
203	DDX46_HUMAN	Probable ATP-dependent RNA helicase DDX46	117.8	35
204	LAR1B_HUMAN	La-related protein 1B	105.8	34
205	ZCH18_HUMAN	Zinc finger CCCH domain-containing protein 18	106.5	34
206	SMC3_HUMAN	Structural maintenance of chromosomes protein 3	141.8	34
207	SORT_HUMAN	Sortilin	n/a	33
208	ANXA2_HUMAN	Annexin A2	118.5	33
209	MORC2_HUMAN	MORC family CW-type zinc finger protein 2	95.3	32
210	JKIP2_HUMAN	Janus kinase and microtubule-interacting protein 2	135.2	32
211	NOMO1_HUMAN	Nodal modulator 1	34.9	32
212	ARGI1_HUMAN	Arginase-1	n/a	32
213	NEST_HUMAN	Nestin	n/a	31
214	KI21B_HUMAN	Kinesin-like protein KIF21B	184.3	31
215	VIME_HUMAN	Vimentin	53.7	31
216	KRT81_HUMAN	Keratin, type II cuticular Hb1	n/a	31
217	CASC5_HUMAN	Protein CASC5	268.2	31
218	GEN_HUMAN	Flap endonuclease GEN homolog 1	n/a	31
219	MTP_HUMAN	Microsomal triglyceride transfer protein large subunit	n/a	31
220	KIF17_HUMAN	Kinesin-like protein KIF17	n/a	31
221	STIM2_HUMAN	Stromal interaction molecule 2	n/a	31

Sample 5: OSR1 S325				
No	**Protein name**		**MW (KDa)**	**Protein Score**
222	STIM1_HUMAN	Stromal interaction molecule 1	n/a	31
223	H2B1D_HUMAN	Histone H2B type 1-D	13.9	31
224	H2B3B_HUMAN	Histone H2B type 3-B	13.9	31
225	H2B1C_HUMAN	Histone H2B type 1-C/E/F/G/I	13.9	31
226	RAE1_HUMAN	Rab proteins geranylgeranyltransferase component A 1	n/a	31
227	CAC1A_HUMAN	Voltage-dependent P/Q-type calcium channel subunit alpha-1A	283.8	30
228	PP6R3_HUMAN	Serine/threonine-protein phosphatase 6 regulatory subunit 3	98.6	30
229	MYOME_HUMAN	Myomegalin	n/a	30
230	KPYM_HUMAN	Pyruvate kinase PKM	58.5	30
231	RM55_HUMAN	39S ribosomal protein L55, mitochondrial	15.1	30
232	RBPMS_HUMAN	RNA-binding protein with multiple splicing	n/a	30
233	NOP14_HUMAN	Nucleolar protein 14	98.3	30
234	DHX37_HUMAN	Probable ATP-dependent RNA helicase DHX37	130.5	30
235	ZBT11_HUMAN	Zinc finger and BTB domain-containing protein 11	121.4	30
236	PCID2_HUMAN	PCI domain-containing protein 2	n/a	30
237	PXDNL_HUMAN	Peroxidasin-like protein	166.2	30
238	RL7A_HUMAN	60S ribosomal protein L7a	30.1	30
239	CC113_HUMAN	Coiled-coil domain-containing protein 113	n/a	30
240	CHD9_HUMAN	Chromodomain-helicase-DNA-binding protein 9		<30
241	FA83C_HUMAN	Protein FAM83C		<30
242	CSPG2_HUMAN	Versican core protein		<30
243	SF3A1_HUMAN	Splicing factor 3A subunit 1		<30
244	MTOR_HUMAN	Serine/threonine-protein kinase mTOR		<30
245	USP9Y_HUMAN	Probable ubiquitin carboxyl-terminal hydrolase FAF-Y		<30
246	USP9X_HUMAN	Probable ubiquitin carboxyl-terminal hydrolase FAF-X		<30
247	PEPL_HUMAN	Periplakin		<30
248	RFIP4_HUMAN	Rab11 family-interacting protein 4		<30
249	SYNE2_HUMAN	Nesprin-2		<30
250	DPOLZ_HUMAN	DNA polymerase zeta catalytic subunit		<30
251	APH1B_HUMAN	Gamma-secretase subunit APH-1B		<30
252	PUF60_HUMAN	Poly(U)-binding-splicing factor PUF60		<30

Sample 5: OSR1 S325				
No	**Protein name**		**MW (KDa)**	**Protein Score**
253	CTNB1_HUMAN	Catenin beta-1		<30
254	RS30_HUMAN	40S ribosomal protein S30		<30
255	PUM2_HUMAN	Pumilio homolog 2		<30
256	CP135_HUMAN	Centrosomal protein of 135 kDa		<30
257	VKGC_HUMAN	Vitamin K-dependent gamma-carboxylase		<30
258	NPM_HUMAN	Nucleophosmin		<30
260	SFI1_HUMAN	Protein SFI1 homolog		<30
261	CCD25_HUMAN	Coiled-coil domain-containing protein 25		<30
262	ATPB_HUMAN	ATP synthase subunit beta, mitochondrial		<30
263	PABP1_HUMAN	Polyadenylate-binding protein 1		<30
264	PABP4_HUMAN	Polyadenylate-binding protein 4		<30
265	DHX36_HUMAN	ATP-dependent RNA helicase DHX36		<30
266	KCNH7_HUMAN	Potassium voltage-gated channel subfamily H member 7		<30
267	S10A3_HUMAN	Protein S100-A3		<30
268	SIN3A_HUMAN	Paired amphipathic helix protein Sin3a		<30
269	TOP1M_HUMAN	DNA topoisomerase I, mitochondrial		<30
270	KCNV2_HUMAN	Potassium voltage-gated channel subfamily V member 2		<30
271	DIAP2_HUMAN	Protein diaphanous homolog 2		<30
272	FSIP2_HUMAN	Fibrous sheath-interacting protein 2		<30
273	BCLF1_HUMAN	Bcl-2-associated transcription factor 1		<30
274	LIMS1_HUMAN	LIM and senescent cell antigen-like-containing domain protein 1		<30
275	BNC2_HUMAN	Zinc finger protein basonuclin-2		<30
276	DHX8_HUMAN	ATP-dependent RNA helicase DHX8		<30
277	C144A_HUMAN	Coiled-coil domain-containing protein 144A		<30
278	ADAM5_HUMAN	Putative disintegrin and metalloproteinase domain-containing protein 5		<30
279	KDM5D_HUMAN	Lysine-specific demethylase 5D		<30
280	RDH16_HUMAN	Retinol dehydrogenase 16		<30
281	PR40A_HUMAN	Pre-mRNA-processing factor 40 homolog A		<30
282	ETS1_HUMAN	Protein C-ets-1		<30
283	RL34_HUMAN	60S ribosomal protein L34		<30
284	KCA10_HUMAN	Potassium voltage-gated channel subfamily A member 10		<30

Sample 5: OSR1 S325				
No	**Protein name**		**MW (KDa)**	**Protein Score**
285	AP2B1_HUMAN	AP-2 complex subunit beta		<30
286	ZCCHV_HUMAN	Zinc finger CCCH-type antiviral protein 1		<30
287	CE350_HUMAN	Centrosome-associated protein 350		<30
288	ALS2_HUMAN	Alsin		<30
289	AR13A_HUMAN	ADP-ribosylation factor-like protein 13A		<30
290	EFCB5_HUMAN	EF-hand calcium-binding domain-containing protein 5		<30
291	PFKAM_HUMAN	ATP-dependent 6-phosphofructokinase, muscle type		<30
292	FADS2_HUMAN	Fatty acid desaturase 2		<30
293	MAGB5_HUMAN	Melanoma-associated antigen B5		<30
294	EF2_HUMAN	Elongation factor 2		<30
295	SYMPK_HUMAN	Symplekin		<30
296	KAISO_HUMAN	Transcriptional regulator Kaiso		<30
297	ANFY1_HUMAN	Rabankyrin-5		<30
298	COL12_HUMAN	Collectin-12		<30
299	CCD62_HUMAN	Coiled-coil domain-containing protein 62		<30
300	HGF_HUMAN	Hepatocyte growth factor		<30
301	K0825_HUMAN	Uncharacterized protein KIAA0825		<30
302	FMO2_HUMAN	Dimethylaniline monooxygenase [N-oxide-forming] 2		<30
303	TNI3K_HUMAN	Serine/threonine-protein kinase TNNI3K		<30
304	XPO2_HUMAN	Exportin-2		<30
305	COQ6_HUMAN	Ubiquinone biosynthesis monooxygenase COQ6, mitochondrial		<30
306	CU129_HUMAN	Putative uncharacterized protein encoded by LINC00479		<30
307	DNLI4_HUMAN	DNA ligase 4		<30
308	DUS2L_HUMAN	tRNA-dihydrouridine(20) synthase [NAD(P)+]-like		<30
309	TLN2_HUMAN	Talin-2		<30
310	GDF7_HUMAN	Growth/differentiation factor 7		<30
311	MOCS1_HUMAN	Molybdenum cofactor biosynthesis protein 1		<30
312	CAR11_HUMAN	Caspase recruitment domain-containing protein 11		<30
313	DLG5_HUMAN	Disks large homolog 5		<30
314	HORN_HUMAN	Hornerin		<30
315	NDUAA_HUMAN	NADH dehydrogenase [ubiquinone] 1 alpha subcomplex subunit 10, mitochondrial		<30

Sample 5: OSR1 S325				
No	**Protein name**		**MW (KDa)**	**Protein Score**
316	THIO_HUMAN	Thioredoxin		<30
317	HEAT6_HUMAN	HEAT repeat-containing protein 6		<30
318	KI13A_HUMAN	Kinesin-like protein KIF13A		<30

7.3. SPAK/OSR1 UBIQUITYLATION AND DEGRADATION UPON CRL4 INHIBITION

7.3.1. WDR3 and WDR6 KO by CRISPR

Figures of sgRNA primer pair in the WDR3/WDR6 locus and plasmid map harbouring the primer pairs are provided in the following pages.

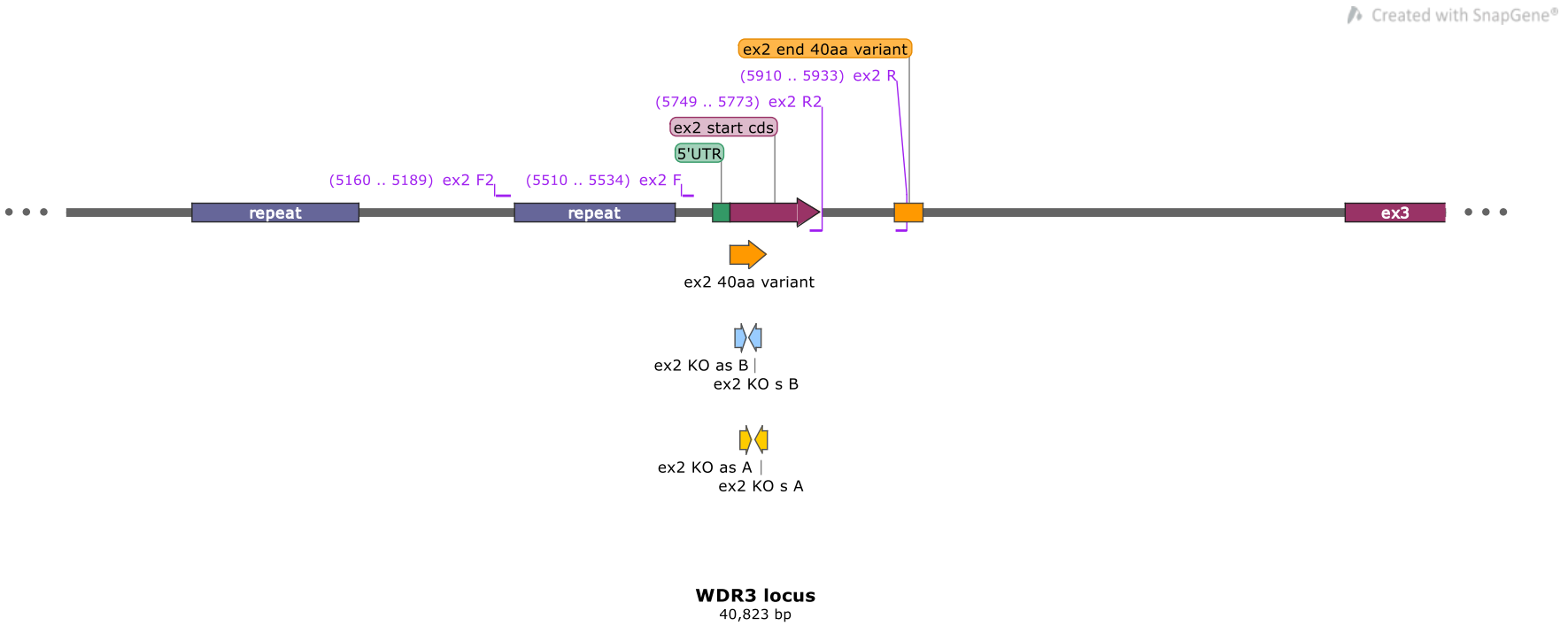

Figure 7.1. Map of WDR3 locus with sgRNA primer pairs for WDR3 knock out by Dual Nickase CRISPR

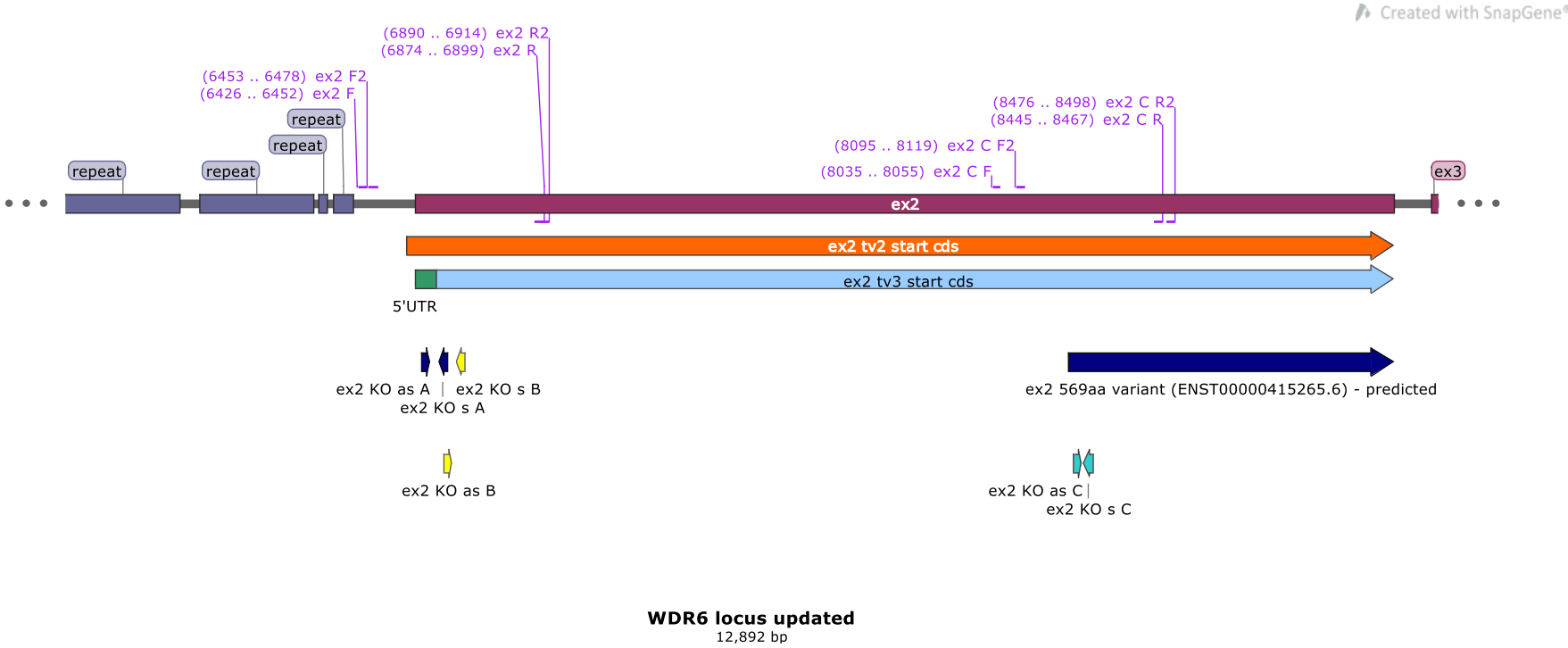

Figure 7.2. Map of WDR6 locus with sgRNA primer pairs for WDR6 knock out by Dual Nickase CRISPR

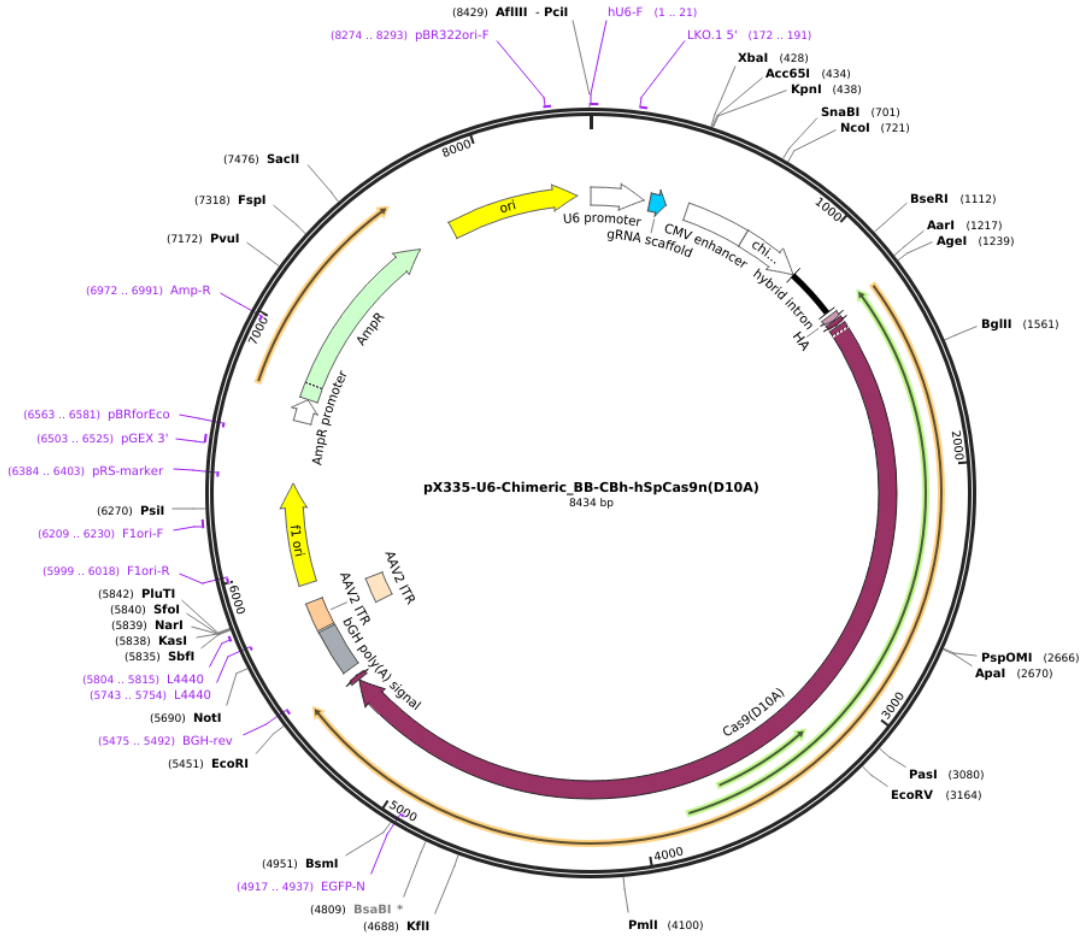

Figure 7.3. Plasmid map of pX335 as parent plasmid of pX335 WDR3 Antisense and pX335 WDR6 Antisense guide. The plasmids were used for WDR3 or WDR6 knockout by CRISPR Dual Nickase (provided by MRC-PPU University of Dundee). The plasmid contained Cas9 (D10A) was inserted by antisense guide primer generated from exon 2 of WDR3 or WDR6 locus.

Figure 7.4. Plasmid map of pBABE as parent plasmid of pBABED WDR3 Sense and pBABED WDR6 Sense guide. The plasmids were used for WDR3 or WDR6 knockout by CRISPR Dual Nickase (provided by MRC-PPU University of Dundee). The plasmid contained Puromycin resistance gene selection marker. Plasmid inserted by sense guide primer generated from exon 2 of WDR3 or WDR6 locus.

7.3.2. WDR3 and WDR6 knockdown by siRNA

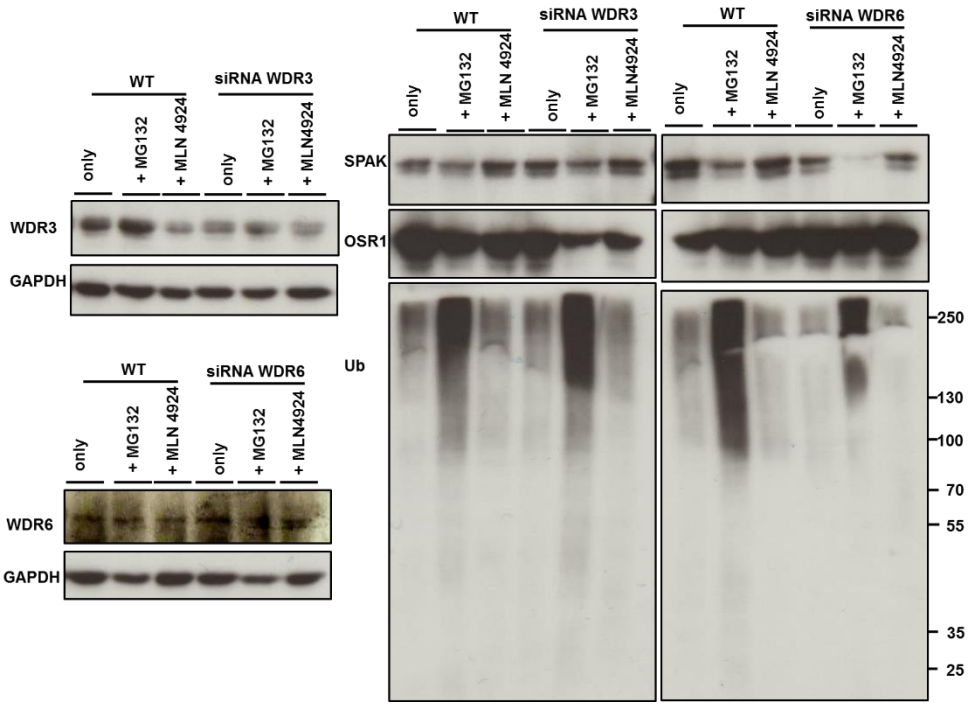

Figure 7.5. siRNA WDR3 and WDR6 did not alter the SPAK and OSR1 level. The cell was treated with 10 µM MG132 for 24 h and 1 µM of MLN4924 for 6 hours before the total protein lysate of both wildtype and siRNA WDR3 and WDR6 cell was used for immunoblotting using WDR3; WDR6; SPAK; OSR1 and ubiquitin antibody to confirm the DDB1 silencing from their protein level. GAPDH immunoblot was used as a loading control. There was an issue with WDR6 antibody sensitivity so the WDR6 knockdown could not be detected.

7.4. CRL4 COMPLEX SUBUNITS ROLE ON SPAK/OSR1 UBIQUITYLATION AND DEGRADATION

7.4.1. Immunoprecipitation of SPAK and OSR1 in U266 cells

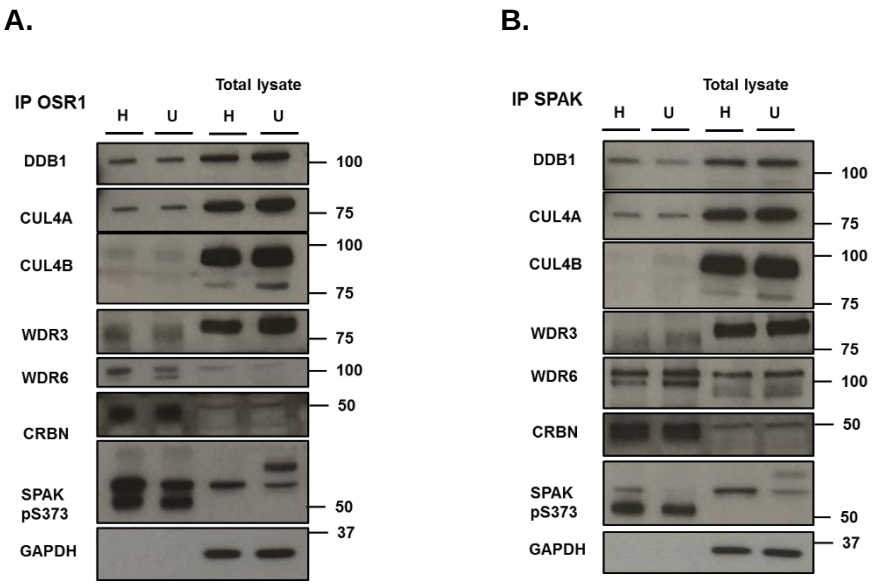

Figure 7.6. Immunoprecipitation of SPAK and OSR1 in U266 cells. Total protein lysate of U266 cell (3mg) on basal (U) or with hypotonic low Cl- stimulation (H) was incubated with Anti-OSR1 **(A)** or Anti-SPAK **(B)** conjugated beads overnight. The elute from washing step was prepared in SDS sample buffer and 0.1 portion precipitate was immunoblotted with all denoted antibodies. SPAK pS373 blot was used as a control for WNK-SPAK/OSR1 signalling activation. Total lysate of U266 cell was used as a control for basal expression of the protein.

7.4.2. Ubiquitin prediction site of OSR1 and SPAK

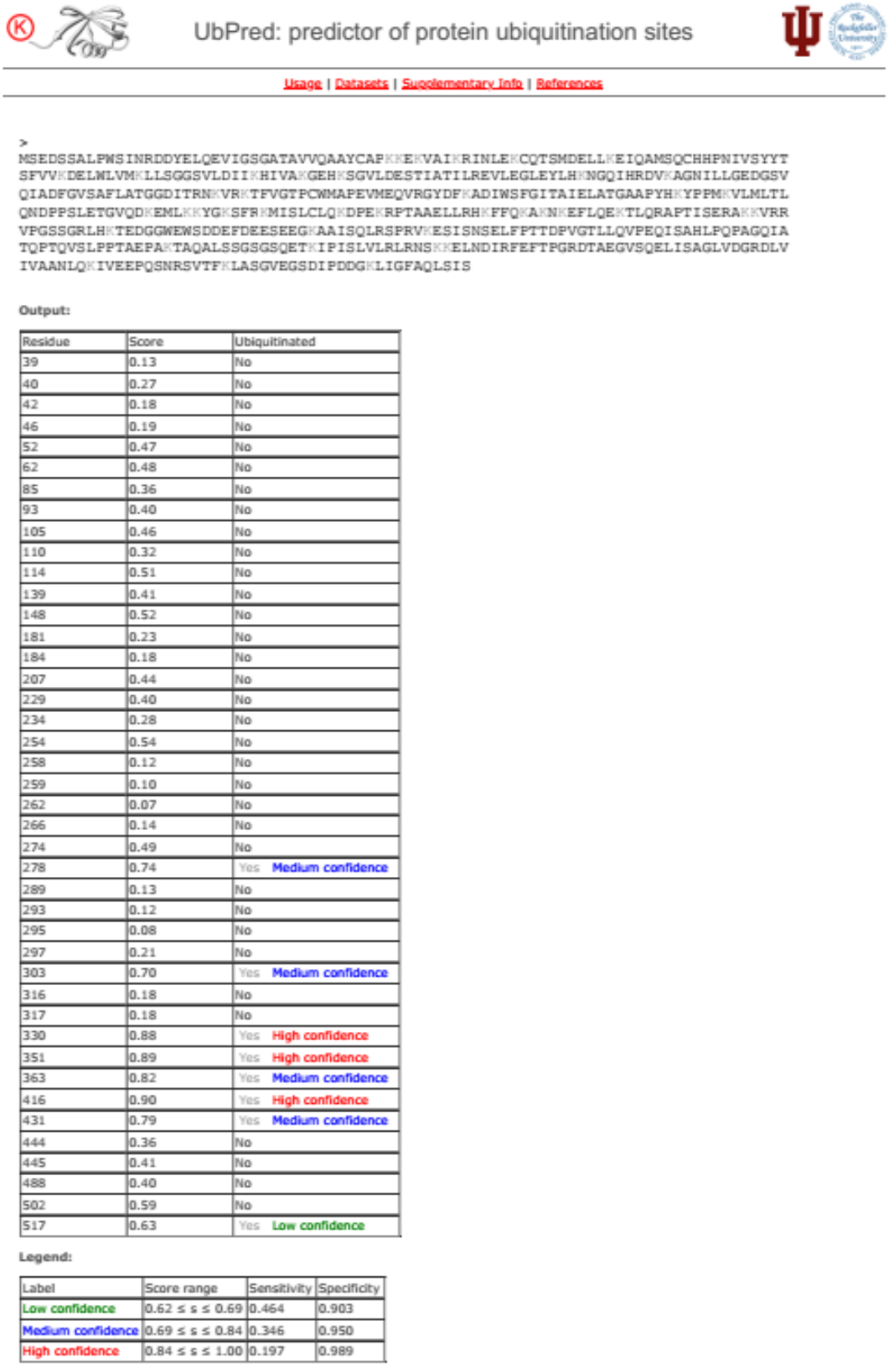

UbPred: predictor of protein ubiquitination sites

Usage | Datasets | Supplementary Info | References

>
MSEDSSALPWSINRDDYELQEVIGSGATAVVQAAYCAPKKEKVAIKRINLEKCQTSMDELLKEIQAMSQCHHPNIVSYYT
SFVVKDELWLVMKLLSGGSVLDIIKHIVAKGEHKSGVLDESTIATILREVLEGLEYLHKNGQIHRDVKAGNILLGEDGSV
QIADFGVSAFLATGGDITRNKVRKTFVGTPCWMAPEVMEQVRGYDFKADIWSFGITAIELATGAAPYHKYPPMKVLMLTL
QNDPPSLETGVQDKEMLKKYGKSFRKMISLCLQKDPEKRPTAAELLRHKFFQKAKNKEFLQEKTLQRAPTISERAKKVRR
VPGSSGRLHKTEDGGWEWSDDEFDEESEEGKAAISQLRSPRVKESISNSELFPTTDPVGTLLQVPEQISAHLPQPAGQIA
TQPTQVSLPPTAEPAKTAQALSSGSGSQETKIPISLVLRLRNSKKELNDIRFEFTPGRDTAEGVSQELISAGLVDGRDLV
IVAANLQKIVEEPQSNRSVTFKLASGVEGSDIPDDGKLIGFAQLSIS

Output:

Residue	Score	Ubiquitinated
39	0.13	No
40	0.27	No
42	0.18	No
46	0.19	No
52	0.47	No
62	0.48	No
85	0.36	No
93	0.40	No
105	0.46	No
110	0.32	No
114	0.51	No
139	0.41	No
148	0.52	No
181	0.23	No
184	0.18	No
207	0.44	No
229	0.40	No
234	0.28	No
254	0.54	No
258	0.12	No
259	0.10	No
262	0.07	No
266	0.14	No
274	0.49	No
278	0.74	Yes Medium confidence
289	0.13	No
293	0.12	No
295	0.08	No
297	0.21	No
303	0.70	Yes Medium confidence
316	0.18	No
317	0.18	No
330	0.88	Yes High confidence
351	0.89	Yes High confidence
363	0.82	Yes Medium confidence
416	0.90	Yes High confidence
431	0.79	Yes Medium confidence
444	0.36	No
445	0.41	No
488	0.40	No
502	0.59	No
517	0.63	Yes Low confidence

Legend:

Label	Score range	Sensitivity	Specificity
Low confidence	0.62 ≤ s ≤ 0.69	0.464	0.903
Medium confidence	0.69 ≤ s ≤ 0.84	0.346	0.950
High confidence	0.84 ≤ s ≤ 1.00	0.197	0.989

Figure 7.7. Ubiquitination prediction site of OSR1 retrieved from www.Ubpred.org

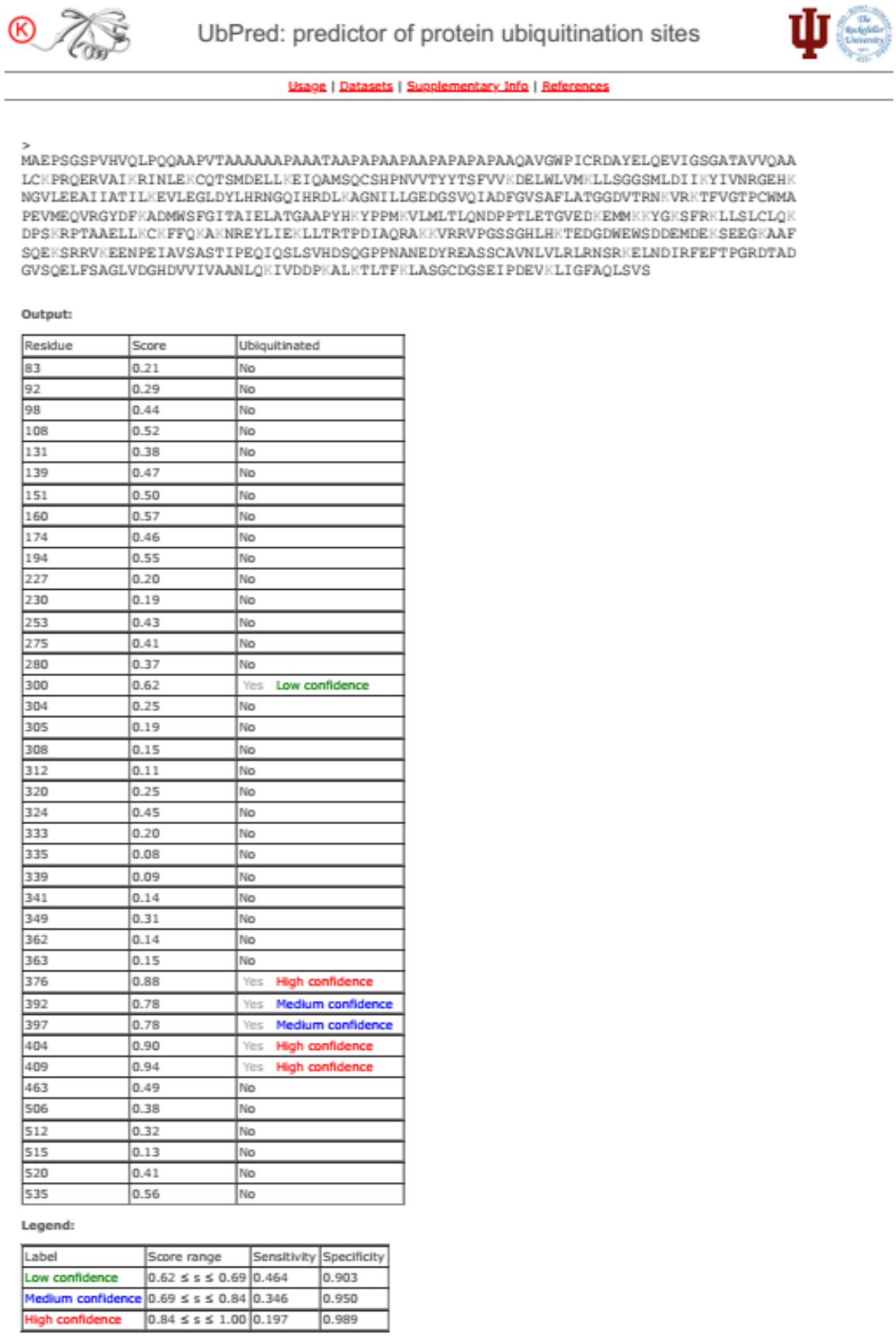

UbPred: predictor of protein ubiquitination sites

Usage | Datasets | Supplementary Info | References

>
MAEPSGSPVHVQLPQQAAPVTAAAAAAPAAATAAPAPAAPAAPAPAPAPAAQAVGWPICRDAYELQEVIGSGATAVVQAA
LCKPRQERVAIKRINLEKCQTSMDELLKEIQAMSQCSHPNVVTYYTSFVVKDELWLVMKLLSGGSMLDIIKYIVNRGEHK
NGVLEEAIIATILKEVLEGLDYLHRNGQIHRDLKAGNILLGEDGSVQIADFGVSAFLATGGDVTRNKVRKTFVGTPCWMA
PEVMEQVRGYDFKADMWSFGITAIELATGAAPYHKYPPMKVLMLTLQNDPPTLETGVEDKEMMKKYGKSFRKLLSLCLQK
DPSKRPTAAELLKCKFFQKAKNREYLIEKLLTRTPDIAQRAKKVRRVPGSSGHLHKTEDGDWEWSDDEMDEKSEEGKAAF
SQEKSRRVKEENPEIAVSASTIPEQIQSLSVHDSQGPPNANEDYREASSCAVNLVLRLRNSRKELNDIRFEFTPGRDTAD
GVSQELFSAGLVDGHDVVIVAANLQKIVDDPKALKTLTFKLASGCDGSEIPDEVKLIGFAQLSVS

Output:

Residue	Score	Ubiquitinated
83	0.21	No
92	0.29	No
98	0.44	No
108	0.52	No
131	0.38	No
139	0.47	No
151	0.50	No
160	0.57	No
174	0.46	No
194	0.55	No
227	0.20	No
230	0.19	No
253	0.43	No
275	0.41	No
280	0.37	No
300	0.62	Yes Low confidence
304	0.25	No
305	0.19	No
308	0.15	No
312	0.11	No
320	0.25	No
324	0.45	No
333	0.20	No
335	0.08	No
339	0.09	No
341	0.14	No
349	0.31	No
362	0.14	No
363	0.15	No
376	0.88	Yes High confidence
392	0.78	Yes Medium confidence
397	0.78	Yes Medium confidence
404	0.90	Yes High confidence
409	0.94	Yes High confidence
463	0.49	No
506	0.38	No
512	0.32	No
515	0.13	No
520	0.41	No
535	0.56	No

Legend:

Label	Score range	Sensitivity	Specificity
Low confidence	0.62 ≤ s ≤ 0.69	0.464	0.903
Medium confidence	0.69 ≤ s ≤ 0.84	0.346	0.950
High confidence	0.84 ≤ s ≤ 1.00	0.197	0.989

Figure 7.8. Ubiquitination prediction site of SPAK retrieved from www.Ubpred.org

7.4.3. Phosphorylation prediction sites in CRL4 subunits

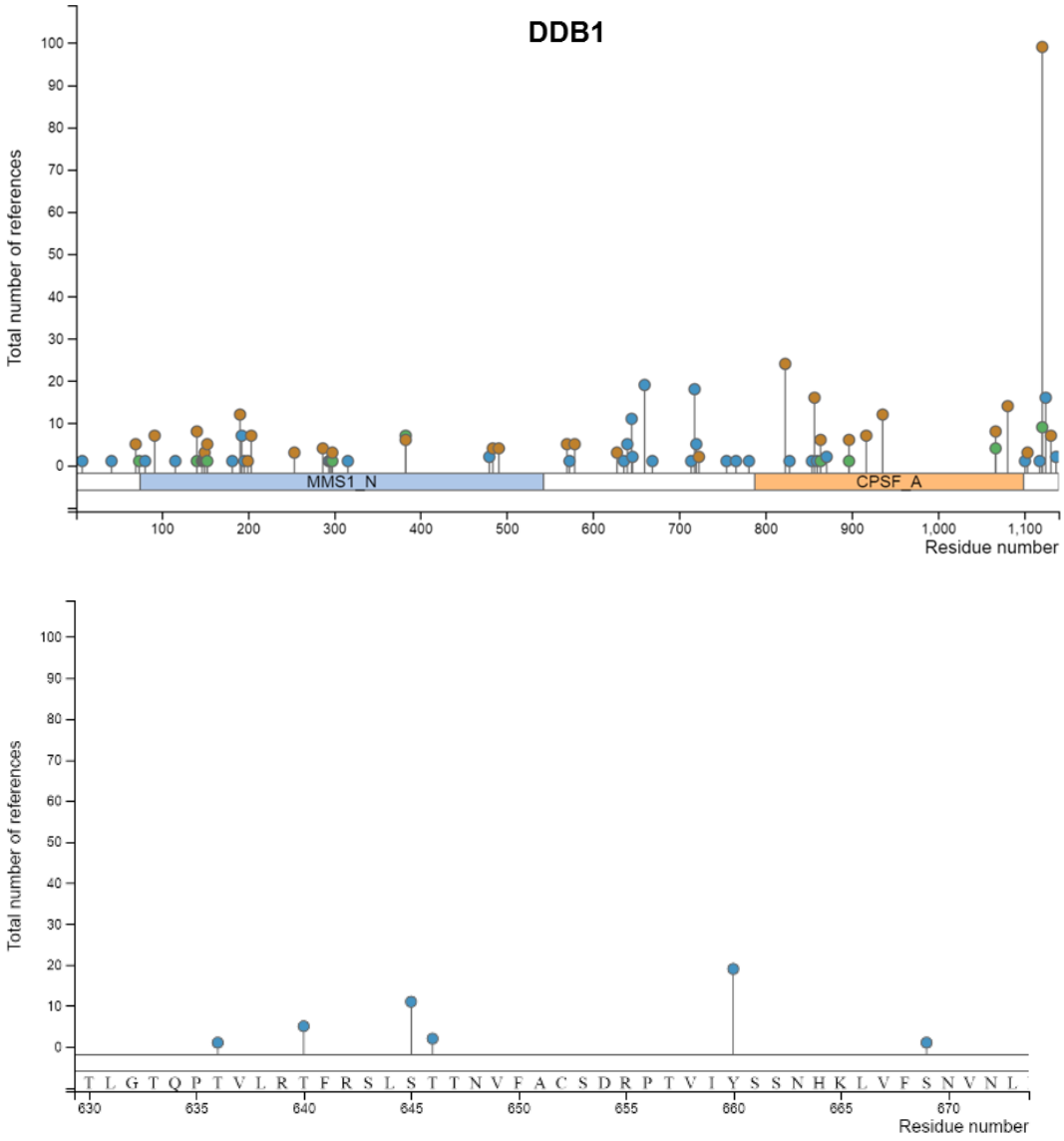

Figure 7.9. Phosphorylation prediction site of DDB1 retrieved from www.phosphosite.org.

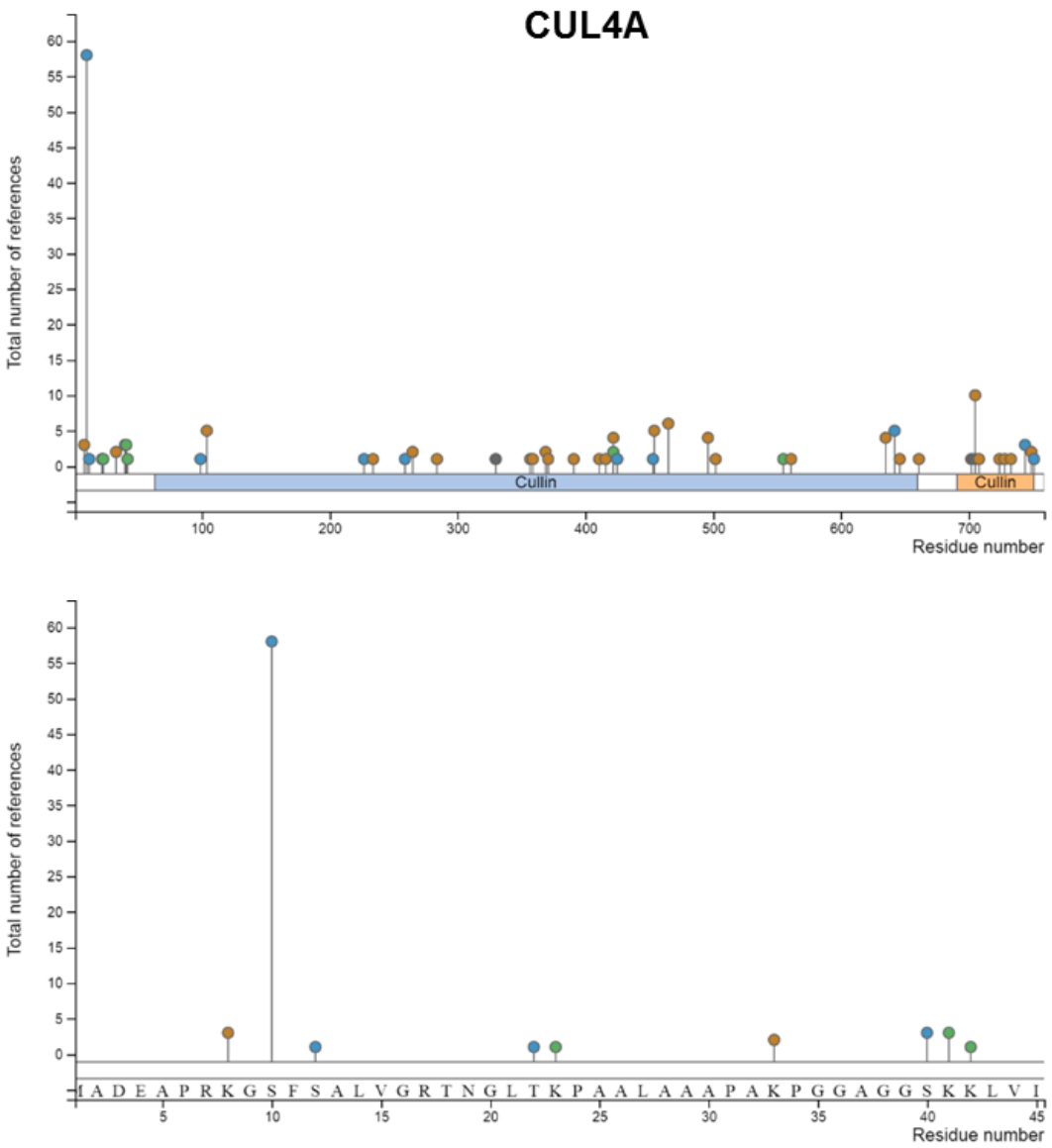

Figure 7.10. Phosphorylation prediction site of CUL4A retrieved from www.phosphosite.org.

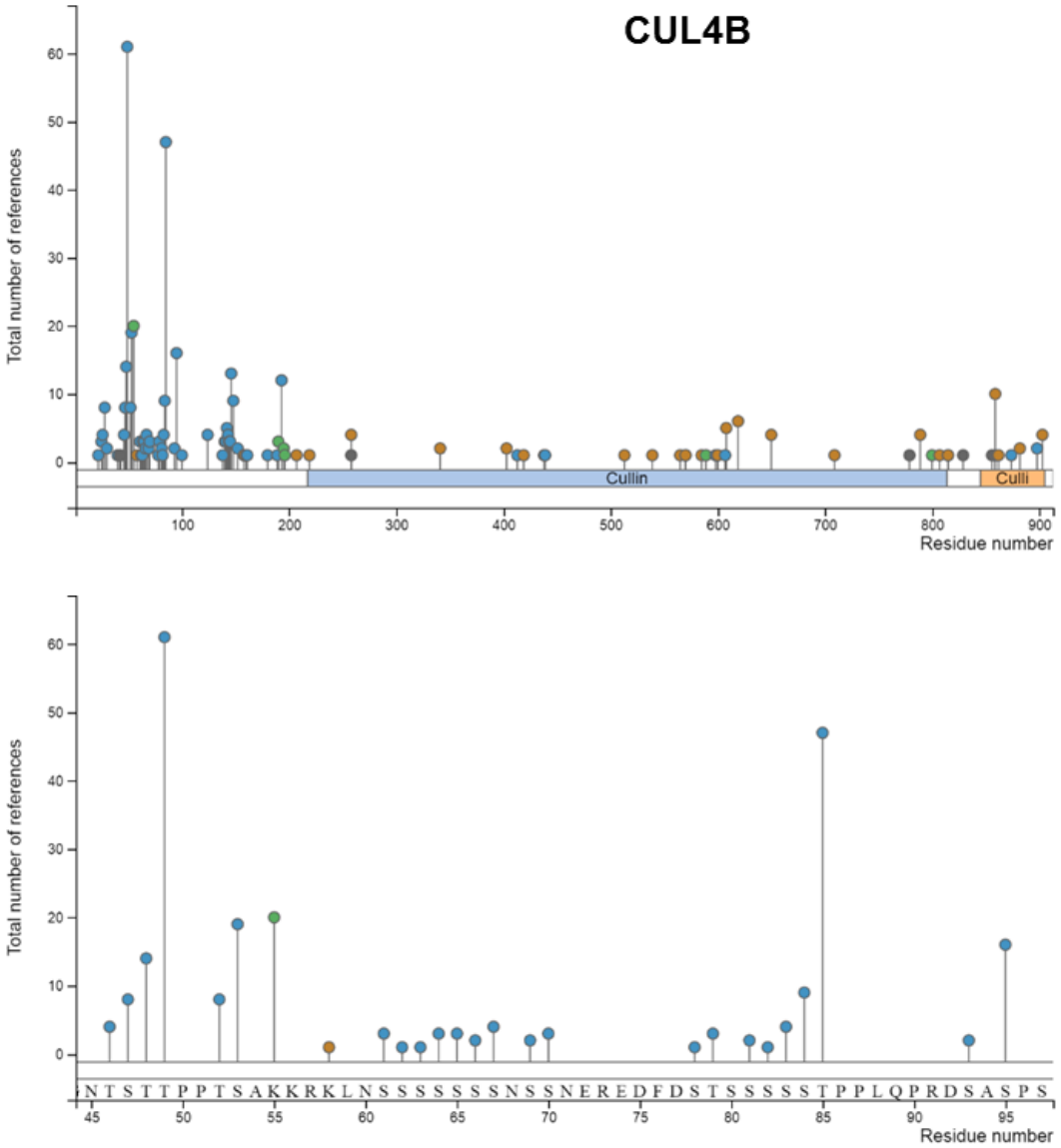

Figure 7.11. Phosphorylation prediction site of CUL4B retrieved from www.phosphosite.org.

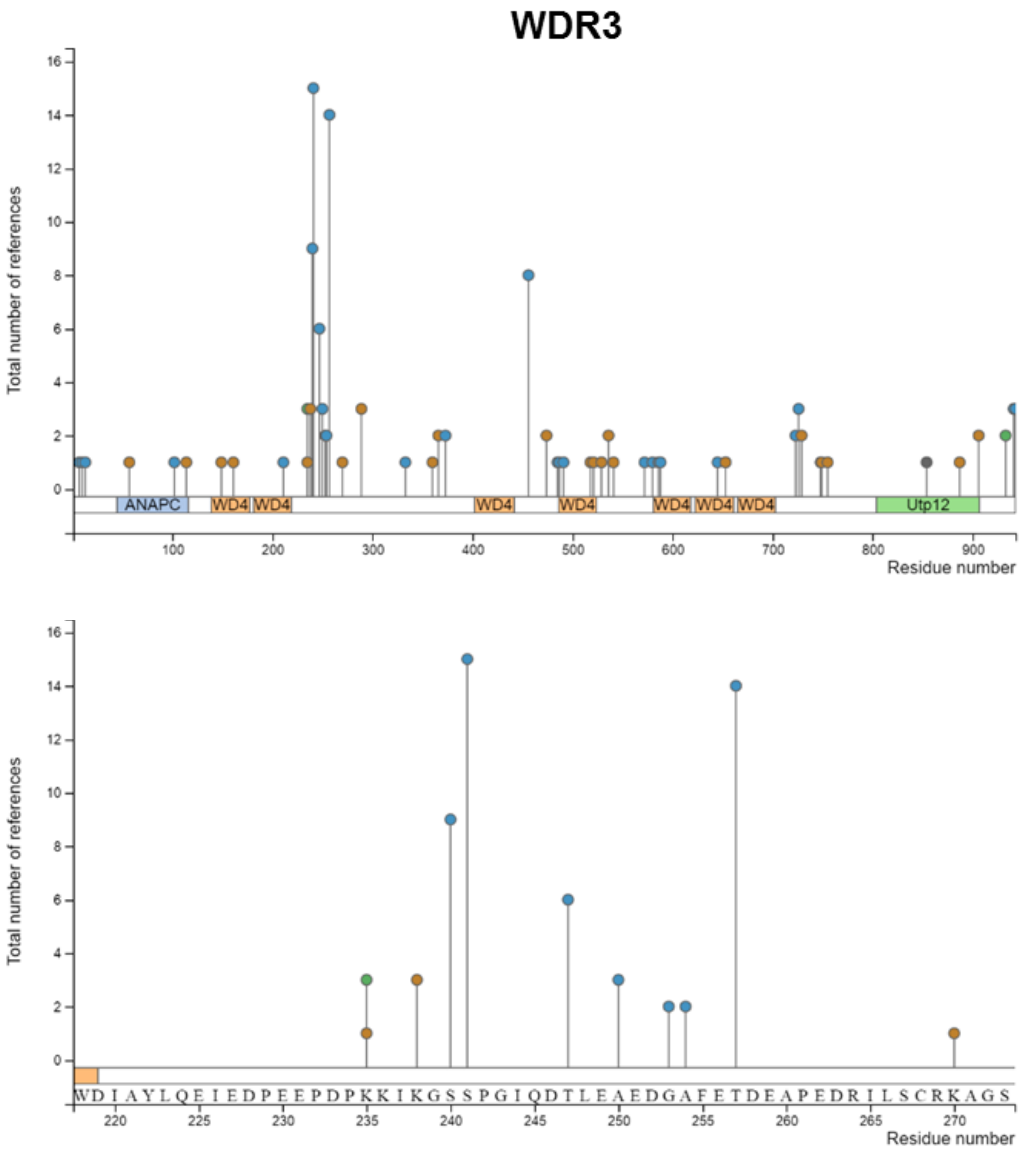

Figure 7.12. Phosphorylation prediction site of WDR3 retrieved from www.phosphosite.org.

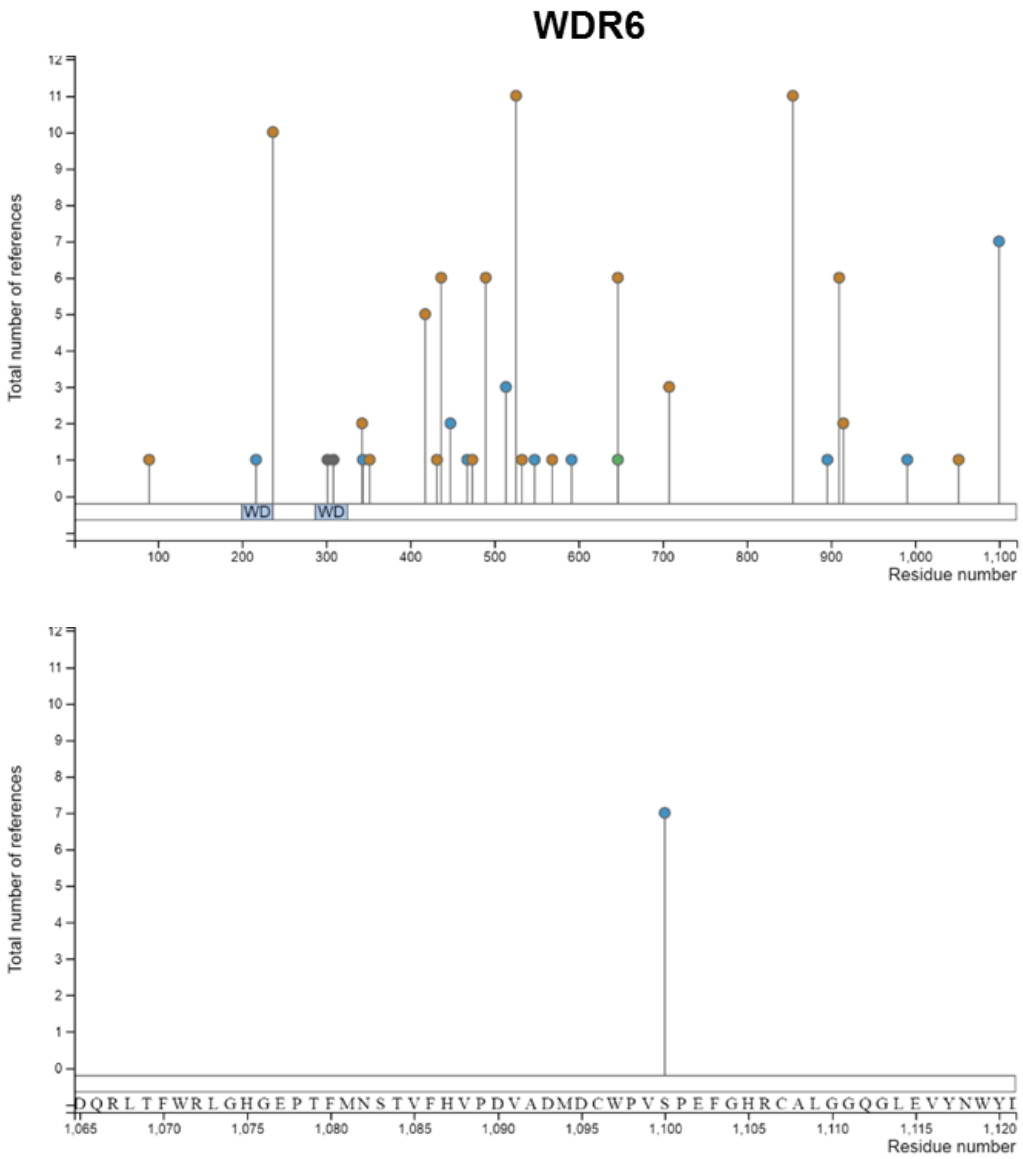

Figure 7.13. Phosphorylation prediction site of WDR6 retrieved from www.phosphosite.org.

7.4.4. HALO-Ubiquilin Protein Expression for TUBE pull-down assay

For preparing the HALO-Ubiquilin tubes protein (MW 59.8 kDa) for TUBE pull down assay, pET28-HALO Ubiquilin (4X UBA) (University of Dundee) (**Figure 7.14.**) was prepared for protein expression. The cDNA plasmid was transformed to BL21 *E.coli* competent cell and grown in LB agar media with 30 µg/ml Kanamycin for overnight. One colony transformant was then cultured in 25 ml of LB broth media as starter culture for 6 hours in 37°C incubator shaker. The culture was then being transferred to the larger batch of 2 litre LB broth media with 30 µg/ml Kanamycin. After reach the cell growth with OD600 ~0.6, the IPTG induction was performed. The optimisation of the induction condition (IPTG concentration, incubation time and temperature) was then performed. The SDS-PAGE analysis and Comassie blue staining was carried out. Gel imaging was performed using SynGene G:Box Chemi XX6 imaging system.

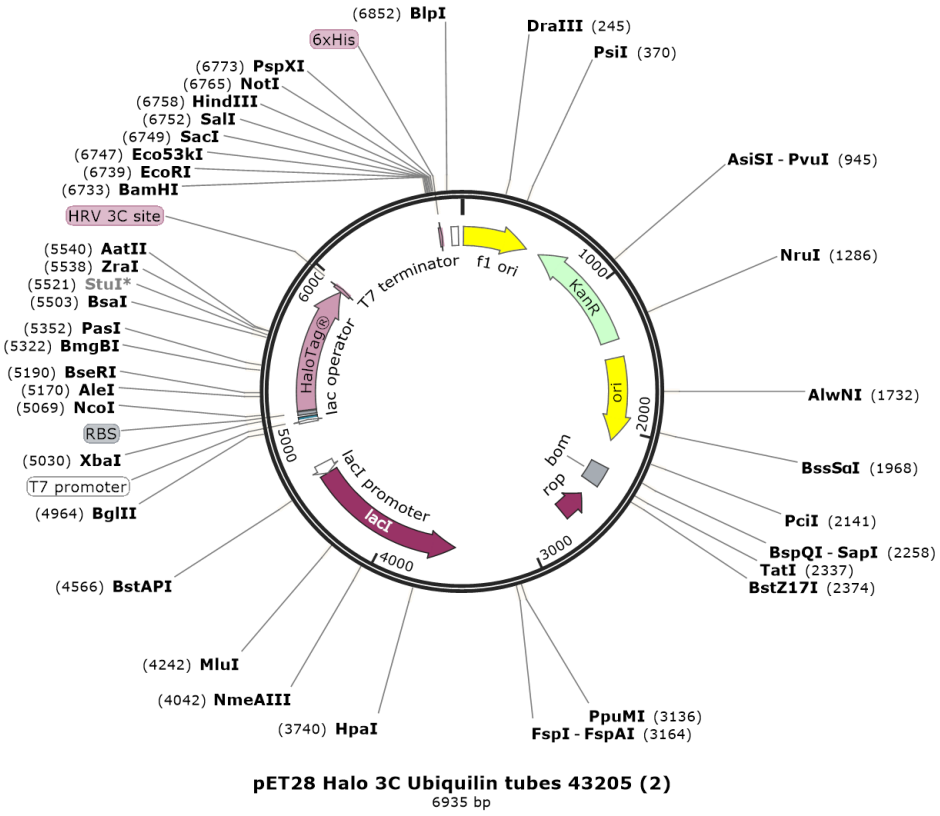

Figure 7.14. Plasmid map of pET28 Halo 3C Ubiquilin tubes. The cDNA plasmid was used for TUBE pull-down assay.

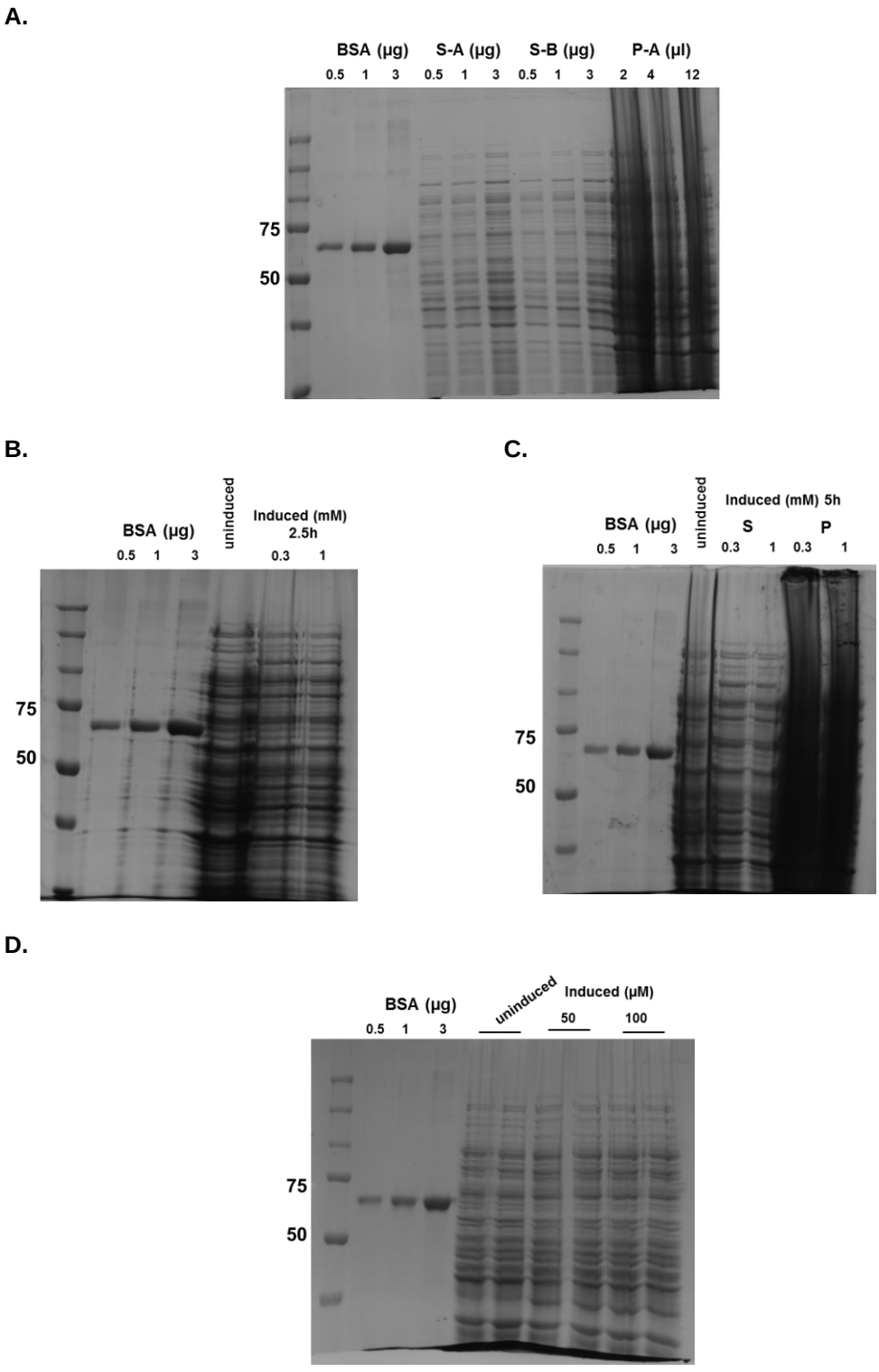

Figure 7.15. Gel image from Comassie blue staining of HALO-Ubiquilin tubes protein (MW ~60 kDa) expression optimisation. (A.) Induction was using IPTG with concentration 0.3 mM at 28°C and sample from the supernatant A (S-A) and B (S-B) as well as pellet A (P-A) in denoted loading amount (µg or µl) for each lane. BSA (Bovine Serum Albumin) as control. (B.) IPTG induction was done for 0.3 and 1 mM for 2.5 and (C.) 5 hours at 37°C. S (supernatant) and P (pellet) sample were loaded 3 µg. Only supernatant sample from 2.5h induction was analysed. (D.) IPTG induction was done for 50 and 100 µM for 17 hours at 16°C. BSA (Bovine Serum Albumin) in defined amount (µg) was used as control.